PLASTIC FLOW AND FRACTURE BEHAVIOR OF DUCTILE MATERIALS INCORPORATING VOID NUCLEATION, GROWTH, AND INTERACTION

by

Arthur L. Gurson

B.S., University of Rochester, 1968
M.S., Brown University, 1970

Thesis

submitted in partial fulfillment of the requirements for the Degree of Doctor of Philosophy in the Division of Engineering at Brown University

June, 1975

This thesis by Arthur L. Gurson

is accepted in its present form by the Division of

Engineering as satisfying the

thesis requirement for the degree of Doctor of Philosophy.

Date 27 May 1975 James R. Rice

Recommended to the Graduate Council

Date 27th May 1975 David K. Gaver

Date 27 May 1975 P S Symonds

Approved by the Graduate Council

Date June 1, 1975 Francis Clauser

Vita

The author was born on April 7, 1948 in New York City. He attended Stuyvesant High School in New York City, from which he graduated in June of 1964. In June of 1968, he received a Bachelor of Science degree in Engineering from the University of Rochester. During the summers of 1967 and 1968, he was employed as an engineering trainee at the Eastman Kodak Company and the Vertol Division of the Boeing Company. He received a Master of Science degree in Engineering from Brown University in June of 1970.

Table of Contents

Acknowledgement

The author wishes to extend sincere appreciation to his thesis advisor, Professor James R. Rice, whose patience, encouragement, and guidance made this work possible. Thanks is also extended to the National Science Foundation and the Atomic Energy Commission, who funded the work, The careful preparation of the manuscript by Leone Cargill and the help of Diane Minter are also gratefully acknowledged.

Introduction

The objective of this work is the development of a reasonable mathematical model of the ductile fracture process. This process involves a first step of macroscopically homogeneous deformation in which the material strain hardens, and voids nucleate and grow. The second step involves a bifurcation of the deformation field, in which the deformation localizes in a band and fracture follows immediately through void linkage by growth or tearing.

A model of the ductile fracture process must therefore contain elements which describe 1) void nucleation, 2) void growth under macroscopically homogeneous deformation, and 3) a criterion for flow localization. To develop such a model, better understanding is needed of the constitutive laws of void containing materials. Towards this goal, the initial plastic yield behavior of some models of void containing materials will be investigated, and approximate yield criteria and flow rules will be developed. These will be combined with the work of other authors on void nucleation and flow localization to model the ductile fracture process.

It is commonly assumed that hydrostatic stress has no effect on plastic yield (1), and in accord with the normal flow rule, that plastic deformation is incompressible. However, many recent experimental [21-35] and theoretical [36-39] studies indicate that when voids are present in ductile materials, the hydrostatic component of stress can cause macroscopic dilatation through the mechanism of void growth. It is postulated that a positive hydrostatic component of stress can aid in the nucleation of voids at strongly bonded inclusions (such as carbides in spheroidized carbon steel) by raising the interfacial stress between the inclusion and the matrix [10,12-14]. A void can be nucleated either by matrix-particle decohesion, or particle cracking [15-20].

It has also been suggested that voids can be nucleated in "pure" materials without the aid of inclusions when the strains are large enough for a dislocation-vacancy mechanism to operate [11].

The aim of this work is to investigate the plastic yield behavior of a model porous (void containing) material. The physical model used is a "unit" cube not unlike that of Bishop and Hill [2], only of a porous material (void-matrix aggregate) instead of a polycrystalline aggregate. The unit cube is by definition large enough to be statistically representative of the properties of the bulk material. As Berg [3,4] has pointed out, the Bishop and Hill analysis of the polycrystalline aggregate applies equally well to a void-matrix aggregate. This allows proof of a macroscopic maximum plastic work principle, if one exists on the microscopic level. Throughout this paper, the adjective "macroscopic" refers to average values of physical quantities (stress, dissipation, velocity, etc.) which represent the behavior of the bulk material. "Microscopic" refers to pointwise properties, such as the stress or velocity fields in the vicinity of a void.

An approximate yield locus is calculated as follows. The von Mises conditions are used to characterize the yield and flow of the matrix material (itself incompressible). A rigid-plastic model is assumed valid because of the large strains involved in ductile fracture [21-35]. A form is then assumed for the velocity field in the aggregate, which allows the voids to grow but requires incompressibility in the matrix. This velocity field must also meet kinematic boundary conditions corresponding to deformation rates on the surface of the unit cube. An upper bound inequality is then used to estimate the macroscopic stress field required to sustain plastic flow. The locus of stress fields for a variety of surface deformation rate fields (one given porosity and

void shape) form the upper bound yield locus for that given unit cube. It is proven in the text that the macroscopic deformation rate tensor lies normal to both the actual and approximate yield loci.

An alternate method for computing macroscopic stresses, based on the work of Rice and Drucker [7], and suggested by Rice [47] is also considered. It is based on the result that the partial derivative of the macroscopic dissipation rate with void volume fraction can be reduced, under certain circumstances, to an integral of dissipation rate over the void surface. The two methods are compared and discussed.

For purposes of analysis, the void-matrix aggregate is idealized as a single void in a rigid-plastic cell; the void volume fraction (f) of the cell equalling that of the aggregate. The cell is presumed to behave under loading as the aggregate would, exhibiting void growth when undergoing yield with a positive component of hydrostatic stress. Two void geometries are considered; the long circular cylindrical void and the spherical void. The outer cell wall is idealized as geometrically similar to, and centered around the void. These two geometries were chosen because they resemble many of the void shapes seen experimentally, they provide the expected isotropy (transverse directions for the cylinder, total for the sphere), and, of course, because their symmetry properties significantly aid the analysis. See figs. 1, 2, and 3.

Once a yield criterion and flow rule have been established, plastic flow can be investigated. Dilation of the bulk material becomes a simple manifestation of the flow rule, which determines the ratio of the deformation rate components. Because the matrix material is incompressible, any increase in volume is due to the generation of empty space within the body, i.e., void growth or void nucleation. Given a proper combination of macroscopic stress

and deformation rate boundary conditions, the amount of void growth per increment of deformation can be determined.

The literature indicates that voids are generated from hard inclusions in a ductile matrix by two mechanisms: matrix-particle decohesion, and particle cracking [12-20]. Void nucleation occurs preferentially in areas of high inclusion concentration. This is explained in the literature by the local stress fields generated by the presence of rigid inclusions when the matrix undergoes plastic flow. High local inclusion concentrations can occur either by close grouping of separate particles, or the presence of one larger-than-average particle. When particle cracking is the mechanism, larger brittle particles are thought to contain more and larger flaws, leading to easier brittle fracture in the particle [19]. For both void generation mechanisms, the size of the generated void is considered equal to that of the generating particle.

Void nucleation and void growth are two separate mechanisms of void volume fraction increase. Nucleation as well as growth can be related to an increment of deformation, when the proper boundary conditions are given. An analytic form is set up which is general enough to include nucleation by both mechanisms discussed above. The theoretical treatment draws heavily on the work done by Argon, et al. [13] with regard to the normal stress generated at the particle matrix interface, and the statistical treatment of a random distribution of particles. As with the voids, only simple particle shapes (spheres and circular cylinders) are considered.

When an inclusion is much weaker than the matrix, or is weakly bonded to the matrix, it is considered to behave as a void from the outset.

Plastic flow is studied in a model bulk material containing voids and/or inclusions, using the yield criteria and flow rules discussed above. Incre-

ments of deformation are applied as boundary conditions, and quantities such as void volume fraction and degree of work hardening are updated with each increment. Work hardening is approximated as homogeneous in the material, and is calculated as a macroscopic average of the dissipation. The matrix is modelled as a rigid-power law hardening material. Void shape is approximated as constant, allowing continued use of yield functions for the spherical or cylindrical shape. For the (predominant) case where the material model possesses the same isotropy properties as the void shape, the approximations made concerning work hardening and subsequent void shape ensure that the isotropy remains after deformation.

Ductile fracture is interpreted here as an unstable bifurcation of the macroscopic flow field in the model bulk material. This bifurcation is the transition from a homogeneous flow field to one in which deformation becomes concentrated in a thin band, with large amounts of void growth. Necking or tearing between voids results, leading immediately to failure.

For isotropic plastic materials, Berg [3,4] has shown that the conditions for band formation are (1) the existence of a surface of zero extension, and (2) a zero rate of hardening in the material. Void nucleation and growth are viable softening mechanisms which can cancel out the hardening of the matrix to give a bulk hardening rate of zero. Rice [45], and Rudnicki and Rice [50] have examined conditions for bifurcation for a wider class of material properties, such as anisotropy and elastic-plasticity. Their results help determine when elastic terms are important, and when they can be ignored.

Calculations of ductility (natural strain to fracture) are carried out for two types of specimen geometries; plane strain, and axial symmetry. A variety of matrix hardening exponents, and void and particle concentrations are considered.

The approximate velocity fields used in the upper bound calculations are developed as follows:

There are an infinity of velocity fields which obey incompressibility and compatibility. A finite number of these are combined to form a general approximate field, containing several undetermined factors which are constant with respect to the geometry of the void-matrix model. The factors are then adjusted so that the velocity field satisfies the displacement boundary conditions, as required by the upper bound method. For very simple fields, only enough factors need be present for this. For more refined fields with additional factors (to give better upper bounds), two more tools are available to determine these factors.

One method is to enforce a condition of zero shear deformation rate at the void surface. For a von Mises material, this means zero shear stress, which would be expected of the true solution. (No such analog exists for normal stress and deformation rate, because the von Mises yield and flow rules are in terms of deviatoric components only.) This makes the approximate field more closely resemble the actual field.

A second method of determining the factors is to find their values which minimize the dissipation in the body for a given set of boundary conditions. A combination of these two methods is found to give better (lower) upper bound solutions.

Two basic types of flow fields are considered. The simplest one to deal with is the type where all of the matrix material is undergoing plastic flow. However, under certain conditions a lower dissipation will result from flow fields where part of the matrix remains rigid. In an attempt to model this, approximate flow fields are developed with rigid-plastic boundaries generated

by radial lines (see figs. 4). For simplicity, only those macroscopic flow fields with a high degree of symmetry are considered. These are; 1) plane strain for the cylindrical model, leading to a rigid wedge symmetric to one of the principal axes, and 2) axially symmetric flow for the spherical model, leading to a rigid circular cone centered on the axis of symmetry. See figs.4.

The angle of the rigid-plastic boundary to an axis of symmetry is the factor which is determined by minization of the dissipation. A criterion of lowest dissipation can also be used to choose between fully plastic flow and flow with a rigid section.

The presence of voids can induce nonuniformity in the microscopic flow field, leading to anistropic hardening. As a first approximation in the ductility analysis, this was changed to isotropic hardening via an averaging process. An assessment of this approximation was considered useful, and is carried out as follows:

The simplest case to consider is the cylindrical void in plane strain, essentially a two-dimensional problem. Instead of using an average value of work hardening, material points are labelled and the total strain (and thus yield stress) is carried through several increments of deformation. Both fully plastic and rigid wedge flow fields are considered. The latter naturally lead to a greater level of anisotropy.

Strong experimental evidence of the contribution of void growth and coalescence to ductile fracture comes from many recent optical and electron microscopic studies [21-35]. Bluhm and Morrissey [26] show photographs of sectioned tensile specimens (steel and copper) where fracture at the neck was stopped before complete separation. Significant void growth is clearly evident; with void elongation in the axial direction, and transverse isotropy.

Beachem [25] has shown that void growth is part of the fracture mechanism for a wide range of engineering materials, under shear as well as tensile loading. Studies by Edelson and Baldwin[21] and Rostoker and Liu [22] on scintered compacts whose porosity was controlled show the loss of ductility caused by second phases (voids and inclusions) in a ductile matrix. ([22], and a paper by Sarin and Grant [23], show that the ductility of the matrix is very dependent on the processing of the powdered metal.) Gurland and Plateau [16] observed that inclusions, once cracked or separated from the matrix, act as voids in the sense that failure occurs by tearing between cavities. Liu and Gurland [29] found that for spheroidized carbon steels, failure occurred by void growth and coalescence for %C < 0.30%. (With higher percentages, voids do not grow very much, and linking up is by some form of inter-void "cracking".

Some of the theoretical work done on yield behavior of porous materials is as follows: McClintock's [36] work includes a fracture criterion based on his analysis of a cylindrical cavity in an infinite matrix subject to axial and transverse stresses. A strong (exponential) dependence of void growth rate on transverse stress in found. Rice and Tracey [37] consider a spherical void in an infinite matrix, and an exponential dependence of growth rate on triaxial stress also results. Kahlow and Avitzur [38] study the problem of the critical pressure needed to prevent void growth during axially symmetric deformation. Their model is a closed cylinder with a cylindrical hole at the center, and their upper bound approach is in some ways similar to that used here. Thomason [9,10] works with a rigid-perfectly plastic plane strain model; a periodic array of rectangular voids. He compares the energy necessary for two types of deformation; homogeneous, and necking between voids. When necking is preferred, he considers fracture to follow immediately.

A study which provides useful material for comparison is one by Nagpal, McClintock, Berg, and Subudhi [44]. They present plane strain slip line solutions for a band of evenly spaced holes under varying ratios of shear and normal traction. Their results can be compared to the yield loci developed here for plane strain deformation in a plastic material with cylindrical voids whose axes are parallel to the plane strain axis.

The author knows of two finite element studies of void growth, both for the two-dimensional case (plane strain, cylindrical voids) [41,42]. Both use an elastic-plastic constitutive relation. The results are very useful in deciding what types of velocity fields to employ.

2. General Theory - Upper Bound Approach

The general model considered here is a "unit" cube of porous material of volume V, large enough to be statistically representative of the properties of the aggregate (Fig. 1). The matrix material (though not the void-matrix aggregate) is considered a homogeneous, incompressible, rigid-plastic, von Mises material. The yield and flow relation for the matrix material are

$$\frac{3}{2} s_{ij} s_{ij} = \sigma_o^2 \quad (a), \qquad s_{ij}(\underset{\sim}{\dot{\epsilon}}) = \frac{\sqrt{\frac{2}{3}}\,\sigma_o\,\dot{\epsilon}_{ij}}{(\dot{\epsilon}_{kl}\,\dot{\epsilon}_{kl})^{1/2}} \quad (b)$$

$$\dot{\epsilon}_{ij} = \frac{1}{2}\left(\frac{\partial \dot{u}_i}{\partial x_j} + \frac{\partial \dot{u}_j}{\partial x_i}\right), \qquad \dot{\epsilon}_{kk} = 0 \quad (c) \tag{2.1}$$

where σ_o is the yield stress in tension of the matrix, s_{ij} is microscopic deviatoric stress, $\dot{\epsilon}_{ij}$ is the microscopic rate of deformation, and $\dot{u}_i$ is the microscopic velocity field, and x_i is the position of a material point.

The macroscopic rate of deformation is defined, as in Bishop and Hill [2], as an averaged quantity in terms of the velocity field on the surface of the unit cube

$$\dot{E}_{ij} = \frac{1}{V}\,\frac{1}{2}\int_S (\dot{u}_i n_j + \dot{u}_j n_i)\, dS \tag{2.2}$$

where $\underset{\sim}{n}$ is the unit outward normal on the outer surface. Using the Gauss theorem and eqn. 2.1c, it can be shown that

$$\dot{E}_{ij} = \frac{1}{V}\int_V \dot{\epsilon}_{ij}\, dV . \tag{2.3}$$

Where $\underset{\sim}{n}$ is still a surface normal in the outward direction, this can be separated into integrals over the matrix material and the void surface:

$$\dot{E}_{ij} = \frac{1}{V}\int_V \dot{\epsilon}_{ij}\, dV + \frac{1}{V}\frac{1}{2}\int_{S_{voids}} (\dot{u}_i n_j + \dot{u}_j n_i)\, dS \qquad (2.4)$$

Since $\dot{\epsilon}_{ij}$ is incompressible, the last term above includes the dilatational part of $\dot{E}_{ij}$. The fields considered are derived from incompressible velocity fields which must meet displacement boundary conditions on the outer surface, as expressed in terms of the $\dot{E}_{ij}$. It is important to note that the $\dot{E}_{ij}$ are average quantities (eqn. 2.2) and can represent many different boundary distributions of $\dot{u}_i$.

The velocity field must also meet the constraint that it be continuous in the matrix. Thus, velocity fields which involve matrix separation are excluded.

Among the infinity of incompressible $\dot{u}_i$ fields which meet the above conditions, the actual $\dot{u}_i$ field is characterized by its generation of the minimum of the dissipation $\dot{W}$;

$$\dot{W} = \frac{1}{V}\int_V s_{ij}(\underset{\sim}{\epsilon})\, \dot{\epsilon}_{ij}\, dV \qquad (2.5)$$

where the terms in the integrand are related to $\dot{u}_i$ by eqns. 2.1. All physical quantities (T_i, $\dot{\epsilon}_{ij}$, s_{ij}, σ_{ij}, $\dot{W}$) associated with the actual $\dot{u}_i$ field will be labeled with the superscript "A", since they are also actual solutions. Quantities associated with other $\dot{u}_i$ fields are merely approximate solutions. An important property of σ^A_{ij} is that it is an equilibrium stress field.

Actual macroscopic stress, Σ_{ij}^A, is defined as in Bishop and Hill [2]; area averages of the forces on the faces of the unit cube. Their three postulates regarding the unit cube are also adopted: 1) The unit cube is large enough to be statistically representitive of the void-matrix aggregate, 2) no correlation exists between microscopic stress and position over any plane section through the unit cube, and 3) no correlation exists between microscopic stress and displacement over any plane section theough the unit cube. Postulate (2) assures zero moments on the cube, and therefore symmetry of Σ_{ij}^A. Postulate (3) is instrumental in proving a maximum plastic work principle for the aggregate. This is developed below, drawing heavily on the example of Bishop and Hill.

Consider the actual dissipation

$$\dot{W}^A = \frac{1}{V}\int_S T_i^A \dot{u}_i^A \, dS = \frac{1}{V}\int_V \sigma_{ij}^A \dot{\epsilon}_{ij}^A \, dV = \frac{1}{V}\int_V s_{ij}(\underset{\sim}{\epsilon}^A)\,\dot{\epsilon}_{ij}\, dV \qquad (2.6)$$

by the principle of virual work, incompressibility, and eqns. 2.1. The principle of virtual work requires an equilibrium stress field, as assured only by the actual solution. Using

$$T_i^A\Big|_S = \sigma_{ij}^A n_j\Big|_S \qquad (2.7)$$

eqn. 2.6 can be written as

$$\dot{W}^A = \frac{1}{V}\int_S \sigma_{ij}^A n_j \dot{u}_i^A \, dS = \frac{1}{V}\sum_{\text{faces}} \int_A \sigma_{ij}^A \dot{u}_i^A n_j \, dS, \qquad (2.8)$$

a sum of integrals over the faces of the unit cube. $\underset{\sim}{n}$ is a constant on any

plane surface. With postulate (3), the integrals in the sum become

$$n_j \int_A \sigma_{ij}^A \dot{u}_i^A \, dS = \frac{1}{A} \int_A \sigma_{ij}^A \, dS \int_A \dot{u}_i^A n_j \, dS \tag{2.9}$$

The actual macroscopic stress is defined as

$$\Sigma_{ij}^A = \frac{1}{A} \int_A \sigma_{ij}^A \, dS \tag{2.10}$$

The actual dissipation thus becomes

$$\dot{W}^A = \frac{1}{V} \int_V s_{ij}(\dot{\underset{\sim}{\epsilon}}^A) \dot{\epsilon}_{ij}^A \, dV = \frac{1}{V} \Sigma_{ij}^A \int_S \dot{u}_i^A n_j \, dS \tag{2.11}$$

where S is the entire outer surface of the unit cube. Using symmetry and eqn. 2.2, this becomes

$$\dot{W}^A = \frac{1}{V} \int_V \sigma_{ij}^A \dot{\epsilon}_{ij}^A \, dV = \Sigma_{ij}^A \dot{E}_{ij} \, . \tag{2.12}$$

It is noteworthy that this result can be obtained directly from the first part of eqn. 2.8 when either of the following is true: 1) The surface tractions are related to Σ_{ij}^A as follows:

$$T_i \Big|_S = \Sigma_{ij} n_j \Big|_S \tag{2.13}$$

or, 2) The surface velocities are related to $\dot{E}_{ij}$ as follows;

$$\dot{u}_i \Big|_S = \left(\dot{E}_{ik} X_k + C_i + \Omega_{ij} X_j \right) \Big|_S \tag{2.14}$$

where the C_i are constants meant to accommodate rigid body translation, and the Ω_{ij} accommodate rigid body rotation (thus, both drop out when $\dot{\epsilon}_{ij}$ are calculated). Note that, to within the C_i and $\Omega_{ij}x_j$, the $\dot{u}_i$ on the outer surface are uniquely determined by the $\dot{E}_{ij}$, without any other conditions (compare to eqn. 2.2).

These conditions trivially satisfy postulate (3) by making either the stress or velocity (rate of displacement) on any plane section a constant.

The sequence of eqns. 2.6 through 2.14 could be carried out with equal validity (except for defining dissipation) for an actual stress field σ_{ij}^{A*} corresponding to a $\dot{u}_i^{A*}$ and $\dot{E}_{ij}^{*}$ different from $\dot{u}_i^{A}$ and $\dot{E}_{ij}$, giving

$$\Sigma_{ij}^{A*}\dot{E}_{ij} = \frac{1}{V}\int_V \sigma_{ij}^{A*}\dot{\epsilon}_{ij}^{A}\,dV \quad . \tag{2.15}$$

Combining with eqn. 2.14 gives

$$\left(\Sigma_{ij}^{A} - \Sigma_{ij}^{A*}\right)\dot{E}_{ij} = \frac{1}{V}\int_V \left(\sigma_{ij}^{A} - \sigma_{ij}^{A*}\right)\dot{\epsilon}_{ij}^{A}\,dV \quad . \tag{2.16}$$

If maximum plastic work applies to the matrix material (as it does to a von Mises material, i.e.,

$$\left(\sigma_{ij}^{A} - \sigma_{ij}^{A*}\right)\dot{\epsilon}_{ij} \geq 0 \quad , \tag{2.17}$$

then,

$$\left(\Sigma_{ij}^{A} - \Sigma_{ij}^{A*}\right)\dot{E}_{ij} \geq 0 \quad . \tag{2.18}$$

This proves maximum plastic work for the aggregate, with Σ_{ij}^{A} and $\dot{E}_{ij}$ as defined above. The yield locus of Σ_{ij}^{A} thus has the properties of convexity

and normality. Normality and eqn. 2.12 give

$$\delta \dot{W}^A = \Sigma^A_{ij}\, \delta \dot{E}_{ij} + \delta \Sigma^A_{ij}\, \dot{E}_{ij}, = \Sigma^A_{ij}\, \delta \dot{E}_{ij},$$

$$\text{since } \delta \Sigma^A_{ij}\, \dot{E}_{ij} = 0 \text{ by normality,} \qquad (2.19)$$

$$\text{and thus, } \Sigma^A_{ij} = \frac{\partial \dot{W}^A}{\partial \dot{E}_{ij}}$$

Eqation 2.5 defines an approximate macroscopic dissipation when $\dot{W}$ is not minimized with respect to all acceptable (incompressible, compatible with $\dot{E}_{ij}$, continuous) velocity fields;

$$\dot{W} = \frac{1}{V}\int_V S_{ij}(\underset{\sim}{\epsilon})\, \dot{e}_{ij}\, dV \qquad (2.5)$$

The approximate velocity fields used here will have the functional form

$$\dot{u}_i = \dot{u}_i(\underset{\sim}{\dot{E}}, f, \underset{\sim}{x}) \qquad (2.20)$$

where x is the coordinate vector of a material point in the matrix. There may be an additional dependence on other parameters q_1, q_2, ---, as in

$$\dot{u}_i = \dot{u}_i(\underset{\sim}{\dot{E}}, f, \underset{\sim}{x}, q_1, q_2, \cdots) \qquad (2.21)$$

with the q_i's chosen to minimize the plastic dissipation. For their optimal values,

$$q_i = q_i(\underset{\sim}{\dot{E}}, f) \qquad (2.22)$$

so the form of eqn. 2.21 ultimately reduces to the form of eqn. 2.20. All of the velocity fields considered here are, like the actual field, homogeneous of degree one in the components of $\underset{\sim}{\dot{E}}$, i.e.,

for C = a constant,

$$\dot{u}_i(C\dot{E}_{11}, C\dot{E}_{22}, \cdots) = C\dot{u}_i(\dot{E}_{11}, \dot{E}_{22}, \cdots) \quad . \tag{2.23}$$

It is easily seen from eqns. 2.1 and 2.5 that $\dot{\varepsilon}$ and $\dot{W}$ are then also homogeneous of degree one in the $\dot{E}_{ij}$, giving

$$\dot{W} = \frac{\partial \dot{W}}{\partial \dot{E}_{ij}} \dot{E}_{ij} \tag{2.24}$$

Define the approximate macroscopic stress needed to cause macroscopic yielding in a way analogous to eqn. 2.19:

$$\Sigma_{ij} = \frac{\partial \dot{W}}{\partial \dot{E}_{ij}} \quad , = \frac{1}{V}\int_V S_{kl}(\underline{\dot{\epsilon}}) \frac{\partial \dot{\epsilon}_{kl}}{\partial \dot{E}_{ij}} \, dV \tag{2.25}$$

due to normality for $s_{ij}(\dot{\epsilon})$. This gives, with eqn. 2.24,

$$\Sigma_{ij}\dot{E}_{ij} = \frac{\partial \dot{W}}{\partial \dot{E}_{ij}} \dot{E}_{ij} = \dot{W} \quad . \tag{2.26}$$

This shows that Σ_{ij} as defined above is a work conjugate to $\dot{E}_{ij}$, as is Σ^A_{ij}. By a trivial rearrangement of the steps in eqn. 2.19, normality is thus established for the approximate yield locus (generated by the locus of stress states Σ_{ij} defined by eqn. 2.25 for all possible directions of $\dot{E}_{ij}$) .

The actual yield surface obeys both normality and convexity; it is desirable to examine if the approximate Σ_{ij} surface is convex. Consider two approximate stress fields Σ_{ij} and Σ^*_{ij} ; which correspond to $\dot{E}_{ij}$ and $\dot{E}^*_{ij}$ respectively through eqns. 2.1, 2.2, 2.5, 2.20, and 2.25. Write the following:

$$\left(\Sigma_{ij}-\Sigma^{*}_{ij}\right)\dot{E}_{ij} = \frac{1}{V}\int_{V}\left\{s_{kl}(\underset{\sim}{\dot{\varepsilon}})\frac{\partial\dot{\epsilon}_{kl}}{\partial\dot{E}_{ij}} - s_{kl}(\underset{\sim}{\dot{\varepsilon}}^{*})\frac{\partial\dot{\epsilon}^{*}_{kl}}{\partial\dot{E}^{*}_{ij}}\right\}\dot{E}_{ij}\,dV \qquad (2.27)$$

Convexity can be proven if, in addition to eqn. 2.23, $\dot{\epsilon}_{ij}$ is homogeneous and linear in $\dot{E}$. This means:

$$\frac{\partial\dot{\epsilon}^{*}_{kl}}{\partial\dot{E}^{*}_{ij}}\cdot\dot{E}_{ij} = \frac{\partial\dot{\epsilon}_{kl}}{\partial\dot{E}_{ij}}\dot{E}_{ij} = \dot{\epsilon}_{kl} \qquad (2.28)$$

Equation 2.27 then becomes

$$\left(\Sigma_{ij}-\Sigma^{*}_{ij}\right)\dot{E}_{ij} = \frac{1}{V}\int_{V}\left(s_{kl}(\underset{\sim}{\dot{\varepsilon}}) - s_{kl}(\underset{\sim}{\dot{\varepsilon}}^{*})\right)\dot{\epsilon}_{kl}\,dV \geq 0, \qquad (2.29)$$

since $s_{ij}(\epsilon)$ obeys maximum plastic work. A maximum plastic work principle is thus proven for Σ_{ij}, giving convexity as well as normality for the Σ_{ij} yield surface, when linearity (eqn. 2.28) applies.

Equation 2.28 applies to one class of velocity fields used later on. A second class, to which it does not apply, is of the form

$$\dot{u}_{i} = \dot{u}_{i}\left(\underset{\sim}{\dot{E}}, \Psi, f, \underset{\sim}{X}\right) \qquad (2.30)$$

where $\dot{u}_{i}$ (and thus $\dot{\epsilon}_{ij}$ and $\dot{W}$) is homogeneous and linear in the $\dot{E}_{ij}$ for a fixed value of ψ. ψ is an additional parameter which is dependent on $\dot{E}$ and f (see eqn. 2.21), and has the effect of making $\dot{u}_{i}$ homogeneous of degree one, but no longer linear, in the $\dot{E}_{ij}$. The approximate dissipation thus has the form

$$\dot{W} = \dot{W}\left(\underset{\sim}{\dot{E}}, \Psi(\underset{\sim}{\dot{E}}, f), f\right) \qquad (2.31)$$

Equation 2.25 gives

$$\Sigma_{ij} = \left.\frac{\partial \dot{W}}{\partial \dot{E}_{ij}}\right|_{\psi = \text{const.}} + \left.\frac{\partial \dot{W}}{\partial \psi}\right|_{\dot{E} = \text{const.}} \left.\frac{\partial \psi}{\partial \dot{E}_{ij}}\right| \qquad (a) \qquad (2.32)$$

As discussed for eqns. 2.21 and 2.22, $\psi(\dot{E},f)$ is determined by minimizing $\dot{W}$ with respect to ψ, so

$$\frac{\partial \dot{W}}{\partial \psi} = 0 \qquad (b) \qquad (2.32)$$

Since Σ_{ij} as given above is a work conjugate of $\dot{E}_{ij}$, normality is proven as in eqn. 2.19.

Unfortunately, the dependence of ψ on $\dot{E}$ makes it impossible to prove convexity as in eqn. 2.29. Convexity can be used, however, to help judge the value of the approximate yield surfaces generated with this formulation. Since the object is to approximate the yield and flow behavior of a real material (with a convex yield surface), an approximation which violates convexity should be considered a bad approximation.

To prove that the approximate yield locus lies outside the actual yield locus in stress space, write the principle of maximum plastic work in the following form:

$$\frac{1}{V}\int_V \left(s_{ij}(\dot{\epsilon}) - s^A_{ij}\right)\dot{\epsilon}_{ij}\, dV \geq 0 , \qquad (2.33)$$

where s^A_{ij} is $s_{ij}(\dot{\epsilon}^A_{ij})$, and both $\dot{\epsilon}_{ij}$ and $\dot{\epsilon}^A_{ij}$ are compatible with the same macroscopic rate of deformation $\dot{E}_{ij}$. Using eqn. 2.5, the principle of

virtual work, and the result that Σ_{ij} and Σ^A_{ij} are work conjugates to $\dot{E}_{ij}$, eqn. 2.33 becomes

$$\left(\Sigma_{ij} - \Sigma^A_{ij}\right)\dot{E}_{ij} \geq 0 \tag{2.34}$$

Since $\dot{E}_{ij}$ is an outward normal to both the Σ_{ij} and Σ^A_{ij} yield loci, this shows that the surface always lies on or outside the Σ^A_{ij} surface.

For the porous material described here, it has been shown that the actual yield locus has the properties of normality and convexity if they are present in the matrix. The most important properties established for the approximate macroscopic yield stress Σ_{ij} are its upper bound relation to Σ^A_{ij}, the convexity and normality properties of its yield surface (given the conditions described above), and the equation relating it to $\dot{E}_{ij}$:

$$\Sigma_{ij} = \frac{1}{V}\int_V S_{kl}(\dot{\underset{\sim}{\epsilon}})\,\frac{\partial \dot{\epsilon}_{kl}}{\partial \dot{E}_{ij}}\,dV \tag{2.25}$$

A subsequent section of this paper is devoted to the solution of eqn. 2.25 for various void volume fractions and the two void geometries discussed earlier. Varying the $\dot{E}_{ij}$ field results in the generation of an approximate yield surface for a particular void geometry and volume fraction.

3. General Theory - Expansion Technique

The purpose of this section is the development of a method for rigorously expanding solutions of Σ for a given E and f to obtain Σ for E and $f + \Delta f$, where $\Delta f << 1$. When f approaches zero, this allows comparison of solutions by other authors for the isolated void in an infinite rigid-perfectly plastic body with results for small (but finite) f obtained via eqn. 2.25. Since no approximations to void spacing are made for the isolated void in an infinite body, the comparison allows some judgement of the effects of the void spacing approximation evident in Figs. 1, 2, and 3. (The comparisons are made in sections 5 and 6.) Under certain restrictions on the form of the flow field the expansion technique allows the calculation of Σ for E and a range of f with much less numerical work then with the previous method. The expansion method also offers some insight into how the actual stress boundary conditions on the void surface (zero traction) should affect the flow field.

Consider this general form for the approximate dissipation (as in eqns. 2.25 and 2.31).

$$\dot{W} = \dot{W}\left(\dot{\underline{E}}, f\right) \tag{3.1}$$

$\dot{W}$ is completely determined by $\dot{E}$ and f. Define the following quantities:

$$\Sigma_{ij} = \frac{\partial \dot{W}}{\partial \dot{E}_{ij}} \quad (a), \qquad \dot{w} = -\frac{\partial \dot{W}}{\partial f} \tag{3.2}$$

where Σ_{ij} is the same as in eqn. 2.25, and $-\dot{w}$ is the change in $\dot{W}$ with f for a fixed $\dot{E}$ field. This gives

$$d\dot{W} = \Sigma_{ij}\, d\dot{E}_{ij} - \dot{w}\, df \tag{3.3}$$

It is intended to relate Σ_{ij} and f through a Maxwell (reciprocal) relation. This is simplest when f is not allowed to be zero, so the aggregate is not incompressible and the $\dot{E}_{ij}$ are six independent quantities. Equations 3.2 and 3.3 then give

$$\frac{\partial \Sigma_{ij}}{\partial f} = \frac{\partial^2 \dot{W}}{\partial f \, \partial \dot{E}_{ij}} = \frac{-\partial \dot{w}}{\partial \dot{E}_{ij}} \tag{3.4}$$

Development of a Maxwell relation is made more difficult when the possibility of $f = 0$ (and thus $\dot{E}_{kk} = 0$) is included, since the six components of E are no longer independently variable. The new function $\dot{V}$, derived below, resolves this problem. Rewrite eqn. 3.3 in terms of deviatoric and hydrostatic components of Σ and $\dot{E}$

$$d\dot{W} = \Sigma'_{ij} \, d\dot{E}'_{ij} + \tfrac{1}{3} \Sigma_{kk} \, d\dot{E}_{\ell\ell} - \dot{w} \, df \,, \tag{3.5}$$

where Σ' and E' are deviatoric quantities. Define $\dot{V}$ as follows:

$$\dot{V} = \dot{V}\left(\underset{\sim}{\dot{E}}', \Sigma_{kk}, f\right) = \dot{W} - \tfrac{1}{3} \Sigma_{kk} \dot{E}_{\ell\ell} \,, \tag{3.6}$$

where only five of the E'_{ij} are independent, the sixth defined from $E'_{kk} = 0$. Then,

$$d\dot{V} = \Sigma'_{ij} \, d\dot{E}'_{ij} - \tfrac{1}{3} \dot{E}_{\ell\ell} \, d\Sigma_{kk} - \dot{w} \, df \tag{3.7}$$

Since variations in dE'_{ij} are constrained by

$$\delta_{ij} \, d\dot{E}'_{ij} = 0 \,, \tag{3.8}$$

the coefficient of dE'_{ij} in the expression for $d\dot{V}$ can only be determined to within a hydrostatic part when $\dot{V}$ is given. This is, however, immaterial since the hydrostatic part of Σ' is zero. Hence, one may write

$$\Sigma'_{ij} = \frac{\partial \dot{V}}{\partial \dot{E}'_{ij}} \quad , \tag{3.9}$$

the partial derivative notation being understood in recognition of the constraint. Also, $\dot{w}$ can be re-expressed as

$$\dot{w} = -\frac{\partial \dot{W}}{\partial f} = -\frac{\partial \dot{V}}{\partial f} \quad , \tag{3.10}$$

and therefore,

$$\frac{\partial \Sigma'_{ij}}{\partial f} = \frac{\partial^2 V}{\partial f \, \partial \dot{E}'_{ij}} = \frac{-\partial \dot{w}}{\partial \dot{E}'_{ij}} \tag{3.11}$$

Another reciprocal relation which results from eqn. 3.7 is

$$\frac{1}{3}\frac{\partial \dot{E}_{kk}}{\partial f} = \frac{-\partial^2 V}{\partial f \, \partial \Sigma_{kk}} = \frac{\partial \dot{w}}{\partial \Sigma_{kk}} \tag{3.12}$$

The general extrapolation procedure is, given $\Sigma_{ij}(\dot{\underset{\sim}{E}}, f)$:

from eqn. 3.4,

$$\Sigma_{ij}(\dot{\underset{\sim}{E}}, f+\Delta f) = \Sigma_{ij}(\dot{\underset{\sim}{E}}, f) - \frac{\partial \dot{w}(\dot{\underset{\sim}{E}}, f)}{\partial \dot{E}_{ij}} \Delta f \, , \quad (a)$$

from eqn. 3.11 (3.13)

$$\Sigma'_{ij}(\dot{\underset{\sim}{E}}', \Sigma_{kk}, f+\Delta f) = \Sigma'_{ij}(\dot{\underset{\sim}{E}}' \Sigma_{kk}, f) - \frac{\partial \dot{w}(\dot{\underset{\sim}{E}}', \Sigma_{kk}, f)}{\partial \dot{E}'_{ij}} \Delta f \quad (b)$$

rigorous to first order in Δf. Given $\dot{E}_{kk}(\dot{E}', \Sigma_{\ell\ell}, f)$, eqn. 3.12 yields

$$\frac{1}{3}\dot{E}_{kk}\left(\underset{\sim}{\dot{E}}', \Sigma_{kk}, f + \Delta f\right) =$$

$$\frac{1}{3}\dot{E}_{kk}\left(\underset{\sim}{\dot{E}}', \Sigma_{kk}, f\right) + \frac{\partial \dot{W}\left(\underset{\sim}{\dot{E}}', \Sigma_{kk}, f\right)}{\partial \Sigma_{kk}} \Delta f \qquad (3.14)$$

again, rigorous to first order in Δf. "Rigor to first order in Δf" as used here is analogous to "within errors due to numerical integration" for eqn. 2.25. Note that because the relationship of Σ to $\dot{W}$ is the same in eqns. 3.2 and 2.25, the Σ_{ij} calculated by the expansion procedure are also upper bound stresses to first order in Δf.

Eqns. 3.13b and 3.14 can be used to extrapolate solutions for $f = 0$ into the domain of nonzero f. References 36 and 37 give results which enable the calculation of $\dot{W}$ as a function of $\dot{E}$ and the remote uniform stress field for an isolated void in an infinite body (which is $\Sigma_{ij}(\dot{E},0)$). Then,

$$\Sigma'_{ij}\left(\underset{\sim}{\dot{E}}, \Sigma_{kk}, f\right) = \Sigma'_{ij}\left(\underset{\sim}{\dot{E}}', \Sigma_{kk}, 0\right) - \frac{\partial \dot{W}\left(\underset{\sim}{\dot{E}}', \Sigma_{kk}, 0\right)}{\partial \dot{E}'_{ij}} f \qquad (a)$$

(3.16)

$$\frac{1}{3}\dot{E}_{kk}\left(\underset{\sim}{\dot{E}}', \Sigma_{kk}, f\right) = \frac{1}{3}\dot{E}_{kk}\left(\underset{\sim}{\dot{E}}', \Sigma_{kk}, 0\right) + \frac{\partial \dot{W}\left(\underset{\sim}{\dot{E}}', \Sigma_{kk}, 0\right)}{\partial \Sigma_{kk}} f \qquad (b)$$

to first order in f.

The term $\dot{W}$ will now be examined in greater detail. From eqns. 3.2b and 2.5;

$$\dot{w} = -\frac{\partial \dot{W}}{\partial f} = -\frac{\partial}{\partial f}\left[\frac{1}{V}\int_V s_{ij}(\underset{\sim}{\dot{\epsilon}})\,\dot{\epsilon}_{ij}\,dV\right] \qquad (3.17)$$

Using Leibnitz's rule and normality of $s_{ij}(\dot{\epsilon})$;

$$\dot{w} = \frac{1}{V}\int_{S_v} s_{ij}(\underset{\sim}{\epsilon})\,\dot{\epsilon}_{ij}\,dS_v \;-\; \frac{1}{V}\int_{V} s_{ij}(\underset{\sim}{\epsilon})\,\frac{\partial \dot{\epsilon}_{ij}}{\partial f}\,dV \qquad (3.18)$$

where S_v is the surface of the void. Only when the volume integral above is small with respect to the surface integral can $\dot{w}$, and thus $\partial\dot{w}/\partial\dot{E}_{ij}$, be accurately approximated by the surface integral alone (and numerical work greatly reduced).

Consider the case where $\dot{\epsilon}_{ij}$ is the actual macroscopic strain rate field. Using incompressibility, the volume integral in eqn. 3.18 becomes

$$\frac{1}{V}\int_{V} \sigma_{ij}^{A}\,\frac{\partial \dot{\epsilon}_{ij}^{A}}{\partial f}\,dV \;.$$

A proof analogous to that for the principle of virtual work gives

$$\frac{1}{V}\int_{V} \sigma_{ij}^{A}\,\frac{\partial \dot{\epsilon}_{ij}^{A}}{\partial f}\,dV \;=\; \frac{1}{V}\int_{S+S_v} T_i^{A}\,\frac{\partial \dot{u}_i^{A}}{\partial f}\,dS \qquad (3.19)$$

where $S + S_v$ is both the outer surface of the body and the void surface. For velocity fields whose behavior on S is independent of f (as in eqn. 2.14), the volume integral becomes

$$\frac{1}{V}\int_{V} \sigma_{ij}^{A}\,\frac{\partial \dot{\epsilon}_{ij}^{A}}{\partial f}\,dV \;=\; \frac{1}{V}\int_{S_v} T_i^{A}\,\frac{\partial \dot{u}_i^{A}}{\partial f}\,dV, \;=\; 0, \qquad (3.20)$$

since the void surface is traction-free.

The condition of a relatively small volume integral is satisfied automatically for the actual velocity field. This says nothing about the use of an

approximate velocity field, since the related microscopic stress field has no relationship to equilibrium. Another way of satisfying the condition is to choose a special form of $\dot{u}_i(\dot{E},f,x)$ such that the volume integral remains small. This form can simply be independent of f, or undetermined to the extent that the condition of smallness on the volume integral can be used to completely determine $\dot{u}_i$. In any case, it should be emphasized that the volume integral of eqn. 3.18 being zero is a necessary, but by no means sufficient condition for $\dot{\epsilon}_{ij}$ to be $\dot{\epsilon}^A_{ij}$.

4. Approximate Velocity Fields and Geometries - General Comments

The approximations made to the void and matrix geometry of the unit cube (Figs. 2 and 3) make possible the construction of approximate velocity fields. In order to meet the requirements of the upper bound method, these velocity fields in the matrix must be kinematically admissible (obey compatibility, and the displacement b.c. on the outer surface - eqn. 2.2 or 2.14), and be incompressible (in keeping with the von Mises assumption). The general velocity field is constructed as a sum of a finite number of incompressible fields, each multiplied by an undetermined macroscopic factor. There must be at least enough terms present so that a solution can be found which meets the displacement b.c.. Any extra terms indicate a more refined velocity field. The extra macroscopic factors are determined as follows:

It seems reasonable to make the $\dot{\varepsilon}_{ij}$ field resemble the $\dot{\varepsilon}^{A}_{ij}$ field as closely as possible. One such opportunity is presented by the knowledge that the actual shear stresses on the void surface, and thus the corresponding shear components of $\dot{\varepsilon}^{A}_{ij}$ (eqn. 2.1b) on the void surface are zero. By analogy, setting the corresponding components of $\dot{\varepsilon}_{ij}$ to zero seems reasonable, and helps solve for any remaining macroscopic factors. No such opportunity is presented by the zero normal stress condition on the void surface, because the von Mises flow rule is in terms of deviatoric stresses only. It has been found, as expected, that this process results in a lower approximate dissipation for a given $\dot{E}$ than if the extra terms were just discarded, indicating a better guess at $\dot{u}_i$.

Another method of determing unknown macroscopic factors is to treat them as variables, and solve for their values which minimize $\dot{W}$ for a given $\dot{E}$. This will give the least upper bound on $\dot{W}$ within the limits of the velocity field approximation.

Two basic types of velocity fields are considered. The simplest is the type where all of the matrix material is undergoing plastic flow, and the velocity boundary conditions are as shown in eqn. 2.14 (pointwise surface velocities uniquely determined by $\dot{E}_{ij}$ to within a rigid body motion). This type of flow field is subjected to both of the refinement procedures discussed above. Another type of field, suggested by some finite element studies [41,42], allows part of the matrix to remain rigid. This velocity field is related to $\underset{\sim}{\dot{E}}$ through eqn. 2.2, the averaged boundary condition. The model employs an idealized rigid-plastic boundary (Fig. 4); a radial plane for the cylinder and a centered circular cone for the sphere. Because of the symmetries involved, this model is limited to axially symmetric deformation in the spherical case, and zero shear along the axis in the cylindrical case. Equation 2.30 describes the velocity field, with ψ being the angle between the rigid-plastic boundary and the axis of symmetry. ψ_{opt} is determined as in equation 2.33. Similarly, a choice is made between the yield loci generated by the two types of flow fields on the basis of which gives the lower value of dissipation for a given $\underset{\sim}{\dot{E}}$.

It is necessary to discuss how the geometric approximations evident in Figs. 1,2, and 3 affect the analysis. The cylindrical model is intended to represent the behavior of an aggregate with voids randomly shaped and dispersed in the transverse directions, but elongated along the axis. The spherical model approximates an aggregate with voids randomly shaped and dispersed in all three directions.

The upper bound result (eqn. 2.34) requires that $\underset{\sim}{\Sigma}^A$ and $\underset{\sim}{\Sigma}$ be computed from the same geometry. When this is the random geometry, for which the non-correlation criteria and boundary conditions of the type eqn. 2.2 are used,

the following assumption must be made: The $\underset{\sim}{\Sigma}$ field behavior of the approximate (cylindrical or spherical) model must resemble that of the random model closely enough so that $\underset{\sim}{\Sigma}$ computed from the approximate model is an upper bound to $\underset{\sim}{\Sigma}^A$ of the random model:

$$\left[\Sigma_{ij}\Big|_{\substack{approx.\\model}} - \Sigma^A_{ij}\Big|_{\substack{random\\model}}\right]\dot{E}_{ij} \geq 0 \qquad (4.1)$$

Another approach is to agree that eqn. 2.34 holds when both $\underset{\sim}{\Sigma}^A$ and $\underset{\sim}{\Sigma}$ are computed from the approximate geometries. The symmetries of these geometries imply violation of the non-correlation criteria, so this approach is limited to cases where boundary conditions as in eqns. 2.13 and 2.14 apply. Then, it must be assumed (as before) that the approximate model behaves enough like the random model so that eqn. 4.1 is valid.

In both cases, a valid extrapolation between the unit cube (random geometry) and the approximate (cylinder, sphere) geometries must be assumed.

5a. Long Circular Cylindrical Voids - Fully Plastic Flow

This void geometry is meant to represent one limit of random void shape. Long, roughly cylindrical voids are seen to appear at the necks of tensile bars after large deformation (see, for example, ref. 26). They would also result from long cylindrical inclusions which decohere from the matrix after straining, or, on a larger scale, from drilled holes in a homogeneous material. The centered and geometrically similar matrix displays the transverse isotropy expected of an isotropic material with a void distribution which is random in the transverse directions.

For the fully plastic case, the velocity b.c. will be related to E through eqn. 2.14. The velocity field will be broken up into four separate parts which should, when combined in various proportions, satisfy any set of velocity boundary conditions. These parts are 1) plane strain ($E_{i3} = \epsilon_{i3} = 0$, $i = 1,3$) with no dilatation, 2) uniform deformation in the axial direction, 3) shearing normal to the axial direction, and 4) general dilatation. Rice and Tracey [37] employ a similar technique in their treatment of a spherical cavity in an infinite matrix, splitting their strain field into parts due to macroscopic shape change and volume change.

Only the axially symmetric parts of the flow field can be determined completely from incompressibility and symmetry. For the other parts, the general solution to an analogous viscous problem is used to guess some reasonable solutions to use in the manner outlined in section 4. The viscous problem is solvable analytically because the constitutive laws give a linear relationship between stress and strain rate. As is necessary, all the solutions obey incompressibility. The solutions are general enough to satisfy the velocity b.c. on the outer surface, the zero shear strain rate condition on the inner surface

and to allow the dissipation to be further minimized. The cases where the two latter conditions are enforced and ignored will be carried along simultaneously.

Since the cylindrical model is transversely isotropic, it is convenient to work in terms of the following set of axes. The (3) axis is along the axis of the cylinder, and the (1) and (2) axes are in the transverse plane, and rotated such that $\dot{E}_{12} = 0$. This direction can always be found, and its angle β from the initial axes is given by

$$\tan(2\beta) = \frac{2\dot{E}_{12}}{(\dot{E}_{11}-\dot{E}_{22})} \tag{5.1}$$

For plane strain with no dilatation, the viscous problem is solved as follows. An angular dependence of relevant quantities is assumed, with barred quantities dependent only on r :

$$\begin{aligned}
\sigma_{rr} &= \bar{\sigma}_{rr}\cos(2\theta) \\
\sigma_{\theta\theta} &= \bar{\sigma}_{\theta\theta}\cos(2\theta) \\
\sigma_{r\theta} &= \bar{\sigma}_{r\theta}\sin(2\theta)
\end{aligned} \tag{5.2}$$

$$\begin{aligned}
v_r &= \bar{v}_r\cos(2\theta) \\
v_\theta &= \bar{v}_\theta\sin(2\theta)
\end{aligned}$$

where v_i and $\dot{u}_i$ are unterchangeable. An example with this type of angular dependence for a similar elastic problem (circular hole in a plate) can be found in ref. [46].

There are five equations in the five barred quantities in eqn. 5.2; two equilibrium, one incompressibility, and two constitutive. These are

$$\frac{d\bar{\sigma}_{rr}}{dr} + \frac{(\bar{\sigma}_{rr} - \bar{\sigma}_{\theta\theta})}{r} + \frac{2\bar{\sigma}_{r\theta}}{r} = 0$$

$$\frac{d\bar{\sigma}_{r\theta}}{dr} + \frac{2\bar{\sigma}_{r\theta}}{r} - \frac{2\bar{\sigma}_{\theta\theta}}{r} = 0$$

$$\frac{d\bar{v}_r}{dr} + \frac{2\bar{v}_\theta}{r} + \frac{\bar{v}_r}{r} = 0$$

$$(\bar{\sigma}_{\theta\theta} - \bar{\sigma}_{rr}) = 2G\left[\frac{2\bar{v}_\theta}{r} + \frac{\bar{v}}{r} - \frac{d\bar{v}_r}{dr}\right] \qquad (5.3)$$

$$\bar{\sigma}_{r\theta} = G\left[\frac{-2\bar{v}_r}{r} - \frac{\bar{v}_\theta}{r} + \frac{d\bar{v}_\theta}{dr}\right]$$

where G is the shear modulus. These equations are manipulated to eliminate the stresses, leaving the following;

$$\bar{v}_\theta = -\frac{1}{2}\left[r\,\bar{v}_{r,r} + \bar{v}_r\right] \qquad (a)$$

$$r^4\bar{v}_r^{(4)} + 6r^3\bar{v}_r^{(3)} - 3r^2\bar{v}_r^{(2)} - 9\bar{v}_r^{(1)} + 9\bar{v}_r = 0 \qquad (b) \qquad (5.4)$$

where superscript (n) denotes differentiation of order n in r. Equation 5.4b has the general solution

$$\bar{V}_r = C_1 r^3 + C_2 r + C_3 r^{-1} + C_4 r^{-3} \qquad (5.5)$$

$$C_i = \text{constants}$$

which gives

$$\bar{V}_\theta = -2C_1 r^3 - C_2 r + C_4 r^{-3} \qquad (5.6)$$

The resulting strain rate field is

$$\begin{aligned} \dot{\epsilon}_{rr} &= \bar{\dot{\epsilon}}_{rr} \cos(2\theta) \\ \dot{\epsilon}_{\theta\theta} &= \bar{\dot{\epsilon}}_{\theta\theta} \cos(2\theta) \\ \dot{\epsilon}_{r\theta} &= \bar{\dot{\epsilon}}_{r\theta} \sin(2\theta) \end{aligned} \qquad (5.7)$$

where

$$\begin{aligned} \bar{\dot{\epsilon}}_{rr} &= 3C_1 r^2 + C_2 - C_3 r^{-2} - 3C_4 r^{-4} \\ \bar{\dot{\epsilon}}_{\theta\theta} &= -\bar{\dot{\epsilon}}_{rr} \\ \bar{\dot{\epsilon}}_{r\theta} &= -\left[3C_1 r^2 + C_2 + C_3 r^{-2} + 3C_4 r^{-4}\right] \end{aligned} \qquad (5.8)$$

It should be emphasized that eqns. 5.5 to 5.8 are only reasonable guesses at the velocity and strain rate fields for the rigid-plastic case, gleaned from the solution to a different problem. Any compatible and incompressible velocity

field would be permissible. It is felt that eqns. 5.8 are general enough to give a good approximation to the true strain rate field when properly optimized.

Uniform axial deformation involves no shear components on the void surface. Here, microscopic and macroscopic strain rates are equal:

$$\dot{\epsilon}_{33} = \dot{E}_{33} \tag{5.9}$$

Shearing with components in the axial (3) direction is related to the macroscopic strain rates $\dot{E}_{13}$ and $\dot{E}_{23}$. The flow field approximation is constructed with a viscous analog, in a manner similar to that used previously for plane strain with zero dilatation. Consider the components $\dot{E}_{13}$ and $\dot{E}_{23}$. It is easily shown that a rotation θ around the (3) axis results in

$$\dot{E}^{\star}_{13} = 0$$

$$\dot{E}^{\star}_{23} = \dot{E}_{23}(max.) = -\sin(\theta^{\star})\dot{E}_{13} + \cos(\theta^{\star})\dot{E}_{23} \tag{5.10}$$

$$at \quad \tan(\theta^{\star}) = -\frac{\dot{E}_{13}}{\dot{E}_{23}}$$

As before, the analysis can proceed more simply from a special set of axes which can always be found (i.e., where $\dot{E}^{\star}_{13} = 0$), with no loss of generality.

Where γ is the polar angle measured from the $2^{\star}$ axis, the assumed velocity field can be written

$$V_{\bar{z}} = \bar{V}_{\bar{z}}(r)\cos(\gamma), \quad V_r = \bar{V}_r(r)\,2\cos(\gamma), \tag{5.11}$$

$$V_{\alpha} = -\bar{V}_r(r)\,2\sin(\gamma)$$

The following equations for the analogous viscous problem (equilibrium, constitutive relations) lead to forms for $\bar{v}_z$ and $\bar{v}_r$:

$$\sigma_{rz,r} + \frac{1}{r}\sigma_{rz,\theta} + \sigma_{zz,z} + \frac{1}{r}\sigma_{rz} = 0 \qquad (a)$$

$$\sigma_{rz} = 2G\epsilon_{rz}, \quad \sigma_{\theta z} = 2G\epsilon_{\theta z}, \quad \sigma_{zz} = 0 \qquad (b) \qquad (5.12)$$

$$\epsilon_{rz} = \frac{1}{2}\left(v_{z,r} + v_{r,z}\right), \quad \epsilon_{\theta z} = \frac{1}{2}\left(v_{\theta,z} + \frac{1}{r}v_{z,\theta}\right) \qquad (c)$$

When combined with eqns. 5.11 and 5.12b and c, eqn. 5.12a becomes

$$\bar{v}_{z,rr} + \frac{1}{r}\bar{v}_{z,r} - \frac{1}{r^2}\bar{v}_z + \bar{v}_{r,r} = 0 \qquad (5.13)$$

Since $\bar{v}_r$ and $\bar{v}_z$ are independent quantities, they go to zero separately. The general solution is then

$$\bar{v}_r = \text{constant} \equiv V_{32}$$

$$\bar{v}_z = C_5 r + C_6 r^{-1}$$

C_5 and C_6 constant w.r.t. geometry (5.14)

$$\dot{\epsilon}_{rz} = \frac{1}{2}\left[C_5 - C_6 r^{-2} + V_{32}\right]\cos(\gamma)$$

$$\dot{\epsilon}_{\theta z} = -\frac{1}{2}\left[C_5 + C_6 r^{-2} + V_{32}\right]\sin(\gamma)$$

V_{32} is simply the shearing velocity per unit axial length on the (3) plane. The contribution to $\dot{\epsilon}_{r\gamma}$ is

$$\dot{\epsilon}_{r\gamma} = \frac{1}{2}\left(\frac{1}{r}V_{r,\gamma} + V_{\gamma,r} - \frac{1}{r}V_{\gamma}\right) \tag{5.15}$$

$$= \frac{1}{2}V_{32}z\left(-\frac{1}{r}\sin(\gamma) + 0 + \frac{1}{r}\sin(\gamma)\right) = 0$$

The velocity field due to pure dilatation is derived from three-dimensional incompressibility with no angular dependence, and is independent of constitutive laws. Using eqn. 5.9;

$$\dot{\epsilon}_{kk} = 0 = \frac{dV_r^D}{dr} + \frac{V_r^D}{r} + \dot{E}_{zz} = 0, \tag{5.16}$$

where the superscript D refers to "dilatational". The solution is

$$V_r^D = \frac{C_7}{r} - \dot{E}_{zz}\frac{r}{2}, \qquad V_\theta^D = 0$$

$$\dot{\epsilon}_{rr}^D = -C_7 r^{-2} - \frac{1}{2}\dot{E}_{zz} \tag{5.17}$$

$$\dot{\epsilon}_{\theta\theta}^D = +C_7 r^{-2} - \frac{1}{2}\dot{E}_{zz}$$

C_7 is constant w.r.t. geometry

The general form of the velocity and strain rate fields results from combining eqns. 5.5 through 5.17:

$$V_r = \left(C_1 r^3 + C_2 r + C_3 r^{-1} + C_4 r^{-3}\right)\cos(2\theta) + C_7 r^{-1} - \frac{1}{2}\dot{E}_{zz} r + V_{32} z \cos(\gamma) \quad (a) \qquad (5.18)$$

$$V_\theta = \left(-2C_1 r^3 - C_2 r + C_4 r^{-3}\right)\sin(2\theta) - V_{32} z \sin(\gamma) \quad (b)$$

$$V_z = \left(C_5 r + C_6 r^{-1}\right)\cos(\gamma) + \dot{E}_{zz} z \quad (c)$$

$$\dot{\epsilon}_{rr} = \left(3C_1 r^2 + C_2 - C_3 r^{-2} - 3C_4 r^{-4}\right)\cos(2\theta) - C_7 r^{-2} - \frac{1}{2}\dot{E}_{zz} \quad (a)$$

$$\dot{\epsilon}_{\theta\theta} = \left(-3C_1 r^2 - C_2 + C_3 r^{-2} + 3C_4 r^{-4}\right)\cos(2\theta) + C_7 r^{-2} - \frac{1}{2}\dot{E}_{zz} \quad (b)$$

$$\dot{\epsilon}_{zz} = \dot{E}_{zz} \quad (c) \qquad (5.19)$$

$$\dot{\epsilon}_{r\theta} = -\left(3C_1 r^2 + C_2 + C_3 r^{-2} + 3C_4 r^{-4}\right)\sin(2\theta) \quad (d)$$

$$\dot{\epsilon}_{rz} = \frac{1}{2}\left(C_5 - C_6 r^{-2} + V_{32}\right)\cos(\gamma) \quad (e)$$

$$\dot{\epsilon}_{\theta z} = -\frac{1}{2}\left(C_5 + C_6 r^{-2} + V_{32}\right)\sin(\gamma) \quad (f)$$

In applying the external boundary conditions (at r=b, see fig. 2), it is to be understood that the angle θ is measured from the (2) axis where $\dot{E}_{12} = 0$ and $\dot{E}_{22} > \dot{E}_{11}$, and the angle γ is measured from the (2*) axis where $\dot{E}_{13} = 0$. A new quantity whose meaning will become apparent is V_{23}, a normalized shear velocity parallel to the (3) axis and in the same spirit as V_{32} (see eqn. 5.14). Some new macroscopic quantities which will be useful are

$$\dot{E}' \equiv \frac{1}{2}\left(\dot{E}_{22} - \dot{E}_{11}\right)$$

$$\dot{E} \equiv \frac{1}{2}\dot{E}_{kk} \equiv \frac{1}{2}\left(\dot{E}_{11} + \dot{E}_{22} + \dot{E}_{33}\right) \tag{5.20}$$

$$\dot{E}_{23} = \dot{E}_{32} \equiv \frac{1}{2}\left(V_{23} + V_{32}\right)$$

repeated Latin indices meaning sum over 1,2,3.

The velocity field on the outer surface is, in terms of the macroscopic quantities;

$$V_r = \dot{E}' b \cdot \cos(2\theta) + \frac{1}{2}\left(\dot{E}_{22} + \dot{E}_{11}\right) \cdot b + V_{32} \cdot z \cdot \cos(\gamma)$$

$$V_z = V_{23}\, b \cos(\gamma) + \dot{E}_{zz} \cdot z \tag{5.21}$$

$$V_\theta = -\dot{E}' b \cdot \sin(2\theta) - V_{32} \sin(\gamma)$$

The condition of zero shear stress-zero shear strain rate on the void surface is

$$\dot{\epsilon}_{r\theta}\Big|_{r=a} = \dot{\epsilon}_{rz}\Big|_{r=a} = 0 \tag{5.22}$$

Equations 5.18 and 5.21 give

$$C_1 b^2 + C_2 + C_3 b^{-2} + C_4 b^{-4} = E'$$

$$C_7 b^{-1} - \frac{1}{2}\dot{E}_{zz} b = \frac{1}{2}\left(\dot{E}_{11} + \dot{E}_{22}\right), \quad C_7 = E b^2 \qquad (5.23)$$

$$C_5 + C_6 b^{-2} = V_{23}$$

Equations 5.19 and 5.22 give

$$3C_1 a^2 + C_2 + C_3 a^{-2} + 3C_4 a^{-4} = 0$$

$$C_5 - C_6 a^{-2} + V_{32} = 0 \qquad (5.24)$$

C_5 and C_6 are now determined uniquely. Using the following;

$$f = \frac{a^2}{b^2}, \qquad \lambda \equiv \frac{r^2}{b^2} \qquad (5.25)$$

these are

$$C_5 = \frac{V_{23} - f V_{32}}{(1+f)}, \quad C_6 = \frac{a^2\left(V_{23} + V_{32}\right)}{(1+f)} \qquad (5.26)$$

Equations 5.19e and f now become

$$\dot{\epsilon}_{rz} = \frac{\left(1 - f/\lambda\right)}{(1+f)} \dot{E}^{*}_{23} \cos(\gamma), \equiv \bar{\dot{\epsilon}}_{rz} \cos(\gamma)$$

$$\dot{\epsilon}_{\theta z} = -\frac{\left(1 + f/\lambda\right)}{(1+f)} \dot{E}^{*}_{23} \sin(\gamma), \equiv \bar{\dot{\epsilon}}_{\theta z} \sin(\gamma) \qquad (5.27)$$

Equations 5.23a and 5.24a are two equations in the four unknowns C_1 through C_4. The procedure adopted here is to set $C_1 = 0$, and solve for C_3 and C_4 in terms of C_2 and the known macroscopic quantities. C_2 is then determined numerically as the value which minimizes the dissipation, and is thus considered a function of E' and f (as suggested by eqn. 5.23 and born out by numerical calculations). The reason for assuming a value for C_1 is simply that the numerical minimization problem is much more complex and time consuming for two variables than for one. The value zero was chosen because; 1) C_1 goes to zero for small f in the previously cited elastic example [46], and 2) it is felt that for this type of problem the velocity field should approach linearity in r for $r >> a$, and only the $C_1 r^3$ term violates this for nonzero C_1. Therefore, discarding the term seems to be reasonable, especially coupled with the minimization with respect to C_2.

Solving eqns. 5.23a and 5.24a for C_3 and C_4 (with $C_1=0$) gives

$$C_3 = \frac{b^2}{(3-f)}\left[3E' - (3-f^2)C_2\right]$$

$$C_4 = \frac{a^2 b^2}{(3-f)}\left[C_2(1-f) - E'\right] \qquad (5.28)$$

Equations 5.19a, b, and d can be written more compactly when the coefficients of the trigonometric functions are written as single terms. Using this, and eqns. 5.23b and 5.25, they become

$$\dot{\epsilon}_{rr} = \bar{\dot{E}}_{rr}\cos(2\theta) - E\lambda^{-1} - \frac{1}{2}\dot{E}_{zz}$$

$$\dot{\epsilon}_{\theta\theta} = -\bar{\dot{E}}_{rr}\cos(2\theta) + E\lambda^{-1} - \frac{1}{2}\dot{E}_{zz} \qquad (5.29)$$

$$\dot{\epsilon}_{r\theta} = \bar{\dot{E}}_{r\theta}\sin(2\theta)$$

Adopting the form

$$C_2 = C_2'(f)\, E' \tag{5.30}$$

and defining

$$A = \frac{\lambda(3-f^2) - 3f(1-f)}{\lambda^2(3-f)} \tag{5.31}$$

it can be shown that

$$\bar{\dot{\epsilon}}_{rr} = \dot{E}'\left[C_2'(1+A) - \frac{3(\lambda-f)}{\lambda^2(3-f)}\right] \qquad (a)$$

$$\bar{\dot{\epsilon}}_{r\theta} = -\dot{E}'\left[C_2'(1-A) + \frac{3(\lambda-f)}{\lambda^2(3-f)}\right] \qquad (b) \tag{5.32}$$

The numerical minimization of $\dot{W}$ with respect to C_2' resulted in the following empirical form (an approximation to a finite number of data points), which is accurate for $0 \leq f \leq 0.5$:

$$C_2'(f) \sim 1 - f - 0.27\left(1 - \exp(-18.5 \cdot f)\right) \qquad (a)$$

For very small f (≤ 0.01) (5.33)

$$C_2'(f) \sim 1 - 6f \qquad (b)$$

is sufficient.

Equations 5.27 through 5.33 result from meeting both shear strain rate b.c. on the void surface, displacement b.c. on the outer surface, and minimization wrt C_2'. It is useful to consider the simpler form which results when the

strain rate b.c. are ignored, and dependence of $\bar{\dot{\varepsilon}}_{rr}$, $\bar{\dot{\varepsilon}}_{r\theta}$, $\bar{\dot{\varepsilon}}_{rz}$, and $\bar{\dot{\varepsilon}}_{\theta z}$ on λ is eliminated. This is equivalent to assuming that the portion of the velocity field related to macroscopic shearing is independent of f, and equal to the homogeneous results for $f = 0$. The only effect of void volume fraction on the nondilatational velocity field is then the removal of material whose straining would contribute to the macroscopic dissipation. The result is

$$\bar{\dot{\varepsilon}}_{rr} = \dot{E}', \quad \bar{\dot{\varepsilon}}_{r\theta} = -\dot{E}', \quad C_2' = 1$$

$$\bar{\dot{\varepsilon}}_{rz} = \dot{E}^*_{23}, \quad \bar{\dot{\varepsilon}}_{\theta z} = -\dot{E}^*_{23} \tag{5.34}$$

Equations 5.29a,b show the dependence of the dilatational portion of the microscopic strain rate field on λ.

The dissipation can now be written in the following form:

$$\dot{W} = \frac{1}{V}\int_V S_{ij}(\underset{\sim}{\dot{\varepsilon}})\,\dot{\varepsilon}_{ij}\,dV = \frac{1}{V}\int_V \sqrt{\frac{2}{3}}\,\sigma_o\,(\dot{\varepsilon}_{ij}\,\dot{\varepsilon}_{ij})^{1/2} \tag{2.5}$$

Using the definitions

$$\mu = \cos(2\Theta)$$

$$\eta = \cos(\gamma) \tag{5.35}$$

and eqns. 5.27 and 5.29, this becomes

$$\dot{W} = \frac{1}{V}\int_V \frac{2}{\sqrt{3}}\,\sigma_o \Big\{ \mu^2 \bar{\dot{\varepsilon}}^2_{rr} + (1-\mu^2)\,\bar{\dot{\varepsilon}}^2_{r\theta} - 2\mu\,\bar{\dot{\varepsilon}}_{rr}\,E\lambda^{-1} + \dot{E}^2\lambda^{-2} + \frac{3}{4}\dot{E}^2_{33} + \eta^2\,\bar{\dot{\varepsilon}}^2_{rz} + (1-\eta^2)\,\bar{\dot{\varepsilon}}^2_{\theta z} \Big\}^{1/2} dV \tag{5.36}$$

The upper bound macroscopic stresses needed to enforce the deformation are then given by eqn. 2.25.

The locus of the stress vectors in stress space needed to enforce various modes of deformation is the yield locus. For the cylindrical model, it is expected that the yield function can be formulated in terms of equivalent macroscopic tensile stress

$$\Sigma_{eqv} = \left(\frac{3}{2}\Sigma'_{ij}\Sigma'_{ij}\right)^{\frac{1}{2}} \tag{5.37}$$

and the sum of the two transverse normal stresses

$$\Sigma_{\gamma\gamma} = \Sigma_{11} + \Sigma_{22} \tag{5.38}$$

The dilatation should be affected by $\Sigma_{\gamma\gamma}$ alone.

For the transverse axes oriented such that $\dot{E}_{12} = 0$, it can be shown that the dissipation has the general form

$$\dot{W} = \dot{W}\left(\dot{E}', \dot{E}, \dot{E}_{i3}\right) \quad i = 1, 2, 3 \tag{5.39}$$

i.e., $\underset{\sim}{\dot{E}}$ determines $\dot{W}$ uniquely. Consider a rotation θ about the 3 axis from the principle transverse axes to, say, the $\hat{}$ axes (an arbitrary rotation). It is easily shown that

$$\begin{aligned} \hat{\dot{E}}_{12} &= \sin(2\theta)\dot{E}' \\ \frac{1}{2}\left(\hat{\dot{E}}_{22} - \hat{\dot{E}}_{11}\right) \equiv \hat{\dot{E}}' &= \cos(2\theta)\dot{E}' \\ \text{i.e., } \left[(\hat{\dot{E}}')^2 + (\hat{\dot{E}}_{12})^2\right]^{1/2} &= \dot{E}' \end{aligned} \tag{5.40}$$

Equation 2.29 then gives

$$\hat{\Sigma}_{12} = \frac{\partial \dot{W}}{\partial \hat{E}_{12}} = \frac{\partial \dot{W}}{\partial \dot{E}'} \frac{\partial \dot{E}'}{\partial \hat{E}_{12}} = \frac{\partial \dot{W}}{\partial E'} \frac{\hat{E}_{12}}{\left[(\hat{E}')^2 + (\hat{E}_{12})^2\right]} \tag{5.41}$$

Therefore, $\Sigma_{12} = 0$ in the principle transverse coordinates of $\dot{\underset{\sim}{E}}$, and the macroscopic equivalent tensile stress in these coordinates is

$$\Sigma_{eqv}^2 = \frac{3}{4}\left(\Sigma_{22} - \Sigma_{11}\right)^2 + \frac{9}{4}\Sigma_{33}'^2 + \frac{3}{2}\left(\Sigma_{\alpha 3}\Sigma_{\alpha 3} + \Sigma_{3\alpha}\Sigma_{3\alpha}\right) \qquad \alpha = 1, 2 \tag{5.42}$$

Using eqns. 5.20 and 2.25, it can be shown that

$$\Sigma_{22} = \frac{\partial \dot{W}}{\partial \dot{E}_{22}} = \frac{1}{2}\left(\frac{\partial \dot{W}}{\partial \dot{E}'} + \frac{\partial \dot{W}}{\partial \dot{E}}\right) \qquad (a)$$

$$\Sigma_{11} = \frac{\partial \dot{W}}{\partial \dot{E}_{11}} = \frac{1}{2}\left(-\frac{\partial \dot{W}}{\partial \dot{E}'} + \frac{\partial \dot{W}}{\partial \dot{E}}\right) \qquad (b)$$

$$\text{so, } \left(\Sigma_{22} - \Sigma_{11}\right) = \frac{\partial \dot{W}}{\partial \dot{E}'} \quad (c), \quad \Sigma_{\alpha\alpha} = \frac{\partial \dot{W}}{\partial \dot{E}} \quad (d) \tag{5.43}$$

$$\Sigma_{33} = \frac{\partial \dot{W}}{\partial \dot{E}_{33}} \quad (e), \qquad \Sigma_{33}' = \frac{2}{3}\left(\frac{\partial \dot{W}}{\partial \dot{E}_{33}} - \frac{1}{2}\frac{\partial \dot{W}}{\partial \dot{E}}\right) \quad (f)$$

$$\Sigma_{\alpha 3} = \frac{\partial \dot{W}}{\partial \dot{E}_{\alpha 3}} \quad (g)$$

where a repeated Greek index ($\alpha\alpha$) means sum over 1 and 2. It is useful to remember that $\dot{W}$ is homogeneous of order 1 in $\dot{E}$. Therefore, the stresses can be calculated given only the direction of $\dot{E}$, or some normalized value.

Now, the details of solving for the upper bound yield locus for fully plastic flow (both numerically and analytically) will be discussed. First, note that in transforming back to the transverse axes where $\dot{E}_{12} = 0$,

$$\left(\dot{E}^{*}_{23}\right)^2 = \dot{E}^2_{13} + \dot{E}^2_{23} \tag{5.44}$$

Then, using eqns. 5.27 and 5.32, or eqn. 5.34, eqn. 5.36 becomes

$$\dot{W} = \frac{1}{3}\int_V \frac{2}{\sqrt{3}}\sigma_o\left\{K_1\dot{E}'^2 - 2\mu K_2\dot{E}'\dot{E}\lambda^{-1} + \dot{E}^2\lambda^{-2} + \frac{3}{4}\dot{E}^2_{33} + \frac{1}{2}K_3\left(\dot{E}_{\alpha 3}\dot{E}_{\alpha 3} + \dot{E}_{3\alpha}\dot{E}_{3\alpha}\right)\right\}^{\frac{1}{2}} dV \tag{5.45}$$

where K_1, K_2, and K_3 are geometric factors which go to 1 when eqns. 5.34 are used. Noting eqns. 5.31, 5.33, and 5.35;

$$K_1 = (C_2')^2\left[(1-A)^2 + 4A\mu^2\right] + \frac{6C_2'(\lambda-f)(1-2\mu^2-A)}{\lambda^2(3-f)} + \left(\frac{3(\lambda-f)}{\lambda^2(3-f)}\right)^2 \tag{5.46}$$

$$K_2 = C_2'(1+A) - \frac{3(\lambda-f)}{\lambda^2(3-f)}$$

$$K_3 = \frac{1}{(1+f)^2}\left[1 + \frac{2f}{\lambda}(1-2\eta^2) + \frac{f^2}{\lambda^2}\right]$$

Before applying eqns. 5.43, it is convenient to define some more new variables. First, a normalizing factor for the strain rates is defined:

$$\bar{\dot{E}} = \left(\frac{1}{2} \dot{E}'_{ij} \dot{E}'_{ij} \right)^{1/2} \tag{5.47}$$

This is convenient because for plane strain with no dilatation,

$$\bar{\dot{E}} = \dot{E}'$$

For general states of strain, define

$$G_1 = \frac{\dot{E}'}{\bar{\dot{E}}}, \qquad G_2 = \frac{\dot{E}}{\bar{\dot{E}}}$$

$$G_3 = \frac{\left(\dot{E}_{\alpha 3} \dot{E}_{\alpha 3} + \dot{E}_{3\alpha} \dot{E}_{3\alpha} \right)^{1/2}}{\bar{\dot{E}}}, \qquad G_4 = \frac{\dot{E}_{33}}{\bar{\dot{E}}} \tag{5.48}$$

$$Q = \left\{ K_1 G_1^2 - 2\mu K_2 \frac{G_1 G_2}{\lambda} + \frac{G_2^2}{\lambda^2} + \frac{K_3}{2} G_3^2 + \frac{3}{4} G_4^2 \right\}$$

Equations 5.43 then become

$$(\Sigma_{22} - \Sigma_{11}) = \frac{1}{V} \int_V \frac{2}{\sqrt{3}} \sigma_o Q^{-1/2} \left[K_1 G_1 - \mu K_2 \frac{G_2}{\lambda} \right] dV \qquad (a)$$

$$\Sigma_{\gamma\gamma} = \frac{1}{V} \int_V \frac{2}{\sqrt{3}} \sigma_o \frac{Q^{-1/2}}{\lambda} \left[\frac{G_2}{\lambda} - \mu K_2 G_1 \right] dV \qquad (b)$$

$$\Sigma'_{33} = \left[\frac{1}{V} \int_V \frac{2}{\sqrt{3}} \sigma_o Q^{-1/2} dV \right] \frac{G_4}{2} \qquad (c) \tag{5.49}$$

$$\Sigma_{33} = \frac{3}{2} \left(\Sigma'_{33} + \frac{1}{3} \Sigma_{\gamma\gamma} \right) \qquad (d)$$

$$\Sigma_{\alpha 3} = \left[\frac{1}{V} \int_V \frac{2}{\sqrt{3}} \sigma_o Q^{-1/2} K_3 \right] \frac{1}{2} \frac{\dot{E}_{\alpha 3}}{\bar{\dot{E}}} \qquad (e)$$

The volume integral is done as follows: Consider a volume element of axial length L, inner radius a, and outer radius b. Since the integrals are volume-averaged, only the ratio a/b is important. The yield stress of the void is zero, so the integral is carried out over $a \leq r \leq b$:

$$\frac{1}{V}\int_V dV = \frac{1}{\pi b^2 L}\int_0^{2\pi}\int_a^b\int_0^L r\,dr\,d\theta\,dL \tag{5.50}$$

Given no dependence of the integrand on L, and using

$$\lambda = \frac{r^2}{b^2}, \quad d\lambda = \frac{2r\,dr}{b^2}, \quad r\,dr = \frac{b^2}{2}\,d\lambda \tag{5.51}$$

eqn. 5.50 becomes

$$\frac{1}{V}\int_V dV = \frac{1}{2\pi}\int_0^{2\pi}\int_f^1 d\lambda\,d\theta \tag{5.52}$$

Figures 5 present the results of carrying out the integrals of eqns. 5.49 numerically. Each point on any line represents Σ_{eqv} vs. $\frac{1}{2}\Sigma_{YY}$ for a given $\dot{E}$ and f. The convenient normalization

$$\underset{\sim}{T} \equiv \frac{\underset{\sim}{\Sigma}}{\sigma_o} \tag{5.53}$$

is used; here, σ_o is constant throughout the matrix. As can be seen, the smallest value of T_{eqv} for a given $\frac{1}{2}T_{YY}$ and f occurs for plane strain deformation (3 axis). This is because in plane strain, the load carrying capability of the body suffers most from the zero shear stress condition on the

void surface. It is the plane strain part of the flow field which is affected by the minimization of $\dot{W}$ with respect to C_2'. Note that a similar minimization is not carried out for the flow field due to $\dot{E}_{23}$, since the form assumed did not leave an extra coefficient equivalent to C_2 (see eqn. 5.14).

The simplest case to deal with analytically is axially symmetric deformation ($\dot{E}' = \dot{E}_{23} = 0$). Here, the microscopic flow field is completely determined by symmetry and incompressibility, and the zero shear stress b.c. on the void surface is automatically satisfied. All angular dependence disappears from eqns. 5.49, and the stresses as defined in eqns. 5.49 b and c can be related without approximation as follows [47]:

For axially symmetric deformation,

$$T_{eqv} = \frac{3}{2} T'_{33}$$

$$G_1 = G_3 = 0, \quad (T_{22} - T_{11}) = T_{23} = 0 \tag{5.54}$$

$$Q = G_2^2 \lambda^{-2} + \frac{3}{4} G_4^2$$

Using the substitutions

$$X = G_2 \lambda^{-1}, \quad d\lambda = -G_2 X^{-2} dX, \quad (a)$$

$$a = \frac{3}{4} G_4^2 \quad (b) \tag{5.55}$$

"a" is used as a temporary variable, not to be confused with void radius (a).

eqns. 5.49 b and c become

$$T_{\gamma\gamma} = \frac{-2}{\sqrt{3}} \int_{\frac{G_2}{f}}^{G_2} \left(a + X^2\right)^{-\frac{1}{2}} dX \tag{5.56}$$

$$T_{eqv} = \sqrt{a}\, G_2 \int_{G_2}^{\frac{G_2}{f}} X^{-2} \left(a + X^2\right)^{-\frac{1}{2}} dX$$

These integrals can be found in many standard reference tables (e.g., ref. [48]. The results are:

$$T_I = \frac{\sqrt{3}}{2} T_{\gamma\theta} = \ln\left[\frac{\sqrt{af^2+G_2^2}+G_2}{f\left(\sqrt{a+G_2^2}+G_2\right)}\right] \quad (a)$$

$$T_{II} = T_{eqv}\, a^{-1/2} = \sqrt{a+G_2^2} - \sqrt{af^2+G_2^2} \quad (b) \qquad (5.57)$$

The object now is to eliminate (a) between these two equations, giving one relationship between T_{eqv} and $T_{\gamma\gamma}$ at yield (a yield function). This is accomplished as follows:

Define the variables

$$Z_1 = \sqrt{a+G_2^2} + G_2$$
$$Z_f = \sqrt{af^2+G_2^2} + G_2 \qquad (5.58)$$

Equations 5.57 and 5.58 then give

$$Z_1 = \frac{T_{II}}{(1-f\,e^{T_I})}, \qquad Z_f = \frac{T_{II}\, f\, e^{T_I}}{(1-f\,e^{T_I})} \qquad (5.59)$$

Equations 5.58 can be rearranged to give

$$G_2 = \frac{Z_1^2 - a}{2Z_1} = \frac{Z_f^2 - af^2}{2Z_f} \qquad (5.60)$$

Substituting eqns. 5.59 into eqns. 5.60 gives

$$T_{II}^2\, a^{-1} = (1-f\,e^{T_I})(1-f\,e^{-T_I}) = 1+f^2-2f\cosh(T_I) \qquad (5.61)$$

Using eqn. 5.57, this becomes

$$\phi = T_{eqv}^2 + 2f\cosh\left(\frac{\sqrt{3}}{2}T_{\gamma\gamma}\right) - 1 - f^2 = 0, \qquad (5.62)$$

which is the yield function for axially symmetric deformation.

It can now be shown that eqn. 5.62 sets the form for all yield functions for fully plastic flow in the cylindrical model, whatever the direction of $\dot{E}$. First, consider the approximate flow field which results when

$$K_1 = K_2 = K_3 = 1$$

This approximation allows the integration of eqns. 5.49 with respect to λ. The result is then expanded in a power series around $\mu = 0$, and integrated with respect to θ for an approximate result.

Define the following;

$$X = G_2\lambda^{-1}, \quad d\lambda = G_2 X^{-2} dX \qquad (a)$$

$$a = G_1^2 + \tfrac{1}{2}G_3^2 + \tfrac{3}{4}G_4^2 \qquad (b) \qquad (5.63)$$

which are identical to eqns. 5.55 for axial symmetry ($G_1 = G_3 = 0$). Using

$$\int \frac{dX}{Q^{1/2}} = \ln\left[Q^{\frac{1}{2}} + X - \mu G_1\right] \equiv F(\mu) \qquad (5.64)$$

$$\int \frac{dX}{XQ^{1/2}} = \frac{-1}{a^{1/2}}\ln\left[\frac{Q^{1/2} + a^{1/2} - \mu G_1}{X}\right] = \frac{-1}{a^{1/2}}G(\mu)$$

$$\int \frac{dX}{X^2Q^{1/2}} = -\frac{Q^{1/2}}{aX} + \frac{\mu}{a}\int \frac{dX}{XQ^{1/2}} \equiv -H(\mu) - \frac{\mu}{a^{1/2}}G(\mu)$$

it can be shown that, to first order in $\underline{E}$:

$$T_{eqv} = -a^{1/2} G_2 H(o)\Big|_{G_2}^{G_1/f} = a^{-1/2}\left[\sqrt{a+G_2^2} - \sqrt{af^2+G_2^2}\right]$$

$$T_{\gamma\gamma} = \frac{2}{\sqrt{3}} F(o)\Big|_{G_2}^{G_1/f} = \frac{2}{\sqrt{3}} \ln\left[\frac{\sqrt{af^2+G_2^2}+G_2}{f\left(\sqrt{a+G_2^2}+G_2\right)}\right] \qquad (5.65)$$

The above eqns. are the equivalent to eqns. 5.57, the only difference being a more general definition of (a). Eliminating (a) between them gives

$$T_{eqv}^2 + 2f\cdot\cosh\left(\frac{\sqrt{3}}{2} T_{\gamma\gamma}\right) - 1 - f^2 = 0 \qquad (5.66)$$

for all directions of the stress tensor.

When K_1 , K_2 , and K_3 are defined as in eqn. 5.46, the stress field for a given E must be computed numerically. The results can be written, to a good approximation, as

$$C_{TQV}\, T_{eqv}^2 + 2f\cdot\cosh\left(\frac{\sqrt{3}}{2} T_{\gamma\gamma}\right) - 1 - f^2 = 0, \qquad (5.67)$$

where C_{TQV} is a function of f and the direction of E . Equation 5.62 is the exact solution, and gives

$$C_{TQV} = 1 \quad \text{for axial symmetry.} \qquad (5.68)$$

The numerical results for plane strain can be approximated closely by this empirical form

$$C_{TQV} \simeq \left(1 + 3f + 24 f^6\right)^2 \quad \text{for } \dot{E}_{33} = 0 . \qquad (5.69)$$

The values of C_{TQV} for other strain rate fields will lie between these two values.

McClintock [36] has examined the problem of void growth for the axially symmetric deformation of a long cylindrical void in an infinite plastic matrix, and has given

$$\frac{\dot{a}}{a} = \dot{E}_{zz}\left[\frac{\sqrt{3}}{2}\sinh\left(\frac{\sqrt{3}}{2}T_{rr}\right) - \frac{1}{2}\right] \tag{5.70}$$

The strain rate field at the void surface (r = a) is

$$\dot{\epsilon}_{rr} = -\left(\frac{\dot{a}}{a} + \dot{E}_{zz}\right), \quad \dot{\epsilon}_{\theta\theta} = \frac{\dot{a}}{a}, \quad \dot{\epsilon}_{zz} = \dot{E}_{zz} \tag{5.71}$$

$$\text{from } \dot{u}_r = -\frac{1}{2}\dot{E}_{zz}\,r + \frac{1}{r}\left(\frac{\dot{a}}{a} + \frac{\dot{E}_{zz}}{2}\right)$$

The last term in eqn. 3.18 is zero here, since the flow field has no dependence on f. Therefore, using 5.52

$$\dot{W} = \frac{1}{V}\int_V s_{ij}(\dot{\underline{\epsilon}})\,\dot{\epsilon}_{ij}\,dV = \frac{1}{2\pi}\int_0^{2\pi}\int_f^1 \sqrt{\frac{2}{3}}\,\sigma_o\left(\dot{\epsilon}_{ij}\,\dot{\epsilon}_{ij}\right)^{\frac{1}{2}} d\lambda\, d\theta \tag{5.72}$$

Using axial symmetry and Leibnitz's rule,

$$\dot{w} = -\frac{\partial \dot{W}}{\partial f} = \sqrt{\frac{2}{3}}\,\sigma_o\left(\dot{\epsilon}_{ij}\,\dot{\epsilon}_{ij}\right)^{1/2}\Big|_{\lambda = f} \tag{5.73}$$

Using eqn. 5.71,

$$\dot{w} = \sigma_o \dot{E}_{zz} \cosh\left(\frac{\sqrt{3}}{2} T_{rr}\right) \tag{5.74}$$

Since the extrapolation makes use of the flow field at $f = 0$ (infinite matrix), the form

$$\frac{\partial \Sigma'_{ij}}{\partial f} = -\frac{\partial \dot{w}}{\partial \dot{E}'_{ij}} \tag{3.11}$$

is appropriate. The result is

$$\frac{\partial T'_{33}}{\partial f} = \cosh\left(\frac{\sqrt{3}}{2} T_{rr}\right), \tag{5.75}$$

$$T'_{33}\Big|_{f=0} - T'_{33}\Big|_{f} \simeq f \cosh\left(\frac{\sqrt{3}}{2} T_{rr}\right)$$

$$\text{and } \frac{\partial T'_{rr}}{\partial f} = 0, \quad T'_{rr} = \text{constant} \tag{5.76}$$

Since T'_{rr} is a constant,

$$\left|T'_{33}\right|_f - \left|T'_{rr}\right| = T_{eqv}\Big|_f \tag{5.77}$$

So one can write

$$T_{eqv}\Big|_o - T_{eqv}\Big|_f = f \cosh\left(\frac{\sqrt{3}}{2} T_{rr}\right) \tag{5.78}$$

$$\text{where } T_{eqv}\Big|_o = 1$$

Therefore,

$$T_{eqv}\Big|_f \simeq 1 - f\cosh\left(\frac{\sqrt{3}}{2}T_{rr}\right) \quad (a)$$

(5.79)

and

$$\frac{dT_{eqv}}{dT_{rr}} \simeq -\frac{\sqrt{3}}{2} f\cdot\sinh\left(\frac{\sqrt{3}}{2}T_{rr}\right) \quad (b)$$

Equations 5.79 are to be compared with the yield function (for small f) which results from the upper bound approach:

$$\phi = T_{eqv}^2 + 2f\cdot\cosh\left(\frac{\sqrt{3}}{2}T_{rr}\right) - 1 - f^2 = 0 \quad (a)$$

$$\delta\phi = 0 = \frac{\partial\phi}{\partial T_{eqv}}dT_{eqv} + \frac{\partial\phi}{\partial T_{rr}}dT_{rr}, \quad (5.80)$$

$$\frac{dT_{eqv}}{dT_{rr}} = -\frac{\sqrt{3}\, f\cdot\sinh\left(\frac{\sqrt{3}}{2}T_{rr}\right)}{2T_{eqv}} \quad (b)$$

Equations 5.79 and 5.80 are very similar when the transverse stress and f are not too large. Also, note that T_{eqv} can be obtained to first order in f from eqn. 5.80 via an expansion

$$T_{eqv} = \left[1 + f^2 - 2f\cdot\cosh\left(\frac{\sqrt{3}}{2}T_{rr}\right)\right]^{\frac{1}{2}} \quad (5.81)$$

$$\simeq 1 + \frac{1}{2}\left[-2f\cosh\left(\frac{\sqrt{3}}{2}T_{rr}\right) + f^2\right]$$

$$\simeq 1 - f\cdot\cosh\left(\frac{\sqrt{3}}{2}T_{rr}\right)$$

The result is eqn. 5.79a, and the expansion is accurate for

$$2f \cdot \cosh\left(\frac{\sqrt{3}}{2} T_{rr}\right) - f^2 \ll 1 \qquad (5.82)$$

i.e., for small values of f and T_{YY}.

5b. Long Circular Cylindrical Voids - Flow with Rigid Section

The geometry considered here is the same as in section 5a, however, the flow field has an important difference. For the case of plane strain (no deformation in the direction of the cylinder axis), part of the matrix remains rigid while the other part flows plastically to accommodate the macroscopic deformation.

Plane strain deformation of a matrix containing cylindrical cavities as described above has been studied previously via elastic-plastic finite elements [41,42] and (rigid-perfectly plastic) slip line theory [44]. All of these support the idea of only part of the matrix deforming plastically. The finite element solutions suggest that a radial line might be a suitable approximation to the rigid-plastic boundary, and that the non-plastic region is symmetric around the principle axis along which there is the largest absolute strain (see fig. 4).

The rigid-plastic analog studied here is a circular cylindrical matrix with a circular cylindrical void at its center, undergoing plane strain deformation. There are wedges of rigid material centered around the (2) axis, with radial planes as boundaries (see above). An approximate velocity field will be constructed which allows for this rigid-plastic boundary. As discussed previously, the proper angle, ψ_{opt}, between the boundary and the (2) axis is the angle for which the dissipation is minimized for a given $(\dot{E}_{11}, \dot{E}_{22})$ (applied via eqn. 2.2). ψ_{opt} is found numerically.

This formulation leads to some interesting numerical results, but does not lead to a concise derived functional form in the manner that eqn. 5.67 was obtained. Therefore, some parts of the formulation will be outlined, omitting the kind of detail given in section 5a. The main concern of this section will be plane strain, as in references [41,42,44]. Velocity fields due to $\dot{E}_{13}$,

$\dot{E}_{23}$, and $\dot{E}_{33}$ can presumably be superimposed, as in section 5a, if results for $\dot{E}_{13} \neq 0$ are desired.

The model is illustrated in fig. (6). Boundary velocity is specified at $\alpha = 0$ and $\alpha = \frac{\pi}{2}$, and the rigid-plastic boundary is at angle ψ measured from the (2) axis. The general procedure will be to find the velocity field in terms of V_1, V_2, and ψ, then to use eqn. 2.2 to obtain V_1 and V_2 for a given $\dot{E}_{11}$, $\dot{E}_{22}$ and ψ. ψ will then be varied to locate ψ_{opt}. Because of symmetry, the entire velocity field can be found by considering a 90° slice.

Besides the velocity b.c., a major constraint is that the rigid section move without deformation. This establishes the velocity b.c. at the rigid-plastic boundary, where the velocity must have no radial dependence. Symmetry requires that v_r be symmetric, and v_α be antisymmetric, about the (1) axis. As with the previous case, incompressibility is required.

Using the above conditions, the approximate velocity field (v_r, v_α) can be constructed as follows:

Instead of trying to solve a similar viscous problem as in section 5a, the simpler approach of starting with a generalized series solution will be used. Write

$$v_r = a_m r^m \cos(n_m \alpha) + b_m r^m \sin(n_m \alpha)$$
$$v_\alpha = c_m r^m \cos(n_m \alpha) + d_m r^m \sin(n_m \alpha) \qquad (5.83)$$

Symmetry immediately gives

$$b_m = c_m = 0 \qquad (5.84)$$

Incompressibility is, for plane strain,

$$v_{r,r} + \frac{1}{r}\left(v_{\alpha,\alpha} + v_r\right) = 0 \tag{5.85}$$

giving, for all α,

$$r^m \cos(n_m \alpha)\left[(m+1)\, a_m + n_m d_m\right] = 0,$$

$$d_m = -(m+1)\frac{a_m}{n_m} \tag{5.86}$$

Equations 5.83 thus become

$$v_r = a_m r^m \cos(n_m \alpha)$$

$$v_\alpha = -(m+1)\frac{a_m}{n_m} r^m \sin(n_m \alpha) \tag{5.87}$$

The rigid-plastic boundary requires that v_r and v_α be independent of r at $\alpha = \frac{\pi}{2} - \psi$. Terms with $m = 0$ obviously meet this condition. Because $\sin(x)$ and $\cos(x)$ never are both zero for the same value of x, meeting the condition for $m \neq 0$ requires that the coefficient of either $\sin(n_m \alpha)$ or $\cos(n_m \alpha)$ vanish. This is fulfilled only when $m = -1$. Equations 5.87 thus become

$$v_r = a_0 \cos(n_0 \alpha) + a_{-1} r^{-1} \cos(n_{-1} \alpha)$$

$$\text{where } n_{-1} = \frac{1}{1 - \frac{2}{\pi}\psi} \tag{5.88}$$

$$v_\alpha = -\frac{a_0}{n_0} \sin(n_0 \alpha)$$

Boundary conditions are first imposed as the surface velocities at $\alpha = 0$ and $\alpha = \frac{\pi}{2}$ (see Fig. 6). Due to symmetry, these are purely radial velocities. V_1^N and V_2^N are the velocities normalized with respect to the outer radius b. The rigid section moves uniformly in the (2) direction with velocity $V_2^N b$, and imposes this velocity on the rigid-plastic boundary. The boundary conditions on the plastic region are then, using eqn. 5.88:

$$\text{at} \begin{pmatrix} \alpha = 0 \\ r = b \end{pmatrix} \quad V_r = V_1^N b = a_0 + a_{-1} b^{-1} \qquad (a)$$

$$\text{at} \begin{pmatrix} \alpha = \frac{\pi}{2} - \psi \\ r = b \end{pmatrix} \quad V_r = V_2^N b \cdot \cos(\psi) = a_0 \cdot \cos\left[n_0 \left(\frac{\pi}{2} - \psi\right)\right] \qquad (5.89)$$

$$V_\alpha = V_2^N b \cdot \sin(\psi) = -\frac{a_0}{n_0} \cdot \sin\left[n_0 \left(\frac{\pi}{2} - \psi\right)\right]$$

The following changes of variable are useful:

$$A_0 = \frac{a_0}{b V_2^N}, \quad A_{-1} = \frac{a_{-1}}{b^{-1} V_1^N} \qquad (5.90)$$

Equations 5.88 and 5.89 then give

$$V_1^N = A_0 V_2^N + A_{-1} V_1^N \qquad (a)$$

$$\cos(\psi) = A_0 \cos\left[n_0 \left(\frac{\pi}{2} - \psi\right)\right] \qquad (b) \qquad (5.91)$$

$$n_0 \sin(\psi) = -A_0 \sin\left[n_0 \left(\frac{\pi}{2} - \psi\right)\right] \qquad (c)$$

For a given ψ, eqns. 5.91 b and c can be solved numerically for n_0 and A_0. It is important to note that A_0, n_0, and n_{-1} (see eqn. 5.88) are functions only of ψ, and not of V_1^N and V_2^N.

Using λ as defined in eqn. 5.25, eqns. 5.88 can be written:

$$v_r = b\left[A_o V_2^N \cos(n_o\alpha) + A_{-1} V_1^N \lambda^{-1/2} \cos(n_{-1}\alpha)\right] \quad (a)$$

$$v_\alpha = -b \frac{A_o}{n_o} V_2^N \sin(n_o\alpha) \quad (b) \qquad (5.92)$$

Using eqn. 5.91a,

$$v_r = b\left[A_o V_2^N \left(\cos(n_o\alpha) - \lambda^{-1/2}\cos(n_{-1}\alpha)\right) + V_1^N \lambda^{-\frac{1}{2}} \cos(n_{-1}\alpha)\right] \quad (c)$$

For a given ψ, v_r and v_α for the plastic region are now linear functions of V_1^N and V_2^N.

The rigid section has the velocity field

$$v_r = V_2^N \sin(\alpha) \qquad (5.93)$$

$$v_\alpha = V_2^N \cos(\alpha),$$

so the total velocity field is piecewise linear in V_1^N and V_2^N. This makes the determination of V_1^N and V_2^N (for a given ψ) from $\dot{E}_{11}$ and $\dot{E}_{22}$ rather straightforward.

For principle coordinates, eqn. 2.2 becomes

$$\dot{E}_{\alpha\underline{\alpha}} = \frac{1}{V}\int_S v_\alpha n_{\underline{\alpha}}\, dS, \qquad (5.94)$$

where a bar under a subscript indicates no sum. Let $C_{\alpha\beta}^N$ be a series of 2×2 matrices, each one identified by the superscript N. They will be used in the linear transformation between V_1^N, V_2^N, and $\dot{E}_{11}$, $\dot{E}_{22}$.

First, v_r and v_α are piecewise linear functions of V_1^N and V_2^N for a given ψ :

$$\begin{Bmatrix} V_r \\ V_\alpha \end{Bmatrix} = \begin{bmatrix} C_{11}^1 & C_{12}^1 \\ C_{21}^1 & C_{22}^1 \end{bmatrix} \begin{Bmatrix} V_1^N \\ V_2^N \end{Bmatrix} \tag{5.95}$$

The two sets of $C_{\alpha\beta}^1$ are obtainable from eqns. 5.92 and 5.93.

Equation 5.95 can be written

$$V_\gamma = C_{\gamma\delta}^1 V_\delta^N \qquad \gamma, \delta = 1, 2 \tag{5.95}$$

Equation 5.94 requires velocities in cartesian coordinates, and these are obtained by

$$\begin{Bmatrix} V_1 \\ V_2 \end{Bmatrix} = \begin{bmatrix} C_{11}^2 & C_{12}^2 \\ C_{21}^2 & C_{22}^2 \end{bmatrix} \begin{Bmatrix} V_r \\ V_\alpha \end{Bmatrix}, \quad \text{or}$$

$$V_\beta = C_{\beta\gamma}^2 V_\gamma = C_{\beta\gamma}^2 C_{\gamma\delta}^1 V_\delta^N \tag{5.96}$$

Then, eqn. 5.94 becomes

$$\dot{E}_{\beta\underline{\beta}} = \left[\frac{1}{V} \int_S n_\beta C_{\underline{\beta}\gamma}^2 C_{\gamma\delta}^1 \, dS \right] V_\delta^N, \quad \text{or}$$

$$\dot{E}_{\beta\underline{\beta}} = C_{\beta\delta}^3 V_\delta^N \tag{5.97}$$

Note that the surface integral must be carried out over both the plastic and the rigid regions. Inverting eqn. 5.97 gives

$$V_\delta^N = C_{\delta\beta}^4 \dot{E}_{\beta\underline{\beta}} \tag{5.98}$$

Thus, for a given ψ, V_1^N and V_2^N are homogeneous linear functions of $\dot{E}_{11}$ and $\dot{E}_{22}$.

Finding the dissipation corresponding to ψ_{opt} amounts to finding ψ and $W(\psi)$ where

$$\frac{\partial \dot{W}}{\partial \psi} = 0 \quad (a), \qquad \frac{\partial^2 \dot{W}}{\partial \psi^2} > 0 \quad (b) \tag{5.99}$$

and can be done by Newton's method [49] applied to $\partial \dot{W}/\partial \psi$. The dissipation is calculated in general as in eqn. 2.5 :

$$\dot{W} = \frac{1}{V}\int_V S_{ij}(\dot{\underset{\sim}{\epsilon}})\,\dot{\epsilon}_{ij}\,dV = \frac{1}{V}\int_V \sqrt{\tfrac{2}{3}}\,\sigma_o\left(\dot{\epsilon}_{ij}\,\dot{\epsilon}_{ij}\right)^{1/2} dV \,. \tag{2.5}$$

The derivative is calculated numerically;

$$\frac{\partial \dot{W}}{\partial \psi} \simeq \left.\frac{\dot{W}(\psi+\Delta) - \dot{W}(\psi-\Delta)}{2\Delta}\right|_{\dot{E}_{ij}\,=\,\text{constant}}, \quad \Delta \ll \frac{\pi}{2} \,. \tag{5.100}$$

Here, the integral need be done over only the plastic region, since no straining takes place in the rigid region. For plane strain,

$$\dot{\epsilon}_{ij}\,\dot{\epsilon}_{ij} = \dot{\epsilon}_{rr}^2 + \dot{\epsilon}_{\alpha\alpha}^2 + 2\dot{\epsilon}_{r\alpha}^2 \,. \tag{5.101}$$

Using eqns. 5.92,

$$\begin{aligned}
\dot{\epsilon}_{rr} &= v_{r,r} = \left(A_o V_2^N - V_1^N\right)\lambda^{-1}\cos(n_{-1}\alpha) \\
\dot{\epsilon}_{\alpha\alpha} &= \frac{1}{r}\left(v_{\alpha,\alpha} + v_r\right) = -\dot{\epsilon}_{rr} \\
\dot{\epsilon}_{r\alpha} &= \frac{1}{2}\left[v_{\alpha,r} + \frac{1}{r}\left(v_{r,\alpha} - v_\alpha\right)\right] \\
&= -\frac{1}{2}\left[V_2^N A_o \lambda^{-1/2}\left(n_o - \frac{1}{n_o}\right)\sin(n_o\alpha)\right. \\
&\quad \left. + \left(V_1^N - A_o V_2^N\right)\lambda^{-1} n_{-1}\sin(n_{-1}\alpha)\right]
\end{aligned} \tag{5.102}$$

The macroscopic stresses are calculated, as before, via eqn. 2.25. There are some complications, however, due to the dependence of $\dot{E}_{rr}$ and $\dot{E}_{r\alpha}$ on ψ and V_δ^N. First, eqn. 5.25 must be modified to read

$$\Sigma_{ij} = \left.\frac{\partial \dot{W}}{\partial \dot{E}_{ij}}\right|_{\psi = const.} + \left.\frac{\partial \dot{W}}{\partial \psi}\right|_{\dot{E}_{ij} = const.} \cdot \frac{\partial \psi}{\partial \dot{E}_{ij}} \tag{5.103}$$

Because the correct value of ψ is ψ_{opt}, eqn. 5.99a applies and the last term is zero. Equation 5.98 shows that for constant ψ, the V_δ^N are linear in the principle values $\dot{E}_{11}$ and $\dot{E}_{22}$, so eqn. 5.103 can be written, for $\delta, \beta = 1,2$

$$\Sigma_{\beta\beta} = \left.\frac{\partial \dot{W}}{\partial \dot{E}_{\beta\beta}}\right|_{\psi = \psi_{opt}} = \frac{\partial \dot{W}}{\partial V_\delta^N} C_{\delta\beta}^4 \tag{5.104}$$

A much simpler method for calculating $\Sigma_{\alpha\beta}$ was also investigated;

$$\Sigma_{\alpha\beta} = \frac{\partial \dot{W}}{\partial \dot{E}_{\alpha\beta}} \simeq \frac{\dot{W}(\dot{E}_{\alpha\beta} + \Delta) - \dot{W}(\dot{E}_{\alpha\alpha} - \Delta)}{2\Delta}, \quad \Delta \ll (\dot{E}_{ij}\dot{E}_{ij})^{1/2} \tag{5.105}$$

This gave the same results (within numerical errors) as those obtained via eqn. 5.104, and served as a check on the calculation.

For the cylindrical model, the yield function can be expressed in terms of Σ_{eqv} and $\Sigma_{\gamma\gamma}$. For plane strain, these are

$$\Sigma_{eqv} = \frac{\sqrt{3}}{2}\left|\Sigma_{22} - \Sigma_{11}\right|$$

$$\Sigma_{\gamma\gamma} = \Sigma_{22} + \Sigma_{11} \tag{5.106}$$

so the Σ_{13} need not be calculated.

For more general deformation, the Σ_{i3} must be calculated to obtain a yield surface. To apply eqn. 2.25 to the Σ_{i3}, the $\dot{\epsilon}_{ij}$ due to the $\dot{E}_{i3}$ must be superimposed on the $\dot{\epsilon}_{ij}$ for plane strain given in eqns. 5.102. To distinguish between the two, the superscript "ps" will denote $\dot{\epsilon}_{ij}$ due to plane strain, and the superscript "i3" will denote $\dot{\epsilon}_{ij}$ due to $\dot{E}_{i3}$:

$$\dot{\epsilon}_{ij} = \dot{\epsilon}^{ps}_{ij} + \dot{\epsilon}^{i3}_{ij} \tag{5.107}$$

Equations 5.19 give the following as the addition due to an imposed $\dot{E}_{33}$:

$$\begin{aligned} \dot{\epsilon}^{i3}_{rr} &= -\tfrac{1}{2}\dot{E}_{33}(\lambda+1) \\ \dot{\epsilon}^{i3}_{\alpha\alpha} &= +\tfrac{1}{2}\dot{E}_{33}(\lambda-1) \\ \dot{\epsilon}^{i3}_{zz} &= \dot{E}_{33} \end{aligned} \tag{5.108}$$

coordinates (r, α, z).

For $\dot{E}_{13}$ and $\dot{E}_{23}$, eqns. 5.10 and 5.27 give

$$\begin{aligned} \dot{\epsilon}^{i3}_{rz} &= \bar{\dot{E}}_{rz}\cos(\gamma) \\ \dot{\epsilon}^{i3}_{\theta z} &= \dot{\epsilon}^{i3}_{\alpha z} = \bar{\dot{E}}_{\alpha z}\cos(\gamma) \\ \gamma &= \theta - \theta^{*} \end{aligned} \tag{5.109}$$

Where θ is the angle of rotation from the axes in the transverse plane in which $\dot{E}_{12} = 0$ to the axes in the transverse plane in which $\dot{E}_{13} = 0$.

For plane strain, the $\dot{E}_{i3}$ should be set to zero after the derivatives are taken. This gives

$$\Sigma_{33} = \frac{1}{V}\int_V \sqrt{\frac{2}{3}}\,\sigma_o\left(\dot{\epsilon}^{ps}_{ij}\,\dot{\epsilon}^{ps}_{ij}\right)\dot{\epsilon}^{ps}_{rr}\left(-\lambda^{-1}\right)\,dV,$$

$$\Sigma_{13} = \Sigma_{23} = 0 \,. \tag{5.110}$$

For the more general case ($\dot{E}_{i3} \neq 0$), the procedure is straightforward. It should be noted that ψ_{opt} may change for $\dot{E}_{i3} \neq 0$, so the minimization procedure must be repeated.

The yield curves generated by the wedge flow field for plane strain are shown in figs. 7. In comparing these curves with those obtained for fully plastic flow, it is immediately apparent that the slopes of the curves for the wedge model are more negative for the lower values of Σ_{YY}. By the normal flow rule, this means that the wedge model predicts more dilatation than the fully plastic model for low Σ_{YY}. Considering that the effect of a rigid wedge would be to inhibit contraction in the (1) direction (see figs. 4 and 6) this is reasonable.

Dilatation for the plane strain model can be characterized by the ratio

$$\dot{E}_R \equiv \frac{\dot{E}_{11}}{\dot{E}_{22}} \,. \tag{5.111}$$

Figure 8 shows the variation of ψ_{opt} with E_R for a range of f. For small dilatation, ψ_{opt} rises with E_R, indicating growth in the size of the wedge. This is logical, since a larger wedge would interfere more with contraction in the (1) direction. For large dilatation, ψ decreases with increasing E_R. This indicates a growing preference for the fully plastic state.

In a paper by Nagpal, McClintock, Berg, and Subhuti [44], plane strain slip line solutions for bands of evenly spaced cylindrical cavities (long axis in the plane strain direction) are developed. The cross sections of the cavities considered are slits at various angles, and circular holes. The bands also have zero extension in the transverse direction, a result of the fracture criterion being developed there (see fig. 9a). For the cylinders with the circular cross section, an analogy can be made to the cylindrical voids in matrices in plane strain discussed here. The slip line solutions are done for various ratios of shear traction to normal traction, so with a bit of manipulation the results generated here can be directly compared with theirs (Appendix 2).

In order to find equivalent values of Σ_s and Σ_n for the plane strain results generated here, rotation into coordinates where $\dot{E}_{11} = 0$ is required. (Σ_n and Σ_s are not enough to compute Σ_{eqv} and Σ_{YY}). The counterclockwise rotation θ from the original axes is given by

$$\tan^2(\theta) = -\frac{\dot{E}_{11}}{\dot{E}_{22}} \,, \tag{5.112}$$

which shows that a plane of zero extension exists only when $\dot{E}_{11}$ and $\dot{E}_{22}$ are of opposite sign. Then, where the superscript $*$ denotes quantities in the coordinates reached by the rotation;

$$\dot{E}_{11} = \dot{E}^*_{11} = \dot{E}^*_{22} = 0 \tag{5.113}$$

$$\Sigma_n = \Sigma^*_{22} = \sin^2(\theta)\Sigma_{11} + \cos^2(\theta)\Sigma_{22}$$

$$\Sigma_s = \Sigma^*_{11} = \sin(\theta)\cos(\theta)\left(\Sigma_{11} - \Sigma_{22}\right)$$

Any comparison of results requires an interpretation of void volume fraction f in terms of the ratio P/L. In the slip line model, P is the hole radius and L is the inter-void spacing in the band. Figure 9b shows a square array of holes in a matrix, with the two reasonable directions for bands marked. (The bands are shown by dotted lines.) Relating P/L in each band to the void volume fraction of the array, and postulating that these represent bounds on the f represented by any band, the result is

$$\frac{\pi}{4}\left(\frac{P}{L}\right)^2 \leq f \leq \frac{\pi}{2}\left(\frac{P}{L}\right)^2 \tag{5.114}$$

In fig. 10, the slip line results are compared with the results generated here for the fully plastic and wedge models. The wedge model does a much better job in matching the slip line model, particularly for the value of f midway between the bounds given above;

$$f = \frac{3}{8}\pi\left(\frac{P}{L}\right)^2 \tag{5.115}$$

The direction of plastic flow (i.e., the normalized values of the $\dot{E}_{ij}$) is governed by the normality rule, and thus depends on the slope of the yield curve. For this reason, the similarity in slope of the slip line and wedge yield surfaces is particularly satisfying. It also justifies the development of the wedge model.

As noted previously, no functional form for the yield locus emerges from these calculations. However, some success has been achieved in fitting the following empirical form to the data:

$$\phi = T_{eqv}^2 - \left(B_0 + B_1 T_{GH} + B_2 T_{GH}^2\right), \quad T_{GH} = \frac{1}{2} T_{rr} \tag{5.116}$$

The coefficients B_o , B_1 , and B_2 are constant for a given f . They are determined by fitting the function to three numerical data points, spaced as evenly as possible over the computed yield locus. B_o , B_1 , and B_2 are functions of f , so yield functions for values of f between those calculated numerically can be approximated. In figs. 11, the approximations are shown in solid lines, while the numerical data are shown as points. Figure 12 shows the computed values of B_o , B_1 , and B_2 for various values of f . For values of f between those for which numerical data exists, numerical data for the three nearest values of f are used to determine the coefficients on the right-hand side below:

$$B_o = B_{of0} + B_{of1} \cdot f + B_{of2} \cdot f^2$$

$$B_1 = B_{1f0} + B_{1f1} \cdot f + B_{1f2} \cdot f^2 \qquad (5.117)$$

$$B_2 = B_{2f0} + B_{2f1} \cdot f + B_{2f2} \cdot f^2$$

Thus, B_o , B_1 , B_2 are calculated as functions of f for any values of f , and approximate yield loci result. These are shown in Fig. 13 for a range of f .

5c. Composite Yield Functions for Plane Strain

In sections 5a and 5b, upper bound yield loci for the cylindrical model in plane strain were calculated, using two very different microscopic flow fields. Both flow fields give yield curves which are convex to the origin in stress space. Because the curves intersect, neither is the preferred yield curve for the entire range of $\frac{1}{2} T_{YY}$. The preferred (composite) upper bound yield curve is thus comprised of the sections of the two curves which are closest to the origin.

The flow behavior predicted by the actual yield locus (via normality) should obey the following symmetry conditions. For zero dilatation ($\dot{E}_{11} = -\dot{E}_{22}$), radial velocity along the (2) axis should be of opposite value to that along the (1) axis. For pure transverse dilatation ($\dot{E}_{11} = \dot{E}_{22}$), the radial velocity should be constant. It would be reassuring if the composite of the two approximate yield loci also obeyed these symmetry conditions. These correspond to the points of the yield curve for the fully plastic model (at $\frac{1}{2} T_{YY} = 0$, and at $T_{eqv} = 0$), and do not exist for the wedge model due to the inherent asymmetry of the velocity field assumption. Therefore, at these two points, it is not unexpected that the fully plastic curve should be the innermost curve. This is indeed true when the refined fully plastic velocity field is used, but it is noteworthy that for the unrefined field ($K_1=K_2=K_3=0$, see eqns. 5.45, 5.46), it would be untrue. The importance of a refining procedure is thus underscored. Note that the wedge flow field was refined also, by varying the angle of the rigid-plastic boundary.

One way to use the composite yield function is simply to solve a problem using both the wedge and the fully plastic yield functions, and keep the solution which gives the lower dissipation. Another way is to use a functional

form which approximates the entire composite yield surface, if one can be found. One such attempt is discussed below.

Consider figs. 14. They suggest that one approach might be to take the form of the fully plastic solution, and modify it to "compress" the yield curve in the middle range of $\frac{1}{2}T_{YY}$. The form used is

$$\phi = T_{eqv}^2 - \left[1 + f^2 - 2f\cosh\left(\frac{\sqrt{3}}{2}T_{\gamma\gamma}\right)\right]^P = 0, \quad P > 1 \qquad (5.118)$$

When $P = 1$, this reduces to the fully plastic solution for axial symmetry, or for plane strain for the unrefined velocity field. Note that for $T_{eqv}=0$, $\frac{1}{2}T_{YY}$ will be the same as for the fully plastic solution, independent of P.

The proper value of P can be determined by matching eqn. 5.118 to the data. For most cases, P varies between 2 and 3.4, with the higher values of P for the lower values of $\frac{1}{2}T_{YY}$ (see figs. 15). With this wide range of values of P, it is obvious that eqn. 5.118 is useful only when the stress state does not vary too greatly.

The accuracy of the approximation can be judged by two criteria. One is accuracy in predicting yield stress, the other is accuracy in predicting rate of deformation behavior via normality (i.e., predicting the slope of the yield curve). Especially for low $\frac{1}{2}T_{YY}$, the first criterion is much easier to meet than the second. Therefore, when investigating rate of deformation behavior, it is probably better to use eqns. 5.118 and 5.67 (the two separate yield functions), and chose the result which gives the lower dissipation.

6a. Spherical Voids - Fully Plastic Flow

This void geometry is meant to represent a limit of void shape opposite to that of the long circular cylinder. Voids of approximately spherical shape can occur when (approximately equiaxed) inclusions decohere from a matrix, or themselves break apart during deformation. Voids have also been seen to nucleate in materials without inclusions, due to grain boundary misfits caused by straining [11-20]. Metal powder compacts can be specially prepared so that they contain approximately equiaxed voids [21,22]. Voids can also be present by accident, through faulty processing.

Many parts of this analysis are similar to parts of the analysis for the cylindrical geometry. The spherical geometry is simpler to work with because there are no preferred axes (as with the cylinder), but at the same time more complicated because of the spherical geometry. A refinement procedure analogous to that in section 5a was carried out; in contrast to the previous case, little change in the calculated yield loci resulted. For this reason, a refinement calculation will be omitted here.

Figure 16 shows the spherical model in principle axis space. Because there are no preferred axes for the model, the approximate microscopic velocity field will be broken up into only two parts; shape change at constant volume ($\underset{\sim}{v}^s$), and volume change at constant shape ($\underset{\sim}{v}^v$). The total microscopic velocity field is simply

$$\underset{\sim}{v} = \underset{\sim}{v}^s + \underset{\sim}{v}^v \tag{6.1}$$

The $\dot{\epsilon}_{ij}$ field calculated from v_i must, as before, be incompressible, and $\underset{\sim}{v}$ must meet external boundary conditions put in terms of the $\dot{E}_{ij}$.

$$v_i\big|_S = \dot{E}_{ij} x_j\big|_S \tag{6.2}$$

The boundary condition is of the type in eqn. 2.14; as is the case for the fully plastic cylindrical model. Because the two parts of the velocity field (eqn. 6.1) will be constructed separately, it is reasonable to separate the boundary condition as follows:

$$\begin{aligned} \dot{E}_{ij} &= \dot{E}'_{ij} + \tfrac{1}{3}\dot{E}_{nn}\delta_{ij} && (a) \\ v_i^s\big|_S &= \dot{E}'_{ij} x_j\big|_S && (b) \\ v_i^v\big|_S &= \tfrac{1}{3}\dot{E}_{nn} x_i\big|_S && (c) \end{aligned} \tag{6.3}$$

The superscript "s" , meaning "shape changing", should not be confused with the symbol "S" , denoting the outer surface. δ_{ij} is the Kronecker delta.

The deviatoric part of $\dot{E}_{ij}$ is used to construct a simple approximation to the shape changing part of $\underset{\sim}{v}$. In cartesian coordinates,

$$v_i^s = \dot{E}_{ij} x_j \qquad v_i^s = \dot{E}'_{ij} x_j \tag{6.4}$$

This identically satisfies the boundary condition. If the microscopic rate of deformation field is separated as $\underset{\sim}{v}$ is in eqn. 6.1, then

$$\dot{\epsilon}_{ij} = \dot{\epsilon}^s_{ij} + \dot{\epsilon}^v_{ij} \tag{6.5}$$

Equation 6.4 immediately gives

$$\dot{\epsilon}^s_{ij} = \dot{E}'_{ij}$$

which satisfies incompressibility by inspection.

By symmetry, $\underset{\sim}{v}^v$ should consist of a radial component only. Incompressibility is thus written

$$v^v_{r,r} + \frac{2 v^v_r}{r} = 0 \tag{6.6}$$

Integration gives

$$v^v_r = C r^{-2}, \quad C = \text{constant} \tag{6.7}$$

Applying the boundary condition (eqn. 6.3c),

$$v^v_r\Big|_{r=b} = C b^{-2} = \tfrac{1}{3} \dot{E}_{nn} b, \quad C = \tfrac{1}{3} \dot{E}_{nn} b^3 \tag{6.8}$$

The velocity field corresponding to pure dilatation is thus

$$v^v_r = \frac{\dot{E}_{nn}}{3} \frac{b^3}{r^2}, \quad v^v_\theta = v^v_\phi = 0 \tag{6.9}$$

Calculating the $\dot{\varepsilon}^v_{ij}$ in spherical coordinates;

$$\dot{\epsilon}^v_{rr} = \frac{\partial v^v_r}{\partial r} = -\frac{2}{3}\left(\frac{b}{r}\right)^3 \dot{E}_{nn}$$

$$\dot{\epsilon}^v_{\phi\phi} = \frac{1}{r}\frac{\partial v^v_\phi}{\partial \phi} + \frac{v^v_r}{r} = +\frac{1}{3}\left(\frac{b}{r}\right)^3 \dot{E}_{nn} \tag{6.10}$$

$$\dot{\epsilon}^v_{\theta\theta} = \frac{1}{r\sin(\phi)}\frac{\partial v^v_\theta}{\partial \theta} + \frac{v^v_r}{r} + v^v_\phi \frac{\cot(\phi)}{r} = +\frac{1}{3}\left(\frac{b}{r}\right)^3 \dot{E}_{nn}$$

$$\dot{\epsilon}^v_{r\theta} = \dot{\epsilon}^v_{r\phi} = \dot{\epsilon}^v_{\theta\phi} = 0$$

Incompressibility is satisfied, by inspection.

It is useful to write $\dot{\underset{\sim}{\epsilon}}$ (eqn. 6.5) in the following form, using the new variable h_{ij} :

$$\dot{\epsilon}_{ij} = \dot{E}'_{ij} + \frac{1}{3}\dot{E}_{nn}\, h_{ij} \tag{6.11}$$

In spherical coordinates,

$$h_{rr} = -2\left(\frac{b}{r}\right)^3, \quad h_{\phi\phi} = h_{\theta\theta} = +\left(\frac{b}{r}\right)^3 \qquad (a)$$

$$h_{ij}\Big|_{i\neq j} = 0 \qquad (b) \tag{6.12}$$

In cartesian coordinates,

$$h_{ij} = \left(\delta_{ij} - \frac{3x_i x_j}{r^2}\right)\left(\frac{b}{r}\right)^3, = \left(\delta_{ij} - 3n_i n_j\right)\left(\frac{b}{r}\right)^3 \qquad (c)$$

$$r^2 = x_1^2 + x_2^2 + x_3^2 \qquad (d)$$

(6.12)

$$n_i = \frac{x_i}{r} = \text{cartesian components of the normal to a sphere of radius } r \qquad (e)$$

Now that an approximate $\dot{\underset{\sim}{\epsilon}}$ field has been constructed, we may apply eqn. 2.25 and write $\underset{\sim}{\Sigma}$ as a function of $\dot{\underset{\sim}{E}}$ and f.

$$\Sigma_{ij} = \frac{1}{V}\int_V s_{kl}(\dot{\underset{\sim}{\epsilon}})\,\frac{\partial \dot{\epsilon}_{kl}}{\partial \dot{E}_{ij}}\, dV \tag{2.25}$$

Equation 6.11 can be modified as

$$\dot{\epsilon}_{kl} = \dot{E}'_{kl} + \frac{1}{3}\dot{E}_{nn}h_{kl} = \left(\dot{E}_{kl} - \frac{1}{3}\dot{E}_{nn}\,\delta_{kl}\right) + \frac{1}{3}\dot{E}_{nn}\,h_{kl} \tag{6.13}$$

so,

$$\frac{\partial \dot{\epsilon}_{kl}}{\partial \dot{E}_{ij}} = \left(\delta_{ki}\delta_{lj} - \frac{1}{3}\delta_{ij}\delta_{kl}\right) + \frac{1}{3}\delta_{ij}h_{kl} \tag{6.14}$$

Using the fact that $s_{ij}\delta_{ij} = 0$, eqn. 2.25 becomes

$$\Sigma_{ij} = \frac{1}{V}\int_V \left(s_{ij} + \frac{1}{3}\delta_{ij}s_{kl}h_{kl}\right) dV, = \Sigma'_{ij} + \frac{1}{3}\Sigma_{nn}\delta_{ij} \tag{6.15}$$

Matching coefficients of δ_{ij} gives

$$\Sigma'_{ij} = \frac{1}{V}\int_V s_{ij}(\underset{\sim}{\dot{\epsilon}})\, dV \tag{6.16}$$

$$\Sigma_{nn} = \frac{1}{V}\int_V s_{kl}(\underset{\sim}{\dot{\epsilon}})\, h_{kl}\, dV$$

Using $s_{nn} = 0$ and eqn. 6.12, one can write

$$\Sigma_{nn} = \frac{1}{V}\int_V \frac{3}{2} s_{rr}(\underset{\sim}{\dot{\epsilon}})\, h_{rr}\, dV \tag{6.17}$$

In terms of $\dot{\epsilon}_{ij}$ and σ_o, the upper bound macroscopic stresses are (using eqn. 2.16),

$$\Sigma'_{ij} = \frac{1}{V}\int_V \sqrt{\frac{2}{3}}\, \frac{\sigma_o \dot{\epsilon}_{ij}}{\sqrt{\dot{\epsilon}_{kl}\dot{\epsilon}_{kl}}}\, dV \tag{6.18}$$

$$\Sigma_{nn} = \frac{1}{V}\int_V \sqrt{\frac{3}{2}}\, \frac{\sigma_o \dot{\epsilon}_{rr} h_{rr}}{\sqrt{\dot{\epsilon}_{kl}\dot{\epsilon}_{kl}}}\, dV$$

The upper bound macroscopic dissipation is

$$\dot{W} = \frac{1}{V}\int_V \sqrt{\frac{2}{3}}\,\sigma_c\left(\dot{\epsilon}_{kl}\,\dot{\epsilon}_{kl}\right)^{\frac{1}{2}} dV \tag{6.19}$$

Equations 6.18 and 6.19 will be solved in a manner similar to that used in section 5a.

The integrands must first be put in terms of the $\dot{E}_{ij}$, which along with f are the independent variables. To this end, eqn. 6.12 and the coordinate transformation

$$\left[\dot{E}'_{ij}\,n_i n_j\right]_{\substack{\text{cartesian}\\ \text{coords.}}} = \dot{E}'_{rr}\Big|_{\substack{\text{spherical}\\ \text{coords.}}} \tag{6.20}$$

are used to give

$$\dot{\epsilon}_{ij}\,\dot{\epsilon}_{ij} = \dot{E}'_{ij}\,\dot{E}'_{ij} - 2\dot{E}_{nn}\dot{E}_{nn}\dot{E}'_{rr}\left(\frac{b}{r}\right)^3 + \frac{2}{3}\dot{E}^2_{nn}\left(\frac{b}{r}\right)^6 \tag{6.21}$$

The following changes of variable are useful in making eqns. 6.18 and 6.19 more tractable. Where possible, they are similar to steps taken in section 5a. Define the following new variables:

$$D = \frac{\dot{E}_{nn}}{3\sqrt{\frac{2}{3}\dot{E}'_{kl}\dot{E}'_{kl}}}\,, \qquad t_{ij} = \frac{\dot{E}'_{ij}}{\sqrt{\frac{2}{3}\dot{E}'_{kl}\dot{E}'_{kl}}}$$

$$\mu = \frac{\dot{E}'_{rr}}{\sqrt{\frac{2}{3}\dot{E}'_{kl}\dot{E}'_{kl}}} = t_{ij}\,n_i n_j \quad \text{(see Appendix 1)} \tag{6.22}$$

$$\lambda = \left(\frac{r}{b}\right)^3\,, \qquad Q = 1 - 4D\mu\lambda^{-1} + 4D^2\lambda^{-2}$$

The volume integral over the sphere is treated as follows, where Ω as used here is a solid angle.

$$dV = r^2 \, d\Omega \, dr, \quad = r^2 \sin(\phi) \, d\phi \, d\theta \, dr$$

$$r^2 dr = \frac{b^2}{3} d\lambda \quad \Leftarrow \quad r^3 = \lambda b^3 \Rightarrow 3r^2 dr = b^3 d\lambda$$

$$\frac{1}{V}\int_V dV = \frac{1}{\frac{4}{3}\pi b^3}\int_\Omega \int_a^b r^2 \, dr \, d\Omega = \frac{1}{4\pi}\int_\Omega \int_f^1 d\lambda \, d\Omega \qquad (6.23)$$

$$\int_\Omega d\Omega = \int_0^{2\pi}\int_0^{\pi} \sin(\phi) \, d\phi \, d\theta$$

Using the above, and eqns. 6.12, eqns. 6.18 and 6.19 become

$$\dot{W} = \frac{\sqrt{\frac{2}{3}}\,\sigma_o}{4\pi}\left(\dot{E}'_{mn}\dot{E}'_{mn}\right)^{1/2}\int_\Omega \int_f^1 Q^{1/2} \, d\lambda \, d\Omega \qquad (6.24)$$

$$\Sigma'_{ij} = \frac{\sigma_o}{6\pi}\int_\Omega \int_f^1 Q^{-1/2}\left[t_{ij} + (\delta_{ij} - 3n_i n_j) D\lambda^{-1}\right] d\lambda \, d\Omega \quad (a) \qquad (6.25)$$

$$\Sigma_{nn} = \frac{\sigma_o}{6\pi}\int_\Omega \int_f^1 Q^{-1/2}\left(2D\lambda^{-1} - \mu\right)\lambda^{-1} \, d\lambda \, d\Omega \quad (b)$$

These equations show that the macroscopic upper bound stresses depend only on the ratios of the $\dot{E}_{ij}$, and not on their magnitudes. This is to be expected.

Because no refinement procedure has taken place here, eqns. 6.24 and 6.25 are simpler in their dependence on λ than their counterparts for the cylinder

(see eqns. 5.45 through 5.49). Their form is simple enough, in fact that the integral over λ can be carried out analytically for the general case. The necessary integrals can be found in tables once the substitution

$$X = \frac{1}{\lambda}, \quad d\lambda = -\frac{1}{X^2}\,dX, \quad X\Big|_{\lambda=f} = \frac{1}{f}, \quad X\Big|_{\lambda=1} = 1$$

$$\text{so,} \quad \int_f^1 d\lambda = \int_1^{1/f} \frac{dX}{X^2} \tag{6.26}$$

is made (see, for example, ref. [48]). Note; x is not to be confused with the position vector $\underset{\sim}{x}$.

Once eqns. 6.24 and 6.25 have been altered by the above substitution, the integrals over x can be put in terms of the following functions (note the definition of functions $F(x,\mu)$, $G(x,\mu)$, and $H(x,\mu)$:

$$\int \frac{dx}{Q^{1/2}} = \frac{1}{2|D|} \ln\left[Q^{1/2} + 2|D|x - \frac{D}{|D|}\mu\right] \equiv \frac{1}{2|D|} F(x,\mu)$$

$$\int \frac{dx}{xQ^{1/2}} = -\ln\left[\frac{Q^{1/2}+1}{x} - 2D\mu\right] \equiv -G(x,\mu) \tag{6.27}$$

$$\int \frac{dx}{x^2Q^{1/2}} = -\frac{Q^{1/2}}{x} - 2D\mu\, G(x,\mu), \quad H(x,\mu) \equiv \frac{Q^{1/2}}{x}$$

Equations 6.24 and 6.25 now become

$$\dot{W} = \frac{\sqrt{\frac{2}{3}}\sigma_o \left(\dot{E}'_{mn}\dot{E}_{mn}\right)^{1/2}}{4\pi} \int_\Omega \left\{ \left[\frac{X}{2} - \frac{\mu}{4D} \right] Q^{1/2} + \frac{(1-\mu^2)}{4|D|} F(X,\mu) \right\} \Bigg|_{X=1}^{X=1/f} d\Omega \qquad (6.28)$$

$$\Sigma'_{ij} = -\frac{\sigma_o}{6\pi} \int_\Omega \left\{ t_{ij} H(X,\mu) + D \cdot K_{ij} \cdot G(X,\mu) \right\} \Bigg|_{X=1}^{X=1/f} d\Omega \qquad (a)$$

$$\text{where } K_{ij} = (\delta_{ij} - 3n_i n_j) + 2\mu t_{ij} \qquad (6.29)$$

$$\Sigma_{nn} = \frac{\sigma_o}{2\pi} \int_\Omega \left\{ \frac{D}{|D|} F(X,\mu) + \mu G(X,\mu) \right\} \Bigg|_{X=1}^{X=1/f} d\Omega \qquad (b)$$

Some results of the numerical integration of eqns. 6.29a and b can be seen as the discrete points in fig. 17, where

$$T_{eqv} = \frac{\left(\frac{3}{2}\Sigma'_{ij}\Sigma'_{ij}\right)^{1/2}}{\sigma_o}, \quad \frac{1}{3}T_{kk} = \frac{\frac{1}{3}\Sigma_{kk}}{\sigma_o} \qquad (6.30)$$

The curves in fig. 17 are approximate results. Each curve is for a different f. They are all for axially symmetric deformation,

$$\dot{E}'_{11} = \dot{E}'_{22} = -\frac{1}{2}\dot{E}'_{33} \qquad (6.31)$$

and result from varying D between zero and infinity. D is a logical independent variable, representing the ratio of the hydrostatic component of $\dot{\underset{\sim}{E}}$ to a measure of its deviatoric component. Each yield curve intersects the horizontal (hydrostatic) axis at 90°, indicating by normality that $D = \infty$. The value of $\frac{1}{3}T_{kk}$ for $T_{eqv} = 0$ can be easily calculated either by using eqns. 6.18b and 6.11 for $\dot{E}_{11} = \dot{E}_{22} = \dot{E}_{33}$ (all angular dependence disappears), or by using eqn. 6.25b, taking the limit as $D \to \infty$. The result is

$$\frac{\frac{1}{3}\Sigma_{nn}}{\sigma_o} = \frac{\frac{1}{3}T_{nn}}{} = \frac{2}{3}\ln\left(\frac{1}{f}\right) \tag{6.32}$$

As mentioned previously, the points in fig. 17 result from axially symmetric deformation only. Other ratios of the $\dot{E}_{ij}$ were found to give yield curves which were, for the most part, indistinguishable from the axisymmetric results. The largest differences occurred at very high triaxiality (and slope), where, for a given $\frac{1}{3}T_{kk}$ and f, the spread in T_{eqv} for various $\dot{E}'$ was never more than 10% of the T_{eqv} for axial symmetry. At these points, the values of T_{eqv} were themselves quite low.

Numerical calculation of the yield function for all of stress space (resulting from a range of $\dot{E}_{ij}$ covering all possibilities) is greatly facilitated by the use of the following symmetry arguments, adapted from ref. [1], p. 18.

The yield surface in stress space can be depicted by the hydrostatic stress ($\frac{1}{3}\Sigma_{kk}$) and π plane projection (figs. 18) of the yield surface at that hydrostatic stress. The π plane is simply the plane perpendicular to the line

$$\Sigma_{11} = \Sigma_{22} = \Sigma_{33}$$

in principle stress space. The perpendicular distance from this line to a point on the yield surface is simply

$$r = \left(\Sigma'_{ij}\,\Sigma'_{ij}\right)^{1/2}$$

Referring to the form of eqns. 6.24 and 6.25, noting that the spherical model is isotropic, and using principle axes, the following arguments can be made:

If $(\Sigma_a, \Sigma_b, \Sigma_c)$ is a plastic state with $\Sigma_a > 0$, so is $(\Sigma_a, \Sigma_c, \Sigma_b)$ due to isotropy. Therefore, the π plane intersection of the yield surface is

symmetric about the positive 1 axis. Due to isotropy, the same symmetric form surrounds the positive 2 and 3 axes. The same arguments apply separately to the negative 1, 2, and 3 axes, though there is nothing to show any similarity between the points surrounding the positive and negative axes. Therefore, the intersection of the yield locus with the π plane between any positive axes and a neighboring negative axis (60°) gives, through symmetry, the entire 360° intersection. Figures 18a shows the $\dot{E}_{ij}$ used to calculate a typical 60° segment. (Unfortunately, slightly different values of $\dot{E}_{kk}$ were required to get equal values of Σ_{kk}, for the π plane projection in stress space). Figure 18b shows a π plane projection in stress space with the deviation exaggerated for clarity. Corresponding $\dot{E}_{ij}$ directions, located by normality, are shown.

Examination of eqns. 6.24 and 6.25 shows another area where symmetry can be exploited. It can be shown that if (T'_{ij}, T_{kk}) is on the yield surface, so is $(-T'_{ij}, -T_{kk})$. This allows prediction of the effects of hydrostatic pressure from the results for hydrostatic tension if the effects of inclusion fragments within the void are ignored.

The approximate yield functions developed below involve only the first and second invariants of stress. Therefore, the π plane projections in stress space will be circles.

The gross effect of the hydrostatic stress in the approximate fully plastic yield function is to change the von Mises cylinder into a closed body of revolution about the cylinder axis. This has been approximated previously [4] by closing the von Mises cylinder with a hemispherical cap.

The next step is to find approximate analytic solutions to eqns. 6.29, 6.30, which can be combined to give an approximate upper bound yield function. The

method used is to expand the functions F, G, and H in a power series in μ around $\mu = 0$, and then integrate over Ω. The expansion is used because the expressions are too complicated for exact integration. Good accuracy results from truncating the expansions after the second order term in μ.

Equation 6.22c defines μ in terms of the $\dot{E}_{ij}$ and the angular position of the radius vector. It can be shown that the absolute value of μ never exceeds 1, which makes μ particularly attractive as an expansion variable. If a Lode variable [1] ν is defined in terms of principle values of $\dot{E}'_{ij}$ (as in ref. [37]),

$$\nu = \frac{-3\dot{E}'_{III}}{\dot{E}'_{I} - \dot{E}'_{II}}, \quad \dot{E}'_{I} \geq \dot{E}'_{III} \geq \dot{E}'_{II} \tag{6.33}$$

then it can be shown that

$$\mu = \frac{1}{2\sqrt{3+\nu^2}}\left[\nu\left(1-3\cos^2(\phi)+3\sin^2(\phi)\cos(2\theta)\right)\right] \tag{6.34}$$

$\mu_{max.} = +1$ occurs at $\nu = +1$, $\phi = (2n-1)\frac{\pi}{2}$, $\theta = n\frac{\pi}{2}$,
n = even integer

$\mu_{min} = -1$, at $\nu = -1$, ϕ and θ as above, n = odd integer

When the expansions are written out, a superscript in parentheses will indicate the number of derivatives with respect to μ imposed on that term. A bar above the symbol $F^{(n)}$, $G^{(n)}$, or $H^{(n)}$ will indicate as follows:

$$\bar{F}^{(n)} = \left(F^{(n)}(x,\mu)\right)_{\mu=0}\Bigg|_{x=1}^{x=\frac{1}{f}} \tag{6.35a}$$

etc. Thus, the expansions are of the form

$$F(x,\mu)\Big|_{x=1}^{x=\frac{1}{f}} = \bar{F}^{(0)} + \mu \bar{F}^{(1)} + \tfrac{1}{2}\mu^2 \bar{F}^{(2)} + \ldots . \qquad (6.35b)$$

The approximate stress integrals thus become, to second order in μ,

$$\Sigma'_{ij} \simeq -\frac{\sigma_o}{6\pi}\int_\Omega \Big[t_{ij}\left(\bar{H}^{(0)} + \mu\bar{H}^{(1)} + \tfrac{1}{2}\mu^2\bar{H}^{(2)}\right) + 2D t_{ij}\left(\mu\bar{G}^{(0)} + \mu^2\bar{G}^{(1)}\right) + \left(\delta_{ij} - 3n_i n_j\right)\left(\bar{G}^{(0)} + \mu\bar{G}^{(1)} + \tfrac{1}{2}\mu^2\bar{G}^{(2)}\right)\Big] d\Omega \qquad (6.35c)$$

$$\Sigma_{kk} \simeq \frac{\sigma_o}{2\pi}\int_\Omega \Big[\frac{D}{|D|}\left(\bar{F}^{(0)} + \mu\bar{F}^{(1)} + \tfrac{1}{2}\mu^2\bar{F}^{(2)}\right) + \left(\mu\bar{G}^{(0)} + \mu^2\bar{G}^{(1)}\right)\Big] d\Omega$$

Using the results derived in Appendix (1) and dropping the smaller terms, carrying out the integral over Ω gives

$$T'_{ij} = -t_{ij}\left(\tfrac{2}{3}\bar{H}^{(0)} + \tfrac{1}{15}\bar{H}^{(2)} + \tfrac{4}{15}D\bar{G}^{(1)}\right) \qquad (6.36)$$

$$T_{kk} = \frac{D}{|D|}\left[2\bar{F}^{(0)} + \tfrac{1}{5}\bar{F}^{(2)}\right] + \tfrac{2}{5}\bar{G}^{(1)}$$

Again dropping smaller terms, the equivalent tensile stress can be calculated to second order:

$$T_{eqv}^2 = \frac{3}{2} T'_{ij} T'_{ij} \simeq \frac{3}{2} t_{ij} t_{ij} \left(\frac{4}{9} \bar{H}^{(0)2} + \frac{4}{45} \bar{H}^{(0)} \bar{H}^{(2)} \right)$$

$$= \bar{H}^{(0)2} + \frac{1}{5} \bar{H}^{(0)} \bar{H}^{(2)}$$

$$T_{eqv} \simeq \left[\bar{H}^{(0)2} + \frac{1}{5} \bar{H}^{(0)} \bar{H}^{(2)} \right]^{1/2} \tag{6.37}$$

$$\simeq \left| \bar{H}^{(0)} \right| \left[1 + \frac{1}{5} \frac{\bar{H}^{(2)}}{\bar{H}^{(0)}} \right]^{1/2}$$

$$\simeq \left| \bar{H}^{(0)} \right| + \frac{1}{10} \bar{H}^{(2)} \, sign\left(\bar{H}^{(0)} \right)$$

The following statements can be verified in a straightforward manner from eqn. 6.27:

$$\bar{F}^{(0)} = \ln \left[\frac{(f^2 + 4D^2)^{1/2} + 2|D|}{f\left((1 + 4D^2)^{1/2} + 2|D| \right)} \right]$$

$$\bar{F}^{(2)} = -\left[\frac{1}{(1 + 4D^2 x^2)} + \frac{4D^2 x^2}{(1 + 4D^2 x^2)^{3/2} \left(\sqrt{1 + 4D^2 x^2} + 2|D| x \right)} \right]_{x=1}^{x=\frac{1}{f}}$$

$$\bar{G}^{(1)} = \frac{-2Dx}{(1 + 4D^2 x^2)^{1/2}} \Bigg|_{x=1}^{x=\frac{1}{f}} \tag{6.38}$$

$$\bar{H}^{(0)} = \sqrt{f^2 + 4D^2} - \sqrt{1 + 4D^2}$$

$$\bar{H}^{(2)} = \frac{-4D^2 x}{(1 + 4D^2 x^2)^{3/2}} \Bigg|_{x=1}^{x=1/f}$$

For $D > 0$, these give

$$\frac{T_{kk}}{2} \simeq +\bar{F}^{(0)} - \frac{1}{5}\left.\frac{Dx(2+4D^2x^2)}{(1+4D^2x^2)^{3/2}}\right|_{x=1}^{x=1/f} \tag{6.39}$$

$$T_{eqv} \simeq -\bar{H}^{(0)} + \left.\frac{2D^2x}{5(1+4D^2x^2)^{3/2}}\right|_{x=1}^{x=1/f}$$

The last terms in the above expressions are of second order (order μ^2). Because they are small with respect to the first order terms, they can be dropped for a fairly good first order solution. When this is done, a calculation analogous to that in eqns. 5.57 through 5.62 (with $a \to 1$, $G_2 \to 2D$) gives

$$\phi = T_{eqv}^2 + 2f\cdot\cosh\left(\tfrac{1}{2}T_{kk}\right) - 1 - f^2 = 0, \tag{6.40}$$

the first order yield function.

The second order terms in eqn. 6.39 are

$$T_{k2} \equiv \left.\frac{Dx(2+4D^2x^2)}{5(1+4D^2x^2)^{3/2}}\right|_{x=1}^{x=1/f} \tag{6.41}$$

$$T_{p2} \equiv \left.\frac{-2D^2x}{5(1+4D^2x^2)^{3/2}}\right|_{x=1}^{x=1/f}$$

so the second order yield function is

$$\left(T_{eqv} + T_{p2}\right)^2 + 2f\cdot\cosh\left(\tfrac{1}{2}T_{kk} + T_{k2}\right) - 1 - f^2 = 0 \tag{6.42}$$

The second order terms require that D be known. Because D is itself determined by the yield function via normality,

$$D = \frac{\dot{E}_{nn}}{3\sqrt{\frac{2}{3}\dot{E}'_{k\ell}\dot{E}'_{k\ell}}} = \frac{\phi_{,T_{nn}}}{3\sqrt{\frac{2}{3}\left[\left(\phi_{,T_{k\ell}} - \frac{1}{3}\phi_{,T_{nn}}\delta_{k\ell}\right)(\cdots)\right]}^{1/2}} \qquad (6.43)$$

it should have to be calculated by an iterative process. However, it has been found that if a first order solution is used to calculate the value of D used in the second order terms, these are almost indistinguishable from the results of an iterative process. Therefore, T_{k2} and T_{p2} can be calculated using

$$D = \frac{f \cdot \sinh\left(\frac{1}{2}T_{KK}\right)}{2\,T_{eqv}} \qquad \text{drop terms of order } f^2 \qquad (6.44)$$

The first and second order approximations are shown, with the numerical data, in fig. 17. As can be seen, the second order approximation fits the numerical data almost exactly, and the first order approximaiton is quite reasonable.

Because the simple flow field used here (eqns. 6.4 and 6.9) is independent of f, the expansion method could have been used as an alternative to integrating over λ (eqns. 6.27) with relative ease. The expansion method will be used here to generate a yield function from the results of Rice and Tracey [37] for the fully plastic flow of an infinite body containing a single spherical void. This will be compared with eqns. 6.40 and 6.42.

For axially symmetric deformation (about the (3) axes) with large amounts of triaxiality, Rice and Tracey give the average radial velocity at the void surface as

$$\dot{a} = a \cdot \frac{3}{2}\dot{E}_{33}\exp\left[\frac{T_{kk}}{2} - \frac{5}{3}\right] \qquad (6.45)$$

where "a" is the void radius. When, the exponent is large enough, the dissipation can be calculated to reasonable accuracy by using eqn. 6.45 as in pure radial expansion:

$$\dot{\epsilon}_{rr} = -2\frac{\dot{a}}{a}, \quad \dot{\epsilon}_{\theta\theta} = \dot{\epsilon}_{\phi\phi} = \frac{\dot{a}}{a}, \qquad (6.46)$$

$$\dot{\epsilon}_{r\theta} = \dot{\epsilon}_{r\phi} = \dot{\epsilon}_{\theta\phi} = 0$$

This gives

$$\dot{W} = \frac{1}{4\pi}\int_{\Omega}\sqrt{\frac{2}{3}}\,\sigma_o\left(\dot{\epsilon}_{ij}\dot{\epsilon}_{ij}\right)^{1/2} d\Omega = \sqrt{\frac{2}{3}}\,\sigma_o\sqrt{6}\,\frac{\dot{a}}{a},$$

$$\dot{w} \simeq 3\sigma_o \dot{E}_{33}\cdot exp\left[\frac{T_{kk}}{2} - \frac{5}{3}\right] \qquad (6.47)$$

$$\dot{w} \simeq 3\sigma_o \dot{E}_{33}\, e^{-5/3} exp\left(\tfrac{1}{2}T_{kk}\right) \simeq 0.57\,\sigma_o \dot{E}_{33}\, exp\left(\tfrac{1}{2}T_{kk}\right)$$

By analogy with eqns. 5.75 through 5.78, which are also for axially symmetric deformation,

$$T_{eqv} \simeq 1 - 0.57 f\cdot exp\left(\tfrac{1}{2}T_{kk}\right) \qquad (6.48)$$

$$\simeq 1 - 1.14 f\cdot cosh\left(\tfrac{1}{2}T_{kk}\right)$$

For small f ,

$$T_{eqv}^2 \simeq 1 - 2.28 f\cdot cosh\left(\tfrac{1}{2}T_{kk}\right) \qquad (6.49)$$

which, considering the approximations made, is in reasonable agreement with eqn. 6.40. It can be shown that the "large triaxiality" approximations used above are valid for $T_{kk} \geq 1$.

6b. Spherical Voids - Flow with Rigid Section

Following the example of section 5, the plastic flow of a spherical model with rigid sections is now considered. For simplicity, only axisymmetric deformation is considered. The rigid sections are then idealized as truncated circular cones, capped with spherical sections, whose axes coincide with the tensile axis. The variable ψ is the angle between the tensile axis and the wall of the cone, and is varied to minimize the dissipation. This optimizes the assumed flow field within the limits of the approximation. Flow of this type is considered because of the success achieved with its cylindrical analog. See fig. 4b.

The form of the calculations in this section is very similar to the form of section 5b; the geometry and flow type are the major differences. Again, the calculations do not lead to any concise derived form for the yield function, so some details are omitted. The notation used here for some of the intermediate variables differs somewhat from that used in section 5b.

Consider the model, shown in fig. 19. Boundary velocity is specified at $\alpha = 0$ and $\alpha = \frac{\pi}{2}$, and the rigid-plastic boundary is the cone wall set at angle ψ from the tensile (3) axis. Due to axial symmetry,

$$V_1 = V_2 = V_R\Big|_{\alpha=0} \tag{6.50}$$

so the only boundary velocities which must be specified are V_1 and V_3. As before, the angle ψ is specified. The general procedure is to find the microscopic velocity field in terms of V_1, V_3, and ψ; then to use eqn. 2.2 to obtain V_1 and V_3 for a given $\dot{E}_{11}$ and $\dot{E}_{33}$ ($\dot{E}_{11} = \dot{E}_{22}$ by symmetry). ψ is then varied to locate ψ_{opt}, which gives the lowest dissipation (within the limits of the approximation). Symmetry allows all integrals over the spherical

geometry to be reduced to integrals over a 90° slice between $\alpha = 0$ and $\alpha = \pi/2$.

As before, the constraint of the rigid section establishes velocity b.c. at the rigid-plastic boundary. Here, the velocity must have no radial dependence. Symmetry requires that v_r be symmetric, and v_α antisymmetric, about the (1) axis. Incompressibility is required.

Using the above information, the approximate velocity field (v_r, v_α) is constructed. Using symmetry and a generalized series representation,

$$V_r = \sum_{m,n} A_{nm}\, r^n \cos(m\alpha) \tag{6.51}$$

$$V_\alpha = \sum_{m,n} B_{nm}\, r^n \sin(m\alpha)$$

with infinite summation over n and m . (The two series will be truncated later by restricting the values that can be taken by m and n .) Incompressibility in spherical coordinates gives

$$r V_{r,r} + \left[2V_r - V_\alpha \cdot \tan(\alpha) + V_{\alpha,\alpha}\right] = 0 \tag{6.52}$$

with commas indicating partial differentiation. Substituting eqns. 6.51 into eqn. 6.52 gives, for each coefficient of r^n ,

$$\sum_m \Big[(n+2) A_{nm} \cos(m\alpha) + B_{nm}\left(-\sin(m\alpha)\tan(\alpha) + m\cdot\cos(m\alpha)\right)\Big] = 0 \tag{6.53}$$

The factor $\tan\alpha$ in the coefficient of B_{nm} has the effect of eliminating most values of m from consideration (i.e., their companion A_{nm} and B_{nm} must be zero for eqn. 6.53 to hold). However, the following trigonometric identities

$$\sin(2\alpha)\tan(\alpha) = 1 - \cos(2\alpha)$$

$$\sin(4\alpha)\tan(\alpha) = -1 + 2\cos(2\alpha) - \cos(4\alpha) \qquad (6.54)$$

allow terms with $m = 0, 2$, and 4 to remain. Also note that for $n = -2$, A_{nm} does not enter into the incompressibility condition and $B_{nm} = 0$ for all m.

Limiting m to 0, 2, and 4 when $n \neq -2$, and using eqns. 6.54, incompressibility gives

$$A_{n4} = 5(3A_{no} + A_{n2})$$

$$B_{n2} = -(n+2)(2A_{no} + A_{n2}) \qquad (6.55)$$

$$B_{n4} = -(n+2)(3A_{no} + A_{n2})$$

Eqns. 6.51 thus become

$$v_r = A_{oo}(1 + 15\cos(4\alpha)) + A_{o2}(\cos(2\alpha) + 5\cos(4\alpha)) + \sum_m A_{-2m} r^{-2} \cos(m\alpha)$$

$$v_\alpha = -A_{oo} \cdot 2 \cdot (2\sin(2\alpha) + 3\sin(4\alpha)) - A_{o2} \cdot 2 \cdot (\sin(2\alpha) + \sin(4\alpha)) \qquad (6.56)$$

Note that for the terms with $n = -2$, A_{nm} and m are still unidentified.

Let the rigid-plastic boundary be at the angle

$$\alpha = \alpha^* = \frac{\pi}{2} - \psi$$

Then, the boundary conditions imposed by the rigid cone are

$$\text{at } \alpha = \alpha^*, \quad V_r = r_o V_{3N} \sin(\alpha^*) \qquad (a)$$

$$V_\alpha = r_o V_{3N} \cos(\alpha^*) \qquad (b) \qquad (6.57)$$

$$V_r \text{ and } V_\alpha \text{ independent of } r \qquad (c)$$

The other boundary conditions are

$$\text{at } \alpha = 0, \; r = r_o, \quad V_r = r_o V_{1N} \qquad (a)$$

$$V_\alpha = 0 \qquad (b) \qquad (6.58)$$

The subscript "N" denotes normalization by the outer radius r_o :

$$V_{1N} = \frac{V_1}{r_o}, \quad V_{3N} = \frac{V_3}{r_o} \qquad (6.59)$$

Equation 6.57c requires that, for $n = -2$,

$$\cos(m\alpha^*) = 0 \qquad (6.60)$$

There are an infinity of values of m which satisfy this condition. In constructing the approximate velocity field, only this one value of m will be used (the series is truncated):

$$m = \frac{\pi}{2\alpha^*} \qquad (6.61)$$

Λ_{-2m} can be found in terms of the other coefficients via eqn. 6.58a:

$$\frac{A_{-2m}}{r_o^3 V_{1N}} = 1 - \frac{V_{3N}}{V_{1N}}\left(\frac{16\,A_{00}}{V_{3N}\,r_o} + \frac{6\,A_{02}}{V_{3N}\,r_o}\right) \tag{6.62}$$

This form is used to underscore the following normalizing scheme, similar to that used in eqn. 5.90:

$$A_0 = \frac{A_{00}}{V_{3N}\,r_o}\,, \quad A_2 = \frac{A_{02}}{V_{3N}\,r_o}\,, \quad A_{-2} = \frac{A_{-2m}}{V_{1N}\,r_o^3}$$
$$A_{-2} = 1 - \frac{V_{3N}}{V_{1N}}\left(16\,A_0 + 6\,A_2\right) \tag{6.63}$$

These are all nondimensional quantities. Using the definition of λ found in eqn. 6.22 (with $r_o \equiv b$), eqns. 6.56 become

$$V_r = V_{3N}\,r_o\left\{A_0\left(1+15\cos(4\alpha)\right) + A_2\left(\cos(2\alpha) + 5\cos(4\alpha)\right)\right\}$$
$$+ V_{1N}\,r_o\,A_{-2}\,\lambda^{-\frac{2}{3}}\cos(m\alpha)$$

(6.64)

$$V_\alpha = V_{3N}\,r_o\left\{-2A_0\left(2\sin(2\alpha) + 3\sin(4\alpha)\right)\right.$$
$$\left. - 2A_2\left(\sin(2\alpha) + \sin(4\alpha)\right)\right\}$$

As a check on the calculations, eqn. 6.52 can be applied to the above. It shows that incompressibility is satisfied for arbitrary values of A_{-2}, A_0, A_2, V_{1N}, and V_{3N}.

The boundary conditions at the rigid-plastic boundary (eqns. 5.57), when applied to eqns. 6.64, give A_0 and A_2 as functions of α^* only. (Note that the factors $V_{3N}\,r_o$ cancel, and use is made of eqn. 6.60). Eqn. 6.63 then gives A_{-2}, also a function of α^* only. The general procedure now follows

the form of eqns. 5.95 through 5.100. Appropriate changes are made for geometry, and the Greek subscripts are now 1 and 3. Thus v_r and v_α are obtained in terms of $\dot{E}_{11}$, $\dot{E}_{33}$, and ψ; then the solution is optimized with respect to ψ.

The microscopic rates of deformation for axially symmetric deformation are

$$\begin{aligned}
\dot{\epsilon}_{\phi\phi} &= \dot{\epsilon}_{\alpha\alpha} = \frac{1}{r}\left(V_{\alpha,\alpha} + V_r\right) \\
\dot{\epsilon}_{\theta\theta} &= \frac{1}{r}\left(V_r - V_\alpha \tan(\alpha)\right) \\
\dot{\epsilon}_{r\alpha} &= \frac{1}{2r}\left(-V_{r,\alpha} + V_\alpha\right) \\
\dot{\epsilon}_{r\theta} &= \dot{\epsilon}_{\alpha\theta} = 0
\end{aligned} \tag{6.65}$$

These can be calculated using eqn. 6.64. The derivatives are

$$\begin{aligned}
V_{r,r} &= -2\,V_{1N}\,A_{-2}\,\lambda^{-1}\cos(m\alpha) \\
V_{\alpha,\alpha} &= -2\,V_{3N}\,r_o\left\{2\cos(2\alpha)\left(2A_0 + A_2\right)\right. \\
&\qquad \left. + 4\sin(4\alpha)\left(3A_0 + A_2\right)\right\} \\
V_{r,\alpha} &= V_{3N}\,r_o\left\{-60A_0\sin(4\alpha) - A_2\left(2\sin(2\alpha) + 20\sin(4\alpha)\right)\right\} \\
&\qquad - V_{1N}\,r_o\,A_{-2}\,\lambda^{-2/3}\,m\cdot\sin(m\alpha)
\end{aligned} \tag{6.66}$$

The approximate dissipation $\dot{W}$ is computed via eqn. 2.5. For axial symmetry

$$\dot{W} = \int_0^{\alpha^*}\int_f^1 \sqrt{\frac{2}{3}}\,\sigma_o\left(\dot{\epsilon}_{rr}^2 + \dot{\epsilon}_{\theta\theta}^2 + \dot{\epsilon}_{\alpha\alpha}^2 + 2\dot{\epsilon}_{r\alpha}^2\right) d\lambda\, d\alpha \tag{6.67}$$

Note that the integral is taken only over that part of the geometry which is undergoing plastic flow, and much use is made of symmetry.

Stresses are calculated numerically as in eqns. 5.103 through 5.105. The yield curves are given in terms of the following:

$$T_{eqv} \equiv |T_{33} - T_{11}|$$
$$T_H \equiv \frac{1}{3} T_{kk} = \frac{1}{3}(2T_{11} + T_{33}) \qquad (6.68)$$

The results are shown for a range of f in figs. 20, along with the variation in ψ_{opt}. Their appearance is very similar to the results for the cylindrical model in plane strain (fig. 7), so a similar type of polynomial approximation (eqns. 5.116, 5.117) is attempted. The results are shown in fig. 21.

The results of fully plastic flow and flow with a rigid section are compared in figs. 22. The symmetry conditions of section 5c do not apply to axially symmetric deformation, so it is not necessarily to be expected that the fully plastic solution gives the better (lower) upper bound when $T_{kk} = 0$. Symmetry does, however, require that the fully plastic solution apply at $T_{eqv} = 0$, and this is indeed obeyed by the results.

Some further comment on the solution at $T_{kk} = 0$ is in order. As seen from fig. 22, the fully plastic solution dominates at lower values of f (less than around 0.01), while the rigid section solution dominates for higher values of f. It is physically reasonable that a fully plastic solution should increasingly dominate as f decreases. This is also true for the entire yield surface.

A choice between the two competing yield surfaces is made in the same manner as discussed in section 5c; the innermost yield surface is preferred.

At the time of writing, the author knows of no other theoretical or numerical work done for the type of problem considered in this section. Therefore, a comparison with results generated by another method (as was done in section 5b) cannot be made here.

7. Normality, Plastic Flow, Void Growth, and Work Hardening

In chapter 2, the normality of the macroscopic rate of deformation tensor to the upper bound yield function was established. This means that the yield function can be used as a plastic potential (see ch. 3 in ref. [1]), which gives the direction of $\dot{E}_{ij}$ once the stress state for yield has been specified:

$$\dot{E}_{ij} = \Lambda \frac{\partial \phi}{\partial \Sigma_{ij}} , \quad = \dot{E}_{ij}\left(\Sigma_{ij}, f, \dot{\Sigma}_{ij}\right) \tag{7.1}$$

Λ is a scalar factor, the "magnitude" of $\dot{E}$, determined from consistency conditions and a given hardening law. (This will be derived later.) For a given yield function, this allows calculation of the rate of volume change in a dilatant material which is caused by a given rate of stress or strain:

$$\dot{V} = V \cdot \dot{E}_{kk} = V \cdot \Lambda \cdot \left(\frac{\partial \phi}{\partial \Sigma_{11}} + \frac{\partial \phi}{\partial \Sigma_{22}} + \frac{\partial \phi}{\partial \Sigma_{33}} \right), \equiv V \Lambda \frac{\partial \phi}{\partial \Sigma_{kk}} \tag{7.2}$$

Because the matrix is incompressible, all volume change in the aggregate is due to void growth. (The reverse is also true here; void nucleation will not be considered until a later chapter.) It can be shown that

$$\dot{f} = (1-f)\dot{E}_{kk} = (1-f)\Lambda \frac{\partial \phi}{\partial \Sigma_{kk}} \tag{7.3}$$

Dilatation, which weakens the aggregate, is thus closely related to the influence of hydrostatic stress in the yield function.

The two types of upper bound yield functions (fully plastic flow, flow with rigid section) developed in chapters 5 and 6 resulted from the imposition of $\dot{E}$ fields, and calculation of upper bounds to the stresses necessary to maintain those fields. Given the same ratio of T_{eqv} to T_{HYD}, the two types of yield functions can lead to very different amounts of dilatation. The following example is illustrative:

A state of simple tension is imposed on an aggregate containing spherical voids.

$$T_{11} = T_{22} = 0, \quad T_{eqv} = T_{33}, \quad T_{HYD} = \tfrac{1}{3} T_{33} \tag{7.4}$$

$$\dot{E}_{33} \text{ is known}, \quad \Lambda = \frac{\dot{E}_{33}}{\phi, \Sigma_{33}}$$

(Note that the size of T_{HYD} here is relatively small.) Two quantities of interest for each type of yield function are T_{33}, and the ratio $(\dot{E}_{KK}/\dot{E}_{33})$. The former can be obtained when the yield functions are specialized by eqn. 7.4:

$$\phi = T_{33}^2 + 2f \cdot \cosh\left(\tfrac{1}{2} T_{33}\right) - 1 - f^2 = 0, \text{ or} \tag{7.5}$$

$$\phi = T_{33}^2 - B_0 - B_1 \cdot \tfrac{1}{3} T_{33} - B_2 \tfrac{1}{9} T_{33}^2 = 0$$

When the flow rule is used, the yield function must remain unspecialized:

using $\underset{\sim}{T} = \frac{\underset{\sim}{\Sigma}}{\sigma_o}$,

$$\dot{E}_{ij} = \Lambda \phi_{,\Sigma_{ij}} = \Lambda \frac{1}{\sigma_o}\left(3T'_{ij} + f\cdot\sinh\left(\tfrac{1}{2}T_{kk}\right)\delta_{ij}\right), \text{ or} \tag{7.6}$$

$$\dot{E}_{ij} = \Lambda \phi_{,\Sigma_{ij}} = \Lambda \frac{1}{\sigma_o}\left[3T'_{ij} - \delta_{ij}\left(\tfrac{1}{3}B_1 + \tfrac{2}{3}B_2\cdot\tfrac{1}{3}T_{kk}\right)\right]$$

Specializing the $\dot{E}$ to eqn. 7.4 gives, for fully plastic flow,

$$\frac{\dot{E}_{kk}}{\dot{E}_{33}} = \frac{3f\cdot\sinh\left(\tfrac{1}{2}T_{33}\right)}{2T_{33} - f\cdot\sinh\left(\tfrac{1}{2}T_{33}\right)} \tag{7.7}$$

For flow with a rigid section, the result is

$$\frac{\dot{E}_{kk}}{\dot{E}_{33}} = \frac{-B_1 - B_2\cdot\tfrac{2}{3}\cdot T_{33}}{2T_{33} - B_1\cdot\tfrac{1}{3} - B_2\cdot\tfrac{2}{9}T_{33}} \tag{7.8}$$

Both of these ratios must use the relevant value of T_{33} . The results, for a range of values of f , are given in fig. 23.

The figure shows that the rigid cone model predicts considerably more dilatation relative to the fully plastic model, especially at lower values of f.

It also generates lower values of T_{33} (and is thus preferable as an upper bound solution) for all but the smallest values of f.

The curves generated by the rigid cone model appear to have a discontinuous slope at several points. This is because values of $B_i(f)$ were obtained by linear interpolation between known values of B_i for $f = .01, .05, .10,$ and $.20$.

Work hardening in the aggregate can be approached in two ways. One is to consider the local microscopic strain and corresponding local flow stress of individual points in the matrix; the other is to continue to treat the matrix as if its flow stress was uniform (as in the virgin material), assigning an average value. The latter is explored below:

The "average" values of microscopic equivalent yield stress and total strain are

$$\sigma_o, \bar{\epsilon}, \text{ where } \sigma_o = f(\bar{\epsilon}), \frac{d\sigma_o}{d\bar{\epsilon}} = f'(\bar{\epsilon}) = h(\bar{\epsilon}) \tag{7.9}$$

where the functions $f(\bar{\epsilon})$ and $h(\bar{\epsilon})$ describe, respectively, the stress-strain curve and its slope for the matrix material (h is not to be confused with h_{ij} in eqn. 6.12). The average rate of plastic work is equal to the volume average (over the matrix, but not the voids) of the macroscopic rate of plastic work:

$$\sigma_o \dot{\bar{\epsilon}} = \frac{\Sigma_{ij} \dot{E}_{ij}}{(1-f)} \tag{7.10}$$

This gives

$$\dot{\bar{\epsilon}} = \frac{T_{ij}\,\dot{E}_{ij}}{(1-f)} \tag{7.11}$$

as an average rate of plastic straining on the microscale. From eqn. 7.9,

$$\dot{\sigma}_o = h\,\dot{\bar{\epsilon}} = h\,\frac{T_{ij}\,\dot{E}_{ij}}{(1-f)} \tag{7.12}$$

As an example of the form taken by h, consider the case of power law hardening (where $*$ indicates values at first yield),

$$\frac{\sigma_o}{\sigma_o^*} = \left(\frac{\bar{\epsilon}}{\bar{\epsilon}^*}\right)^n, \quad \dot{\sigma}_o = \sigma_o \frac{n}{\bar{\epsilon}}\,\dot{\bar{\epsilon}} \tag{7.13}$$

Using all of the above, it is possible to determine Λ. First, apply consistency to the yield function

$$\phi = \phi(\Sigma_{ij}, \sigma_o, f) = 0 \tag{7.14a}$$

For the specific forms developed in chapters 5 and 6, this can be written as

$$\phi = \phi(T_{ij}, f) = \phi\left(\frac{\Sigma_{ij}}{\sigma_o}, f\right) = 0 \tag{7.14b}$$

It is "consistent" that since the yield function equals zero, so does its total derivative:

$$\dot{\phi} = 0 = \frac{\partial \phi}{\partial \Sigma_{ij}} \dot{\Sigma}_{ij} + \frac{\partial \phi}{\partial \sigma_o} \dot{\sigma}_o + \frac{\partial \phi}{\partial f} \dot{f} \,, \tag{7.15}$$

$$\dot{\phi} = 0 = \frac{\partial \phi}{\partial \Sigma_{ij}} \dot{\Sigma}_{ij} + \frac{\partial \phi}{\partial \sigma_o} \frac{h T_{ij}}{(1-f)} \frac{\partial \phi}{\partial \Sigma_{ij}} \Lambda + \frac{\partial \phi}{\partial f} (1-f) \frac{\partial \phi}{\partial \Sigma_{kk}} \Lambda$$

This gives, for Λ

$$\Lambda = - \frac{\partial \phi}{\partial \Sigma_{ij}} \dot{\Sigma}_{ij} \left[\frac{\partial \phi}{\partial \sigma_o} \frac{h T_{ij}}{(1-f)} \frac{\partial \phi}{\partial \Sigma_{ij}} + \frac{\partial \phi}{\partial f} (1-f) \frac{\partial \phi}{\partial \Sigma_{kk}} \right]^{-1} \tag{7.16}$$

Λ can also be calculated from rate of deformation boundary conditions (eqn.7.1).

8. Void Nucleation at Particles

So far, while investigating the behavior of porous materials, no mention has been made of the origin of the porosity. Some materials are naturally porous. Others acquire porosity during deformation when second phases fracture, either internally or along the interface with the surrounding matrix. In this chapter, void nucleation at rigid particles embedded in a work hardening matrix undergoing plastic flow will be investigated.

Two reasonable ideas have been put forward to explain void nucleation at rigid particles; a critical strain in the matrix, and a critical stress normal to the matrix-particle interface. Both are investigated here, with the bulk of the space devoted to the latter. In both cases, extensive use is made of work by other authors. An attempt is made to put both theories into the same framework.

The change in f during an increment of deformation is now broken into two parts: That due to the growth of existing voids, and that due to the nucleation of new voids.

$$df = df\Big|_{growth} + df\Big|_{nucl} \tag{8.1}$$

Here, the second term is investigated. The first was dealt with in the previous chapter (see eqn. 7.3).

In some recent work on spheroidized 1.05%C steel, Gurland [19] finds that the variation of the fraction of particles broken with strain is very close to linear and homogeneous. The experiments were done in tension, compression, and torsion (essentially low levels of triaxial stress - judged here to be too low to demonstrate the role of the first stress invariant in a critical stress nu-

cleation criterion). If a cracked particle is presumed to behave like a void, these experiments suggest the form

$$df\big|_{nucl} \simeq C_1 \, d\bar{\epsilon}, \tag{8.2}$$

where C_1 is a constant for a given volume fraction of particles. (It was learned [54] that the volume fraction of particles, f_p, was approximately 0.15.) Note that for these experiments,

$$d\bar{\epsilon} \simeq d\bar{E} \tag{8.3}$$

because there was negligible void growth in the specimens used for measurements, and the initial void volume fraction f was zero.

Where P_f denotes the fraction of the particles which are fractured at a given value of $\bar{\epsilon}$, Gurland's data at $\bar{\epsilon} = 0.30$ gives (for tension experiments)

$$\frac{dP_f}{d\bar{\epsilon}} \simeq \frac{.06}{.30} = 0.2 \tag{8.4}$$

which would lead to

$$C_1 = f_p \frac{dP_f}{d\bar{\epsilon}} = 0.03 \tag{8.5}$$

However, larger particles were found to fracture preferentially, necessitating a correction factor (the ratio of the average volume of fractured particles to the average volume of all the particles). Where the average size of the broken particles is proportional to 2.2, and that of the unbroken particles proportional to 1.3;

$$P_f = 0.06,$$

$$C_1 = \frac{0.03 \times 2.2}{(1-P_f)\cdot 1.3 + P_f \cdot 2.2} = 0.043, \simeq 0.04 \tag{8.6}$$

It is interesting to speculate on the functional dependence of C_1 on the volume fraction of unfractured particles (f_{up}). One expects the dependence to be approximately linear and homogeneous at low values of f_{up}. Because eqn. 8.2 is in terms of the microscopic matrix material quantity $d\bar{\underset{\sim}{\varepsilon}}$ (and not, for instance, $d\bar{\underset{\sim}{E}}$), it is not unreasonable to expect this dependence to continue as f_{up} becomes larger. A more universal expression in place of eqn. 8.2 might then be

$$df\big|_{nucl} \simeq C_1^* f_{uP}\, d\bar{\varepsilon} \tag{8.7}$$

where C_1^* did not vary greatly with f_{up}. For the example above,

$$C_1^* = \frac{C_1}{f_{uP}} \simeq \frac{0.043}{0.15} \simeq 0.29 \tag{8.8}$$

Argon, et al. [13] study the case of rigid particles which adhere to a plastic matrix, eventually coming loose. They favor a critical value of the stress normal to the matrix particle interface as the criterion for this event. In their calculations, they examine this stress, and how its value is amplified via interaction with neighboring particles when the matrix undergoes plastic flow. Due in part to their work (as modified in Appendix 3), the following form is suggested

$$\sigma_i = A \cdot \sigma_o + \frac{\Sigma_H}{(1-f)} \tag{8.9}$$

A is an amplification factor (Appendix 3, and fig. 26) and σ_i is the interfacial stress, and is a monotonically rising function of the local particle concentration c. The amplification occurs only for shear deformation, so the last term is added to include the hydrostatic contribution to σ_i. The factor (1-f) is an approximate way of accounting for the fact that the voids do not carry any stress:

$$\sigma_H \simeq \frac{\Sigma_H}{(1-f)} \tag{8.10}$$

Matrix-particle separation occurs when

$$\sigma_i = \sigma_i^c \tag{8.11}$$

the critical value.

Using the above criterion, say that c^* is the lowest value of c for which matrix particle separation can occur. Then Argon, et al. have shown, via a statistical model for randomly distributed particles of equal size that the fraction of particles which have nucleated voids (separated from the matrix) is

$$(1-P) = 0.4412 \int_{c^*/\bar{c}}^{\infty} \frac{dx}{\Gamma(x+1)} \tag{8.12}$$

P is the fraction of the particles which have not separated, $\bar{c}$ is the average particle fraction, and $\Gamma(n+1)$ is the Gamma function.

It is pointed out in ref. [13] that even though this model was developed for particles of equal size, a relative particle size factor is evident. This is because the local concentration c near a large particle is likely to be

larger than that near a small particle, and is thus more likely to attain c^*. Experimental observations [17-20,53] support the idea that nucleation occurs preferentially at larger particles.

Using Leibnitz's rule for differentiation of definite integrals [49] on eqn. 8.12 gives

$$\frac{\partial(1-P)}{\partial c^*} = \frac{-0.4412}{\Gamma\left(\frac{c^*}{\bar{c}}+1\right)} \frac{1}{\bar{c}}, \text{ i.e.,}$$

$$\Delta(1-P) = \frac{-0.4412}{\Gamma\left(\frac{c^*}{\bar{c}}+1\right)} \frac{\Delta c^*}{\bar{c}} \tag{8.13}$$

where Δ indicates a small change. If the assumption is made that once a particle has separated from the matrix, it behaves like a void of equal volume, then eqn. 13 gives

$$df\big|_{nucl} = \frac{-0.4412}{\Gamma\left(\frac{c^*}{\bar{c}}+1\right)} dc^* \tag{8.14}$$

Now, the problem is to find dc^*, using eqns. 8.9 and 8.11.

Imagine an increment in c^*. Now ask what increment in stress is necessary to enforce this. Equation 8.4 at matrix-particle separation is

$$\sigma_i = \sigma_i^c = A(c^*)\,\sigma_0 + \frac{\Sigma_H}{(1-f)} \tag{8.15}$$

c^* can be determined (numerically) from this equation. Impose a variation on c^* and find how the other quantities must vary to maintain the separation

condition:

$$d(\sigma_i^c) = 0 = \left.\frac{dA}{dc}\right|_{c^*} dc^* \cdot \sigma_o + A(c^*)\, d\sigma_o + d\left(\frac{\Sigma_H}{1-f}\right) \qquad (8.16)$$

For a hardening material;

$$\sigma_o = f(\bar{\varepsilon}), \quad d\sigma_o = h(\bar{\varepsilon})\, d\bar{\varepsilon} \qquad (8.17)$$

Using the above and eqn. 8.14, eqn. 8.16 becomes

$$0 = -\frac{dA}{dc^*}\frac{\Gamma\left(\frac{c^*}{\bar{c}}+1\right)}{0.4412}\sigma_o\, df|_{nucl} + A(c^*)\, h\, d\bar{\varepsilon} + d\left(\frac{\Sigma_H}{1-f}\right) \qquad (8.18)$$

$$df|_{nucl} = \frac{0.4412}{\Gamma\left(\frac{c^*}{\bar{c}}+1\right)}\frac{1}{\frac{dA}{dc^*}}\left[A(c^*)\frac{h}{\sigma_o}\, d\bar{\varepsilon} + \frac{1}{\sigma_o}\, d\left(\frac{\Sigma_H}{1-f}\right)\right]$$

(It is noted that the last term can itself be a linear function of df/nucl . This will be taken into account shortly.)

Equations 8.18 and 8.2 can be combined into the following general form:

$$df|_{nucl} = M_1\, d\bar{\varepsilon} + M_2\, d\left(\frac{\Sigma_H}{1-f}\right) \qquad (8.19)$$

For the model based on Gurland's results,

$$M_1 = \text{constant w.r.t. } \bar{\varepsilon}, \quad M_2 = 0 \qquad (8.20)$$

In order to make all the terms in eqn. 8.18 readily calculable, and to identify all coefficients of $df|_{nucl}$, the last term should be expanded:

$$d\left(\frac{\Sigma_H}{1-f}\right) = \frac{d\Sigma_H}{1-f} + \frac{\Sigma_H}{(1-f)^2}\,df \tag{8.21}$$

$$= \frac{d(\sigma_o T_H)}{(1-f)} + \frac{\sigma_o T_H}{(1-f)^2}\left(df|_{growth} + df|_{nucl}\right)$$

Using eqns. 7.3 and 7.12, this becomes

$$d\left(\frac{\Sigma_H}{1-f}\right) = \frac{\sigma_o\, dT_H}{1-f} + \frac{T_H}{(1-f)}\,h(\bar{\varepsilon})\,d\bar{\varepsilon} \tag{8.22}$$

$$+ \frac{\sigma_o T_H}{(1-f)^2}\left[(1-f)\,dE_{kk} + df|_{nucl}\right]$$

The term dT_H can be expressed in terms of df if enough is known about the relationship between the first two invariants of macroscopic stress. Express the yield function as

$$\phi = \phi(T_{eqv}, T_H, f) \tag{8.23}$$

Then, consistency gives

$$\delta\phi = 0 = \frac{\partial\phi}{\partial T_{eqv}}\,dT_{eqv} + \frac{\partial\phi}{\partial T_H}\,dT_H + \frac{\partial\phi}{\partial f}\,df, \tag{8.24}$$

$$\left[\frac{\partial\phi}{\partial T_{eqv}}\,\frac{dT_{eqv}}{dT_H} + \frac{\partial\phi}{\partial T_H}\right]dT_H + \frac{\partial\phi}{\partial f}\,df = 0$$

The term dT_{eqv}/dT_H is known, for instance, in the example given in chapter 7 (eqn. 7.4).

It is thus possible to write down a complete expression for df/nucl , which depends on c^* , $\bar{c}$, A(c) , the stress state, the yield function, and Λ . For the critical stress criterion,

$$M_2 = \frac{0.4412}{\Gamma\left(\frac{c^*}{\bar{c}}+1\right)} \frac{1}{\frac{dA}{dc^*}} \cdot \frac{1}{\sigma_o} , \quad M_1 = M_2 \cdot A(c^*) \cdot h \tag{8.25}$$

Equations 8.24, 8.22, and 8.19 can then be used to obtain

$$df\Big|_{nucl} = \left[\frac{1}{M_2 \sigma_o} - \frac{1}{(1-f)_o} \left(\frac{d T_H}{df} + \frac{T_H}{(1-f)} \right) \right]^{-1} \cdot \Lambda \times$$

$$\left[\left(\frac{M_1}{M_2 \sigma_o} + \frac{T_H}{(1-f)} \frac{h}{\sigma_o} \right) T_{ij} \phi_{,\Sigma_{ij}} + \frac{1}{(1-f)} \left(\frac{d T_H}{df} + \frac{T_H}{(1-f)} \right) (1-f) \phi_{,\Sigma_{kk}} \right] \tag{8.26}$$

A quantity which must be known to carry out the above calculation for the critical stress criterion (see eqn. 8.9) is the ratio of the critical interfacial stress to the initial matrix tensile yield stress,

$$\frac{\sigma_i^c}{\sigma_o^*}$$

This allows calculation of $A(c^*)$, and thus (by numerical means),

$$c^* \quad and \quad \frac{dA}{dc^*}$$

A range of values considered reasonable for the stress ratio is

$$1 < \frac{\sigma_i^c}{\sigma_o^*} < 6 \tag{8.27}$$

This is based on data from [12] and [20]. The references reported strain to void nucleation, from which α_i^c can be inferred. Iron and copper alloys were considered.

Some results of calculations using eqn. 8.26 are shown in figs. 27 and 28. The quantities plotted are

$$\frac{df|_{nucl}}{df|_{growth}} \quad vs. \quad \frac{\sigma_o}{\sigma_o^*} \text{ , or } \frac{\bar{\epsilon}}{\bar{\epsilon}_y}$$

The geometry considered was plane strain, with parallel cylindrical voids and particles oriented in the direction of zero strain. The transverse stress is zero, and the boundary conditions are in terms of $\dot{E}_{22}$:

$$\dot{E}_{33} = 0, \; T_{11} = 0, \; \dot{E}_{22} = known, \; \Lambda = \frac{\dot{E}_{22}}{\phi, \Sigma_{22}} \qquad (8.28)$$

Each graph is for constant values of f and $\bar{c}$, and each line is for a constant stress ratio. Calculations are carried out for both fully plastic and rigid wedge yield functions.

9. Yield Function and Plastic Potential with Void Nucleation

It has been shown that, prior to the consideration of void nucleation as a mechanism for porosity increase, the yield function could be used as a plastic potential (see, for example, eqn. 7.1). In this chapter, the effects of void nucleation on this dual purpose of the yield function are examined.

First, it would be wise to define the two quantities separately. A plastic potential is a function which defines the direction of plastic flow, given a state of stress sufficient for yield. (In hardening materials, it also gives the magnitude of plastic flow, via consistency.) In eqns. 7.1 and 7.16, ϕ is used as a plastic potential. A yield function defines the locus of points in stress space for which the aggregate, at a certain state of deformation, will first attain plastic yield. For a more detailed discussion, see chapter 2 of ref. [1].

The major difference between void nucleation (critical stress criterion) and void growth as mechanisms for porosity increase can be seen from eqns. 8.18 and 7.3. A component of $df|_{nucl}$ is dependent directly on the change in stress; it is independent of the magnitude of the plastic flow increment. In contrast, an increment of void growth is a homogeneous and linear function of Λ.

One might ask if the plastic potential changes when the void nucleation mechanism is included. This question can be answered by considering the proof of normality given in chapter 2. The rate of deformation tensor $\dot{\underset{\sim}{E}}$ is proven to lie normal to the locus of those stresses defined by

$$\Sigma_{ij} = \frac{\partial \dot{W}}{\partial \dot{E}_{ij}} \quad \text{where} \quad \dot{W} = \frac{1}{V}\int_V S_{kl}(\dot{\underset{\sim}{E}})\,\dot{e}_{kl}\,dV \tag{9.1}$$

It is postulated that if the void nucleation mechanism does not change any of

these quantities, then ϕ as a plastic potnetial will remain unchanged. The key quantity above is

$$\dot{\underset{\sim}{\epsilon}}_1 = \dot{\underset{\sim}{\epsilon}}\left(\dot{E}, f\right) \tag{9.2}$$

$\dot{\underset{\sim}{\epsilon}}$ is not a function of the rate of change of f. Because nucleation does not affect the current value of f, but only its rate of change, the plastic potential is unchanged by nucleation.

The yield function, however, does change. Consider an aggregate of work hardening matrix, voids, and rigid inclusions, of the type described in chapter 8. If the aggregate is at yield, it is interesting to compare the tangent to the yield function and the tangent to the plastic potential. These tangents can be put in terms of the first two stress invariants:

$$\text{tangent} = \frac{d\Sigma_{eqv}}{d\Sigma_H}, \quad d\Sigma_H = \frac{1}{3} d\Sigma_{nn} \tag{9.3}$$

To find the tangent, write the consistency relation in terms of these two stress variables, with nucleation taken into account (a portion of df is now a function of $d\underset{\sim}{\Sigma}$). Write the increment in df as follows:

$$df = a_{f1}\, d\Sigma_{eqv} + a_{f2} d\Sigma_H + a_{f3}\, d\Lambda \tag{9.4a}$$

$$\text{or,} \quad df = b_{ij}\, d\Sigma_{ij} + a_{f3}\, d\Lambda \tag{9.4b}$$

The a_{fi} and b_{ij} are differential coefficients, and will be determined later. Consistency is now written

$$\delta\phi(\Sigma_{eqv}, \Sigma_H, f) = 0$$

$$= \left(\phi_{,\Sigma_{eqv}} + \phi_{,f}\, a_{f1}\right) d\Sigma_{eqv} + \left(\phi_{,\Sigma_H} + \phi_{,f}\, a_{f2}\right) d\Sigma_H \qquad (9.5)$$

$$+ \left(\phi_{,\sigma_o}\, \sigma_o\, \bar{\varepsilon}_{,\Lambda} + \phi_{,f}\, a_{f3}\right) d\Lambda$$

where commas indicate partial differentiation. When moving along the yield function of a hardening material, no plastic flow takes place, so $d\Lambda = 0$. The tangent to the yield function is thus

$$\frac{d\Sigma_{eqv}}{d\Sigma_H} = \frac{-\left(\phi_{,\Sigma_H} + \phi_{,f}\, a_{f2}\right)}{\left(\phi_{,\Sigma_{eqv}} + \phi_{,f}\, a_{f1}\right)} \qquad (9.6)$$

Note that for the critical stress criterion developed in chapter 8,

$$a_{f1} = 0$$

The plastic potential is simply the yield function with nucleation ignored, so its tangent is

$$\frac{d\Sigma_{eqv}}{d\Sigma_H} = \frac{-\phi_{,\Sigma_H}}{\phi_{,\Sigma_{eqv}}} \qquad (9.7)$$

Some examples of the two tangents, and the differences between them, are shown in fig. 29.

Using eqn. 8.19, the differential coefficients in eqn. 9.4 can be found as follows:

$$df = a_{f3}\,d\Lambda + b_{ij}\,d\Sigma_{ij}\,, = a_{f1}\,d\Sigma_{eqv} + a_{f2}\,d\Sigma_H + a_{f3}\,d\Lambda$$

$$= df|_{growth} + df|_{nucl} \qquad (9.8a)$$

$$= (1-f)\,dE_{kk} + M_1\,d\bar{\varepsilon} + M_2\,d\left(\frac{\Sigma_H}{1-f}\right)$$

$$df\left(1 - \frac{M_2\Sigma_H}{(1-f)^2}\right) = \left[(1-f)\,\phi_{,\Sigma_{kk}} + M_1\,\frac{T_{ij}\,\phi_{,\Sigma_{ij}}}{(1-f)}\right]d\Lambda \qquad (9.8b)$$

$$+ \frac{M_2}{(1-f)}\,d\Sigma_H$$

where $d\Sigma_H = \frac{1}{3}\,\delta_{ij}\,d\Sigma_{ij}$

The bond between matrix and particle involves surface effects, such as wetting. It is therefore reasonable to assume that $df|_{nucl}$ can never be negative. Therefore, if eqn. 8.19 gives a negative value of $df|_{nucl}$, it should be reset to zero. Matching coefficients for $df|_{nucl} > 0$ gives

$$a_{f1} = 0, \quad b_{ij} = \frac{1}{3}\,a_{f2}\,\delta_{ij}$$

$$a_{f2} = \left(1 - \frac{M_2\Sigma_H}{(1-f)^2}\right)^{-1}\frac{M_2}{(1-f)} \qquad (9.9a)$$

$$a_{f3} = \left(1 - \frac{M_2\Sigma_H}{(1-f)^2}\right)^{-1}\left[(1-f)\,\phi_{,\Sigma_{kk}} + M_1\,\frac{T_{ij}\,\phi_{,\Sigma_{ij}}}{(1-f)}\right]$$

For $df|_{nucl} = 0$,

$$a_{f1} = a_{f2} = b_{ij} = 0,$$
$$a_{f3} = (1-f)\,\phi_{,\Sigma_{kk}} \tag{9.9b}$$

Given a state of yield, any stress increment pointing outside the yield surface will cause plastic flow. This includes increments which lie between the (nucleation) yield surface and the plastic potential, which would cause unloading if nucleation was not considered. Nucleation also affects the consistency relation, and thus the value of $d\Lambda$ for a given $d\underset{\sim}{\Sigma}$:

$$\phi = \phi(\Sigma_{ij}, \sigma_o, f) = 0$$
$$\delta\phi = 0 = \phi_{,\Sigma_{ij}} d\Sigma_{ij} + \phi_{,\sigma_o} d\sigma_o + \phi_{,f}\left(a_{f3}\, d\Lambda + b_{ij}\, d\Sigma_{ij}\right) \tag{9.10}$$
$$= \left(\phi_{,\Sigma_{ij}} + \phi_{,f}\, b_{ij}\right) d\Sigma_{ij} + \left(\phi_{,\sigma_o} h\, \bar{\varepsilon}_{,\Lambda} + \phi_{,f}\, a_{f3}\right) d\Lambda$$

For no plastic flow ($d\Lambda = 0$) , $d\underset{\sim}{\Sigma}$ must move along the yield function. Equation 9.10 then shows that the tensor $\underset{\sim}{Q}$ is normal to the yield function in stress space, where

$$Q_{ij} = \frac{\partial\phi}{\partial\Sigma_{ij}} + \frac{\partial\phi}{\partial f}\, b_{ij} \tag{9.11}$$

By neglecting nucleation, it can be shown that the tensor $\underset{\sim}{N}$ is normal to the plastic potential, where

$$N_{ij} = \frac{\partial\phi}{\partial\Sigma_{ij}} \tag{9.12}$$

The quantities in eqn. 9.9 are functions of current state, and not of increments in $\underset{\sim}{\Sigma}$ or $\underset{\sim}{E}$. Therefore, when eqn. 8.19 becomes negative, a_{f3} and the b_{ij} change abruptly, and a vertex in the yield function is formed. To locate this vertex, examine $df|_{nucl}$ for movement along the yield function. Using $d\Lambda = d\bar{\varepsilon} = df|_{growth} = 0$, eqns. 8.19 and 8.21 become

$$df|_{nucl} = M_2\, d\left(\frac{\Sigma_H}{1-f}\right), \tag{9.13}$$

$$= \frac{d\Sigma_H}{(1-f)}\left[\frac{1}{M_2} - \frac{\Sigma_H}{(1-f)^2}\right]^{-1}$$

Equation 8.25 shows that for all but the most unusual cases, the quantity in square brackets is positive. Then, $df|_{nucl}$ becomes negative (and is therefore set to zero) when the increment $d\Sigma_H$ is negative. The vertex is therefore at the current yield stress state. As shown by eqn. 9.11 with $b_{ij} = 0$, the branch for which $d\Sigma_H < 0$ is coincident with the plastic potential. The direction of the other branch is defined by $\underset{\sim}{Q}$, when $b_{ij} > 0$. See fig. 30.

Note that this is a vertex in the yield function, and not in the plastic potential. The importance of the distinction will be made apparent in chapter 10.

10. Flow Localization

Ductile fracture on a macroscopic level is sometimes observed to occur via the localization of plastic flow in a band of concentrated deformation. In this chapter, a method is presented which predicts this localization in terms of the constitutive behavior of a porous rigid-plastic material. The method is based on some recent work by Rice [45], and thus draws on the work of Berg [3,4], and Hill [55]. In this method, a body with boundary conditions compatible with a homogeneous macroscopic flow field is considered. Conditions are sought for which the flow field is allowed to localize in a band, while still meeting the boundary conditions, obeying compatibility, and obeying conditions imposed by continuing stress equilibrium. The band of localized flow is presumed to be planar. As a first approximation, the localization for this simple case is presumed to apply to cases where the boundary conditions demand nonhomogeneous flow fields.

Consider an aggregate of rigid-work hardening matrix and voids, but no rigid inclusions (coinciding yield function and plastic potential). Using N_{ij} as defined in eqn. 9.12, the flow rule (constitutive law) given in eqn. 7.1 can be rewritten as

$$\dot{E}_{ij} = \frac{1}{H} \frac{N_{ij}\left(N_{kl} \overset{\nabla}{\Sigma}_{kl}\right)}{N_{rs} N_{rs}} , = \Lambda N_{ij} \tag{10.1}$$

H is a macroscopic hardening parameter, not to be confused with the intermediate variable used in eqns. 5.64-5.65, and 6.27-6.30. It relates the rate of deformation $\dot{\underset{\sim}{E}}$ to the component of $\overset{\nabla}{\underset{\sim}{\Sigma}}$ which lies normal to the yield function-plastic potential. $\overset{\nabla}{\Sigma}_{kl}$ is the corotational stress rate. It is used here because large rates of rotation are expected in the incipient band, once localiza-

tion starts. (For a detailed explanation see, for example, ref. [57].) The corotational stress rate is

$$\overset{\nabla}{\Sigma}_{ij} = \dot{\Sigma}_{ij} - \Sigma_{ip}\,\Omega_{pj} - \Sigma_{jp}\,\Omega_{pi} \qquad (10.2)$$

$$\text{where } \Omega_{ij} = \frac{1}{2}\left(\frac{\partial V_j}{\partial x_i} - \frac{\partial V_i}{\partial x_j}\right)$$

Ω_{ij} is the rotation tensor, V_i are components of the macroscopic velocity vector (not to be confused with the V_i in ch. 5b), and x_i are rectangular cartesian spacial coordinates.

Now, consider the hypothetical band which contains the incipient nonhomogeneous velocity field (fig. 31a). For convenience, the 2 axis is oriented normal to the band. Where Δ indicates the difference between a quantity inside and outside band,

$$\Delta(\,) = (\,)\big|_{inside} - (\,)\big|_{outside} \qquad (10.3)$$

compatibility requires that

$$\Delta\left(\frac{\partial V_i}{\partial x_j}\right) = g_i(x_2)\,\delta_{j2} \qquad (10.4)$$

The $g_i(x_2)$ are functions of x_2 which have not yet been defined. (Examples of violations of eqn. 10.4 are given in fig. 31b.) The difference in rate of deformation between the inside and outside of the band is thus

$$\Delta\dot{E}_{ij} = \frac{1}{2}\left(g_i(x_2)\,\delta_{j2} + g_j(x_2)\,\delta_{i2}\right) \qquad (10.5)$$

Using this, and eqn. 10.1, it can be seen that the kinematical condition for localization can be met only if

$$N_{11} = N_{33} = N_{31} = N_{13} = 0 \; , \tag{10.6}$$

there is no extension in the plane of the incipient band. When the plastic potential is smooth, the N_{ij} are functions of the past history and the current stress state, and not a function of any current rates of change. Therefore, eqn. 10.1 gives

$$\Delta \dot{E}_{ij} = \frac{1}{H} N_{ij} \left(N_{kl} \Delta \overset{\nabla}{\Sigma}_{kl} \right) \tag{10.7}$$

(The effects of vertices in the plastic potential will be discussed later.) Using eqn. 10.6 and symmetry, the quantity in parentheses becomes

$$N_{kl} \Delta \overset{\nabla}{\Sigma}_{kl} = 2 N_{21} \Delta \overset{\nabla}{\Sigma}_{21} + N_{22} \Delta \overset{\nabla}{\Sigma}_{22} + 2 N_{23} \Delta \overset{\nabla}{\Sigma}_{23} \tag{10.8}$$

where, from eqns. 10.2 and 10.4,

$$\begin{aligned} \Delta \overset{\nabla}{\Sigma}_{2j} &= \Delta \dot{\Sigma}_{2j} - \Sigma_{2p} \Delta \Omega_{pj} - \Sigma_{jp} \Delta \Omega_{p2} \\ &= \Delta \dot{\Sigma}_{2j} + \tfrac{1}{2} \Sigma_{2p} \left(g_p \delta_{j2} - g_j \delta_{p2} \right) + \tfrac{1}{2} \Sigma_{jp} \left(g_p - g_2 \delta_{p2} \right) \end{aligned} \tag{10.9}$$

(Up to the inception of localization, the stresses inside and outside the band are equal.)

Consider stress equilibrium in the direction normal to the band:

$$\frac{\partial \Sigma_{ij}}{\partial x_i} = 0 \tag{10.10}$$

When this is considered in terms of a jump from inside to outside the band, and the time derivative applied, it becomes (see ref. [45])

$$\Delta \dot{\Sigma}_{2j} = 0 \tag{10.11}$$

Equations 10.9 then become

$$\begin{aligned} \Delta \overset{\nabla}{\Sigma}_{21} &= -\tfrac{1}{2}(\Sigma_{22} - \Sigma_{11})\, g_1 + \tfrac{1}{2}\Sigma_{13}\, g_3 \\ \Delta \overset{\nabla}{\Sigma}_{22} &= \Sigma_{21}\, g_1 + \Sigma_{23}\, g_3 \\ \Delta \overset{\nabla}{\Sigma}_{23} &= -\tfrac{1}{2}(\Sigma_{22} - \Sigma_{33})\, g_3 + \tfrac{1}{2}\Sigma_{31}\, g_1 \end{aligned} \tag{10.12}$$

Equation 10.8, and thus the $\Delta \dot{E}_{2j}$, then become functions only of the $g_i(x_2)$, the current stress state, and the yield function. Two crucial points in the procedure were; 1) the use of compatibility to establish that the incipient band is a plane of zero extension, and 2) the use of continuing equilibrium across the band to eliminate the time derivatives on the right side of eqn.10.9.

For simplicity, define the normalized tensor components

$$N^*_{ij} = \frac{N_{ij}}{N_{rs} N_{rs}} \tag{10.13}$$

Now, eqns. 10.5 and 10.7 can be combined to give

$$\begin{aligned} \Delta \dot{E}_{21} &= \tfrac{1}{2} g_1 = \frac{1}{H} N^*_{21} \left(N^*_{kl}\, \Delta \overset{\nabla}{\Sigma}_{kl} \right) \\ \Delta \dot{E}_{22} &= g_2 = \frac{1}{H} N^*_{22} \left(N^*_{kl}\, \Delta \overset{\nabla}{\Sigma}_{kl} \right) \\ \Delta \dot{E}_{23} &= \tfrac{1}{2} g_3 = \frac{1}{H} N^*_{23} \left(N^*_{kl}\, \Delta \overset{\nabla}{\Sigma}_{kl} \right) \end{aligned} \tag{10.14}$$

These are three linear equations in the g_i , with coefficients in terms of the known quantities $\underset{\sim}{\Sigma}$ and $\underset{\sim}{N}^*$. The homogeneous matrix equation

$$\left[M_{ij} \right] \left\{ \begin{matrix} g_1 \\ g_2 \\ g_3 \end{matrix} \right\} = 0 \qquad (10.15)$$

this arises. When the determinant of [M] (det[M]) is nonzero, the only solution for the g_i are zero. When det[M] is zero, however, nonzero g_i are possible while the velocity field still meets the boundary conditions, and obeys compatibility and equilibrium. Therefore,

$$det\,[M] = 0 \qquad (10.16)$$

is taken as the localization condition. It establishes critical values of H (called H_{CR}) , for which bands of localized deformation will form.

The calculation is straightforward but rather tedious, so it will not be carried out here. (One way to simplify the calculation without loss of generality is to rotate the axes in the band such that $N_{23} = 0$. Because N_{13} is zero due to kinematic conditions, this means that the new 3 axis is a principle axis of $\underset{\sim}{N}$.) The result of the calculation, with the above rotation carried out, is

$$H^2 \left\{ \tfrac{1}{2} H - N_{21}^* \left[\Sigma_{21} N_{22}^* - (\Sigma_{22} - \Sigma_{11}) N_{21}^* \right] \right\} = 0 \qquad (10.17)$$

One obvious solution for the critical hardening rate is $H_{CR} = 0$. The proper solution is, however, the most positive solution, because this will be reached first in the stress-strain history. Sometimes, this is greater than zero.

To investigate this, first put eqn. 10.17 in terms of the principal axes of $\underset{\sim}{\Sigma}$ and $\underset{\sim}{N}^*$. These need not be the same when anisotropic plasticity is considered. For simplicity, assume that the principal (3) axis of $\underset{\sim}{\Sigma}$ and $\underset{\sim}{N}$ coincide. Then the principal axis systems of $\underset{\sim}{\Sigma}$ and $\underset{\sim}{N}$ can be reached, respectively, by CCW rotations of θ and ψ around the 3 axis from the plane of zero extension (fig. 32). Using the fact that $N^*_{11} = 0$, and denoting principal values by Roman numerals, eqn. 10.17 becomes

$$H^2\left\{\frac{1}{2}H + \frac{1}{4}\sin(2\psi)(N^*_{II} - N^*_I)^2 \sin[2(\theta-\psi)](\Sigma_{II} - \Sigma_{II})\right\} = 0 \qquad (10.18)$$

It is noteworthy that $H_{CR} = 0$ is the only solution when either of the following is true: 1) The principal axes of $\underset{\sim}{\Sigma}$ and $\underset{\sim}{N}$ coincide ($\theta = \psi$). This occurs when the material is isotropic, or when the anisotropy and $\underset{\sim}{\Sigma}$ meet certain symmetry conditions. 2) The highly symmetric cases, $N^*_{II} = N^*_I$, or $\Sigma_{II} = \Sigma_I$. A detailed discussion of anisotropic plasticity, albeit for incompressible materials, can be found in chapter 12 of ref. [1].

It is instructive to examine the possible magnitude of H_{CR} as predicted by eqn. 10.18, using the following simple example (plane strain, small f, no dilatation):

$$\psi = \frac{\pi}{4}$$

$$N^*_I = -N^*_{II} = -\frac{1}{\sqrt{2}}, \quad (N^*_{II} - N^*_I)^2 = 2 \qquad (10.19)$$

$$\Sigma_I = 0, \quad \Sigma_{II} = \frac{2}{\sqrt{3}}\Sigma_{equ} \sim \frac{2}{\sqrt{3}}\sigma_o$$

$$\psi > \theta$$

This gives

$$\frac{H_{CR}}{\sigma_o} = \frac{2}{\sqrt{3}} \sin\left[2(\psi - \theta)\right] \tag{10.20}$$

This should represent a maximum, because increased dilation should decrease both $(N^*_{II}-N^*_I)^2$ and $(\Sigma_{II}-\Sigma_I)$.

When the stress dependent void nucleation mechanism (chapter 9) is added, the constitutive law must be changed to

$$\dot{E}_{ij} = \frac{1}{H} N^*_{ij} \left(Q^*_{kl} \overset{\nabla}{\Sigma}_{kl} \right), \quad = \Lambda N_{ij} \tag{10.21}$$

where the Q^*_{ij} are normalized components of Q (as in eqn. 10.13). In carrying out an analysis similar to that which lead to eqn. 10.14, one arrives at

$$\Delta \dot{E}_{ij} = \frac{1}{2}\left(g_i \delta_{j2} + g_j \delta_{i2}\right) = \frac{1}{H} N^*_{ij} \left(Q^*_{kl} \, \Delta \overset{\nabla}{\Sigma}_{kl} \right) \tag{10.22}$$

Carrying the analysis further leads to vastly different results. Because the Q^*_{ij} (i and j not equal to 2) are not identically zero due to kinematics (the N^*_{ij} are; eqn. 10.6), the sum

$$Q^*_{kl} \, \Delta \overset{\nabla}{\Sigma}_{kl}$$

is not homogeneous in the g_i. The sum contains stress rate terms other than those in eqns. 10.12. The matrix equation for the g_i thus becomes

$$\left[\; M_{ij} \; \right] \left\{ \begin{matrix} g_1 \\ g_2 \\ g_3 \end{matrix} \right\} = \left\{ \begin{matrix} \text{some nonzero} \\ \text{functions of } \Delta \overset{\nabla}{\Sigma}_{ij} \end{matrix} \right\} \tag{10.23}$$

Therefore, there is always a nonzero solution for the g_i, no matter what the hardening rate is. It is therefore predicted that localization occurs immediately, at first yield.

This is an important example of the failure of the rigid-plastic model to predict the behavior of more realistic elastic-plastic materials. One does not expect all of these materials to experience flow localization at first yield. The reason for this failure is that all of the $\Delta\overset{\nabla}{\Sigma}_{ij}$ in the incipient band are not expressible in terms of the $\Delta\dot{E}_{ij}$ (the g_i). Put another way, the flow rules (eqns. 10.21 and 10.7) are not invertible. $\Delta\dot{\underset{\sim}{E}}$ is related only to the component of $\Delta\overset{\nabla}{\underset{\sim}{\Sigma}}$ which is normal to the yield function. In contrast, an elastic-plastic model will give an invertible flow rule, so the stress rates can be expressed directly in terms of the strain rates. This is the approach taken in a recent paper [56] by Rudnicki and Rice:

$$\overset{\nabla}{\Sigma}_{ij} = \mathcal{L}_{ijkl}\dot{E}_{kl} \tag{10.24}$$

$$\text{and} \quad \Delta\overset{\nabla}{\Sigma}_{ij} = \mathcal{L}_{ijkl}\Delta\dot{E}_{kl}, = \mathcal{L}_{ijk2}g_k$$

$\mathcal{L}_{ijkl}$ is the constitutive matrix. Writing eqns. 10.12 as

$$\Delta\overset{\nabla}{\Sigma}_{ij} = R_{jk}g_k \tag{10.25}$$

linear homogeneous equations in the g_i result:

$$\left[\mathcal{L}_{ijk2} - R_{jk}\right]\left\{g_k\right\} = 0 \tag{10.26}$$

The localization condition is thus

$$\det\left[\mathcal{L}_{ijk\ell} - R_{jk}\right] = 0 \tag{10.27}$$

In ref. [56], the authors examine the localization behavior of isotropic elastic-plastic models with smooth yield functions, and models whose yield functions develop vertices. For the isotropic-smooth yield function model, they find that the corotational terms R_{ij} produce only very small corrections to the critical value of H. This is because the R_{ij} are on the order of stress, while the $\mathcal{L}_{ijk\ell}$ are on the order of the elastic moduli. Using $R_{ij} = 0$, they arrive at the following:

$$\frac{H_{CR}}{G} = \frac{(1+\nu)}{9(1-\nu)}(\beta - \mu)^2 - \frac{(1+\nu)}{2}\left(\frac{\sqrt{3}\,\Sigma'_{II}}{\Sigma_{eqv}} + \frac{\beta+\mu}{3}\right)^2 \tag{10.28}$$

where Σ'_{II} is the intermediate principal deviatoric stress, G is the elastic shear modulus, and ν is Poisson's ratio. μ and β are related to the tangents to the yield function and the plastic potential as follows:

$$\mu = \frac{1}{\sqrt{3}}\frac{d\Sigma_{eqv}}{d\Sigma_H} \quad \text{for the yield function}$$

$$\beta = \frac{1}{\sqrt{3}}\frac{d\Sigma_{eqv}}{d\Sigma_H} \quad \text{for the plastic potential} \tag{10.29}$$

For the case of the yield function and plastic potential being the same function ($\beta=\mu$), eqn. 10.28 predicts that H_{CR} is nonpositive, and zero only for a suitably chosen stress state. (When there is no dilation, so $\beta = \mu = 0$, this stress state corresponds to that for plane strain when the matrix is a Von Mises

material.) Recall that eqn. 10.18 predicts $H_{CR} = 0$, independent of Σ'_{II}, for an isotropic rigid plastic model where $\underline{\mu} = \beta$. Therefore, where $\underline{\mu} = \beta$ and the hardening behaviors are the same, an elastic plastic isotropic material is more resistant to flow localization than a rigid-plastic isotropic material.

Consider what happens if one attempts to predict rigid-plastic behavior from eqn. 10.28, by letting G approach infinity. For cases other than when the right-hand side is zero, this will mean

$$H_{CR} \longrightarrow \pm\infty \tag{10.30}$$

When $\beta = \underline{\mu}$, only the negative value is possible, and flow localization could never occur.

It is instructive to examine the range of H_{CR} predicted by eqn. 10.28 for some physically reasonable values of the arguments. For instance, for mild steel, the following are reasonable:

$$G = 10^7, \quad \sigma_o^* = 5\times10^4 \text{ psi}, \quad \nu = 0.3 \tag{10.31}$$

$$\therefore \frac{H}{\sigma_o^*} = 200\cdot\frac{H}{G}$$

For low levels of triaxiality (not much greater than Σ_{eqv}), the fully plastic yield function gives

$$\mu, \beta \simeq O(f) \tag{10.32}$$

where "O(f)" means "order of f". It can also be shown that

$$\sqrt{3}\,\frac{\Sigma'_{II}}{\Sigma_{eqv}} \simeq \begin{cases} \pm \frac{1}{\sqrt{3}} \text{ for axisymmetric stress fields} \\ O(f) \text{ for plane strain, low triaxiality} \end{cases} \quad (10.33)$$

with the values for axial symmetry being the upper and lower limits. Using eqns. 10.28 and 10.31, one arrives at

$$\left|\frac{H_{LR}}{\sigma_o^*}\right| \leq O(200) \text{ for axial symmetry}$$

$$\frac{H_{LR}}{\sigma_o^*} \simeq O(200 \cdot f^2) \text{ for plane strain} \quad (10.34)$$

The results for axial symmetry are certainly suggestive of eqn. 10.30, while the results for plane strain are more suggestive of a critical hardening rate of zero, at least when f is small. It is often found experimentally that axisymmetric specimens are more ductile than plane strain specimens. Equations 10.34 concur with this. The reason for the difference is that in plane strain, the kinematic conditions for flow localization are almost always met (very large dilatation might provide an exception), while in axially symmetric deformation, these conditions are very hard to meet. The only possible plane of zero extension is, by symmetry, the plane perpendicular to the axis. For zero extension in this plane, large amounts of dilatation (and stress triaxiality) are required. (When a specimen is loaded in uniaxial tension, large radial stresses can be generated by a neck, or a circumferential notch.) The level of triaxiality needed for this type of localization can be calculated as follows:

Consider the following general form of the yield function for the isotropic spherical model:

$$\phi = \frac{3}{2} T'_{ij} T'_{ij} + G(T_{kk}, f) = 0 \tag{10.35}$$

For the case of axial symmetry,

$$\dot{E}_{11} = \dot{E}_{22} = \dot{E}_{RR} \tag{10.36}$$

$$T_{11} = T_{22} = T_{RR}, \quad T_{eqv} = T_{33} - T_{11} \quad \text{for} \quad T_{33} \geq T_{11}$$

For a plane of zero extension to exist,

$$\dot{E}_{11} = 0 \longrightarrow \phi_{,T_{11}} = 0 = 3T'_{11} + G_{,T_{11}} \tag{10.37}$$

$$\longrightarrow T_{eqv} = G_{,T_{11}}$$

For the fully plastic yield function, the condition for a plane of zero extension to exist is thus

$$T_{eqv,} = \left[1 + f^2 - 2f\cosh\left(\tfrac{1}{2} T_{kk}\right)\right]^{\frac{1}{2}}, = f \cdot \sinh\left(\tfrac{1}{2} T_{kk}\right) \tag{10.38}$$

When the arguments of the hyperbolic functions are large enough, the approximation

$$\sinh(x) = \cosh(x) = \tfrac{1}{2} e^x \tag{10.39}$$

is valid. Substitution into eqn. 10.38 gives

$$\tfrac{1}{2} T_{kk} = \ln\left(\tfrac{1}{f}\right) - 0.19 \tag{10.40}$$

$$= \tfrac{1}{2} T_{kk}\Big|_{T_{33}=0} - 0.19$$

Numerical solution of eqn. 10.38 for $\frac{1}{2} T_{kk}$ shows that eqn. 10.40 is surprisingly accurate; the error at $f = 0.25$ was less than 0.2%.

When $G(T_{kk}, f)$ is zero, there is no mechanism for dilatation. The above calculations then give the well known result that axisymmetric flow in an incompressible rigid-plastic material can never localize.

The kinematic conditions for flow localization at the neck of a tensile bar require further discussion. Considering the geometry of a cup-cone fracture in an axisymmetric tensile bar of ductile material, it is obvious that flow localization takes place on a conic section. See, for example, ref. [26]. This suggests that a valid generalization of the kinematic condition be that a surface of zero extension exists. The experiments also show that the cup and cone do not extend to the axis of the bar; instead, they flatten out. This central region appears to be due mainly to dilatational instability in a plane perpendicular to the axis, with no shear component. See fig. 33a.

It can be seen from fig. 33b that sliding over closed conic surfaces of zero extension is kinematically inadmissible, while sliding over open conic surfaces is indeed admissible. It is therefore required that for flow localization to occur along the surfaces of zero extension at the neck of a tensile bar, an open region must develop at the axis. Since no sliding is permitted prior to the development of this region, it must develop via a purely dilatational flow localization. This can occur only on the plane perpendicular to the axis, which by symmetry does not require any sliding. Stress conditions at the center of the neck for which that plane is a plane of zero extension are thus required if flow localization is to take place. Once this localization occurs, the center of the neck can be considered voided, and the conic surfaces of zero extension are no longer closed. Localization then takes place on these conic surfaces, and fracture follows immediately.

According to the above interpretation, triaxial stress levels as shown in eqn. 10.40 are required only at the center of the neck to start flow localization. If it were required that a plane of zero extension exist across the entire neck, localization would not occur until enormous amounts of void growth had taken place, and strain to fracture had been greatly overestimated. An analysis of the stresses at the neck of a tensile bar such as that of Bridgman [24] shows that the triaxial stress is greatest at the center, and lowest ($\Sigma_{rr}=\Sigma_{\theta\theta}=0$) at the surface of the neck.

The requirement that a plane of zero extension must form across the neck of an axisymmetric specimen made of porous material may itself be too stringent. The amount of porosity at the neck may itself be large enough to allow sliding along the closed conic surfaces, or adjacent open conic surfaces. If this interpretation is correct, kinematics would be less of a problem, and lower estimates of strain to flow localization (fracture) would result.

So far only models which harden isotropically have been considered. These have subsequent yield functions of the form of eqn. 10.35, so for f held constant, the yield functions at two states of hardening will be geometrically similar. Kineamtic hardening, shape change of the yield function, and the development of vertices have been ignored, because of the added complexity they would introduce. Because their effect can be substantial in some cases, they will be discussed here in a qualitative manner. This may illustrate some of the limitations of the isotropic hardening model when used to study flow localization.

Figures 34a, b, c, and d show schematically what is meant by the four hardening phenomena on the microscale. Plastic incompressibility allows all the information to be contained in π-plane projections. In fig. 34a, the

stress increment is accommodated by expansion of the Mises cylinder. In fig. 34b, the stress increment causes the Mises cylinder to move in the π plane, maintaining its size and shape. In fig. 34c, the initial Mises cylinder changes shape and translates. In fig. 34d, the radial stress increment causes a vertex to form.

Shape change and vertex formation can be explained by considering plastic flow and hardening to take place on individual slip systems, each of which has a separate yield function [56,58]. The total yield function is the intersection of the yield functions of all the slip systems. A given stress increment activates only a fraction of the slip systems, whose selective hardening causes the total yield function to change shape and/or form a sharp vertex.

When a sharp vertex forms at the point of loading, the flow rule no longer gives a unique solution to the direction the plastic flow will take. Instead, the flow direction is bounded by a cone of normals to the surface(s) surrounding the vertex (fig. 35). The direction that the flow takes, within this cone, is determined by the next stress increment, which in turn is influenced by flow localization. The result is that the kinematic conditions for localization can be met if the proper flow direction falls within the cone of normals.

Rudnicki and Rice [56] examine this phenomenon for an elastic-plastic model and find that vertices can raise the value of the critical hardening rate, thus allowing it to be reached earlier in the stress history. Their model is developed for rocks with fissures and individually hardening slip planes, and their calculations seek out the slip plane most likely to accept bifurcation. (Kinematic conditions are in terms of plastic components plus elastic components.) With more slip planes able to meet these conditions due to the vertex, one associated with a more positive value of H_{CR} can often be found.

How could the various hardening phenomena shown in figs. 34 affect the hardening behavior of an aggregate of voids and rigid-plastic matrix? To examine this, recall the relationship between macroscopic and microscopic stress and rate of deformation:

$$\Sigma_{ij} = \frac{1}{V}\int_V S_{kl}(\dot{\underset{\sim}{\epsilon}})\,\frac{\partial \dot{\epsilon}_{kl}}{\partial \dot{E}_{ij}}\,dV \tag{10.41}$$

When the fully plastic spherical model is employed, this becomes

$$\Sigma'_{ij} = \frac{1}{V}\int_V S_{ij}(\dot{\underset{\sim}{\epsilon}})\,dV, \qquad \Sigma_H = -\frac{3}{V}\int_V S_{rr}(\dot{\underset{\sim}{\epsilon}})\,\frac{b^3}{r^3}\,dV. \tag{10.42}$$

Consider a porous body which has undergone some plastic work, and has hardened on the microscale according to figs. 34b, c, or d, and compare the subsequent yield function to one that would result from isotropic hardening (as in fig.34a). For simplicity, consider constant increments of $d\underset{\sim}{\Sigma}$ or $d\underset{\sim}{E}$, giving radial paths in the π plane. Use the endpoints of the yield function in the comparison:

$$\Sigma_{eqv}\Big|_{\Sigma_H=0}, \qquad \Sigma_H\Big|_{\Sigma_{eqv}=0}. \tag{10.43}$$

The hardening parameters (initial yield stress and strain, hardening exponent) should be the same for the individual slip planes and the isotropic model.

For the isotropic model, the yield function should expand with hardening

as before. Neglecting df, this means geometric similarity with a proportionality factor

$$\frac{\sigma_o}{\sigma_o^*}$$

For the kinematic and shape change hardening models, one expects Σ_{eqv} to be a function of orientation. When the $\dot{\underset{\sim}{E}}$ field imposed on the macroscopic stress integrals is such that $\dot{\underset{\sim}{\varepsilon}}(\dot{\underset{\sim}{E}})$ is proportional to the hardening increments, the slip planes which have hardened the most should be used preferentially, and Σ_{eqv} should be maximized. The result should be

$$\Sigma_{eqv}\Big|_{\substack{\Sigma_H=0 \\ max.}} = \Sigma_{eqv}\Big|_{\substack{\Sigma_H=0 \\ isotropic\ hardening}} \tag{10.44}$$

However, the maximum value of Σ_H should behave differently. It is assumed here that despite the anisotropy induced by hardening,

$$\begin{aligned} &\Sigma_{eqv} = 0 \rightarrow \dot{E}_{eqv} = 0, \\ &\Sigma_H\Big|_{\Sigma_{eqv}=0} = \Sigma_H\Big|_{max.} \end{aligned} \tag{10.45}$$

Because an $\dot{\underset{\sim}{E}}$ field which is purely hydrostatic will activate all slip planes equally, one expects an averaging process to take place. This means that

$$\Sigma_H\Big|_{\substack{max \\ kinematic\ hrdn}} < \Sigma_H\Big|_{\substack{max \\ isotropic\ hrdn.}} \tag{10.46}$$

and the two types of subsequent yield functions should appear as in fig. 36.

Note that for a given ratio of Σ_{eqv} to Σ_H, the yield function for kinematic hardening has a steeper slope than that for isotropic hardening. This means that the kinematic condition for flow localization in a band in an axisymmetric specimen would be met at a lower level of Σ_H.

11a. Ductility - Numerical Calculations

The total strain to fracture of a specimen is commonly referred to as its ductility. For tension specimens, the strain measure commonly used is the true longitudinal strain, $\ln(A_o/A)$, where A_o is the original cross-sectional area, and A is the cross-sectional area at fracture. Factors affecting the ductility of a given specimen include its loading or deformation history, and the material response to that history. The material response encompasses the yield function and plastic potential, and the hardening behavior. For each increment in the history, and its associated material response, the conditions for flow localization in a band (fracture) may or may not be met. The strain at which they are first met (E_{fr}) is the measure of ductility used here.

In previous chapters, theories for material response and criteria for flow localization have been developed. In this chapter, they will be combined with various types of histories. The effects on ductility of various parameters in the material theories and the history will then be examined.

Here, the history will be imposed in terms of increments of strain. For each increment, elements of the material response such as void nucleation and growth and matrix hardening will be monitored, using the yield function and plastic potential. Increments of macroscopic stress also result, allowing calculation of the hardening rate H. As can be seen from chapter 10, the critical value of H is a function both of the total and the incremental strain response. For the material models used here, H begins as positive, and grown less positive with each increment of strain. When an increment shows $H \leq H_{CR}$, the conditions for flow localization have been fulfilled, and the calculation is stopped.

Several simplifying assumptions are made to the theories of material behavior. 1) For all the examples carried out here, the void shape is idealized as constant; the incremental change in the void boundary is approximated by its average radial value. (Note that the two void geometries considered were long cylindrical and spherical; more general shapes, such as ellipses or ellipsoids were not studied.) This assumption allows continued use of the yield function for the initial void shape. 2) Isotropic hardening on the microscale (fig.34a) is assumed throughout, and the hardening at any material point is approximated by its average over the matrix. This, together with condition (1), leads to continuation of the aggregate's initial isotropy. 3) Only the simpler yield functions and plastic potentials (eqns. 5.62 and 6.40) are used. It was found that the other approximations did not work well when combined with the isotropy assumption.

The first specimen geometry considered is also the simplest: an aggregate of long parallel cylindrical voids in strain hardening matrix. The aggregate undergoes plane strain deformation, with the axis of zero strain (the 3 axis) coincident with the void axis. No inclusions are present. The aggregate behaves like the two-dimensional model in fig. 37. An increment dE_{22} is specified, and T_{11} is specified (as zero) throughout the history. (Necking is ignored, so the $\underset{\sim}{\Sigma}$ and $\dot{\underset{\sim}{E}}$ fields are homogeneous.) This allows calculation of dE_{11} in terms of dE_{22}. The plane strain condition gives $E_{33} = dE_{33} = 0$. The yield function-plastic potential used for this example is

$$\phi(\Sigma_{ij}, \sigma_o, f) = \tfrac{3}{2}\Sigma'_{ij}\Sigma'_{ij} + 2f\sigma_o^2 \cdot \cosh\left(\tfrac{\sqrt{3}}{2}\Sigma_{rr}/\sigma_o\right) - \sigma_o(1+f^2) = 0$$

$$\text{or, } \tfrac{3}{2}T'_{ij}T'_{ij} + 2f\cdot\cosh\left(\tfrac{\sqrt{3}}{2}T_{zz}\right) - 1 - f^2 = 0 \qquad (11.1)$$

One usually starts with the model specimen in the state of the first yield,

$$\bar{\epsilon} = \bar{\epsilon}_Y , \quad \bar{\epsilon}_p = 0$$
$$\dot{E}^p_{ij} = 0 \tag{11.2}$$

where the superscript p denotes plastic components. (Because this is a rigid-plastic model, these superscripts will now be dropped). The incremental procedure is as follows:

First, impose the increment dU_2 . dE_{22} is then calculated from the current configuration. (In the numerical calculations, this is on the order of 0.01.) The flow rule then allows calculation of $d\Lambda$, and thus dE_{11} :

$$dE_{22} = \frac{dU_2}{L} , \quad \Lambda = \frac{dE_{22}}{\Phi_{,\Sigma_{22}}} , \quad dE_{11} = \Lambda \Phi_{,\Sigma_{11}} \tag{11.3}$$

It can be shown by considering the (two-dimensional) hydrostatic component of $\dot{\underset{\sim}{E}}$; and its associated flow field, that

$$df = (1-f)\left(dE_{11} + dE_{22}\right) \tag{11.4}$$

The average increment of equivalent plastic work in the matrix is found from the increment of macroscopic plastic work, per unit volume of matrix:

$$\sigma_o \, d\bar{\epsilon} = \frac{\Sigma_{ij} \, dE_{ij}}{(1-f)} , \longrightarrow d\bar{\epsilon} = \frac{T_{ij} \, dE_{ij}}{(1-f)} \tag{11.5}$$

In this example, this reduces to

$$d\bar{\epsilon} = \frac{T_{22} \, dE_{22}}{(1-f)} \tag{11.6}$$

T_{22} is found numerically from the yield function, eqn. 11.1 :

$$dE_{33} = 0 \rightarrow T'_{33} = 0 \rightarrow T_{kk} = \frac{3}{2} T_{yy}$$
$$\Phi = 0 \text{ and } T_{11} = 0 \rightarrow \frac{3}{4} T_{22}^2 + 2f \cdot \cosh\left(\frac{\sqrt{3}}{2} T_{22}\right) - 1 - f^2 = 0 \tag{11.7}$$

Given f, T_{22} is found via Newton's method (see, for example, [49]). The average hardening increment in the matrix can then be found:

$$d\sigma_o = h(\bar{\epsilon})\, d\bar{\epsilon} \tag{11.8}$$

The macroscopic hardening rate can be calculated using eqn. 10.1, by evaluating it for pre-localization deformation. This involves no rotation prior to localization, so $\overset{\nabla}{\Sigma}_{ij}$ can be replaced by $\dot{\Sigma}_{ij}$. The time derivatives are then replaced by increments:

$$H = \frac{N^*_{22}}{dE_{22}} \left(N^*_{ij}\, d\Sigma_{ij}\right), \quad d\Sigma_{ij} = d(\sigma_o T_{ij})$$
$$\text{here,} \quad H = \frac{N^*_{22}}{dE_{22}} \left(N^*_{22}\, d\Sigma_{22}\right) = \frac{\phi^2_{,\Sigma_{22}}\, d\Sigma_{22}}{(\phi_{,\Sigma_{ij}}\, \phi_{,\Sigma_{ij}})\, dE_{22}} \tag{11.9}$$

$d\Sigma_{22}$ is found by comparing the current value of Σ_{22} with its value at the previous increment. For this example, a plane of zero extension always exists, and

$$H_{CR} = 0 \tag{11.10}$$

Therefore, flow localization is indicated by a nonpositive value of $d\Sigma_{22}$.

The results of carrying out this incremental process are shown in fig. 38. The horizontal axis is the initial void volume fraction (f_i), and the vertical

axis is ductility. The matrix is modeled as a power law hardening von Mises material;

$$h(\bar{\varepsilon}) = \frac{n}{\bar{\varepsilon}} \;, \quad \frac{\sigma_o}{\sigma_o^*} = \left(\frac{\bar{\varepsilon}}{\bar{\varepsilon}_y}\right)^n \tag{11.11}$$

where n is the strain hardening exponent. Each curve represents the variation of ductility with initial f for a given value of n. In this simple example, necking was ignored. It is expected that necking, by inducing a positive T_{11}, would somewhat reduce the ductility. The effect would increase with strain to fracture, and would thus preferentially affect E_{fr} for lower initial values of f.

The numerical problem of solving for the T_{ij} becomes somewhat more complicated if one wishes to use the fully plastic yield function for an aggregate with spherical voids (eqn. 6.40). Equations analogous to eqns. 11.7 are then, using $dE_{33} = T_{11} = 0$:

$$2T_{33} - T_{22} + f \cdot \sinh\left(\tfrac{1}{2}T_{33} + \tfrac{1}{2}T_{22}\right) = 0 \tag{11.12}$$

$$\tfrac{3}{4}T_{22}^2 + \tfrac{1}{4}\left(2T_{33} - T_{22}\right)^2 + 2f \cdot \cosh\left(\tfrac{1}{2}T_{33} + \tfrac{1}{2}T_{22}\right) - 1 - f^2 = 0$$

These nonlinear simultaneous equations can be solved by a generalization of the method used for eqn. 11.7 (same reference). The rest of the iterative process is identical, and the results are shown in fig. 39. The ductility is higher for a given f_i and n than for the cylindrical model. (When comparing figs. 38 and 39, note the differences in scaling.) For this type of history, it is reasonable that spherical model would exhibit less void growth per increment, and thus higher ductility.

Now, consider an axisymmetric specimen which uses the same (spherical voids) yield function. The specimen is shown in fig. 40. Because the problem is now three-dimensional, the incremental equations differ somewhat from those for plane strain. By symmetry,

$$E_{11} = E_{22} = E_{RR}, \quad T_{11} = T_{22} = T_{RR} \tag{11.13}$$

Increments can be put in terms of dE_{RR} or dE_{33}. Using $dE_{RR} \equiv dE_{11}$,

$$\Lambda = \frac{dE_{11}}{\phi_{,\Sigma_{11}}}, \qquad dE_{33} = \Lambda \phi_{,\Sigma_{33}} \tag{11.14}$$

Equation analogous to eqns. 11.4 through 11.9 are then

$$df = (1-f)(2\,dE_{RR} + dE_{33}) \tag{11.15}$$

$$d\bar{\epsilon} = \frac{(2T_{RR}\,dE_{RR} + T_{33}\,dE_{33})}{(1-f)} \tag{11.16}$$

$$\phi = \tfrac{3}{2} T'_{ij} T'_{ij} + 2f \cdot \cosh\left(\tfrac{1}{2} T_{kk}\right) - 1 - f^2 = 0 \qquad (a)$$

$$\longrightarrow (T_{33} - T_{RR})^2 + 2f \cdot \cosh\left(T_{RR} + \tfrac{1}{2} T_{33}\right) - 1 - f^2 = 0 \qquad (b) \tag{11.17}$$

$$H = \frac{\phi_{,\Sigma_{11}}}{dE_{11}} \frac{(2\phi_{,\Sigma_{11}}\,dE_{11} + \phi_{,\Sigma_{33}}\,dE_{33})}{(2\phi_{,\Sigma_{11}}\phi_{,\Sigma_{11}} + \phi_{,\Sigma_{33}}\phi_{,\Sigma_{33}})} \tag{11.18}$$

Given T_{RR}, eqn. 11.17b can be solved numerically for T_{33}. As before, localization and matrix hardening are characterized by eqns. 11.10 and 11.11.

In a uniaxial tensile specimen, $T_{RR} = 0$ prior to necking. For a first example, incremental ductility calculations were carried out for the axisymmet-

ric geometry with necking ignored throughout the strain history. This was done so that a valid comparison could be made with the plane strain geometry, using the same yield function and localization criterion ($H_{CR} \leq 0$). The results for the axisymmetric specimen are shown in fig. 41. Note that for a given n and initial f, the ductility for the axisymmetric case is always higher. This is in qualitative agreement with experimental results. See, for example, references [30] and [31]. This result is expected in light of the higher hydrostatic stress level caused by the plane strain constraint. (The kinematic conditions discussed in chapter 9 are commonly used to explain this phenomenon when plastic incompressibility is assumed.)

Necking will now be accounted for in the case of the axisymmetric model. Use will be made of the theoretical and experimental work of P. W. Bridgman [24]. In his work, Bridgman developed an approximate solution to the stress distribution at the minimum neck section of a tensile bar, as a function of the radius of curvature at the neck surface. Some later work [40,59,60] has served to verify the accuracy of Bridgman's analysis and its underlying assumptions, provided that any initial notch used to start the neck is not very sharp, or is of a certain geometry. The specimen models used here start with either no neck at all, or a very shallow one. Therefore, the Bridgman analysis is considered acceptable.

The stress distribution is most intense at the center of the minimum neck section, so this is where the localization condition will be applied. For his incompressible plastic model, Bridgman found that the stress state here was (see fig. 42),

$$\sigma_{rr} = \sigma_{33}\big|_{r=a} \cdot \ln\left(\frac{a}{2\rho} + 1\right)$$

$$\sigma_{\theta\theta} = \sigma_{rr}, \quad \sigma_{33} = \sigma_{33}\big|_{r=a} + \sigma_{rr} \tag{11.19}$$

$$\sigma_{33}\big|_{r=a} = \sigma_o$$

In adapting this to a porous material, the simple approximation

$$\Sigma_{33}\big|_{r=a} \simeq \sigma_o(1-f) \tag{11.20}$$

will be used. Thus, the approximation used here will be

$$T_{RR} = (1-f)\ln\left(\frac{a}{2\rho}\right), \quad T_{\theta\theta} = T_{RR} \tag{11.21}$$

T_{33} is then calculated from eqn. 11.17b. This approximation ignores most of the effects of dilatancy. It is felt that the factor (1-f), which approximately carries the weakening effects of the porosity, will be sufficient.

Bridgman gives a good deal of experimental data on the relationship between the nondimentional radius of curvature, and the true strain at the neck of axisymmetric tensile bar

$$\frac{\rho}{a} \text{ vs. } E_1 = 2\ln\left(\frac{a_o}{a}\right) = \ln\left(\frac{A_o}{A}\right) \tag{11.22}$$

The subscript o denotes initial values (prior to any deformation). A is the area of the minimum neck section, and a is the outer radius. The result is given in [24] in an experimental curve fit to the data points. It can be fit

rather well with an empirical equation, the form of which was suggested by Tracey [61]. The following is a slight generalization of that form:

$$\frac{\alpha}{\rho} = 3\left[1 - \exp\left(-0.325\left(E - E_{nk}\right)\right)\right] \quad \text{for } E > E_{nk} \tag{11.23}$$

Where E_{nk} is the value of E at which the specimen starts to neck.

Hutchinson and Miles [62] have investigated the theoretical problem of first necking in an incompressible elastic-plastic axisymmetric tensile bar. They found that for reasonably slender bars, the traditional necking criterion of maximum load is accurate. Here, the maximum load criterion will be applied to a tensile bar of dilatational material. Prior to necking, $T_{RR} = 0$, and $\underset{\sim}{T}$ and $\dot{\underset{\sim}{E}}$ are homogeneous in the specimen. Where P is the axial load, the criterion for inception of necking is

$$dP = 0 = d\left(\Sigma_{33} A\right) = d\left(\sigma_o T_{33} A\right) \tag{11.24}$$

$$0 = d\sigma_o T_{33} A + \sigma_o d T_{33} A + \sigma_o T_{33} dA$$

For this simple stress state, the yield function gives

$$T_{33}^2 + 2f \cdot \cosh\left(\tfrac{1}{2} T_{33}\right) - 1 - f^2 = 0 \tag{11.25}$$

Prior to necking, T_{33} is thus a function only of f. Using this, and some previous developments, eqn. 11.24 can be rewritten as

$$dP = 0 = A\, d\Lambda \left\{ \frac{h(\bar{\varepsilon})\, T_{33}^2}{(1-f)} \phi_{,T_{33}} + \sigma_o \frac{dT_{33}}{df}(1-f)\, \phi_{,\Sigma_{kk}} + \sigma_o T_{33} \cdot 2\, \phi_{,\Sigma_{11}} \right\} \tag{11.26}$$

When the quantity in brackets first becomes nonpositive, necking starts, and

E_{nk} equals the current value of E. After necking, the zero value of T_{RR} is replaced in the incremental equation (11.15 through 11.18) by that value resulting from eqns. 11.21 and 11.23.

When $f = 0$ the material is incompressible and $T_{33} = 1$. Equation 11.25 then becomes

$$0 = A\{h(\bar{\varepsilon})\, dE_{33} + \sigma_0 \cdot 2\, dE_{RR}\}$$
$$= A\, dE_{33}\{h(\bar{\varepsilon}) - \sigma_0\} \qquad (11.27)$$

For power law hardening materials, this gives the familiar result that at necking

$$\sigma_0 \frac{n}{\bar{\varepsilon}} - \sigma_0 = 0, \quad \bar{\varepsilon} = n = \ln\left(\frac{A_0}{A}\right) \qquad (11.28)$$

One effect of porosity, however, is to lessen the rate of work hardening. Where n is the hardening exponent of the matrix, it would be interesting to see how the necking strain for a given value of n varies with the initial value of f. This is shown in fig. 43.

Incremental calculations were carried out in which the model axisymmetric tensile bar was loaded uniaxially until necking commenced, after which the necking correction given above was included. As before, the fracture criterion was $\mu_{CR} = 0$. The results are given in fig. 44. The importance of necking is immediately apparent upon comparison with fig. 42. (Note the difference in scaling.) Necking, and the change in the stress state which it causes, decreases the ductility by approximately a factor of 2 for small $f_i (\approx 0.01)$. The factor falls to approximately 1.4 at $f_i = 0.20$. Variation of n does not seem to have much effect on this factor.

Marshall and Shaw [63] conducted experiments which verify the effect of necking on ductility. They found they could increase the ductility in steel and copper round tensile bars by removing them from the testing apparatus somewhere between inception of necking and fracture, and increasing the ratio ρ/a (fig. 42) by machining in a larger value of ρ. This reduced the hydrostatic stress due to the neck. At fracture, they found that higher values of ρ/a (due to increasing it midway through the test) correlated with higher values of ductility for a given type of specimen.

The next step is to investigate the behavior of an aggregate of rigid-work hardening matrix, voids, and rigid inclusions bonded to the matrix. The particles are assumed to be of equal size, and of the same shape (and orientation, for cylinders) as the voids. Within the orientation limitation, random distribution is assumed. Once a particle cracks or breaks loose from the matrix, it is replaced in the calculations by a void of equal size and shape. The void then grows according to the previously established rules. As before, the localization criterion is $H_{CR} \leq 0$.

Adding the void nucleation mechanism to the incremental calculations is fairly straightforward, because the independent variable is strain, not stress. Interpreting and digesting the results, however, is made much more complicated, because of the extra independent variables which enter the problem. For the nucleation criterion in eqn. 8.7, the extra variables are $\bar{c}$ and σ_1^* and for the type which leads to eqn. 8.26, there are

$$\bar{c} \quad \text{and} \quad \frac{\sigma_i^c}{\sigma_o^*}$$

These are added to the initial value of f (f_i) and the matrix hardening exponent n.

These phenomena are illustrated in figs. 45. Ductility is calculated using the plane strain model with parallel cylindrical voids and rigid particles. As before, necking is neglected. The deformation is homogeneous up to flow localization, which is characterized by $H_{CR} \leq 0$. Each plot is for given values of n and σ_i^c/σ_o^*. Note the abrupt degradation of ductility which occurs when the matrix hardening can no longer balance the softening caused by void nucleation and growth. Also note that this degradation spreads across the entire range of f_i for a rather small range of $\bar{c}$. Dotted lines represent sudden changes in ductility between values of f_i for which ductility was calculated.

Prior to deformation, many engineering materials might be better characterized by the initial particle concentration $(\bar{c}_i)$ then by the parameter f_i. This is the basis of the next series of figures. Each line in figs. 46 represents the ductility for a range of $\bar{c}_i$, with fixed values of n and σ_i^c/σ_o^*, and with $f_i = 0$. The lines represent different classes of histories, and are thus not all similar geometrically (as they are for models with no inclusions). Consider fig. 46a, where $n = 0.2$:

For line 1, σ_i^c is relatively low. Therefore, voids are nucleated very early in the stress-strain history, and macroscopic softening due to nucleation does not occur. The data line is almost identical to that for E_{fr} vs. f_i for $n = 0.2$ in fig. 38. Because of the early nucleation, this would be expected.

For curve 2, σ_i^c is somewhat higher, and nucleation is therefore delayed. For part of the range of $\bar{c}_i$ considered, the nucleation rate at some point in the history becomes large enough to cause macroscopic softening (and thus flow localization). For the lower range of $\bar{c}_i$ where this does not happen, later

nucleation causes a very slight increase in ductility. The dotted line indicates a sudden drop in ductility between values of $\bar{c}_i$ for which E_{fr} is calculated.

For lines 3 and 4, σ_i^c is high enough to delay nucleation until late in the history. There the nucleation process becomes more gradual due to the decrease in the matrix hardening rate. These factors combine to make E_{fr} increase with σ_i^c over the entire range of $\bar{c}_i$. The controlling factor is now the strain prior to significant void nucleation.

Similar results for $n = 0.5$ are shown in fig. 46b. As would be expected, larger values of σ_i^c are required to cover the range of phenomena discussed above. (Again; note that the scale for E_{fr} is different from that in fig. 45a.)

The nucleation criterion which is based on accumulated strain (eqns. 8.7 and 8.8) is obviously much simpler to use than the stress-based criterion discussed above. Because the nucleation rate does not become very large, it is expected that the ductility behavior will also be simpler. It is noteworthy that the data in ref. [19] on which this theory is based is the rate of particle cracking with strain, rather than the rate of matrix particle separation. Therefore, the two criteria may be valid for different types of inclusions.

For simplicity, the numerical examples used here are closely linked with the relevant experiments reported in ref. [19]. The data used in eqns. 8.4 through 8.8 is from tensile tests on axisymmetric specimens, so this is the configuration that is used here. A stress-strain curve given in [19] is interpretad here to give

$$\bar{\epsilon}_y \simeq 0.005, \qquad \sigma_o^* = 4\times10^4 \text{ p.s.i.}$$

$$\frac{\sigma_o}{\sigma_o^*} = \left(\frac{\bar{\epsilon}}{\bar{\epsilon}_y}\right)^n, \quad n \simeq 0.25 \tag{11.79}$$

n was calculated using the stress level at $\bar{\epsilon} = 0.05$. In the numerical examples, n = 0.25 will be used as the matrix hardening exponent throughout the strain history. C_1^* as determined in eqn. 8.8 is most probably a function of the geometry and the parameters in eqn. 11.29. It is therefore felt reasonable only to vary $\bar{c}_i$ in the numerical claculation.

The results are presented in figs. 47. Because of the gradual nature of the nucleation criterion, no sudden decreases in ductility are evident.

11b. Ductility - Comparison with Experiment, Comments on the Theory

Clausing's [30,31] investigations into the properties of structural steels include measurements of ductility (for both axisymmetric and plane strain specimens), hardening exponents, and tensile and yield strengths. As explained previously, the ductility for an axisymmetric specimen is always greater than that for a plane strain specimen of the same material. Clausing's data allows determination of the ratio of axisymmetric to plane strain ductility and its variation with hardening exponent. (Clausing examines its variation with initial yield strength, σ_o^*. One expects low σ_o^* to correlate with high n, and vice versa. This is true for Clausing's data.)

The same ratio and its variation with n can be determined from the numerical data in figs. 39 and 41; ductility in plane strain and axial symmetry for an aggregate of matrix and spherical voids. Necking was ignored in the plane strain case because data similar to Bridgman's (eqn. 11.23) was not available. For consistency, necking was ignored for the axisymmetric case also. The ductility ratio may therefore only be considered as indicative of what might result if necking were included. Remember that the kinematic requirement of a plane of zero extension is ignored in the axisymmetric case.

The numerical ductility ratios are compared to Clausing's data in fig. 48. Clausing's results are marked by full circles, while the numerical data points are connected by straight line segments, each line representing a different value of f_i. The agreement is fair for all but the lowest values of n. Even if necking were included in the numerical models, the added requirement of a plane of zero extension across the neck would have made the ductility ratio

a good deal higher. The comparison suggests that the kinematic requirement does not act to delay flow localization in axial symmetry unless n is rather small.

The isotropic hardening model cannot explain this effect. It can be explained, however, in terms of some simple models of vertex formation (hardening on individual slip planes, [50,57]). Consider materials with different strain hardening exponents, but otherwise identical, subject to a given strain history. Where n is very small, hardening on the slip planes is also small, and the vertex will form at an angle close to 180°. According to the model, the stiffness to tangential components of strain increment decrease only as the vertex sharpens. (For no vertex, this stiffness is on the order of the elastic moduli.) A low value of n therefore means that kinematic conditions which require strain increments with relatively large tangential components will be difficult to satisfy. (By "difficult", it is meant that a large negative H_{CR} is required - see [50].) When n is larger, however, the vertex angle decreases, the tangential stiffness decreases, and the kinematic conditions are easier to satisfy. See fig. 49.

An isotropic hardening model may do a reasonable job of predicting pre-localization flow and hardening behavior, but is less likely to predict localization when the kinematic condition is not easily met. It is therefore felt reasonable to "borrow" the vertex model to predict when flow localization is kinematically admissible. Clausing's data supports the notion that only when n is rather small does the kinematic requirement delay localization in axially symmetric deformation. It is therefore felt reasonable to use the critical

hardening rate as the only localization criterion when $n \gtrsim 0.1$.

Some experimental data with which the numerical calculations can be compared is shown in fig. 50. The lines centered in the scatter bands are marked with the author's initials. Edelson and Baldwin [21] reports ductility in copper-base alloys as a function of the second phase-voids, and a variety of inclusions. (Besides their own work, they include a few results by other authors.) Their specimens were round tensile bars, prepared by mixing powders of the constituents, compressing and scintering, and then machining into final shape. By varying the mixture and the scintering procedure, a wide range of particle or void volume fractions was obtained. They found that ductility was determined more by the volume fraction of the second phase than by the type of second phase. Rostoker and Liu [22] also used a scintering process to prepare their specimens; flat bars made from powdered brass, with various amounts of porosity. Liu and Gurland [29] prepared their round tensile bars from eight different types of vacuum cast carbon steels, each with a different carbon content. The specimens were heat treated to spheroidize the carbide, which was the second phase.

The experimental ductility measurements are shown in fig. 50. Edelson and Baldwin reported that their copper matrix had a strain hardening exponent of approximately 0.5, while Rostoker and Liu report a value of approximately 0.3. The difference between their results is therefore somewhat surprising. The reason may lie in the scintering procedure itself, where metal powders are put under pressure and heated at temperatures below the melting temperatures (bonds between particles then form by diffusion). Rostoker and Liu show that ductility can be rather sensitive to the scintering procedure, which is constrained when a certain porosity is the aim. Further evidence comes

from the data of Liu and Gurland, where the specimens were prepared from a melt. Their higher ductility could result partly from this, and partly from the strength and bonding (to the matrix) of the second phase. It is not expected that the matrix would have a higher hardening exponent than that reported by Edelson and Baldwin.

The qualitative behavior of the numerical results is quite reasonable. Ductility increases as the concentration of second phase decreases, with an apparent limit of infinity as both f_i and $\bar{c}_i$ approach zero. Because the matrix is modelled as a perfect von Mises material with no inhomogeneities, this is to be expected. When $\bar{c}_i$ is zero, the ductility steadily decreases with n, as would be expected. When rigid inclusions which adhere to the matrix are added to the model, the behavior of the new aggregate can be interpreted in a reasonable manner.

The experimental results and the numerical examples for round tensile bars (figs. 50 and 44) do not correlate to badly for very small values of f_i. The discrepancy increases dramatically, however, as f_i becomes large. It is necessary, therefore, to review the approximations used in modelling ductile aggregates, and to see if any improvements or corrections can be made.

Consider first the assumptions related to continuing isotropy. At larger deviatoric strains, the constant void shape assumption becomes less accurate. As seen from comparing yield functions for the spherical and cylindrical voids, void shape can have a large influence on the yield function. Using the yield function for fully plastic flow, and averaging the hardening increment over the matrix also becomes less accurate at higher values of f, where a highly

anisotropic flow field (with part of the matrix rigid) becomes energetically preferable (see fig. 22).

Closely related to this is the way in which void interaction was modelled. This was done by considering the void in a finite geometrically similar matrix, rather than an infinite matrix, and using the same void volume fraction as that of the aggregate to be modelled (see figs. 1 through 3). When f is large, the use of a geometrically similar outer boundary for the matrix may underestimate the plastic flow between neighboring voids. Evidence for this was found in three studies of two dimensional aggregates with periodic arrays of voids. Thomason [9] uses a rigid-non hardening plastic matrix, and looks for conditions favorable to necking (concentration of the plastic flow) between cavities. In his finite element study, Needleman [41] uses an elastic-work hardening plastic matrix, and finds that the plastic zone never encompasses the entire matrix. Similar results were found in [42].

Another aspect of void interaction arises if one tries to consider the voids as randomly dispersed in the matrix, as was done for inclusions in chapter 8. Local values of f would then be different from the average value, and local areas would have different plastic behavior. The aggregate behavior might then differ from that predicted by the single void model.

The hardening behavior is another area of interst. The simple flow histories used here should keep the principle axes of $\underset{\sim}{\Sigma}$ and $\underset{\sim}{\dot{E}}$ coincident, so that within the rigid-plastic, isotropic hardening, incremental plasticity assumptions, $H_{CR} = 0$ should be accurate. However, many materials deviate from istropic hardening, which could alter the macroscopic yield function (see

fig. 36). Many materials (such as rocks) do not in general obey normality, and this can lead to values of H_{CR} which are small but positive [50]. The characterization of the matrix hardening by a single hardening exponent is also a notable approximation.

Another approximation worth discussion is the characterization of the matrix material as a perfect von Mises material, without any consideration of structure. In some recent work, Bauer and Wilsdorf [11] report experiments in which silver single crystal ribbons and polycrystalline stainless steel foils showed void nucleation in "clean" areas (no second phases) and at grain boundaries when pulled in tension. The structure of the matrix itself may then be a primary source of void nucleation when other sources are absent. Bauer and Wilsdorf attribute this nucleation to a dislocation-vacancy mechanism.

Summary and Conclusion

The goal of this work was a better understanding of the role of second phases in the plastic behavior of ductile materials. To this end, approximate yield functions were developed for a simple model aggregate (voids and ductile matrix only) which retained the convexity and normality properties of the matrix yield function. Rigid inclusions, which acted as void nucleation sites, were then added to the formulation. The nucleation mechanism was found to change the yield function, but not the plastic potential.

The elements of plastic behavior which were studied with this model were flow, hardening, and ductility (the strain to ductile fracture). The matrix hardening and the aggregate behavior were idealized as isotropic. Even so, there were many independent variables in the formulation. These included the matrix hardening parameter n, the initial void and inclusion concentrations f_i and $\bar{c}_i$, the matrix-inclusion separation stress σ_i^c, and the macroscopic rate of deformation field $\underline{\dot{E}}$.

Plastic flow was directly affected by porosity. By leading to a term in the plastic potential which was a function of the first invariant of stress, it made plastic volume change in the aggregate possible. Because the matrix retained its plastic incompressiblity, the volume change consisted entirely of void growth.

Hardening in the aggregate was composed of three different phenomena: matrix hardening, softening due to void growth, and softening due to void nucleation. Even while the matrix hardened, the aggregate could thus soften.

It was postulated that flow localization led immediately to ductile

fracture. The criteria for flow localization were found to be 1) the existence of a surface of zero extension, and 2) a critical aggregate hardening rate. For an isotropic material, the critical hardening rate was found to be zero.

Ductility was studied as a function of the independent parameters noted above. The results were qualitatively reasonable, and the behavior could be easily explained. Quantitatively, however, numerical predictions of ductility were too high in comparison to the available experimental data, especially for larger values of f_i and $\bar{c}_i$. This might be attributed to some or all of the following: 1) The model of void interaction may have been inadequate. 2) The isotropy assumptions may have hidden important effects of anisotropy at large plastic strains. 3) Vertex formation was not considered in the determination of the critical hardening rate. 4) No account was taken of the matrix structure.

The numerical results are especially interesting with respect to stress induced void nucleation at inclusions. Under certain conditions, the nucleation may become unstable and cause early flow localization. Due to the behavior of the matrix hardening rate, a moderate value of σ_i^c may decrease the ductility more than lower or higher values of σ_i^c.

In the course of this work, several topics have stood out as being in need of further research. Specific to this work are a better understanding of void interaction, and voids of more general shape. (An originally spherical void in the neck of a tensile bar could then be modelled as, say, a continually elongating ellipsoid.) A more accurate modelling of the ductile matrix material, with regard to both hardening and void nucleation, is also needed.

Better understanding is also needed in areas such as plastic anisotropy, the formation and effects of yield vertices, and the behavior of second phase particles.

References

[1] Hill, R. 1950 The Mathematical Theory of Plasticity, The University Press, Oxford.

[2] Bishop, J. F. W., and Hill, R. 1951 "A Theory of the Plastic Distortion of a Polycrystalline Aggregate Under Combined Stresses", Phil. Mag. 42, pp. 414-427.

[3] Berg, C. A. 1972 "Ductile Fracture by Development of Surfaces of Unstable Cavity Expansion" Journal of Research of N.B.S. 76C, nos. 1 and 2, pp. 33-39.

[4] Berg, C. A. 1969 "Plastic Dilation and Void Interaction" in the Proceedings of the Batelle Memorial Institute Symposium on Inelastic Processes in Solids, pp. 171-209.

[5] Rosenfield, A. R. 1968 "Criteria for Ductile Fracture of Two Phase Alloys" Metallurgical Reviews 13, rev. 121.

[6] Hahn, G. T., Kanninen, M. F., and Rosenfield, A. R. 1972 "Fracture Toughness of Materials" Annual Review of Materials Science 2, pp. 381-404.

[7] Rice, J. R., and Drucker, D. C. 1967 "Energy Changes in Stressed Bodies Due to Void and Crack Growth" International Journal of Fracture Mechanics 3, pp. 19-27.

[8] Rice, J. R., and Johnson, M. A. 1970 "The Role of Large Crack Tip Geometry Changes in Plane Strain Fracture" in Inelastic Behavior of Solids (M. F. Kanninen, et al., eds.) McGraw-Hill, pp. 641-672.

[9] Thomason, P. F. 1968 "A Theory for Ductile Fracture by Internal Necking of Cavities" Journal of the Institute of Metals 96, pp. 360-365.

[10] Thomason, P. F. 1971 "The Influence of Matrix/Particle Cohesive Bond Strength on the Internal Necking Mechanism of Ductile Fracture" Metal Science Journal 5, pp. 64-67.

[11] Bauer, R. W., and Wilsdorf, H. G. F. 1973 "Void Initiation in Ductile Fracture" Scripta Metallurgica 7, pp. 1213-1220.

[12] Argon, A. S., and Im, J. 1975 "Separation of Inclusions in Spheroidized 1045 Steel, Cu -0.6% Cr Alloy, and Maraging Steel in Plastic Straining" Metallurgical Transactions, due to appear in 1975.

[13] Argon, A. S., Im, J., and Safoglu, R. 1975 "Cavity Formation from Inclusions in Ductile Fracture" Metallurgical Transactions, due to appear in 1975.

[14] Argon, A. S., Im, J., and Needleman, A. 1975 "Distribution of Plastic Strain and Triaxial Tensile Stress in Necked Steel and Copper Bars" Metallurgical Transactions, due to appear in 1975.

$$\phi = T_{eq}^2 - (B_0 + B_1 T_{eq} + B_2 T_{eq}^2) T_{eq}$$

[15] Rosovsky, E., Hahn, W. C. Jr., and Avitzur, B. 1973 "The Behavior of Particles During Plastic Deformation of Metals" Metallurgical Transactions 4, pp. 927-930.

[16] Gurland, J., and Plateau, J. 1963 "The Mechanism of Ductile Rupture of Metals Containing Inclusions" Transactions of the A.S.M. 56, pp. 443-454.

[17] Gangulee, A., and Gurland, J. 1967 "On the Fracture of Silicon Particles in Aluminum-Silicon Alloys" Transactions of the Metall. Soc. of the A.I.M.E. 239, pp. 269-272.

[18] Lindley, T. C., Oates, G. and Richards, C. E. 1970 "A Critical Appraisal of Carbide Cracking Mechanisms in Ferride/Carbide Aggregates" Acta Metallurgica 18, pp. 1127-1136.

[19] Gurland, J. 1972 "Observations on the Fracture of Cementite Particles in a Spheroidized 1.05%C Steel Deformed at Room Temperature" Acta Metallurgica 20, pp. 735-741.

[20] Easterling, K. E., Fischmeister, H. F., and Navara, E. 1973 "The Particle-to-Matrix Bond in Dispersion-Hardened Austenitic and Ferritic Iron Alloys" Powder Metallurgy 16, pp. 128-145.

[21] Edelson, B. I., and Baldwin, W. M. 1962 "The Effect of Second Phases on the Mechanical Properties of Alloys" Transactions of the A.S.M. 55, pp. 230-250.

[22] Rostoker, W. and Liu, S. Y. K. 1970 "The Influence of Porosity on the Ductility of Sintered Brass" Journal of Materials J.M.L.S.A. 5, pp. 605-617.

[23] Sarin, V. K., and Grant, N. J. 1972 "Cu-Zr and Cu-Zr-Cr Alloys Produced from Rapidly Quenched Powders" Metallurgical Transactions 3, 875-878.

[24] Bridgman, P. W. 1952 Studies in Large Plastic Flow and Fracture Harvard Univ. Press, Cambridge, Mass.

[25] Beachem, C. D. 1963 "An Electron Fractographic Study of the Influence of Plastic Strain Conditions Upon Ductile Rupture Processes in Metals" Transactions of the A.S.M. 56, pp. 318-326.

[26] Bluhm, J. I., and Morrissey, R. J. 1965 "Fracture in a Tensile Specimen" in International Conference on Fracture, Sendai, Japan.

[27] Barnby, J. T. 1967 "The Initiation of Ductile Failure by Fractured Carbides in an Austenitic Stainless Steel" Acta Metallurgica 15, pp. 903-909.

[28] Darlington, H. 1971 "Ductile Fracture Under Axisymmetric Stresses in Electrolytic Iron and Spheroidized Low-Carbon Steel" Ph.D. thesis, Dept. of Metallurgy and Materials Science, Lehigh University, Bethlehem, Pa.

$$\phi = T_{\sigma_H}^{-1} - \left(B_0 + B_1 T_{\sigma_H} + B_2 T_{\sigma_H}^2\right), \; T_{\sigma_H}$$

[29] Liu, C. T., and Gurland, J. 1968 "The Fracture Behavior of Spheroidized Carbon Steels" Transactions of the A.S.M. 61, pp. 156-167.

[30] Clausing, D. P. 1969 "Tensile Properties of Eight Constructional Steels Between 70 and -320 F" Journal of Materials, J.M.L.S.A. 4, pp. 473-492.

[31] Clausing, D. P. 1970 "Effect of Plane Strain State on Ductility and Toughness" Int. J. of Fracture Mechanics 6, pp. 71-84.

[32] Low, J. R., Jr., Van Stone, R. H., and Merchant, R. H. 1972 "An Investigation of Plastic Fracture in Aluminum Alloys" NASA Technical Report #2, NGR 39-087-003, Carnegie-Mellon University.

[33] Cox, T. B., and Low, J. R., Jr. 1972 "Investigation of the Plastic Fracture of High Strength Steels" NASA Technical Report #3, NGR 39-087-003, Carnegie-Mellon University.

[34] Cox, T. B., and Low, J. R., Jr. 1972 "Investigation of the Plastic Fracture of High Strength Steels" NASA Technical Report #4, NGR 39-087-003, Carnegie-Mellon University.

[35] Broek, D. 1972 "Some Contributions of Electron Fractography to the Theory of Fracture" National Aerospace Laboratory (N.L.R.), the Netherlands, NLR TR 72029 U.

[36] McClintock, F. A. 1968 "A Criterion for Ductile Fracture by the Growth of Holes" Journal of Applied Mechanics 35, pp. 363-371.

[37] Rice, J. R., and Tracey, D. M. 1969 "On the Ductile Enlargement of Voids in Triaxial Stress Fields" J. Mech. Phys. Solids 17, pp. 201-217.

[38] Kahlow, K. J., and Avitzur, B. 1969 "Void Behavior as Influenced by Deformation and Pressure" report to the American Iron and Steel Institute. Lehigh University.

[39] Avitzur, B. 1973 "Tensile Strength of Composite Materials" Journal of Engineering for Industry 95, pp. 827-843.

[40] Needleman, A. 1972 "A Numerical Study of Necking in Circular Cylindrical Bars" J. Mech. Phys. Solids 20, pp. 111-127.

[41] Needleman, A. 1972 "Void Growth in an Elastic Plastic Medium" Journal of Applied Mechanics 39, pp. 964-970.

[42] Haward, R. N., and Owen, D. R. J. 1973 "The Yielding of a Two Dimensional Void Assembly in an Organic Glass" Journal of Materials Science 8, pp. 1136-1144.

[43] Hayden, H. W., and Floreen, S. 1969 "Observations of Localized Deformation During Ductile Fracture" Acta Metallurgica 17, pp. 213-224.

$$\Phi = T_{Gav}^2 - (B_0 + B_1 T_{GH} + B_2 T_{GH}^2), \quad T_{Gav}$$

[44] Nagpal, V., McClintock, F. A., Berg, C. A., and Subudhi, M. 1972 "Traction-Displacement Boundary Conditions for Plastic Fracture by Hole Growth" in the Intl. Symposium on Foundations of Plasticity, vol. 1 (A. Sawczuk, ed.), pp. 365-385.

[45] Rice, J. R. 1973 "The Initiation and Growth of Shear Bands" in Plasticity in Soil Mechanics.

[46] Timoshenko, S. P., and Goodier, J. N. 1934, 1951 Theory of Elasticity, p. 78.

[47] Rice, J. R. private communication.

[48] C.R.C. Standard Math Tables The Chemical Rubber Co., Cleveland, Ohio.

[49] Hildebrand, F. B. 1962 Advanced Calculus for Applications Prentice-Hall, Inc., Englewood Cliffs, New Jersey.

[50] Rudnicki, J. W., and Rice, J. R. 1974 "Conditions for the Localization of Deformation in Pressure Sensitive Dilatant Materials" N.S.F. Geophysics Program, GA-43380/2, Brown University.

[51] Cottrell, A. H. 1953 Dislocations and Plastic Flow in Crystals, Oxford, pp. 116-124.

[52] Ilyushin, A. A. 1946 "The Theory of Small Elastic-Plastic Deformations" Applied Mathematics and Mechanics (Translated from the Russian) 10, pp. 347-356.

[53] Palmer, I. G., and Smith, G. C. 1966 "Fracture of Internally Oxidized Copper Alloys" in Oxide Dispersion Strengthening, Metallurgical Society Conferences, vol. 47, pp. 253-290.

[54] Anand, L. private communication

[55] Hill, R. 1958 "A general theory of Uniqueness and Stability in Elastic-Plastic Solids" J. Mech. Phys. Solids 6, pp. 236-249.

[56] Rudnicki, J. W., and Rice J. R. 1974 "Conditions for the Localization of Deformation in Pressure-Sensitive Dilatant Materials", Brown Report #NSF GA-43380/2.

[57] Fung, Y. C. 1965 Foundations of Solid Mechanics Prentice-Hall, Inc., New Jersey.

[58] Batdorf, S. B., and Budiansky, B. 1949 "A Mathematical Theory of Plasticity Based on the Concept of Slip" N.A.C.A. TN1871.

[59] Clausing, D. P. 1969 "Stress and Strain Distribution in a Tension Specimen With a Circumferential Notch", Journal of Materials 4, pp. 566-582.

[60] Earl, J. C., and Brown, D. K. 1975 "Distributions of Stress and Strain in Circumferentially Notched Tension Specimens" submitted to Engineering Fracture Mechanics

[61] Tracey, D. M. 1968 "Strain Hardening and Interaction Effects on the Growth of Voids in Ductile Fracture" U.S.A.E.C. AT(30-1)-2394/34, Brown University

[62] Hutchinson, J. W., and Miles, J. P. 1974 "Bifurcation Analysis of the Onset of Necking in an Elastic/Plastic Cylinder Under Uniaxial Tension" J. Mech. Phys. Solids 22, pp. 61-71.

[63] Marshall, R. R., and Shaw, M. C. 1944 "The Determination of Flow Stress From a Tensile Specimen" Transactions of the A.S.M. 44, pp. 705-725.

[64] McClintock, F. A., and Argon, A. S. 1966 Mechanical Behavior of Materials Addison-Wesley pp. 114-118.

$$\phi = \tau_{eqv}^2 - \left(B_0 + B_1 T_{GH} + B_2 T_{GH}^2\right), \quad T_{GH}$$

Appendix (1)

The integrals in eqns. 6.35 are over the surface of a unit sphere, and lend themselves to solution using symmetry arguments and the Gauss theorem. The solutions are carried out as follows; using the coordinates and definitions in fig. 3.

a) On the surface of a unit sphere, $x_i = n_i$

b) By symmetry, $\int_\Omega x_1^c \, d\Omega = \int_\Omega x_2^c \, d\Omega = \int_\Omega x_3^c \, d\Omega$, c = any exponent

x_i = cartesian coords.

c) $\int_\Omega x_i x_j \, d\Omega = 0 \quad \text{for } i \neq j$

d) State the Gauss theorem;

$$\int_\Omega n_i F_j \, d\Omega = \int_V \frac{\partial}{\partial x_i}\left(F_j\right) dV$$

Here, V is the volume of the unit sphere, and the F_j are the cartesian components of any vector.

e) By definition, $\mu = \dfrac{\dot{E}'_{rr}}{\sqrt{\frac{2}{3}\dot{E}'_{kl}\dot{E}'_{kl}}} = \dfrac{\dot{E}'_{rr}}{\dot{E}_{eqv}}$.

By coordinate transformation, $\dot{E}'_{rr} = C_{ri} C_{rj} \dot{E}'_{ij}$.

On the unit sphere, $C_{ri} = n_i = x_i\big|_S$

So

$$\mu = \frac{\dot{E}'_{ij} n_i n_j}{\dot{E}_{eqv}}$$

The following calculations are self-explanatory:

$$\int_\Omega \mu \, d\Omega = \dot{E}_{eqv}^{-1} \int_\Omega n_i \dot{E}'_{ij} x_j \, d\Omega = \dot{E}_{eqv}^{-1} \dot{E}'_{ij} \int_V \frac{\partial x_j}{\partial x_i} \, dV$$

$$= \frac{\dot{E}'_{ij} \delta_{ij}}{\dot{E}_{eqv}} = 0$$

$$\int_\Omega \mu^2 \, d\Omega = \left\{ \dot{E}_{eqv}^{-2} \dot{E}'_{ij} \dot{E}'_{kl} \right\} \int_\Omega n_i x_j x_k x_l \, d\Omega = \{ \} \int_V \frac{\partial}{\partial x_i} \left(x_j x_k x_l \right) dV$$

$$= \left\{ \dot{E}_{eqv}^{-2} \dot{E}'_{ij} \dot{E}'_{kl} \right\} \int_V \left[\delta_{ij} x_k x_l + \delta_{ik} x_i x_l + \delta_{il} x_i x_k \right] dV$$

$$= 2 \dot{E}_{eqv}^{-2} \dot{E}'_{pq} \dot{E}'_{pl} \int_V x_q x_l \, dV$$

$$= 2 \dot{E}_{eqv}^{-2} \dot{E}'_{pq} \dot{E}'_{pl} \delta_{ql} \cdot \frac{1}{3} \int_V \left(x_1^2 + x_2^2 + x_3^2 \right) dV$$

$$\int_\Omega \mu^2 \, d\Omega = \int_V r^2 \, dV = \frac{4}{5} \pi$$

$$\int_\Omega n_i n_j \, d\Omega = \int_V \frac{\partial x_i}{\partial x_j} \, dV = \frac{4}{3} \pi \delta_{ij}$$

$$\int_\Omega \mu n_i n_j \, d\Omega = \dot{E}_{eqv}^{-1} \int_\Omega n_k \dot{E}'_{kl} x_l x_i x_j \, d\Omega = \dot{E}_{eqv}^{-1} \int_V \frac{\partial}{\partial x_k} \left(\dot{E}'_{kl} x_l x_i x_j \right) dV$$

$$= \dot{E}_{eqv}^{-1} \int_V \dot{E}'_{il} x_l x_j + \dot{E}'_{jl} x_l x_i \, dV = 2 \dot{E}_{eqv}^{-1} \dot{E}'_{ij} \cdot \frac{4\pi}{15} = \frac{8\pi}{15} t_{ij}$$

(see eqn. 6.22)

following empirical form to the data:

$$\phi = T_{eqv}^2 - \left(B_0 + B_1 T_{GH} + B_2 T_{GH}^2 \right), \quad T_{GH}$$

Appendix (2)

The yield surfaces generated for plane strain in ref. [44] are given in terms of the following stress parameters:

$$\frac{t_n}{2k} \quad , \quad \frac{t_s}{2k}$$

where k is the matrix yield stress in shear, t_n is the macroscopic stress at yield normal to the plane of zero extension, and t_s is the shear stress at yield in the plane of zero extension (see fig. 9). In order to transform between t_n and t_s, and the stress parameters used here for the cylindrical void case, the following steps are taken:

Starting from principal axes (principal values indicated by subscripts I and II), find the plane of zero extension. θ is the CCW rotation from the I axis to that plane.

$$\dot{E}^*_{11} = 0 = \cos^2(\theta)\,\dot{E}_I + \sin^2(\theta)\,\dot{E}_{II}$$

$$\tan^2(\theta) = -\frac{\dot{E}_I}{\dot{E}_{II}} \equiv -E_R$$

Note that, in plane strain, $\dot{E}_I$ and $\dot{E}_{II}$ must be of opposite sign for a plane of zero extension to exist. With θ determined,

$$t_n = \sin^2(\theta)\,\Sigma_I + \cos^2(\theta)\,\Sigma_{II}$$

$$t_s = \sin(\theta)\cos(\theta)\left(\Sigma_{II} - \Sigma_I\right)$$

This indicates that, for comparison purposes, t_s should be considered negative. (Due to a difference in sign convention, ref. [44] has t_n positive.)

$$\phi = T_{eqv}^2 - \left(B_0 + B_1 T_{GH} + B_2 T_{GH}^2\right), T$$

For plane strain,

$$\Sigma_{eqv} = \frac{\sqrt{3}}{2}\left(\Sigma_{II} - \Sigma_{I}\right), \quad \Sigma_{rr} = \left(\Sigma_{II} + \Sigma_{I}\right)$$

so,

$$\Sigma_{II} = \frac{1}{2}\Sigma_{rr} + \frac{1}{\sqrt{3}}\Sigma_{eqv}$$

$$\Sigma_{I} = \frac{1}{2}\Sigma_{rr} - \frac{1}{\sqrt{3}}\Sigma_{eqv}$$

Using the normalization conventions,

$$\frac{t_n}{2k} = \frac{\sqrt{3}}{2}\left(\sin^2(\theta)\, T_I + \cos^2(\theta)\, T_{II}\right)$$

$$\frac{t_s}{2k} = \frac{\sqrt{3}}{2}\cdot \sin(\theta)\cos(\theta)\left(T_I - T_{II}\right)$$

Inverting this gives

$$T_{II} = \frac{2}{\sqrt{3}}\left[\frac{t_n}{2k} - \frac{t_s}{2k}\tan(\theta)\right]$$

$$T_{I} = \frac{2}{\sqrt{3}}\left[\frac{t_n}{2k} + \frac{t_s}{2k}\frac{1}{\tan(\theta)}\right]$$

In fig. 10a, points from the yield curves for the slip line model (fig. 7, ref. [44]) are compared with data generated by the wedge model for f = 0.0178, 0.05, and 0.3. These arise from

$$\left(\frac{P}{L}\right) = 0.073$$

$$\left(\frac{P}{L}\right) = 0.123, \quad \frac{3}{8}\pi\left(\frac{P}{L}\right)^2 = 0.0178$$

$$\phi = T_{eqv}^2 - \left(B_0 + B_1 T_{GH} + B_2 T_{GH}^2\right), \; T_{GH}$$

$$\left(\frac{P}{L}\right) = 0.208, \quad \frac{3}{8}\pi\left(\frac{P}{L}\right)^2 = 0.051 \approx 0.05$$

$$\left(\frac{P}{L}\right) = 0.50, \quad \frac{3}{8}\pi\left(\frac{P}{L}\right)^2 = 0.294 \approx 0.30$$

The points from ref. [44] were measured with a ruler, and are connected by straight lines.

In fig. 10b, data from ref. [44] is compared to composite yield curves (like those in fig. 14, but mapped into the coordinates of fig. 10a) for

$$f = \frac{\pi}{4}\left(\frac{P}{L}\right)^2, \quad \frac{3\pi}{8}\left(\frac{P}{L}\right)^2, \text{ and } \quad \frac{\pi}{2}\left(\frac{P}{L}\right)^2$$

The comparison is reasonable, in light of the fact that two different approaches are used in two similar yet different problems. The main geometric difference is the periodic nature of the model used in ref. [44].

It is observed that the dashed lines (composite yield functions) do not extend all the way down to $t_s/2k = 0$. The curves terminate when the yield function gives $E_R \geq 0$. This means that no plane of zero extension exists. A common feature is that the curves end at the abrupt change in slope marking the transition to fully plastic flow. (This point is made clear in the discussion of composite yield functions.)

$$\phi = T_{cbv}^2 - (B_0 + B_1 T_{cH} + B_2 T_{cH}^2), \; T_{ci}$$

Appendix 3

The purpose here is to develop a form for the stress amplification factor A , drawing heavily on the work done in ref. [13] by Argon, et al.. Some small changes are made in their theory, but the basic assumptions and direction of their calculation are followed very closely. Therefore, where applicable, reference will be made to their work for details. Also, some of their notation will be used in this appendix.

In ref. [13], the stress concentration at a rigid particle in a plastic work hardening matrix is investigated. The main concern is the normal interfacial stress, whose attainment of a critical value (at particles above a certain minimal size) is taken as the criterion for void nucleation.

In their first calculation, they look at the two dimensional problem of a circular (cylindrical) rigid particle embedded in a strain hardening material, undergoing simple shear at distant boundaries. There are no other particles for the lone particle to interact with. Using a bounding technique, they arrive at the result

$$\frac{3}{2}k \leq \sigma_{rr} - \sigma_T \leq 2k \qquad \text{(A.3.1)}$$

where k is the flow stress in shear, σ_{rr} is the normal interfacial stress, and σ_T is the hydrostatic component of stress (superimposed at the distant boundary). Given the closeness of the bounds, and using

$$Y(\bar{\epsilon}^p) \equiv \sqrt{3}\,k \simeq 1.75 \cdot k \qquad \text{(A.3.2)}$$

(where $Y(\bar{\epsilon}^p)$ is the current, i.e., work hardened yield stress in tension of the plastic matrix, and $\bar{\epsilon}^p$ is the total equivalent plastic strain), the following is deduced

$$\sigma_{rr} \simeq Y(\bar{\varepsilon}^p) + \sigma_T \qquad (A.3.3)$$

While this calculation was done for a two dimensional case, the above result is implicitly assumed in ref. [13] to be applicable to the three dimensional case of spherical rigid particles in a work hardening matrix.

Argon, et al. then consider a different type of approximation to the normal interfacial stress, based on a quasi-upper bound method. Here, both the cases of non-interacting and interacting rigid inclusions in a work hardening matrix in simple shear are examined. The method involves construction of a plastic flow field in the vicinity of the particle which accommodates in an approximate way the kinematic restrictions imposed by a rigid particle in a matrix undergoing plastic flow. For particle-particle interaction, this local variation in an otherwise homogeneous flow field (the "secondary plastic zone") must interact with the secondary plastic zone of another rigid particle.

Before continuing, the one modification made to the calculations in ref. [13] should be described. This involves the use of the "Taylor factor", defined here as

$$m_1 \simeq 3.1, = \sqrt{3}\,\frac{k_o}{k_s}\left(\frac{\gamma}{\gamma_y}\right)^{1/n} \qquad (A.3.4)$$

where k_o is the initial yield stress in shear, k_s is the plastic drag at a displacement incompatibility, and the last term represents strain hardening (γ is engineering shear strain, γ_y is the value at first yield). The justification for this can be found in ref. [51]. Note, n as used here is the inverse of its value in the rest of the text. Argon, et al. use a similar form, but

$$\phi = T_{GV}^{\lambda} - \left(B_o + B_1 T_{GH} + B_2 T_{GH}^2\right), \; T_G$$

without a work hardening term. "m" is a constant factor which relates plastic drag to the yield stress in shear, commonly taken to be 3.1 (see [51]).

Using eqn. A.3.4 and following through the other parts of the relevant calculation in ref. 13, one arrives at forms for the non-interacting and interacting values of σ_{rr}. They are of course functions of the amount of work hardening, and the latter (as expected) is a function of the local concentration of particles. Both turn out to be larger than the bounded value in eqn. A.3.3. It is postulated here, however, that their ratio is a reasonable approximation to the ratio of the true values for simple shear;

$$A \equiv \frac{\sigma_{rr}|_{interaction}}{\sigma_{rr}|_{noninteraction}} \tag{A.3.5}$$

Thus, the equation

$$\sigma_{rr} \simeq A \cdot \sigma_o + \frac{\Sigma_H}{(1-f)} \tag{A.3.6}$$

arises, where σ_o is the current yield stress in tension. The (1-f) term is intended to account approximately for the fact that voided material (created here by nucleation at particles) does not support stress. Note that f is the void volume fraction, and not the particle volume fraction.

Carrying through the calculations in ref. [13] (but using eqn. A.3.4) yields, for spherical inclusions

$$\sigma_{rr}|_{noninteraction} = k_o \left(\frac{\dot{\gamma}}{\dot{\gamma}_y}\right)^{1/n} \left[1 + \sqrt{3}\left(\frac{\sqrt{6}(n+1)}{m}\right)^{\frac{1}{n+1}}\right] \tag{A.3.7}$$

$$\Phi = T_{eq}^2 - \left(B_0 + B_1 T_{GH} + B_2 T_{GH}^2\right), \quad T_{GH}$$

The extent of the secondary plastic zone (see fig. 24) is given by

$$\frac{\lambda}{\rho} = \frac{m}{\sqrt{2}}\left(\frac{\sqrt{6}(n+1)}{m}\right)^{\frac{1}{n+1}} \qquad (A.3.8)$$

For the case of interacting inclusions, the extent of the secondary plastic zone is governed by the local particle concentration c. This can be derived by considering two particles (of equal size) which are close enough to interact (fig. 25). Their "average" radius is taken to be the radius of a cylinder of equal volume and depth

$$\frac{4}{3}\pi\rho^3 = \pi\rho_{av}^2 \cdot 2\rho \longrightarrow \rho_{av} = \sqrt{\frac{2}{3}}\rho \qquad (A.3.9)$$

The local concentration in a plane is then

$$c = \frac{\pi\rho_{av}^2}{(\lambda + 2\rho_{av})^2}, \longrightarrow \frac{\lambda}{\rho} = \sqrt{\frac{2\pi}{3c}} - \sqrt{\frac{8}{3}} \qquad (A.3.10)$$

Following through the calculation then gives

$$\sigma_{rr}\Big|_{\text{interaction}} = k_o\left(\frac{\gamma}{\gamma_y}\right)^{\frac{1}{n}}\left[1 + \frac{\sqrt{6}}{m}\frac{\lambda}{\rho} + \sqrt{3}Z\right] \qquad (A.3.11)$$

where Z is a nondimensional stress at $x = 0$ (where the secondary plastic zones intersect), and can be found numerically from the equation

$$\frac{\sqrt{6}(n+1)}{m} = \left(\frac{\sqrt{2}}{m}\frac{\lambda}{\rho} + Z\right)^{n+1} - (Z)^{n+1} \qquad (A.3.12a)$$

$$\phi = T_{eqv}^2 - \left(B_o + B_1 T_{GH} + B_2 T_{GH}^2\right), \; T_G$$

Note that when $Z = 0$, this is equivalent to eqn. A.3.8, for noninteraction. Also note that a closed form solution for Z exists for $n = 2$:

$$Z|_{n=2} = \frac{-\sqrt{2}}{2m}\frac{\lambda}{\rho} + \frac{1}{2}\left[\frac{4}{\sqrt{3}}\frac{(n+1)}{\lambda/\rho} - \frac{2}{3m^2}\left(\frac{\lambda}{\rho}\right)^2\right]^{\frac{1}{2}}. \qquad (A.3.12b)$$

Z should never be negative.

Interaction first takes place when the local particle concentration is large enough so that the secondary plastic zones of neighboring particles make contact:

$$\frac{\lambda}{\rho} = \sqrt{\frac{2\pi}{3c}} - \sqrt{\frac{8}{3}} = \frac{m}{\sqrt{2}}\left(\frac{\sqrt{6}\,(n+1)}{m}\right)^{\frac{1}{n+1}} \qquad (A.3.13)$$

So, for interaction, it is required that

$$c \geq \frac{2\pi}{3}\left[\frac{m}{\sqrt{2}}\left(\frac{\sqrt{6}\,(n+1)}{m}\right)^{\frac{1}{n+1}} + \sqrt{\frac{8}{3}}\right]^{-2} \qquad (A.3.14)$$

For concentrations lower than this, $A = 1$.

Using the above forms to calculate A, the work hardening terms cancel out. This leaves A a function of c and n only. In fig. 26, A is plotted as a function of c for various values of n. c reaches a maximum when $\lambda = 0$, indicating that "average" plane sections of neighboring particles are touching. From eqn. A.3.10,

$$c_{max} = \frac{\pi}{4} \qquad (A.3.15)$$

$$\phi = T_{eff}^2 - \left(B_0 + B_1 T_{eH} + B_2 T_{eH}^2\right) T_{eH}$$

An analysis similar to the one described above can be carried out for the case of long (length L , >> radius ρ) parallel cylindrical inclusions. This geometry change is reflected in a new equilibrium equation (analogous to eqn. 7 in ref. 13);

$$\frac{d\sigma}{dx}\cdot\sqrt{2}\rho L - k_s\cdot 2L = 0, \quad \frac{d\sigma}{dx} - \sqrt{2}\frac{k_s}{\rho} = 0 \qquad (A.3.16)$$

Following through the analysis (as modified by eqn. A.3.4) gives the

$$\sigma_{rr}\Big|_{noninteraction} = k_o\left(\frac{\gamma}{\gamma_y}\right)^{\frac{1}{n}}\left[1+\sqrt{3}\left(\frac{\sqrt{\frac{3}{2}}}{m}(n+1)\right)^{\frac{1}{n+1}}\right] \qquad (A.3.17)$$

$$\frac{\lambda}{\rho}\Big|_{noninteraction} = \sqrt{2}\,m\left(\frac{\sqrt{\frac{3}{2}}}{m}(n+1)\right)^{\frac{1}{n+1}} \qquad (A.3.18)$$

In considering the local particle concentration in a plane, the "average" radius and the actual radius are equal:

$$c = \frac{\pi\rho^2}{(\lambda+2\rho)^2}, \longrightarrow \frac{\lambda}{\rho} = \sqrt{\frac{\pi}{c}} - 2 \qquad (A.3.19)$$

Using the above value,

$$\sigma_{rr}\Big|_{interaction} = k_o\left(\frac{\gamma}{\gamma_y}\right)^{\frac{1}{n}}\left[1+\frac{\sqrt{\frac{3}{2}}}{m}\frac{\lambda}{\rho}+\sqrt{3}\,Z\right] \qquad (A.3.20)$$

where Z is obtained from

$$\frac{\sqrt{\frac{3}{2}}}{m}(n+1) = \left(\frac{1}{\sqrt{2}\,m}\frac{\lambda}{\rho}+Z\right)^{n+1} - Z^{n+1} \qquad (A.3.21)$$

$\phi = T_{eqv}^2 - \left(B_o + B_1 T_{GH} + B_2 T_{GH}^2\right), T_G$

In analogy to eqn. A.3.14, the minimum local concentration necessary for interaction is

$$c = \pi\left[\sqrt{2}\, m \left(\frac{\sqrt{\frac{3}{2}}}{m}(n+1)\right)^{\frac{1}{n+1}} + 2\right]^{-2} \qquad \text{(A.3.22)}$$

The relationships between stress and strain in eqns. A.3.7, A.3.11, A.3.17, and A.3.20 have the interesting property that they obey Ilyushin's theorem for power law hardening materials [52]. The theorem states that if, in a body made of power law hardening material;

$$\left(\frac{\gamma}{\gamma_y}\right) = \left(\frac{k}{k_o}\right)^n \qquad \text{(A.3.23)}$$

(k is the current yield stress in shear), the boundary conditions u_i lead to the solution (σ,ε) in the body, then the boundary conditions $\beta\dot{u}_i$ (β is a scalar constant over the body) must lead to the solution $(\beta^{1/n}\sigma, \beta\varepsilon)$ in the body. This theorem is not obeyed when the calculations are not modified by eqn. A.3.4.

$$\Phi = T_{eqy}^2 - \left(B_o + B_1 T_{GH} + B_2 T_{GH}^2\right) T_{GH}$$

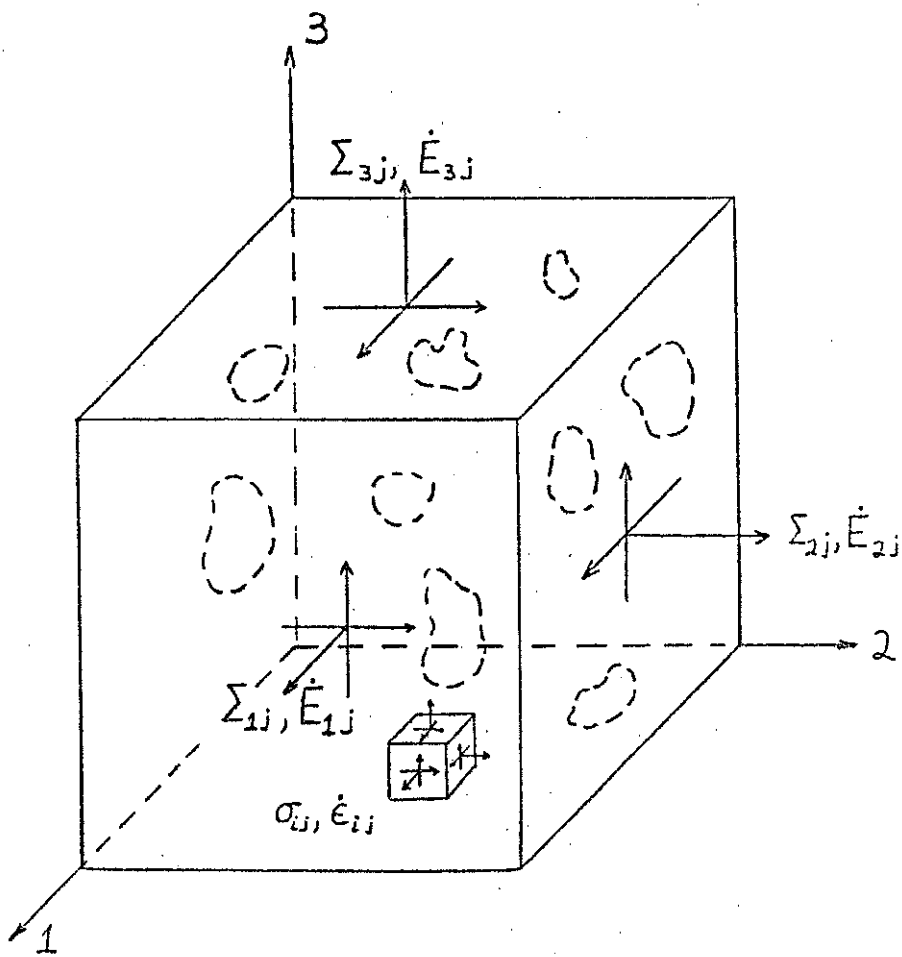

VOID-MATRIX AGGREGATE

RANDOM VOID SHAPES AND ORIENTATIONS

MACROSCOPIC AND MICROSCOPIC TENSOR QUANTITIES

FIGURE 1

$$\Phi = T_{eqv}^2 - \left(B_0 + B_1 T_{GH} + B_2 T_{GH}^2\right), \; T_G$$

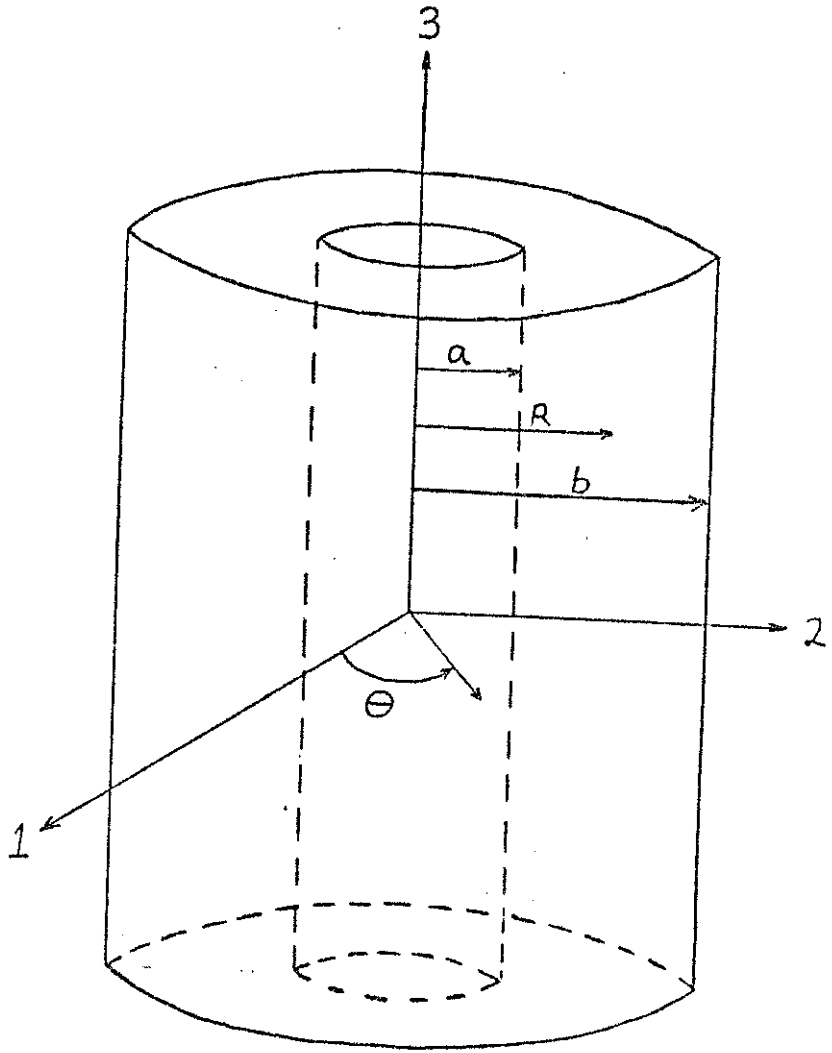

LONG CIRCULAR CYLINDRICAL VOID IN A MATRIX OF RIGID-PERFECTLY PLASTIC VON MISES MATERIAL

FIGURE 2

$$\Phi = T_{eq}^2 - \left(B_0 + B_1 T_{GH} + B_2 T_{GH}^2\right), \quad T_{GH}$$

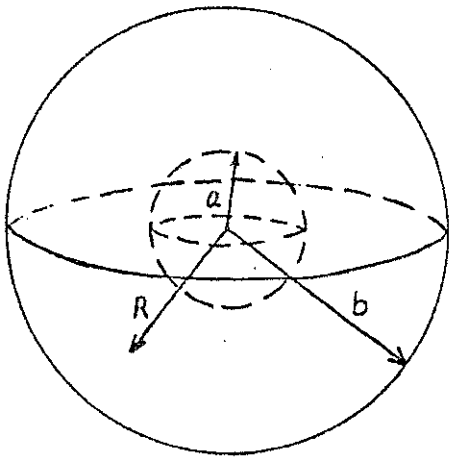

SPHERICAL MODEL

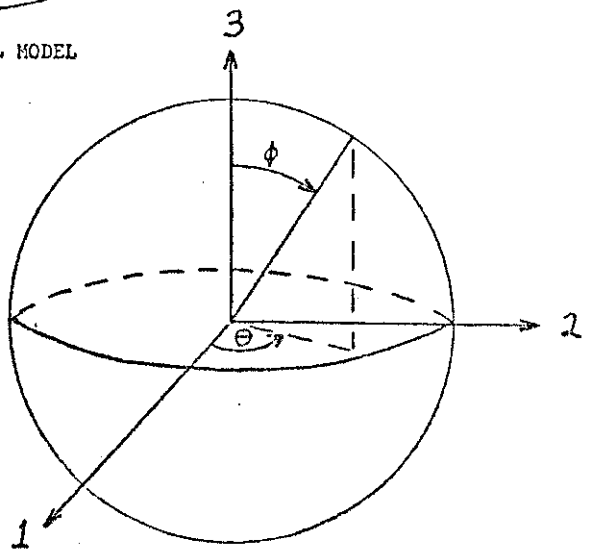

UNIT SPHERE

PRINCIPAL AXIS SYSTEM

FIGURE 3

following empirical form to the data:

$$\phi = T_{eq}^{-1} - \left(B_0 + B_1 T_{GH} + B_2 T_{GH}^2\right), T_G$$

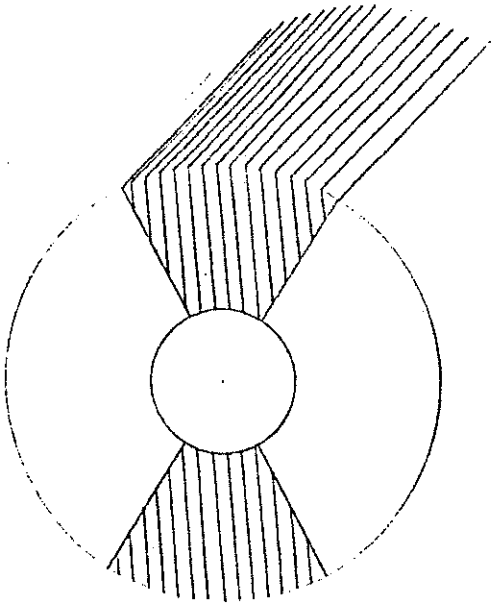

CYLINDRICAL MODEL
RIGID WEDGE
PLANE STRAIN

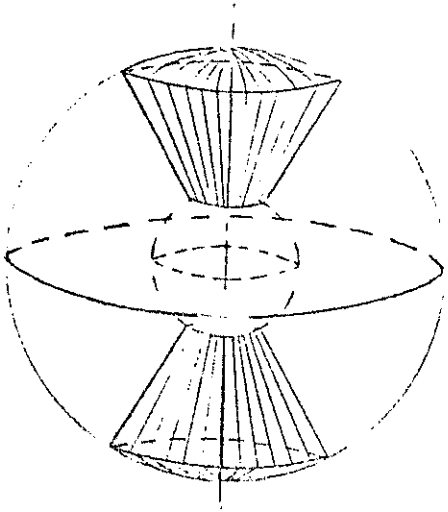

SPHERICAL MODEL
RIGID CONE
AXISYMMETRIC FLOW

FIGURE 4

$$\Phi = T_{GV}^2 - \left(B_0 + B_1 T_{GH} + B_2 T_{GH}^2\right), \; T_{GH}$$

following empirical form to the data:

$$\phi = T_{EQV}^2 - \left(B_0 + B_1 T_{GH} + B_2 T_{GH}^2\right), \quad T_G$$

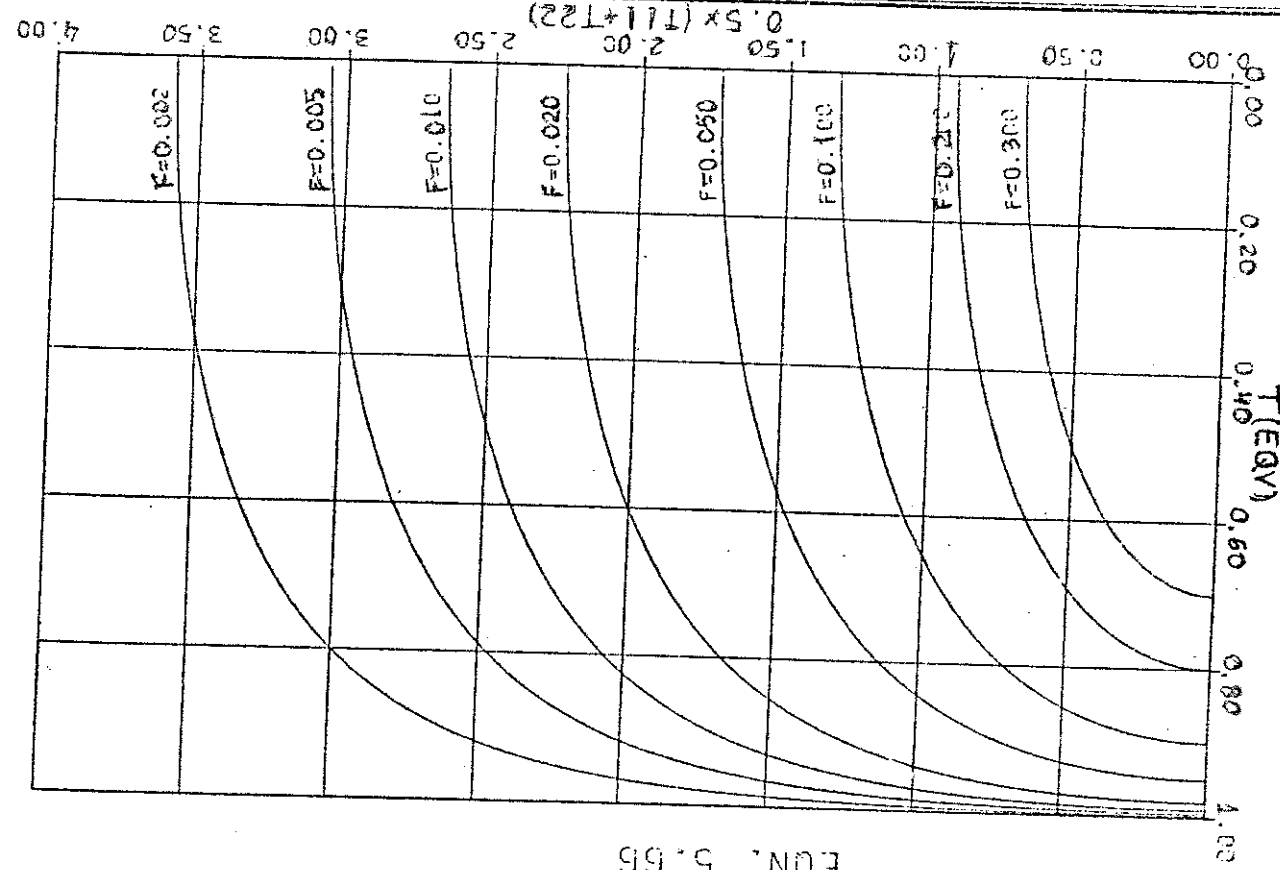

FIG. 5A

$$\phi = T_{eqv}^2 - \left(B_0 + B_1 T_{GH} + B_2 T_{GH}^2\right), T_{GH}$$

FIG. 5B

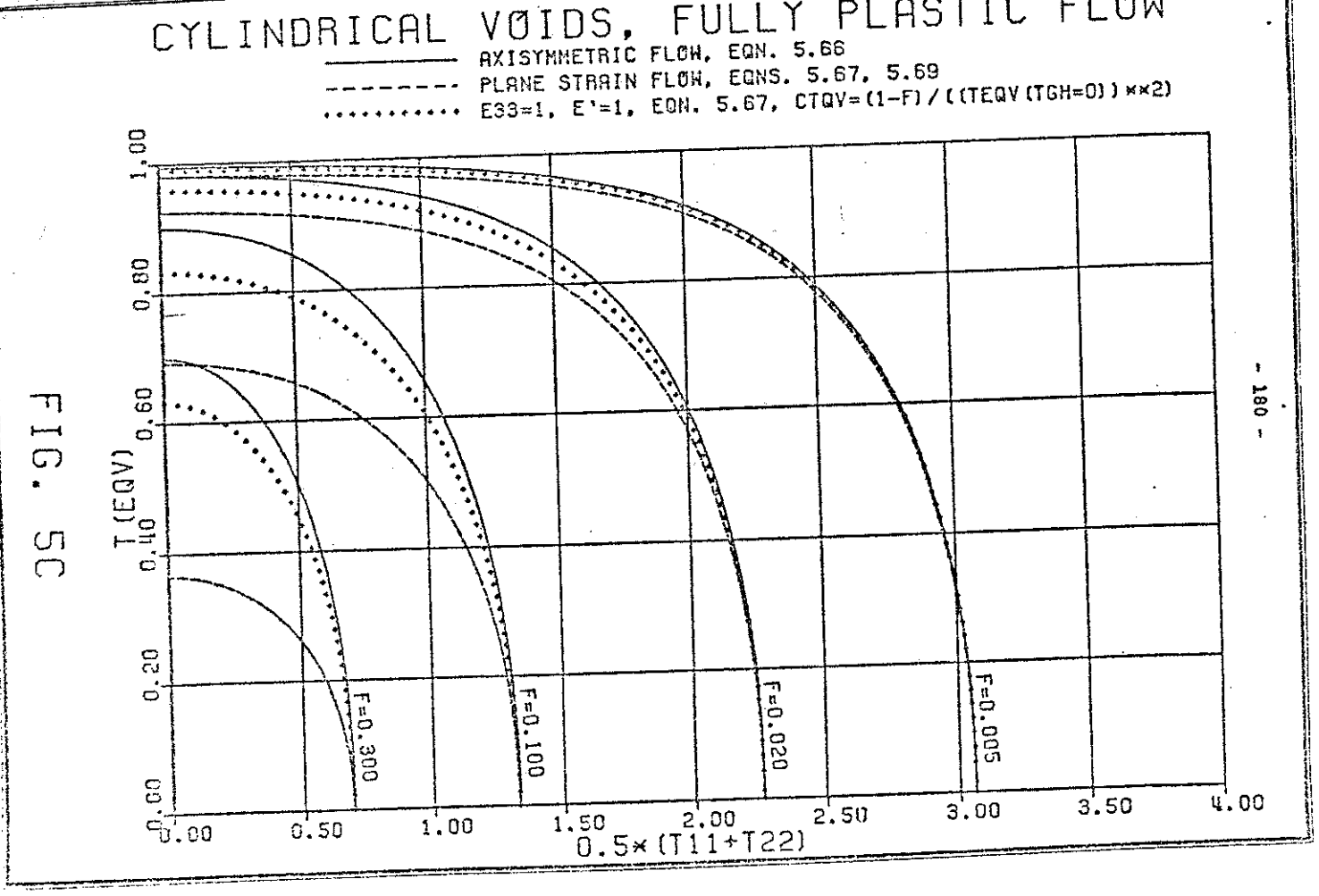

FIG. 5C

following empirical form to the data:

$$\Phi = T_{eqv}^2 - (B_0 + B_1 T_{GH} + B_2 T_{GH}^2), \; T_G$$

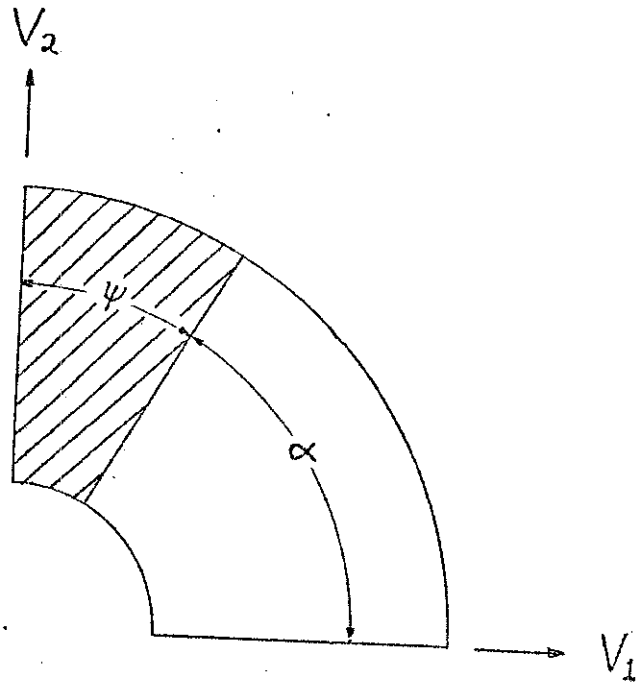

CYLINDRICAL MODEL, RIGID WEDGE
PLANE STRAIN FLOW
QUARTER SECTION

FIGURE 6

$$\phi = T_{c_2 V}^2 - \left(B_0 + B_1 T_{c_H} + B_2 T_{c_H}^2\right), \; T_c$$

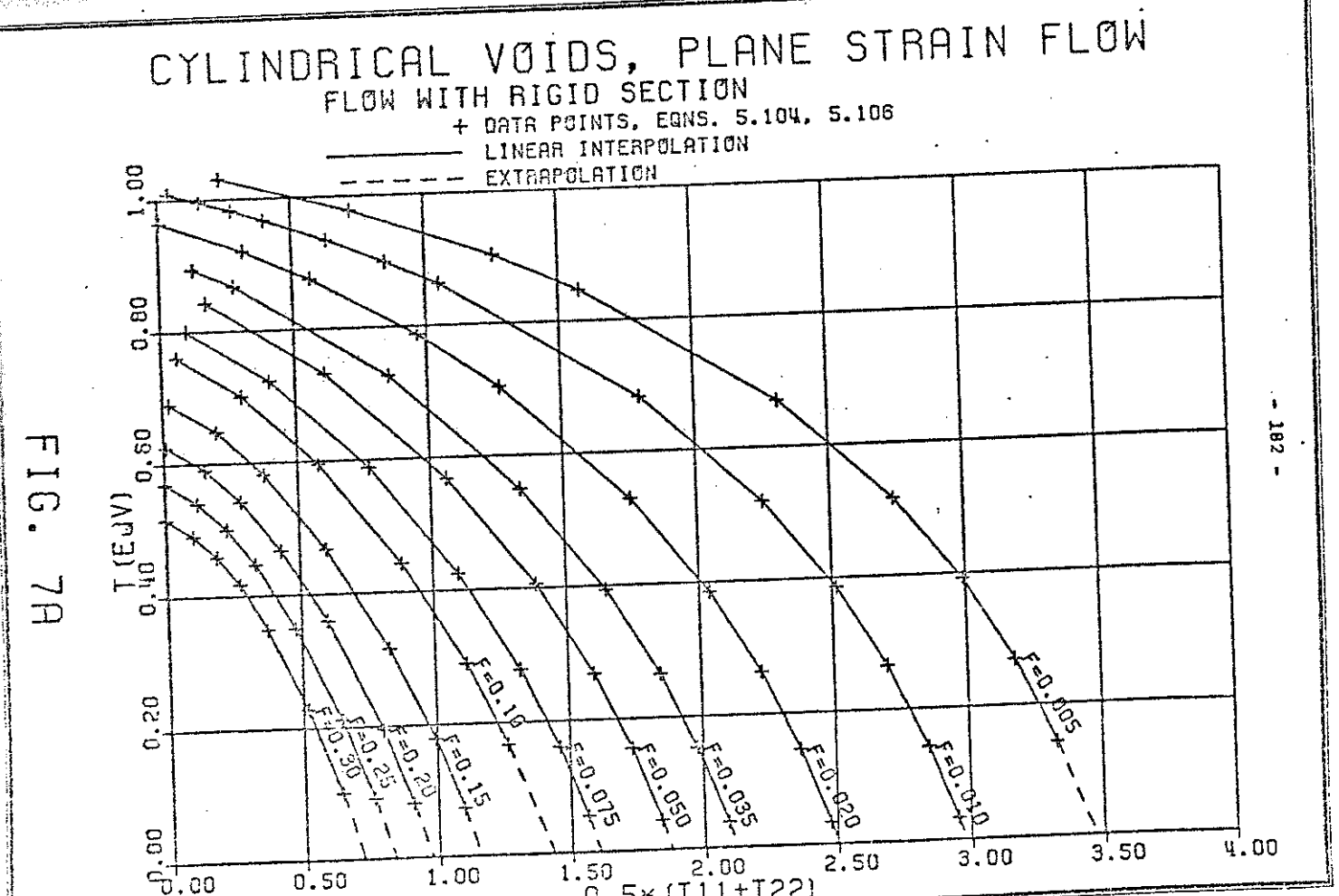

FIG. 7A

following empirical form to the data:

$$\phi = T_{eqv}^2 - (B_0 + B_1 T_{eH} + B_2 T_{eH}^2), \; T_e$$

$$\phi = T_{eqv}^2 - \left(B_0 + B_1 T_{GH} + B_2 T_{GH}^2\right), \; T_{GH}$$

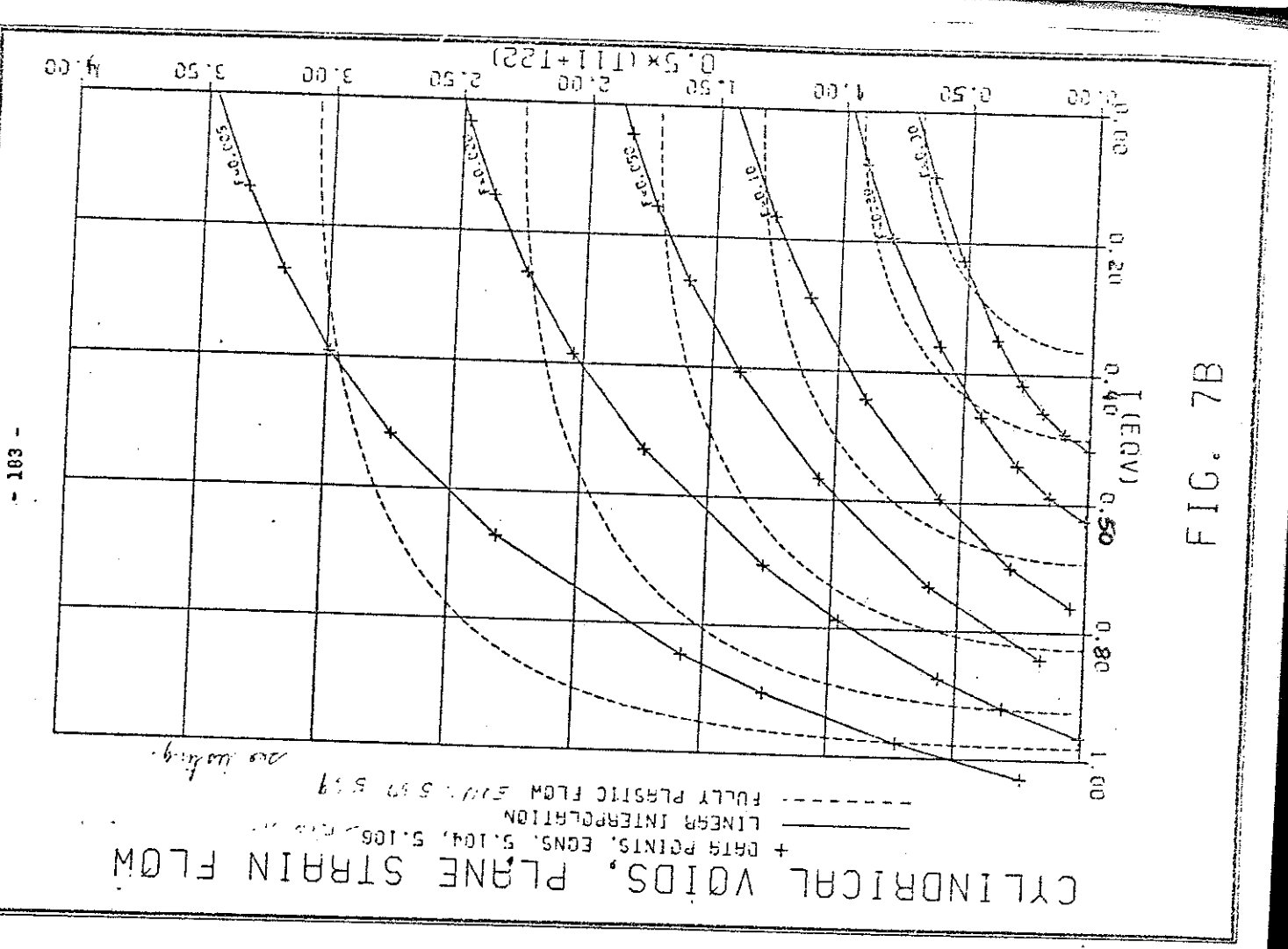

FIG. 7B

FIG. 8

following empirical form to the data:

$$\Phi = T_{eqv}^2 - \left(B_o + B_1 T_{Gn} + B_2 T_{Gn}^2\right), T$$

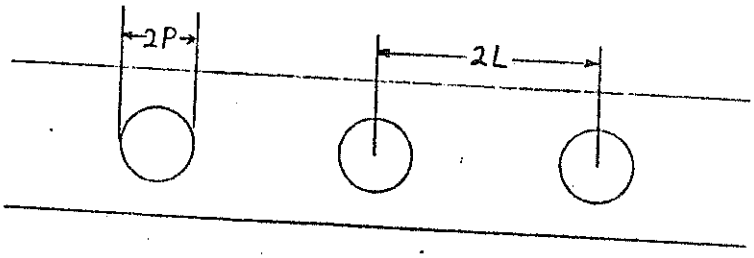

(A) ONE-DIMENSIONAL ARRAY

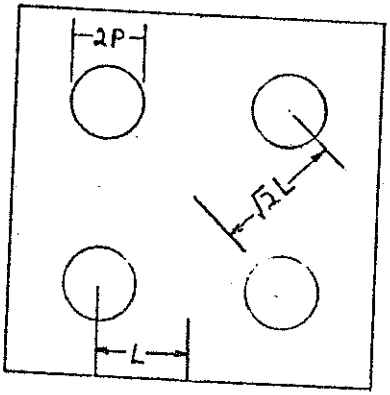

$$\frac{\pi P^2}{4L^2} \leq f \leq \frac{\pi P^2}{2L^2}$$

(B) EXTENSION TO TWO DIMENSIONS

GEOMETRY USED WITH SLIP LINE MODEL

FIGURE 9

following empirical form to the data:

$$\phi = T_{eqv}^2 - \left(B_0 + B_1 T_{GH} + B_2 T_{GH}^2\right), \quad T_{GH}$$

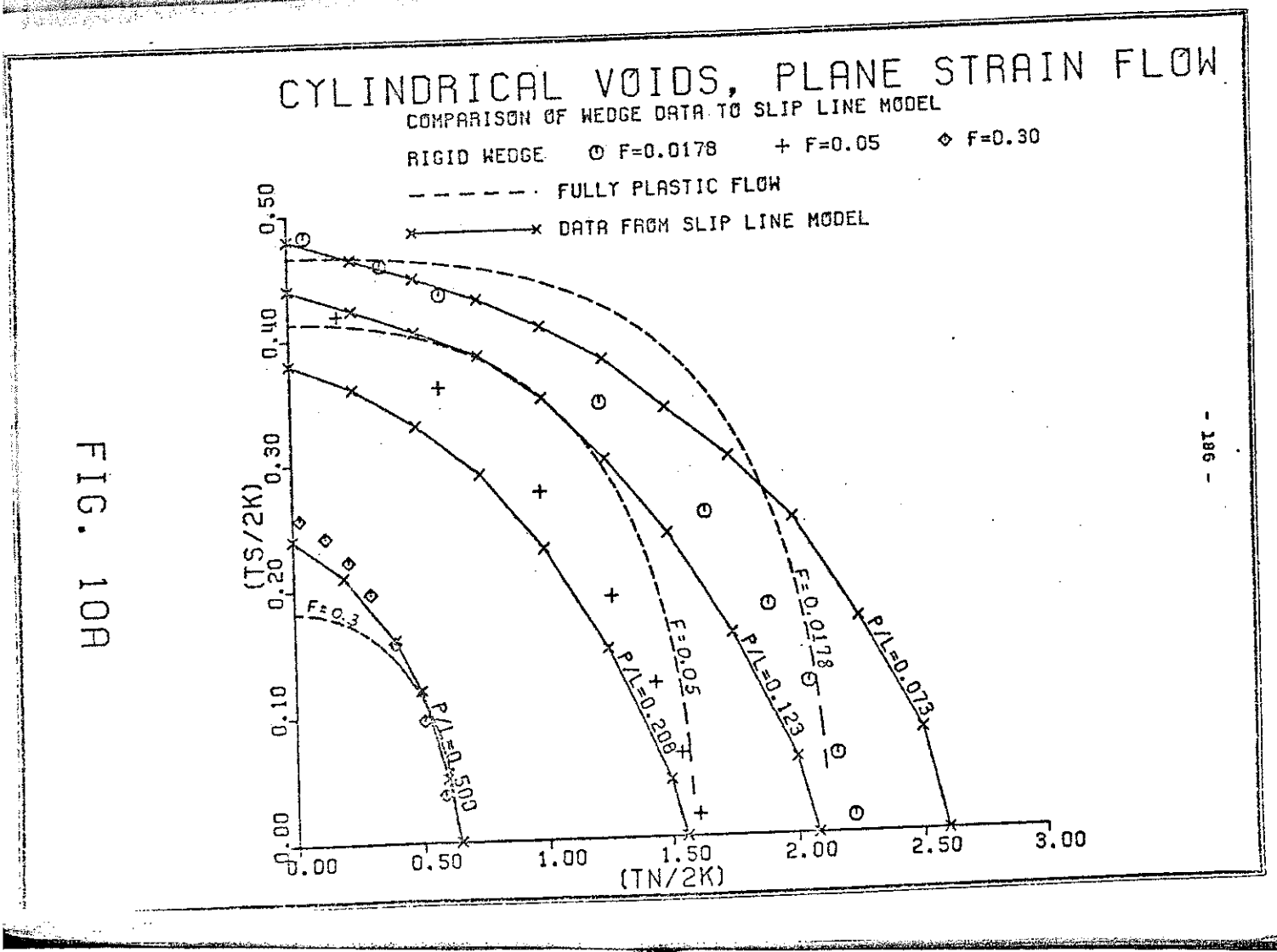

FIG. 10A

following empirical form to the data:

$$\phi = T_{eqv}^2 - \left(B_0 + B_1 T_{eH} + B_2 T_{eH}^2\right), T$$

these calculations. However, some success has been achieve

following empirical form to the data:

$$\phi = T_{eqv}^{2} \left(B_0 + B_1 T_{GH} + B_2 T_{GH}^{2} \right), \quad T_{GH} =$$

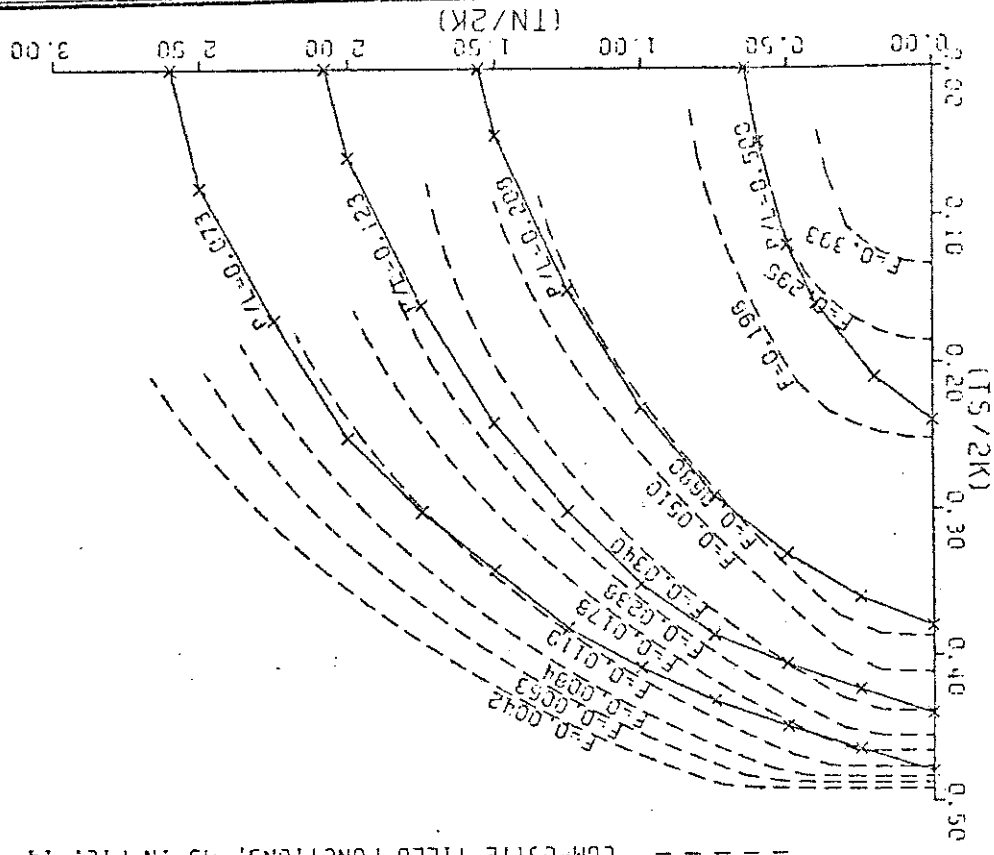

FIG. 10B

these calculations. However, some success has been achieve

following empirical form to the data:

$$\phi = T_{eqv}^{2} - \left(B_0 + B_1 T_{GH} + B_2 T_{GH}^{2}\right), \quad T_{GH}$$

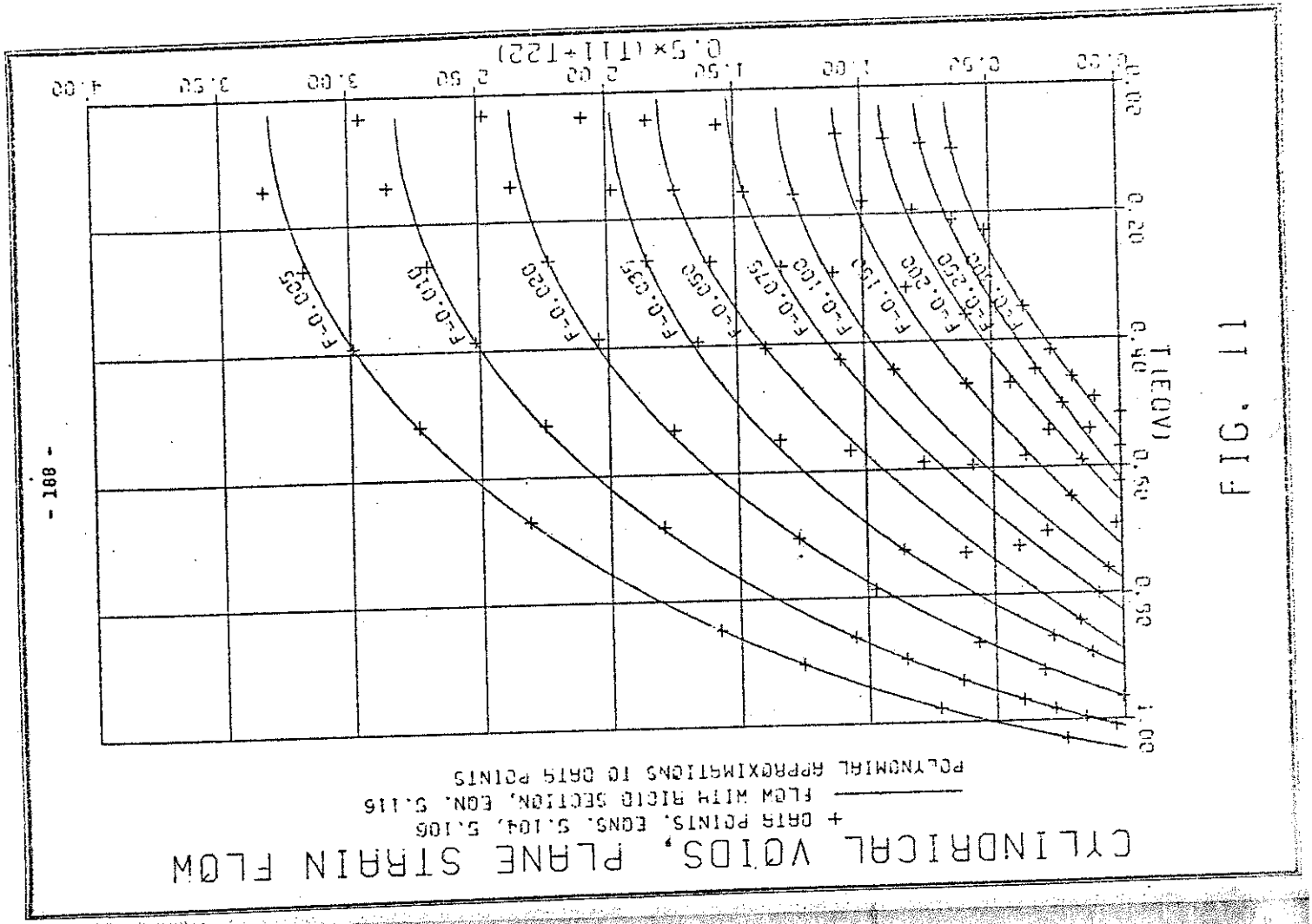

FIG. 11

following empirical form to the data:

$$\phi = T_{eqv}^2 - \left(B_0 + B_1 T_{GH} + B_2 T_{GH}^2\right), \quad T_{GH} = \frac{1}{2}$$

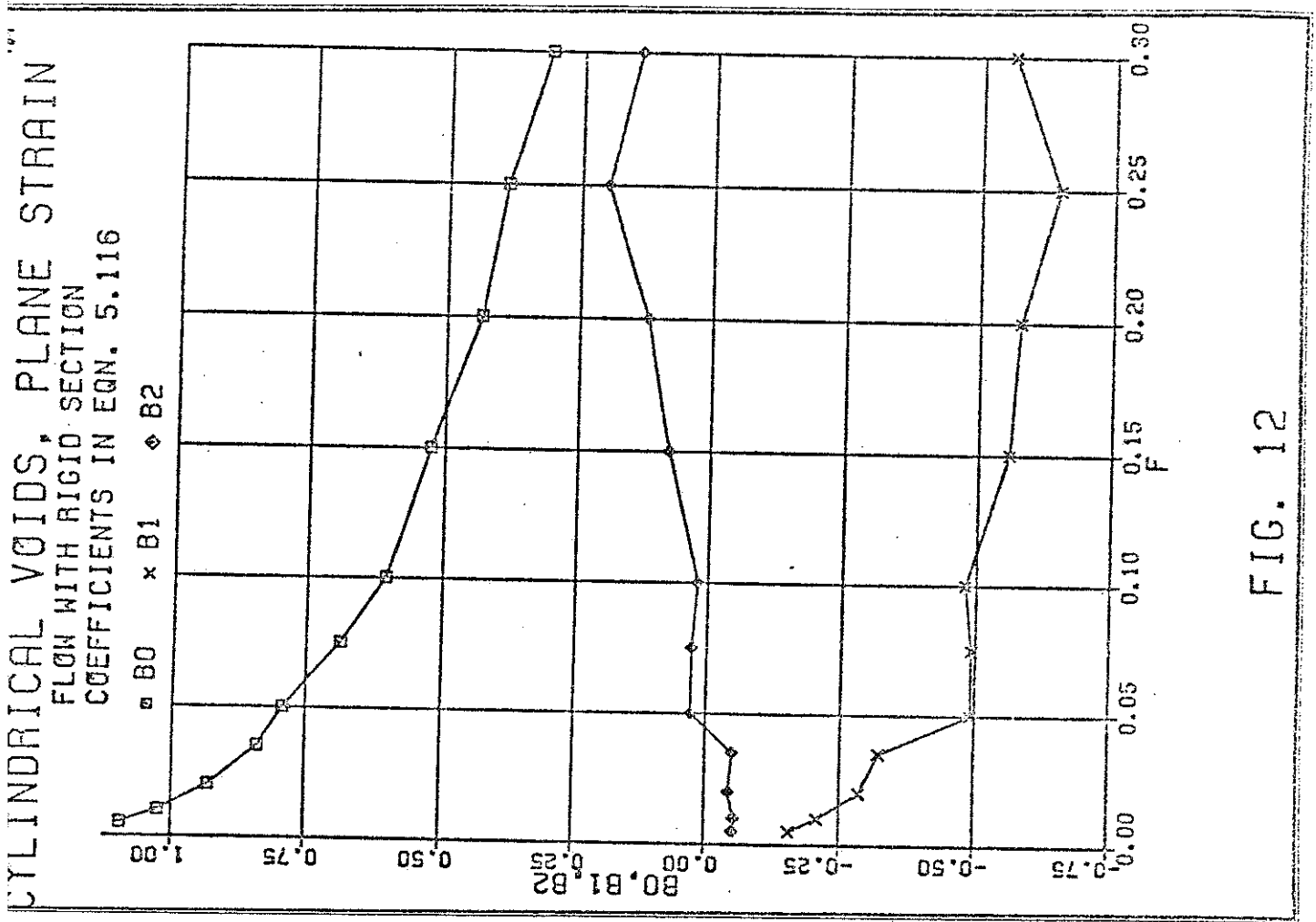

FIG. 12

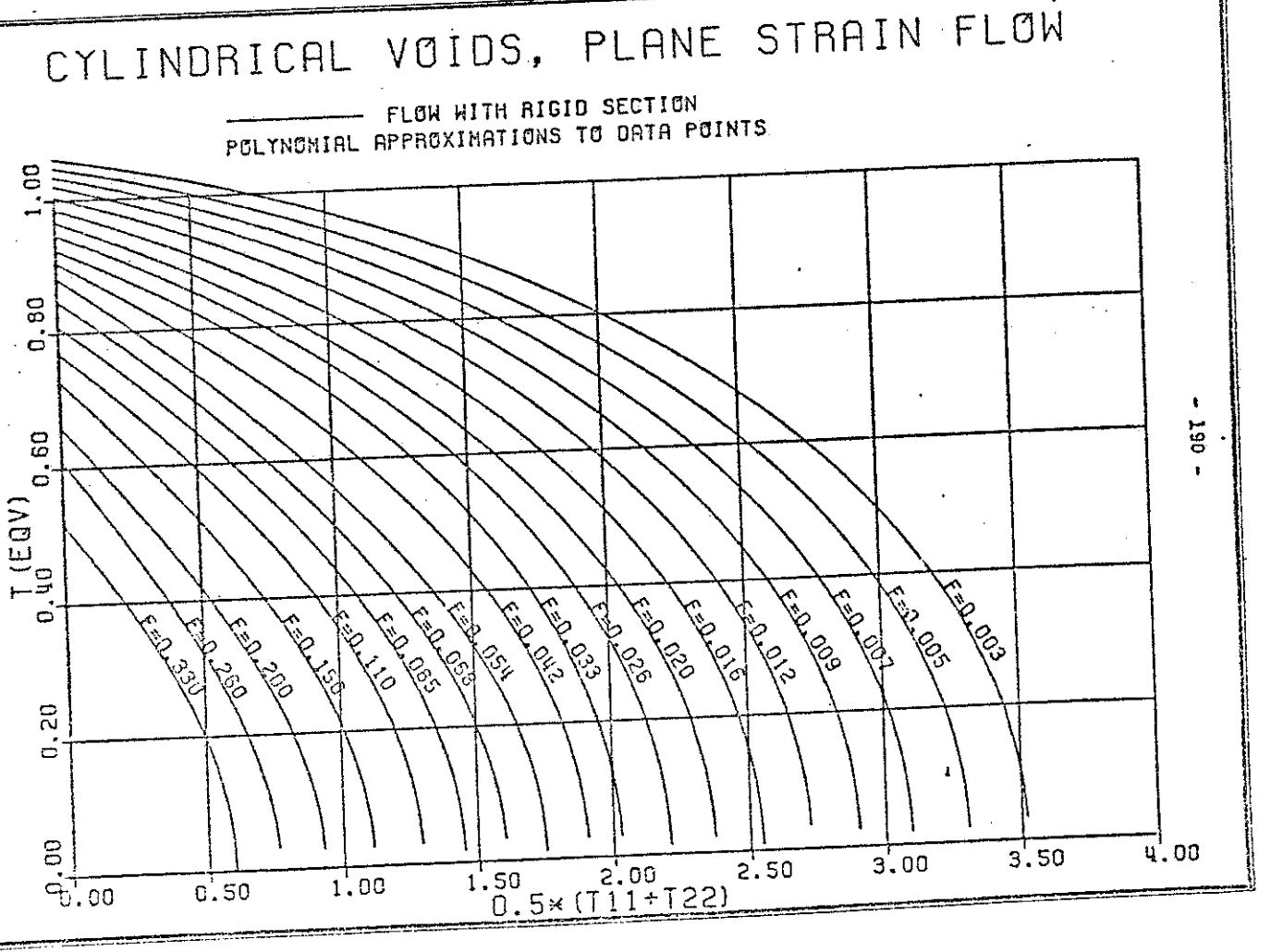
CYLINDRICAL VØIDS, PLANE STRAIN FLØW
FLOW WITH RIGID SECTION
POLYNOMIAL APPROXIMATIONS TO DATA POINTS
T(EQV)
0.5*(T11+T22)
1.00
0.80
0.60
0.40
0.20
0.00
0.00
0.50
1.00
1.50
2.00
2.50
3.00
3.50
4.00
F=0.330
F=0.260
F=0.200
F=0.150
F=0.110
F=0.085
F=0.068
F=0.054
F=0.042
F=0.033
F=0.026
F=0.020
F=0.016
F=0.012
F=0.009
F=0.007
F=0.005
F=0.003

FIG. 13

CYLINDRICAL VOIDS, PLANE STRAIN FLOW
COMPOSITE YIELD FUNCTIONS, COMBINING EQNS. 5.67 AND 5.116
(LINE SEGMENTS CORRESPONDING TO LOWER DISSIPATION)
T (EQV)
0.5×(T11+T22)
F=0.30
F=0.25
F=0.20
F=0.15
F=0.10
F=0.075
F=0.050
F=0.035
F=0.020
F=0.010
F=0.005

FIG. 14

CYLINDRICAL VOIDS, PLANE STRAIN FLOW

APPROXIMATIONS TO COMPOSITE YIELD FUNCTIONS FOR A RANGE OF VALUES OF P, EQN. 5.118 SUPERIMPOSED ON DATA FROM FIG. 14

P= 2.0, 2.5, 3.0, 3.5

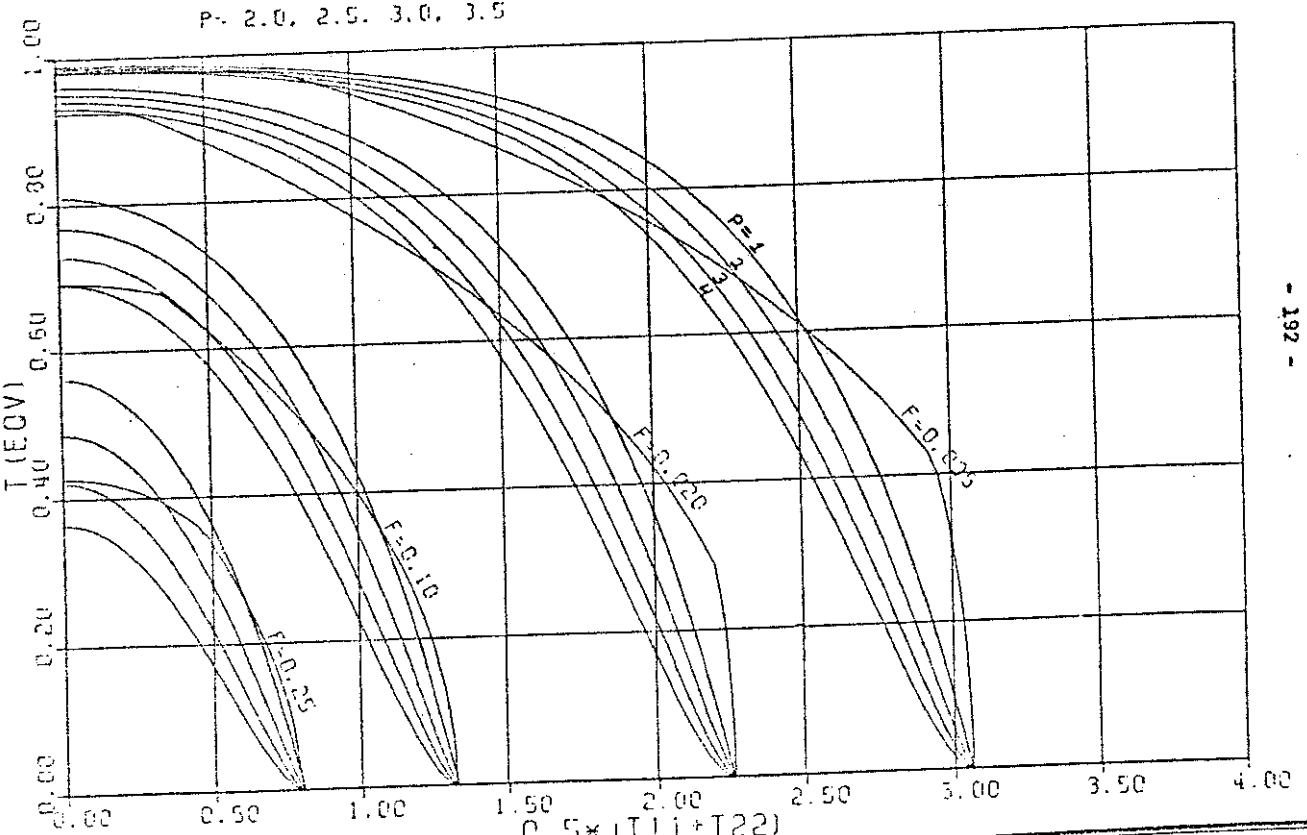

FIG. 15

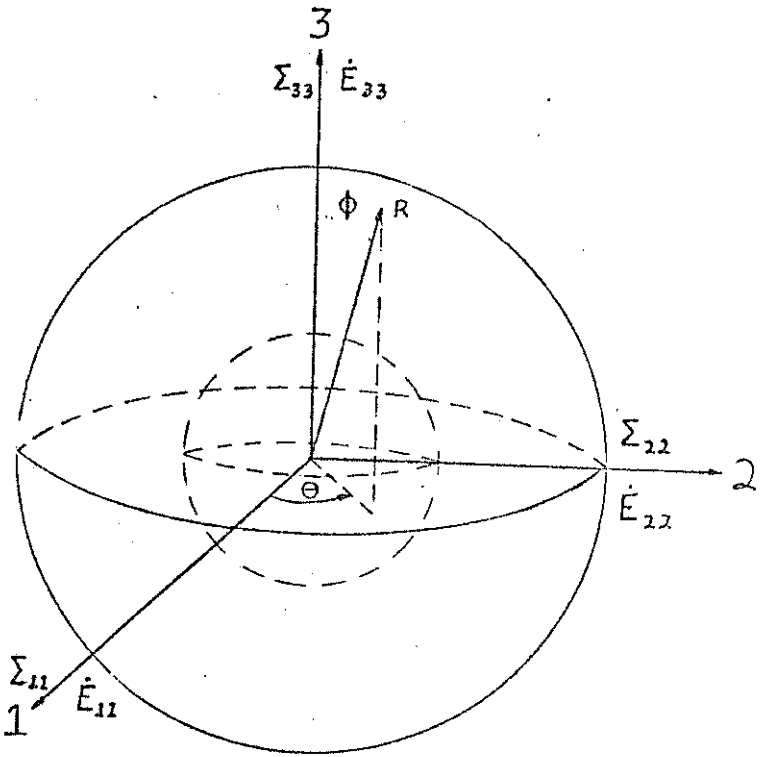

SPHERICAL VOID MODEL, FULLY PLASTIC FLOW

FIGURE 16

SPHERICAL VOIDS, FULLY PLASTIC FLOW
FIRST ORDER SOLUTION, EQN. 6.40
SECOND ORDER SOLUTION, EQN. 6.42
E11=E22, E33>0, AXISYMMETRIC TENSION
E11=E22, E33<0, AXISYMMETRIC COMPRESSION
EQNS. 6.29
F=0.005
F=0.010
F=0.020
F=0.050
F=0.100
F=0.200
F=0.300
T (EQV)
T (HYD)
0.00
0.20
0.40
0.60
0.80
1.00
0.00
0.50
1.00
1.50
2.00
2.50
3.00
3.50
4.00

FIG. 17

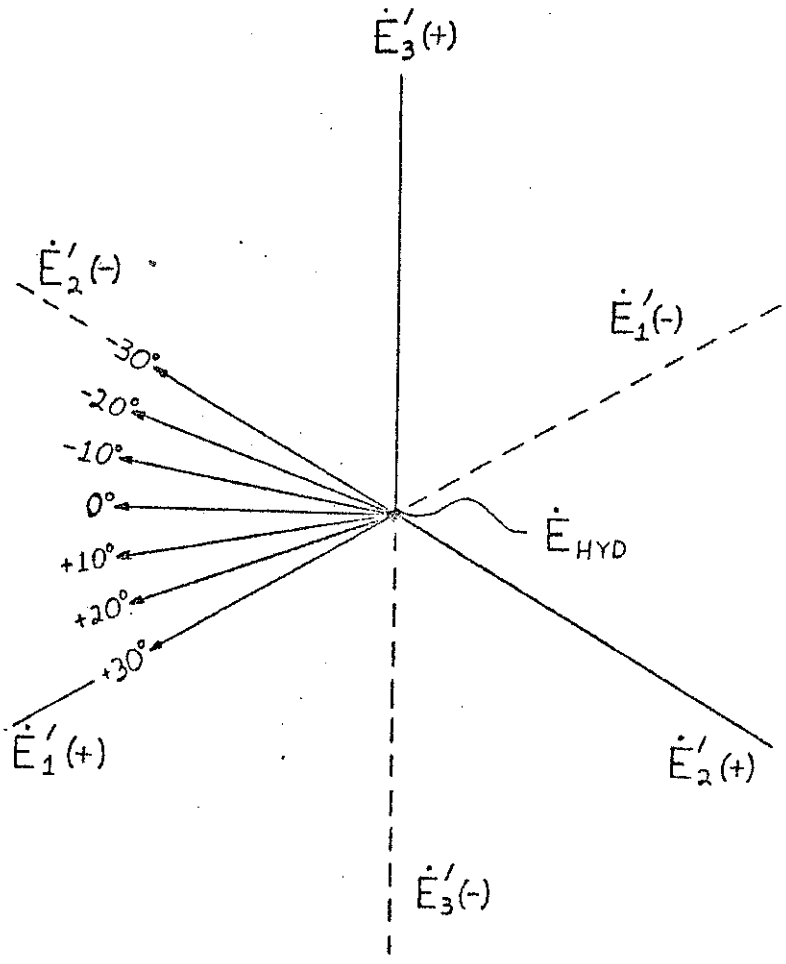

Π PLANE PROJECTION IN $\dot{E}_{ij}$ SPACE
RANGE OF INPUT VALUES COVERING 60°
BY SYMMETRY, GIVES STRESS RESULTS FOR 360°
(SPHERICAL MODEL, FULLY PLASTIC FLOW)

FIGURE 18A

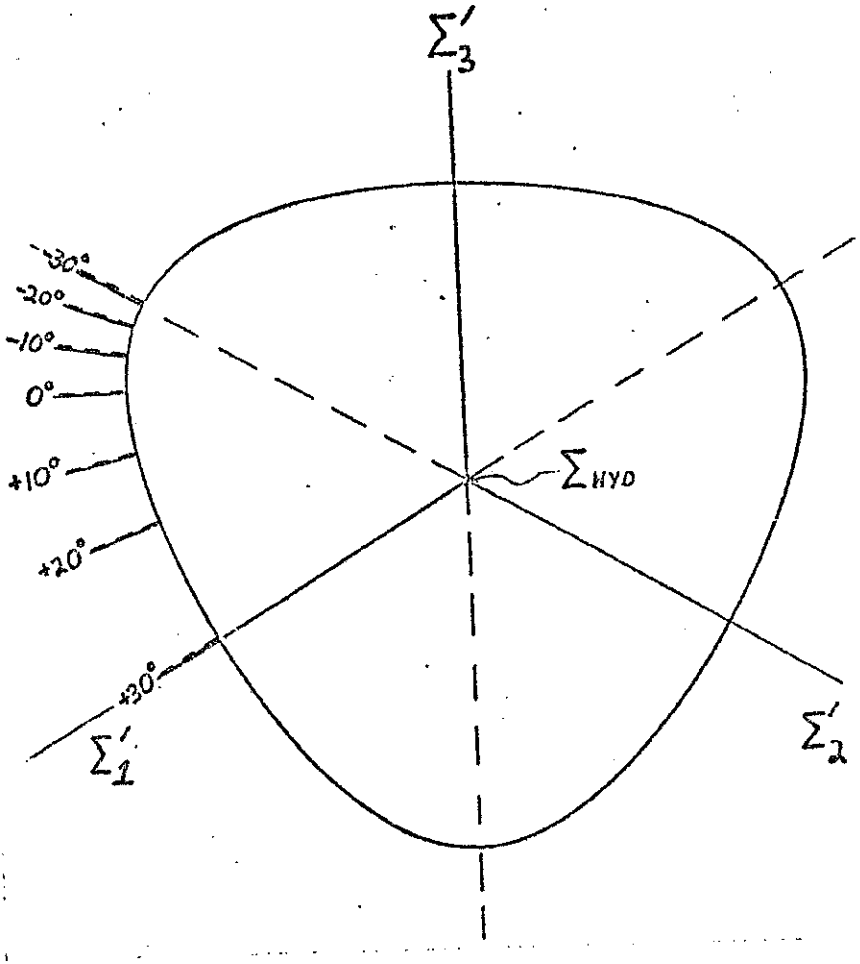

EXAMPLE OF π PLANE PROJECTION OF YIELD LOCUS IN STRESS SPACE
SYMMETRY TO POSITIVE AND NEGATIVE AXES IS SHOWN
DEVIATION FROM CIRCULAR IS EXAGGERATED
PROJECTIONS OF $\dot{E}_{ij}$ INPUT DIRECTIONS DETERMINED BY NORMALITY
(SPHERICAL MODEL, FULLY PLASTIC FLOW)

FIGURE 18B

	T_{eqv}	θ(deg.)
A	0.3301	-30.0
B	0.3296	-21.1
C	0.3281	-11.9
D	0.3262	- 2.4
E	0.3237	+ 7.6
F	0.3216	+18.5
G	0.3156	+30.0

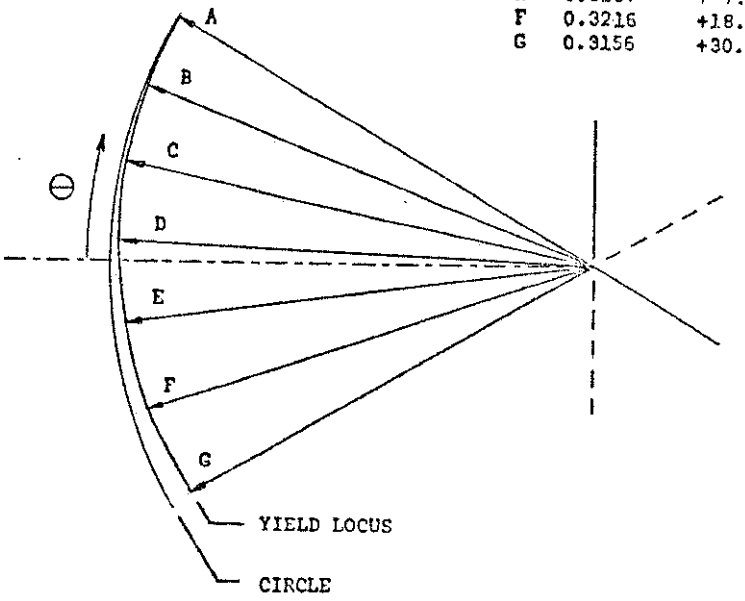

π PLANE PROJECTION OF YIELD LOCUS IN STRESS SPACE
60° SECTION FOR $f = 0.10$, $T_{HYD} = 1.41$ ($T_{eqv} \approx 0.4$)
FROM INTERPOLATION OF DATA POINTS GENERATED WITH EQNS. 6.29
SHOWS ACTUAL DEVIATION FROM CIRCULAR
(SPHERICAL MODEL, FULLY PLASTIC FLOW, EQNS. 6.29)

FIGURE 18C

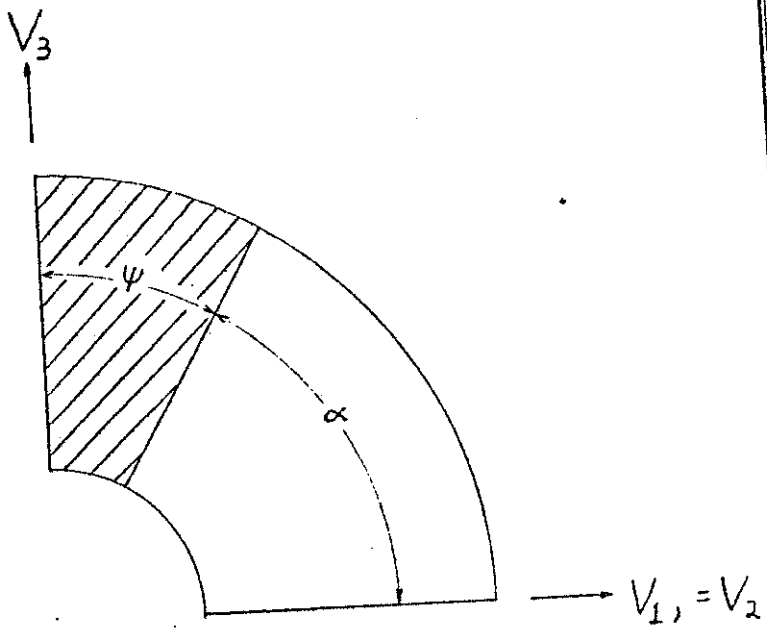

SPHERICAL MODEL, RIGID CONE
AXISYMMETRIC FLOW
RADIAL SECTION

FIGURE 19

FIG. 20A

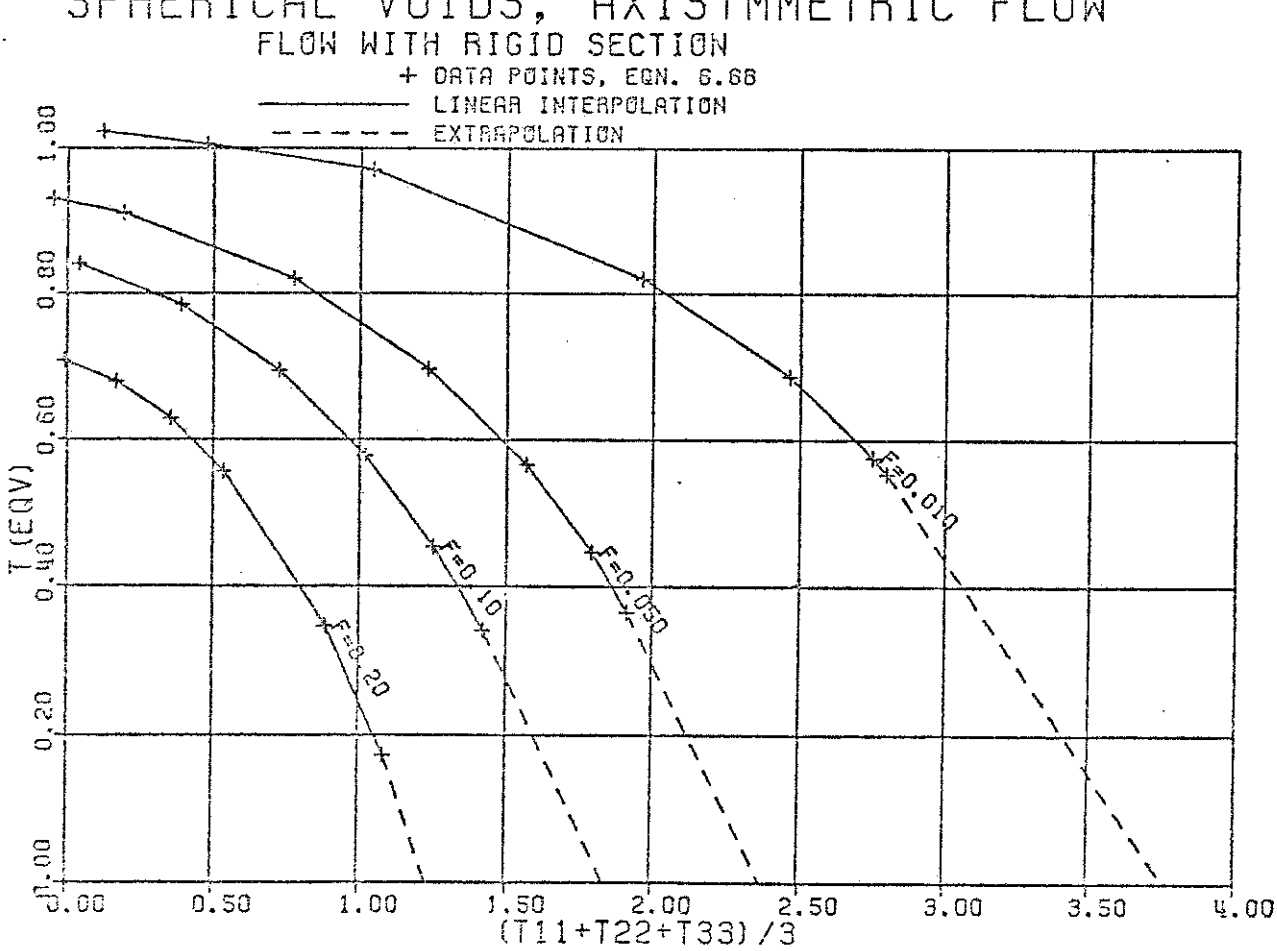
SPHERICAL VØIDS, AXISYMMETRIC FLØW
FLØW WITH RIGID SECTION
+ DATA POINTS, EQN. 6.66
LINEAR INTERPOLATION
EXTRAPOLATION
T(EQV)
1.00
0.80
0.60
0.40
0.20
0.00
F=0.010
F=0.050
F=0.10
F=0.20
0.00
0.50
1.00
1.50
2.00
2.50
3.00
3.50
4.00
(T11+T22+T33)/3

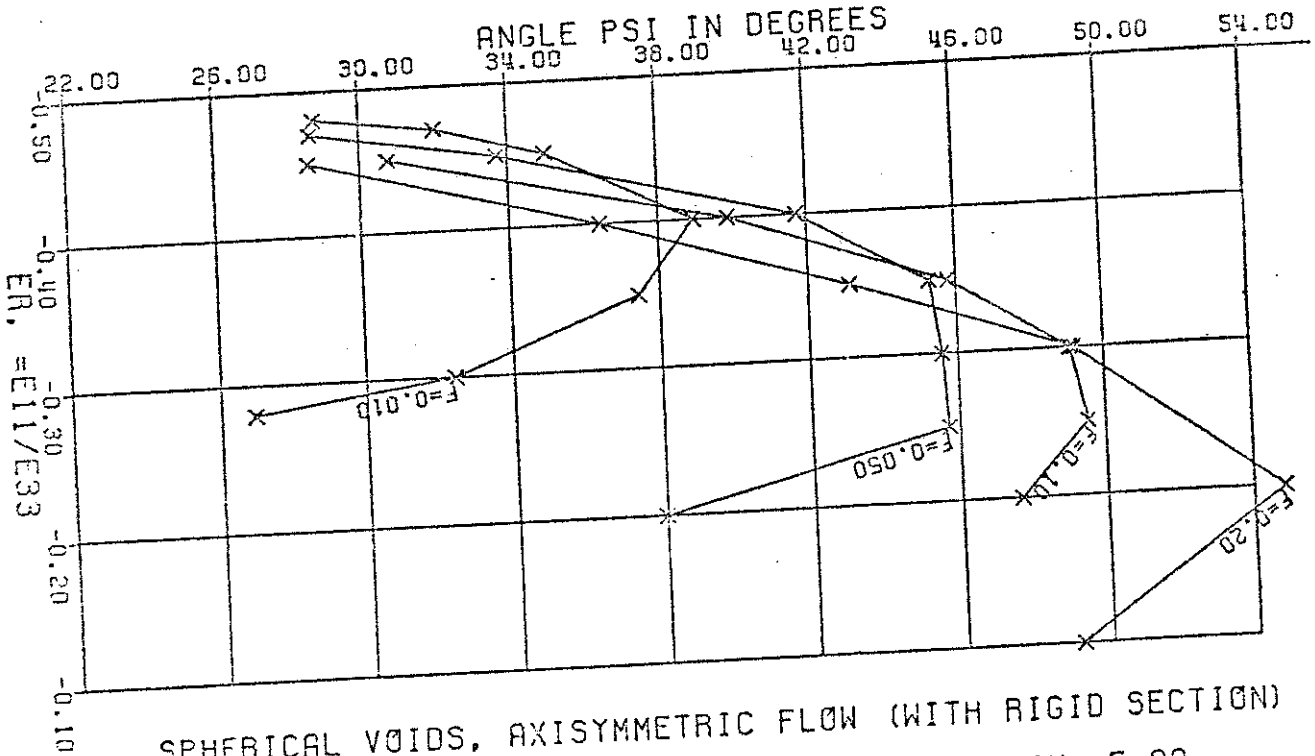

SPHERICAL VØIDS, AXISYMMETRIC FLØW (WITH RIGID SECTION)

ANGLE PSI FØR MINIMUM DISSIPATION, AS IN EQN. 5.99

× DATA POINTS

FIG. 20R

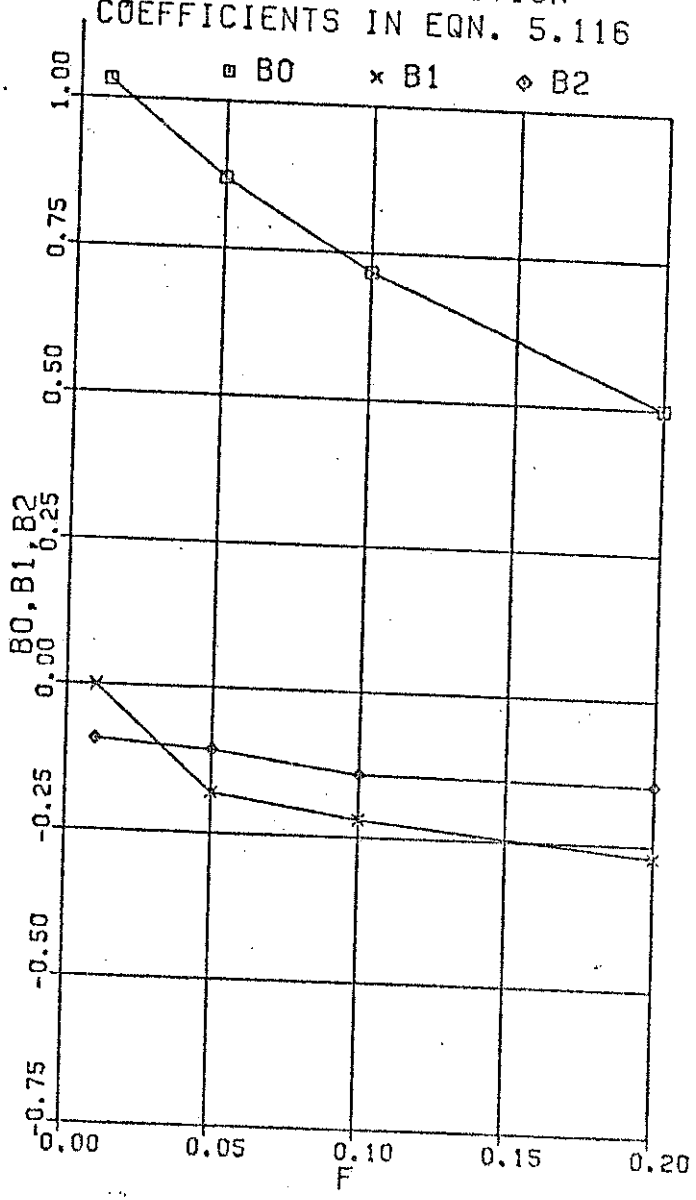
SPHERICAL VOID MODEL
FLOW WITH RIGID SECTION
COEFFICIENTS IN EQN. 5.116
B0
B1
B2
1.00
0.75
0.50
0.25
0.00
-0.25
-0.50
-0.75
B0, B1, B2
0.00
0.05
0.10
0.15
0.20
F

FIG. 20C

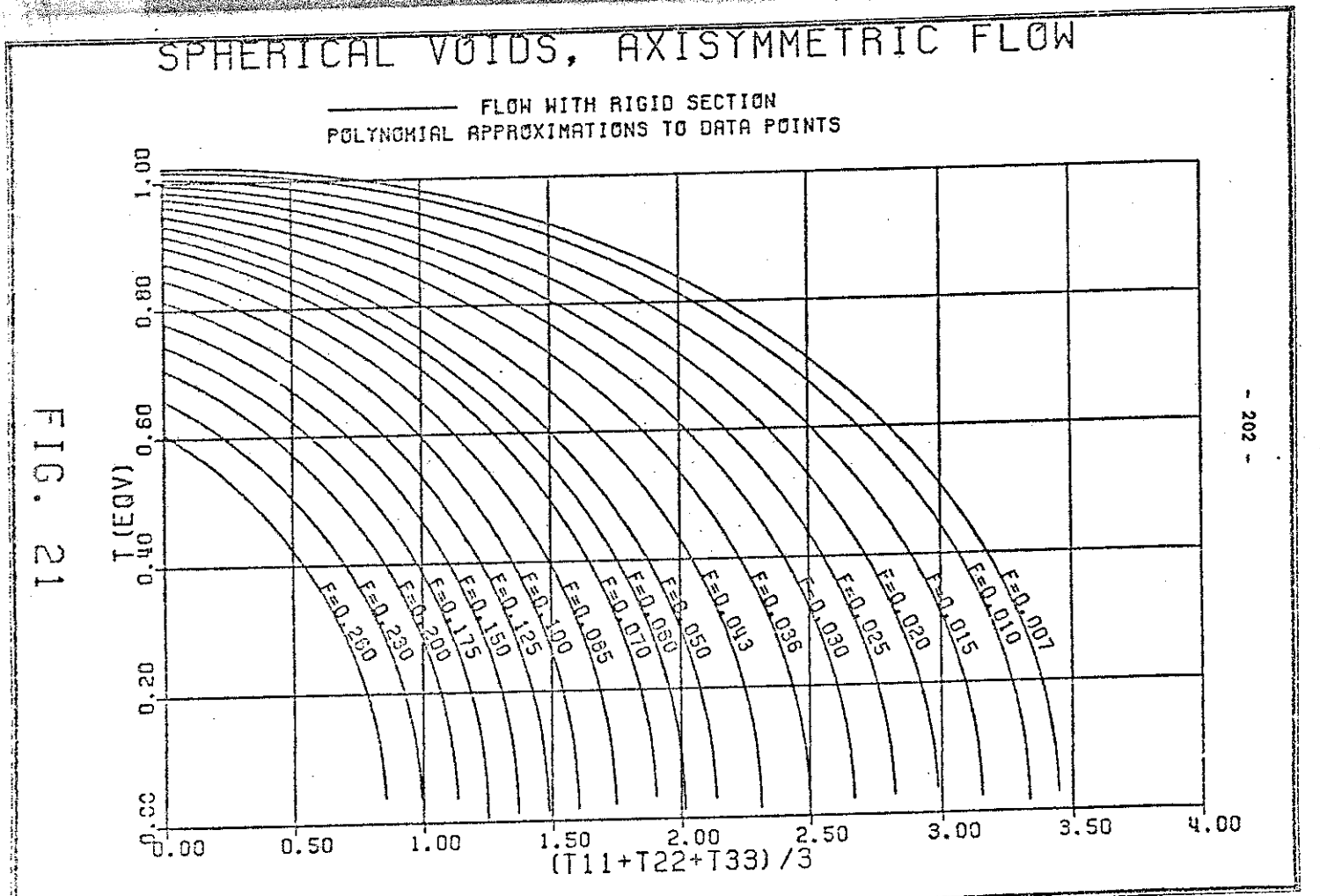
SPHERICAL VOIDS, AXISYMMETRIC FLOW
FLOW WITH RIGID SECTION
POLYNOMIAL APPROXIMATIONS TO DATA POINTS
T(EQV)
1.00
0.80
0.60
0.40
0.20
0.00
0.00
0.50
1.00
1.50
2.00
2.50
3.00
3.50
4.00
(T11+T22+T33)/3
F=0.200
F=0.230
F=0.200
F=0.175
F=0.150
F=0.125
F=0.100
F=0.085
F=0.070
F=0.060
F=0.050
F=0.043
F=0.036
F=0.030
F=0.025
F=0.020
F=0.015
F=0.010
F=0.007

FIG. 21

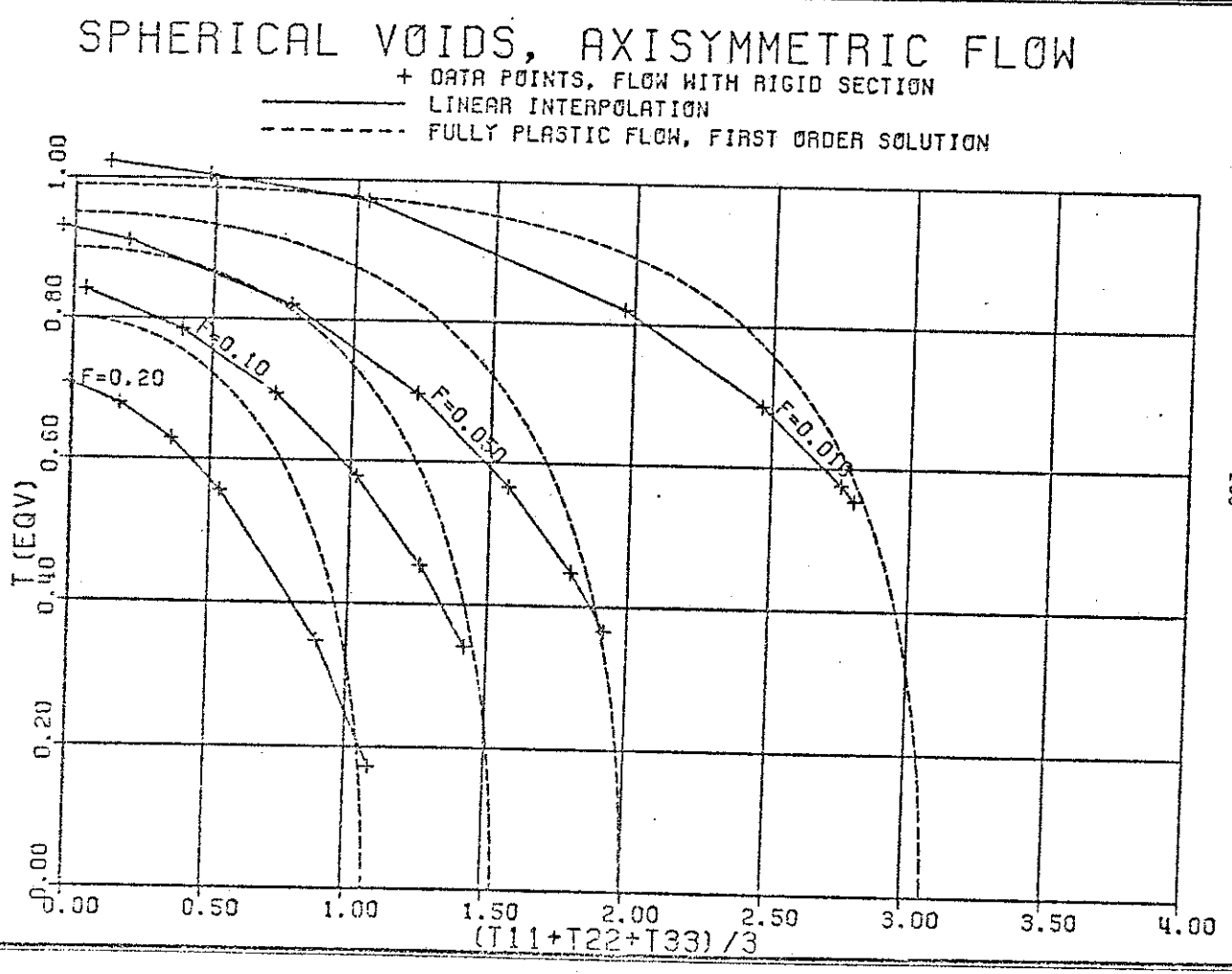
SPHERICAL VØIDS, AXISYMMETRIC FLØW
+ DATA POINTS, FLOW WITH RIGID SECTION
LINEAR INTERPOLATION
FULLY PLASTIC FLOW, FIRST ORDER SOLUTION
F=0.20
F=0.10
F=0.050
F=0.010
T(EQV)
0.00
0.20
0.40
0.60
0.80
1.00
0.00
0.50
1.00
1.50
2.00
2.50
3.00
3.50
4.00
(T11+T22+T33)/3

FIG. 22

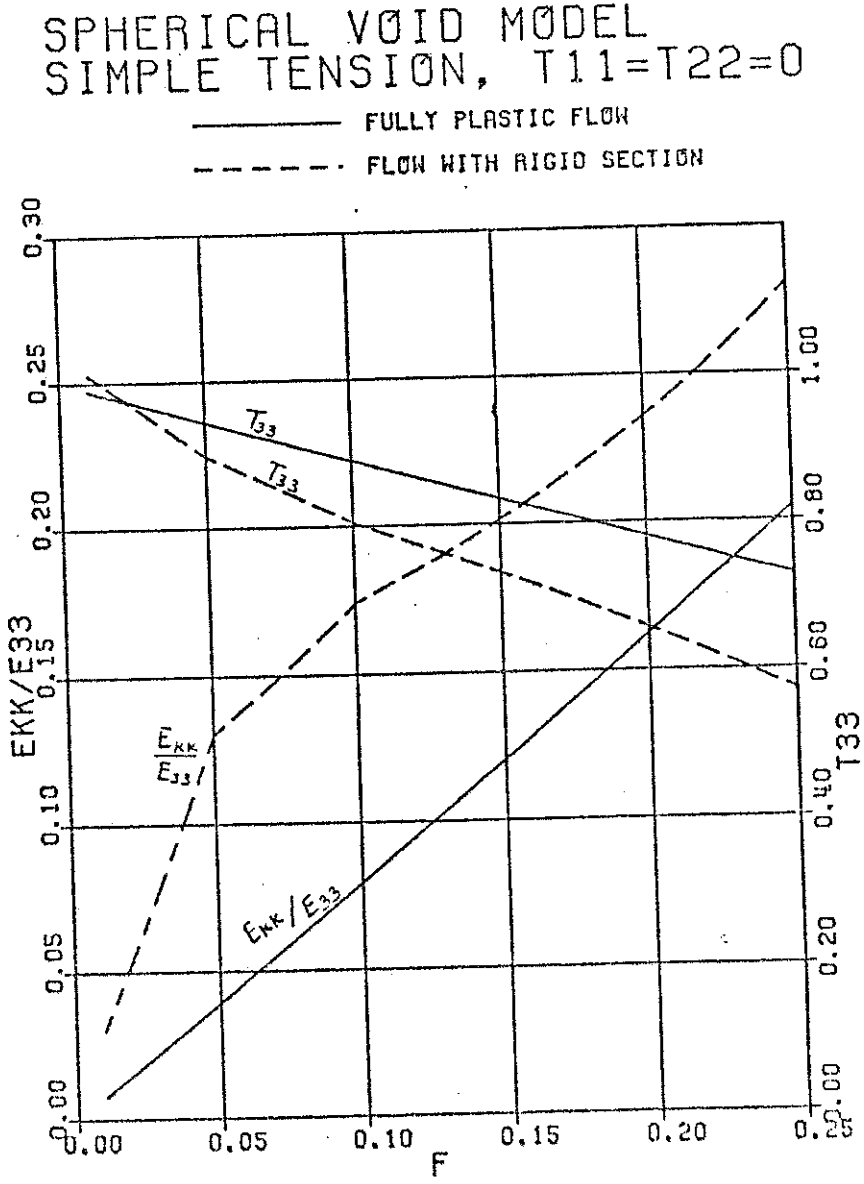
SPHERICAL VØID MØDEL
SIMPLE TENSION, T11=T22=0
FULLY PLASTIC FLOW
FLOW WITH RIGID SECTION
EKK/E33
T33
F
T_{33}
T_{33}
$\frac{E_{KK}}{E_{33}}$
E_{KK}/E_{33}
0.00
0.05
0.10
0.15
0.20
0.25
0.30
0.00
0.20
0.40
0.60
0.80
1.00

FIG. 23

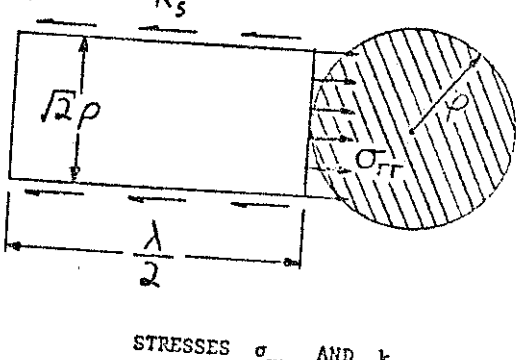

STRESSES σ_{rr} AND k_s
NONINTERACTING SECONDARY PLASTIC ZONE

FIGURE 24

(FIGURES 24 AND 25 ARE COPIED FROM REF. [13])

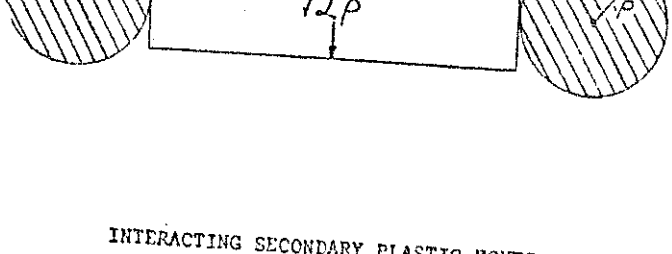

INTERACTING SECONDARY PLASTIC ZONES

FIGURE 25

STRESS AMPLIFICATION DUE TO INTERACTION OF PARALLEL CYLINDRICAL INCLUSIONS

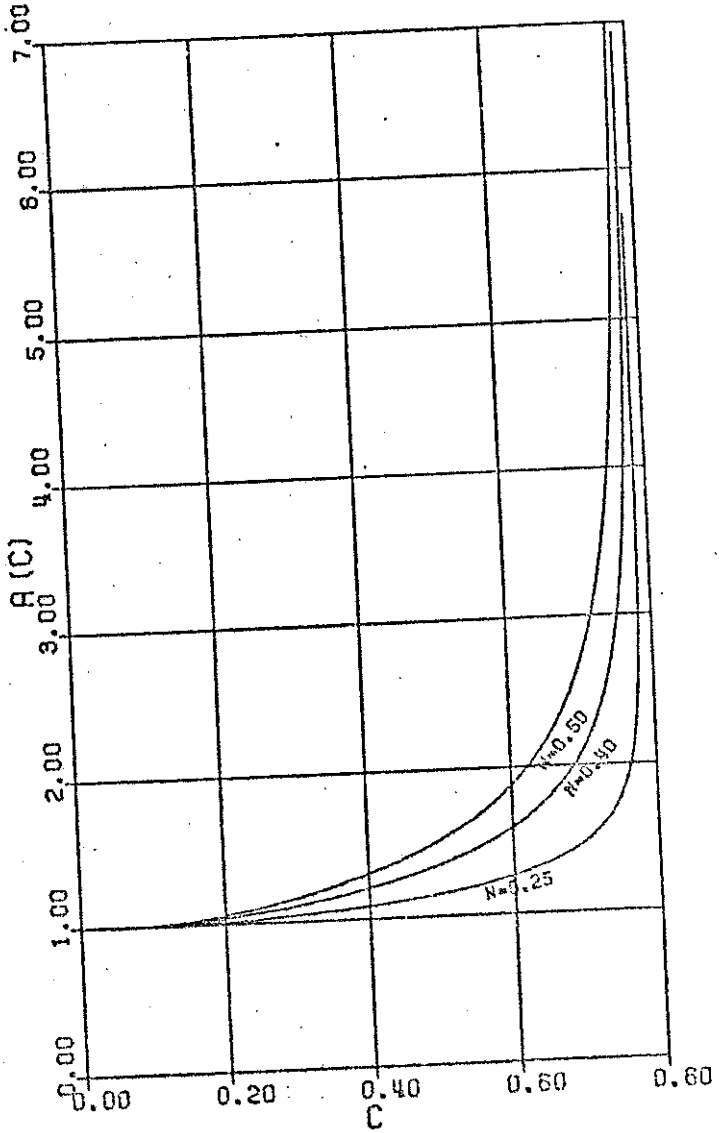

FIGURE 26A

STRESS AMPLIFICATION DUE TO INTERACTION OF SPHERICAL INCLUSIONS

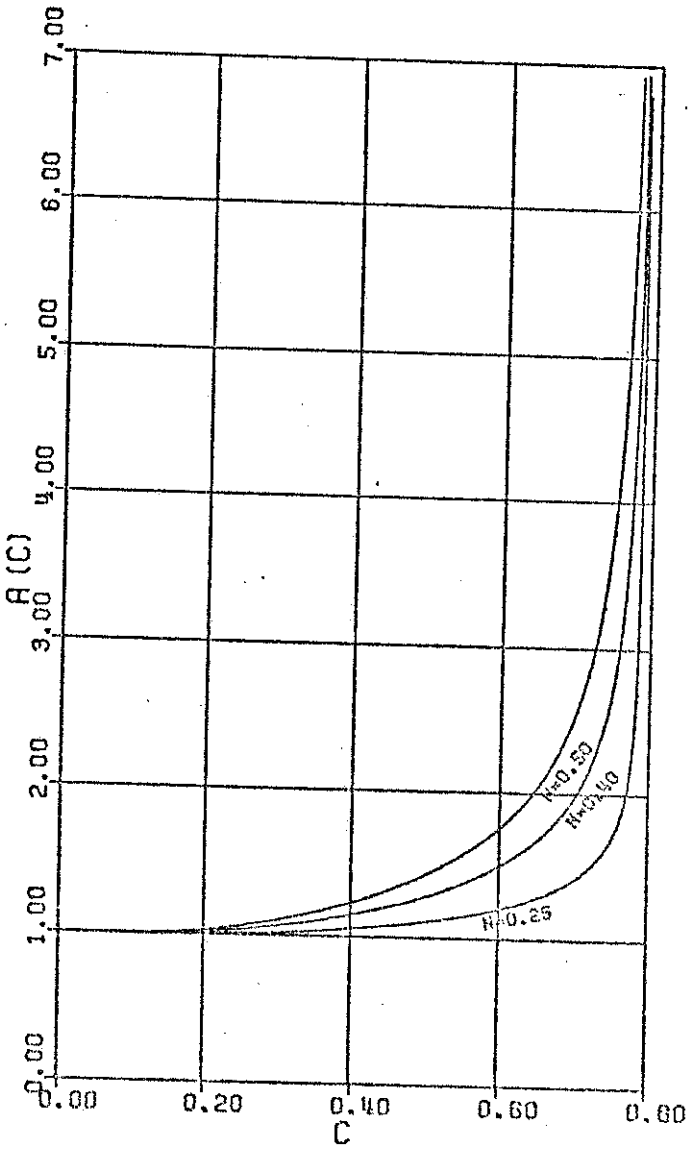

FIGURE 2GB

RELATIVE VØID NUCLEATIØN RATE

FULLY PLASTIC CYLINDRICAL PLASTIC PØTENTIAL

PLANE STRAIN, T11=0 F=0.10, $\bar{C}$=0.10, n=.25

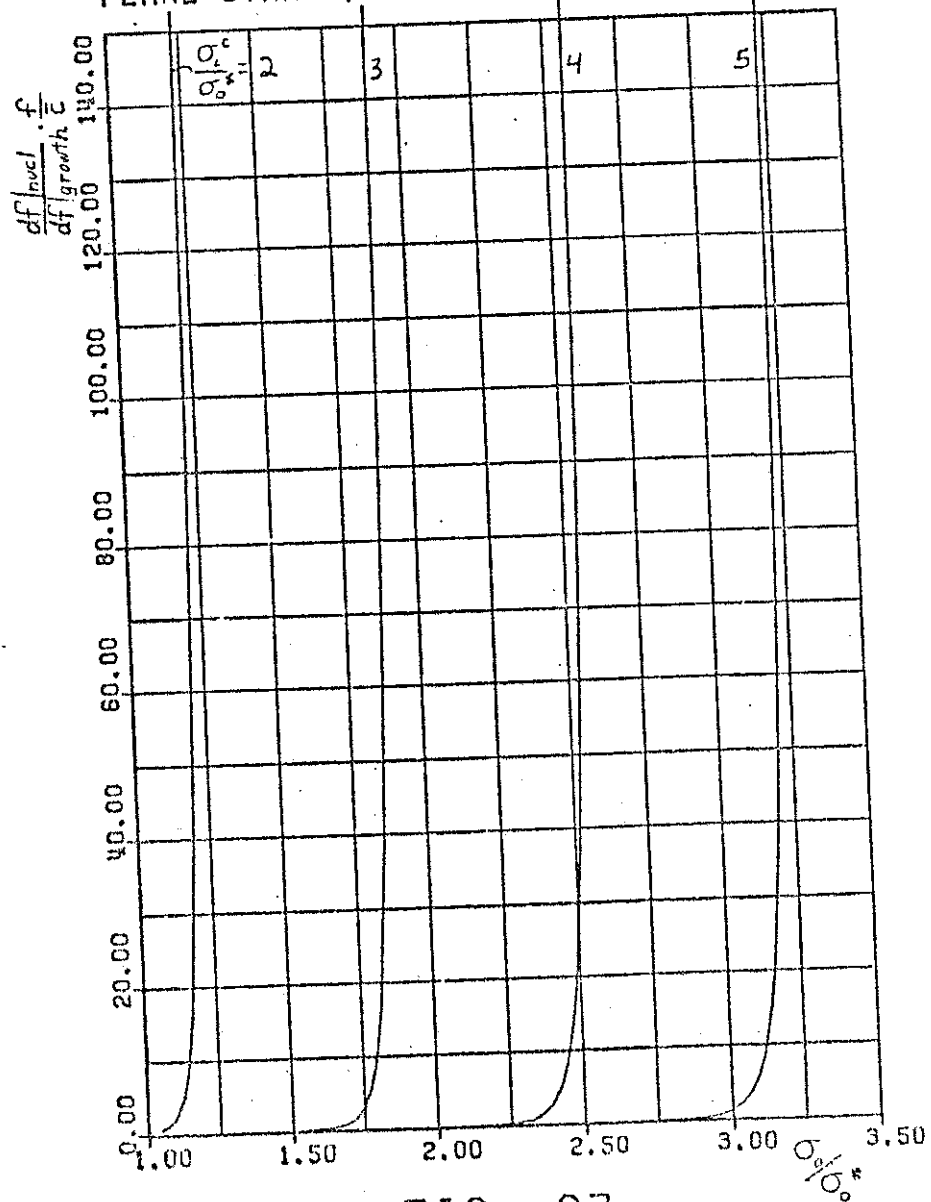

FIG. 27

RELATIVE VOID NUCLEATION RATE

WEDGE MODEL, CYLINDRICAL PLASTIC POTENTIAL

PLANE STRAIN, T11=0 F=0.10, C=0.10, $n=.25$

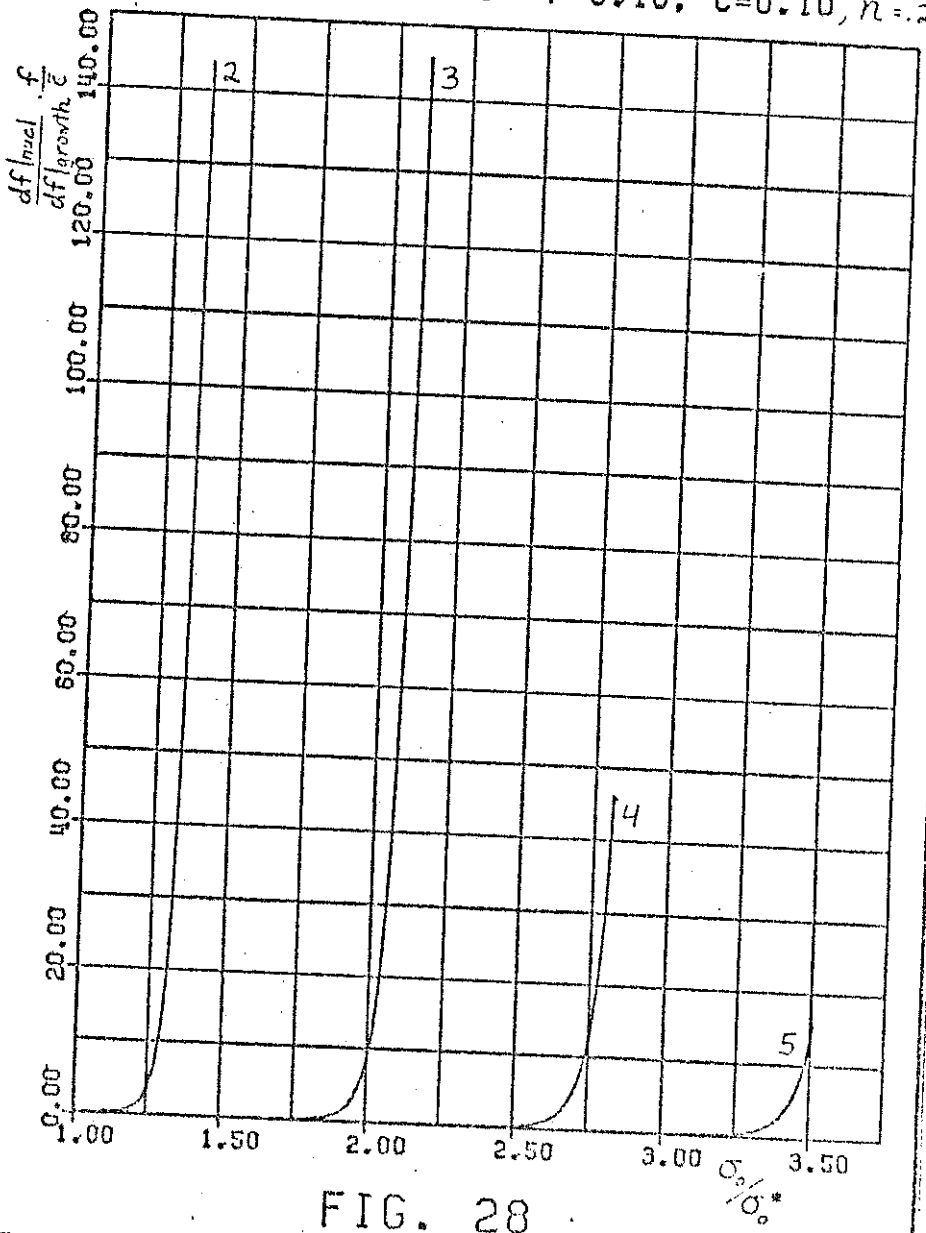

FIG. 28

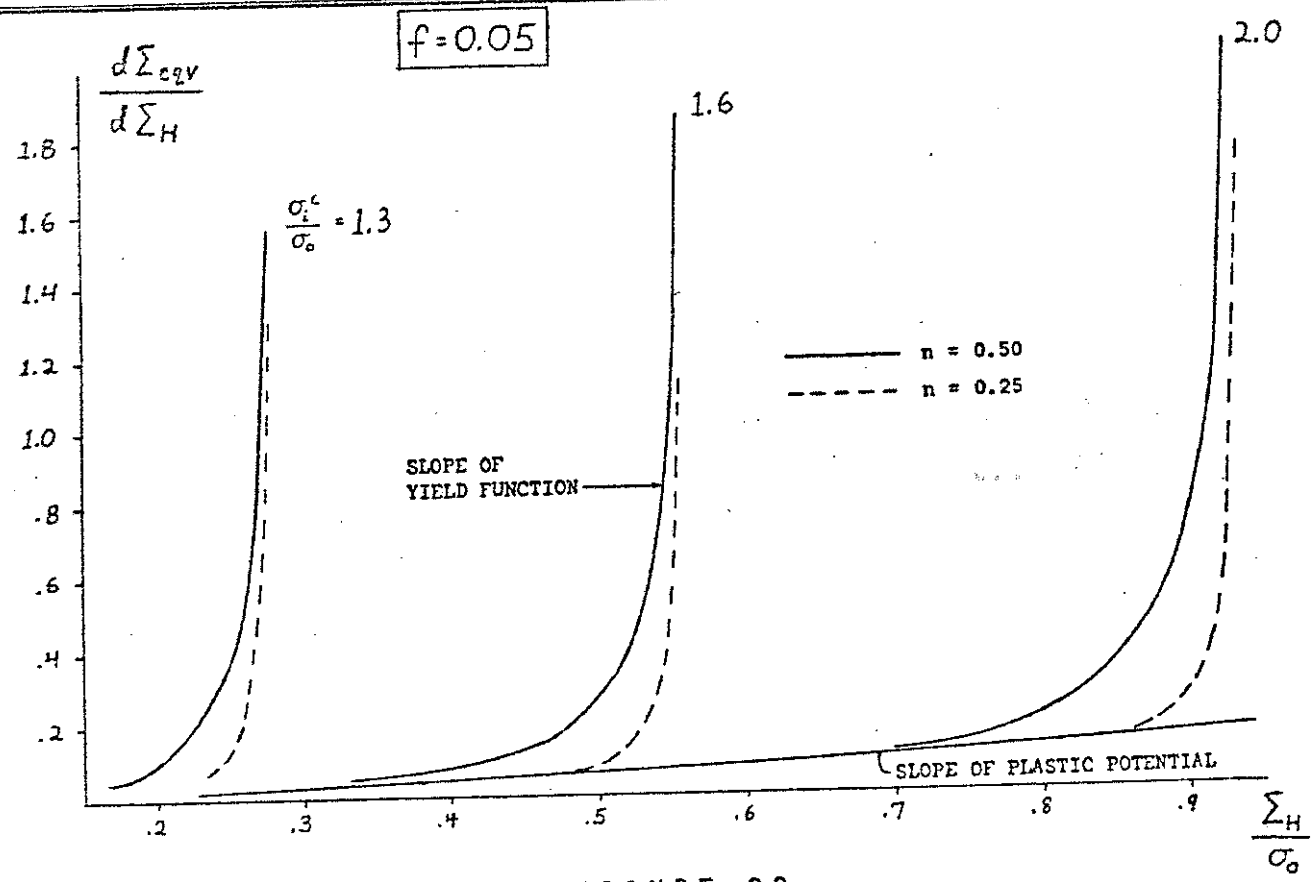
f = 0.05
$\frac{d\Sigma_{eqv}}{d\Sigma_H}$
1.8
1.6
1.4
1.2
1.0
.8
.6
.4
.2
$\frac{\sigma_i^c}{\sigma_o} = 1.3$
1.6
2.0
n = 0.50
n = 0.25
SLOPE OF YIELD FUNCTION
SLOPE OF PLASTIC POTENTIAL
.2
.3
.4
.5
.6
.7
.8
.9
$\frac{\Sigma_H}{\sigma_o}$

FIGURE 29

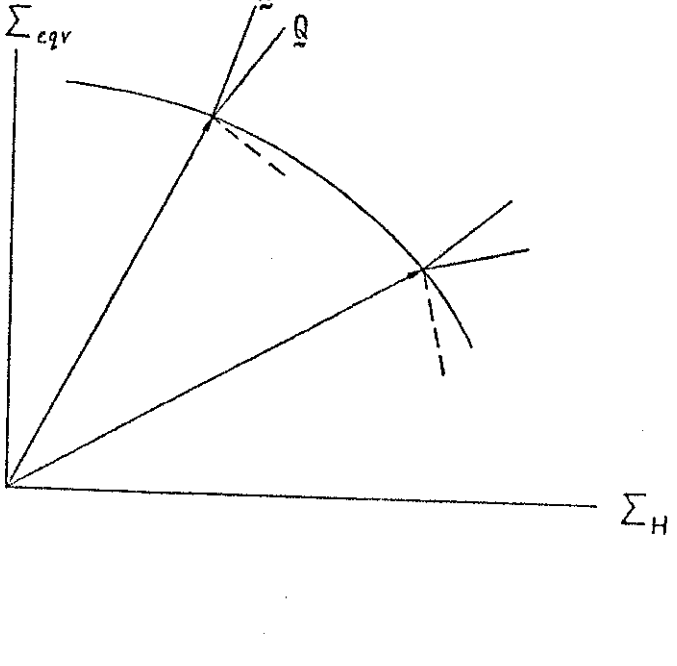

FIGURE 30

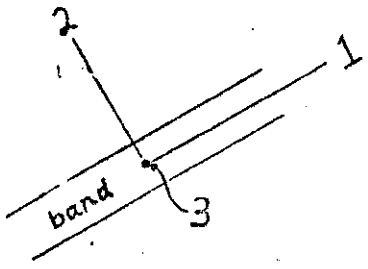

FIGURE 31A

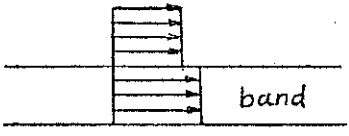

$$\Delta\left(\frac{\partial v_1}{\partial x_1}\right) \neq 0$$

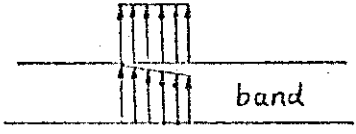

$$\Delta\left(\frac{\partial v_2}{\partial x_1}\right) \neq 0$$

FIGURE 31B

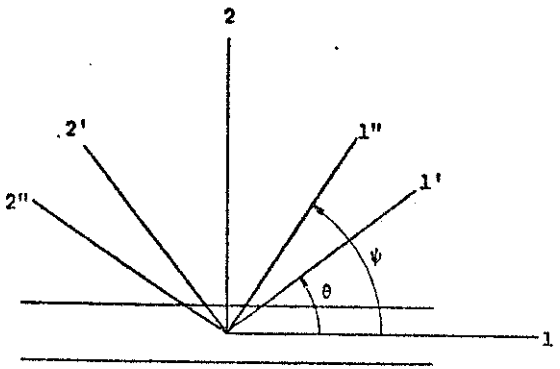

' PRINCIPLE AXES OF $\underset{\sim}{\Sigma}$

" PRINCIPLE AXES OF $\underset{\sim}{N}$

FIGURE 32

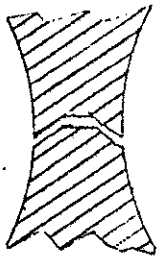

SECTION OF AXISYMMETRIC TENSILE SPECIMEN AFTER FRACTURE

FIGURE 33A

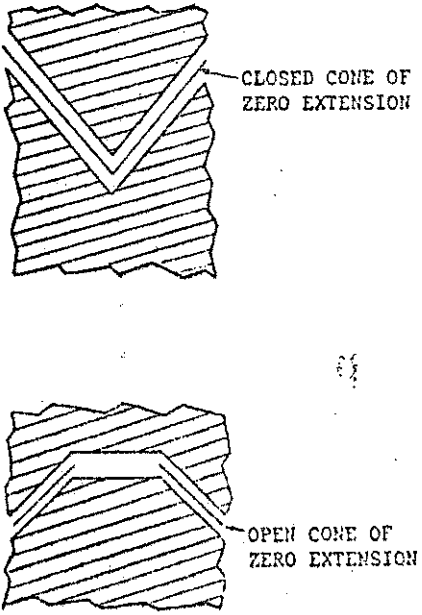

FIGURE 33B

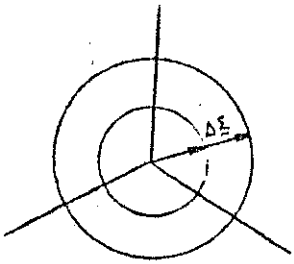

A) ISOTROPIC HARDENING

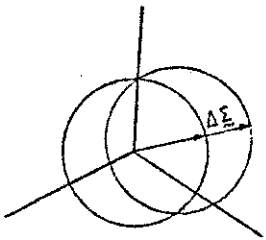

B) KINEMATIC HARDENING

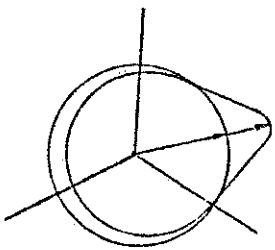

C) SHAPE CHANGE AND KINEMATIC HARDENING

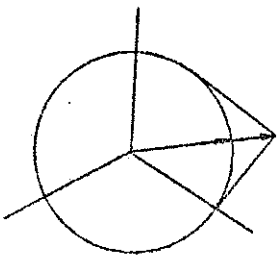

D) VERTEX FORMATION

SUBSEQUENT MICROSCOPIC YIELD FUNCTIONS
π PLANE PROJECTIONS

FIGURE 34

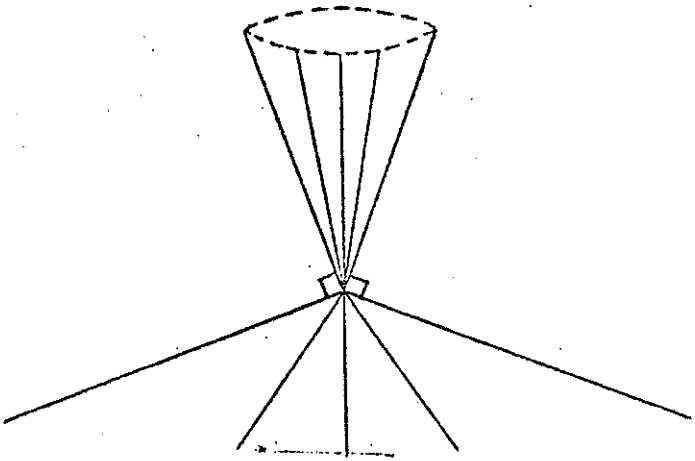

CONE OF NORMALS AT A VERTEX

FIGURE 35

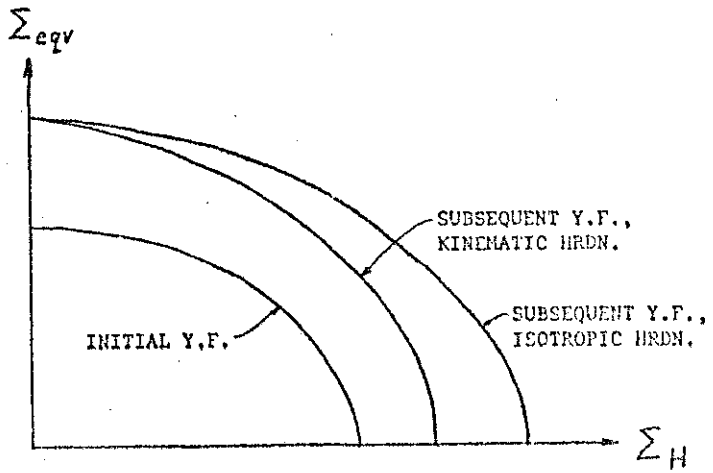

FIGURE 36

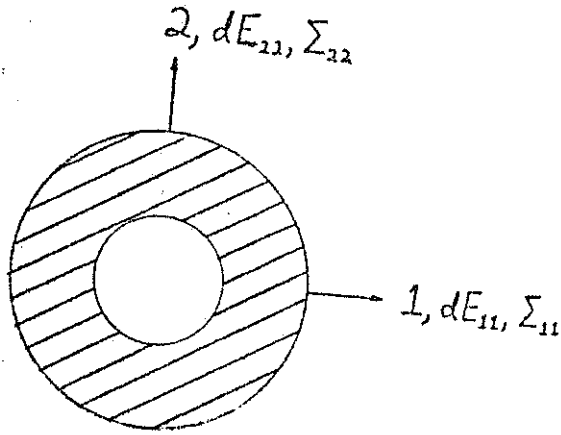

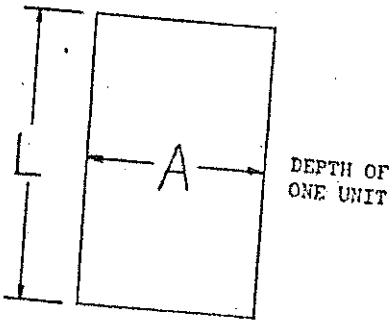

FIGURE 37

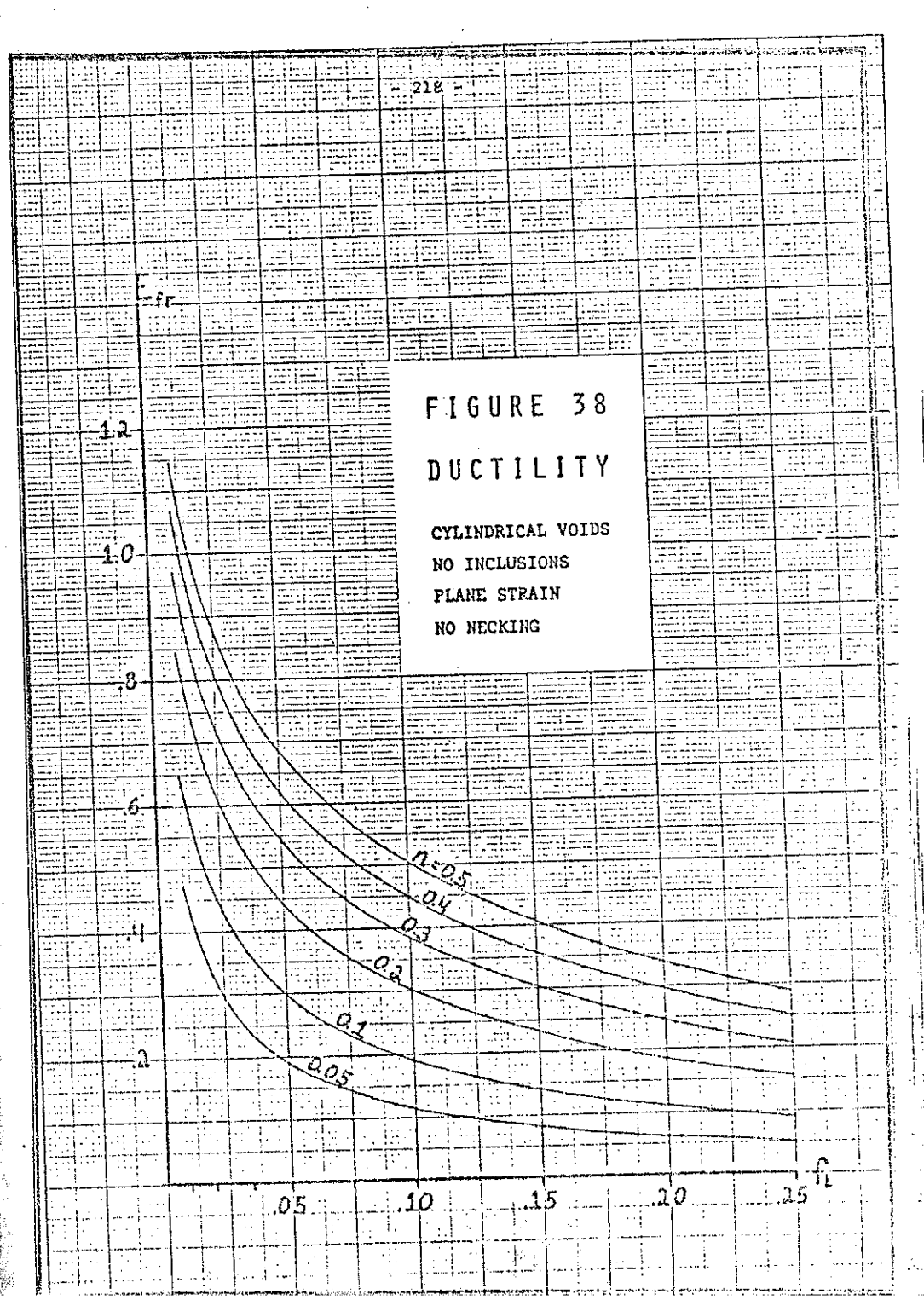

FIGURE 38

DUCTILITY

CYLINDRICAL VOIDS
NO INCLUSIONS
PLANE STRAIN
NO NECKING

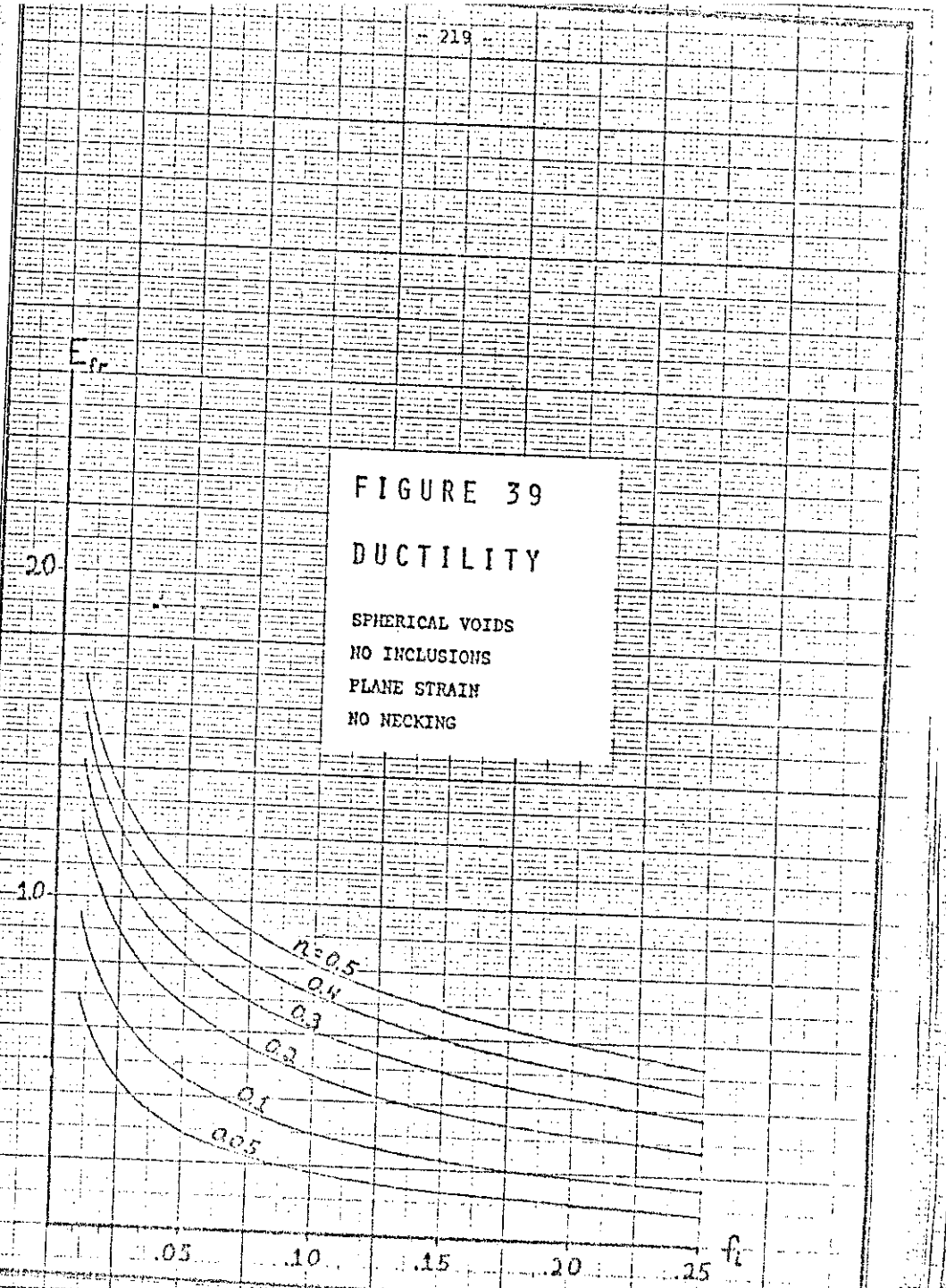

FIGURE 39

DUCTILITY

SPHERICAL VOIDS
NO INCLUSIONS
PLANE STRAIN
NO NECKING

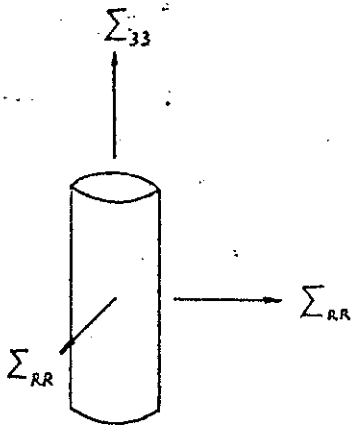

FIGURE 40

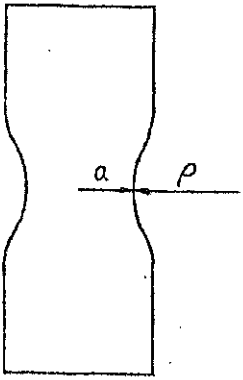

FIGURE 42

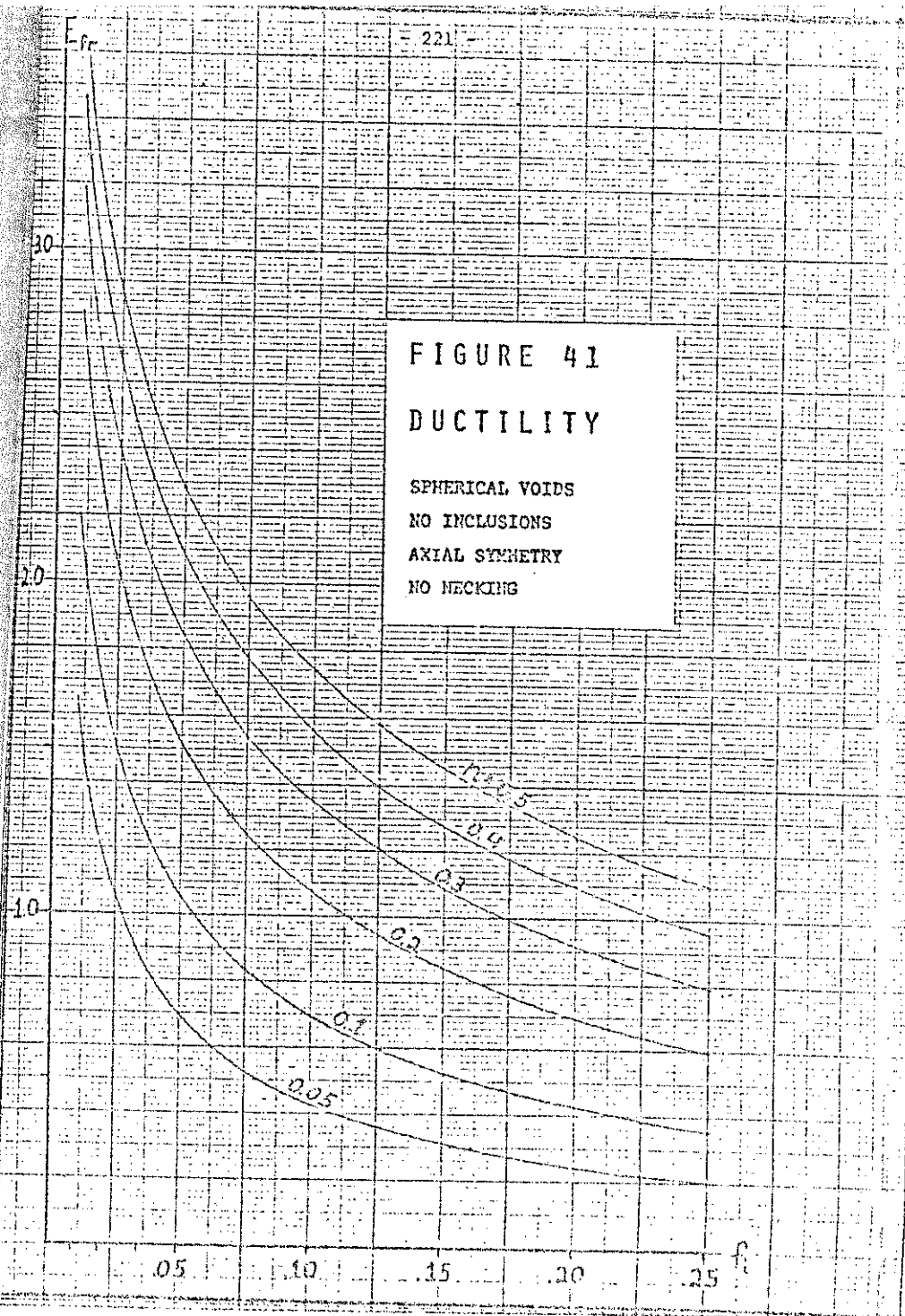

FIGURE 41

DUCTILITY

SPHERICAL VOIDS
NO INCLUSIONS
AXIAL SYMMETRY
NO NECKING

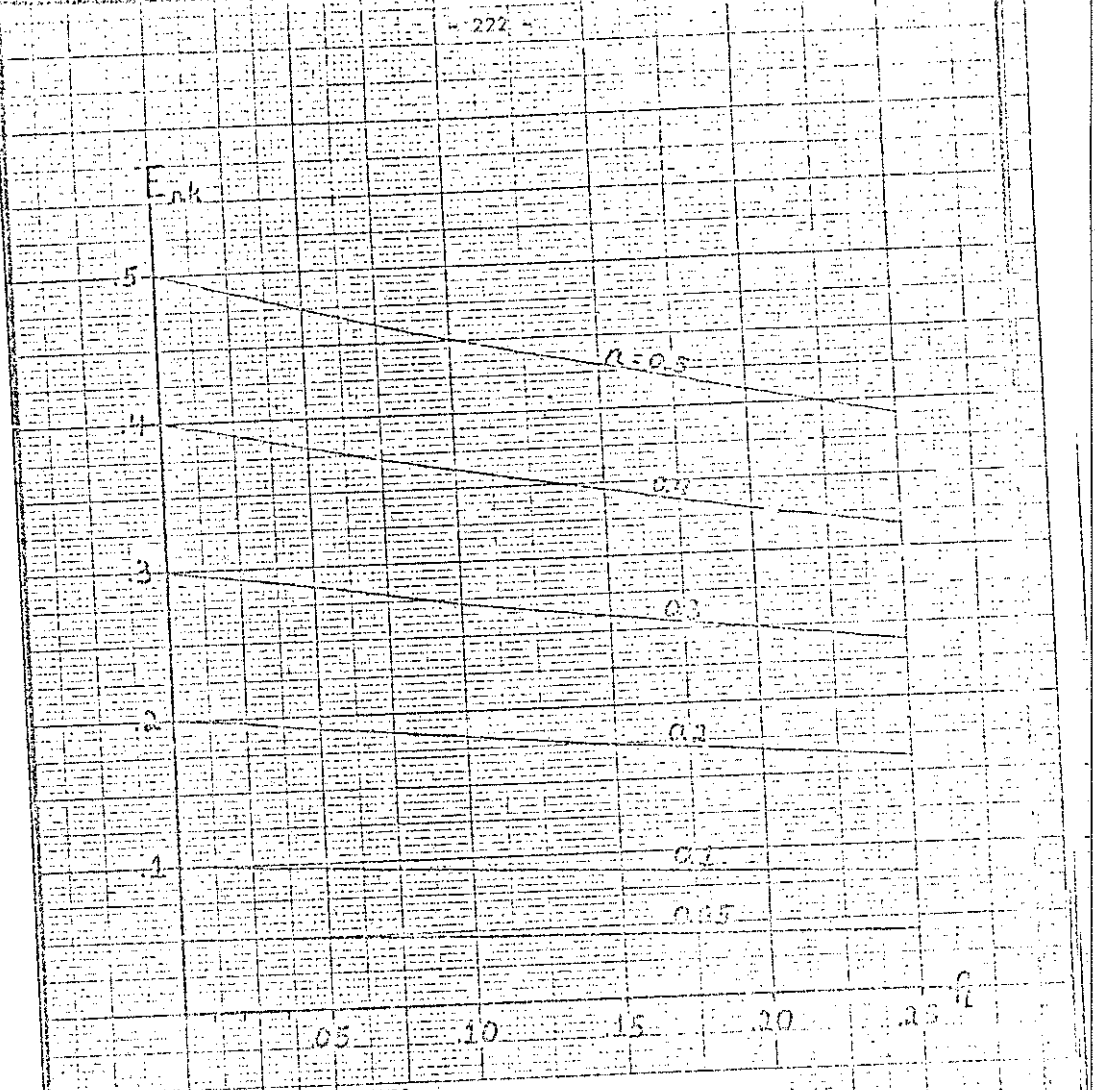

FIGURE 43

NECKING STRAIN

SPHERICAL VOIDS

NO INCLUSIONS

AXIAL SYMMETRY

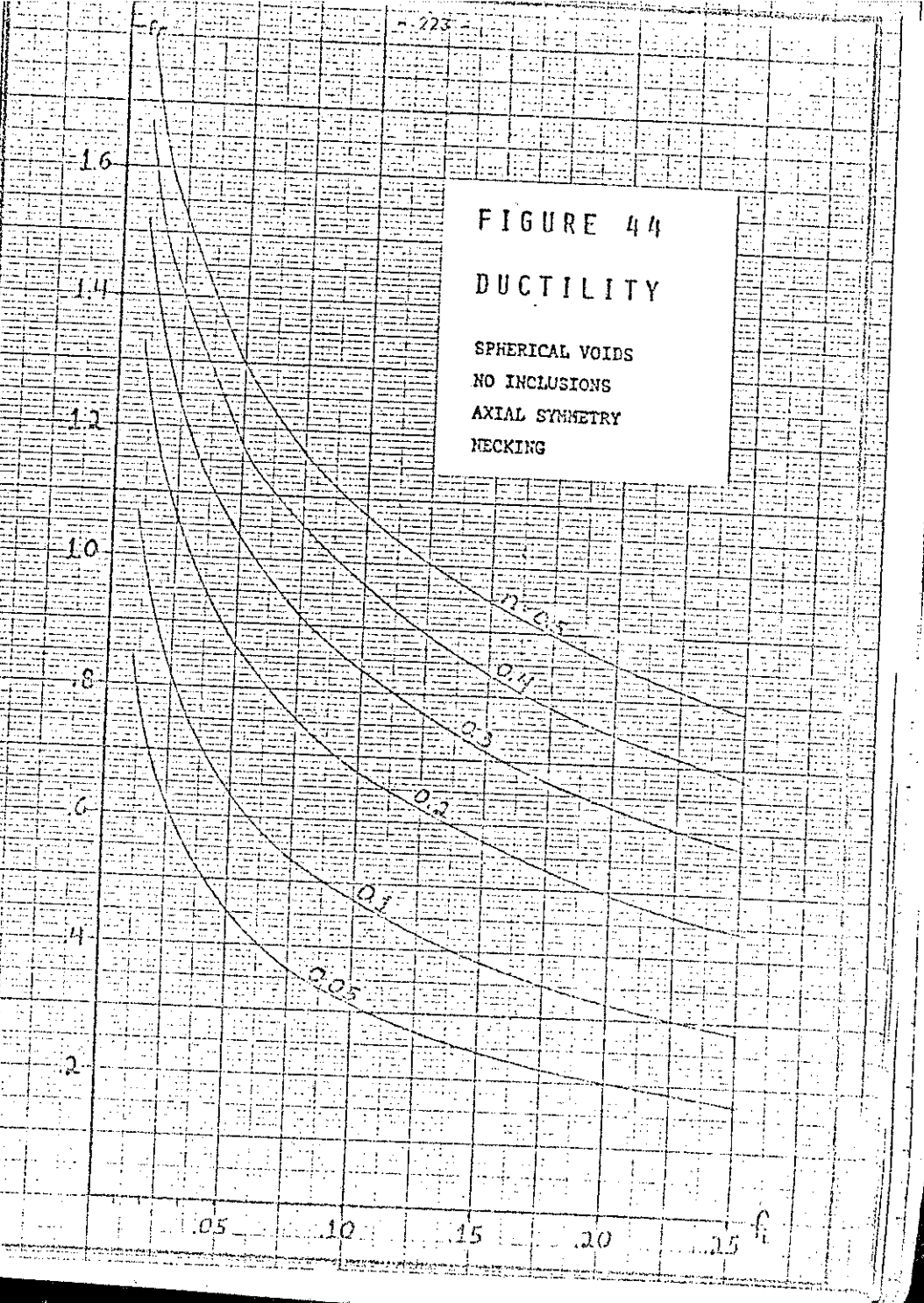

FIGURE 44

DUCTILITY

SPHERICAL VOIDS
NO INCLUSIONS
AXIAL SYMMETRY
NECKING

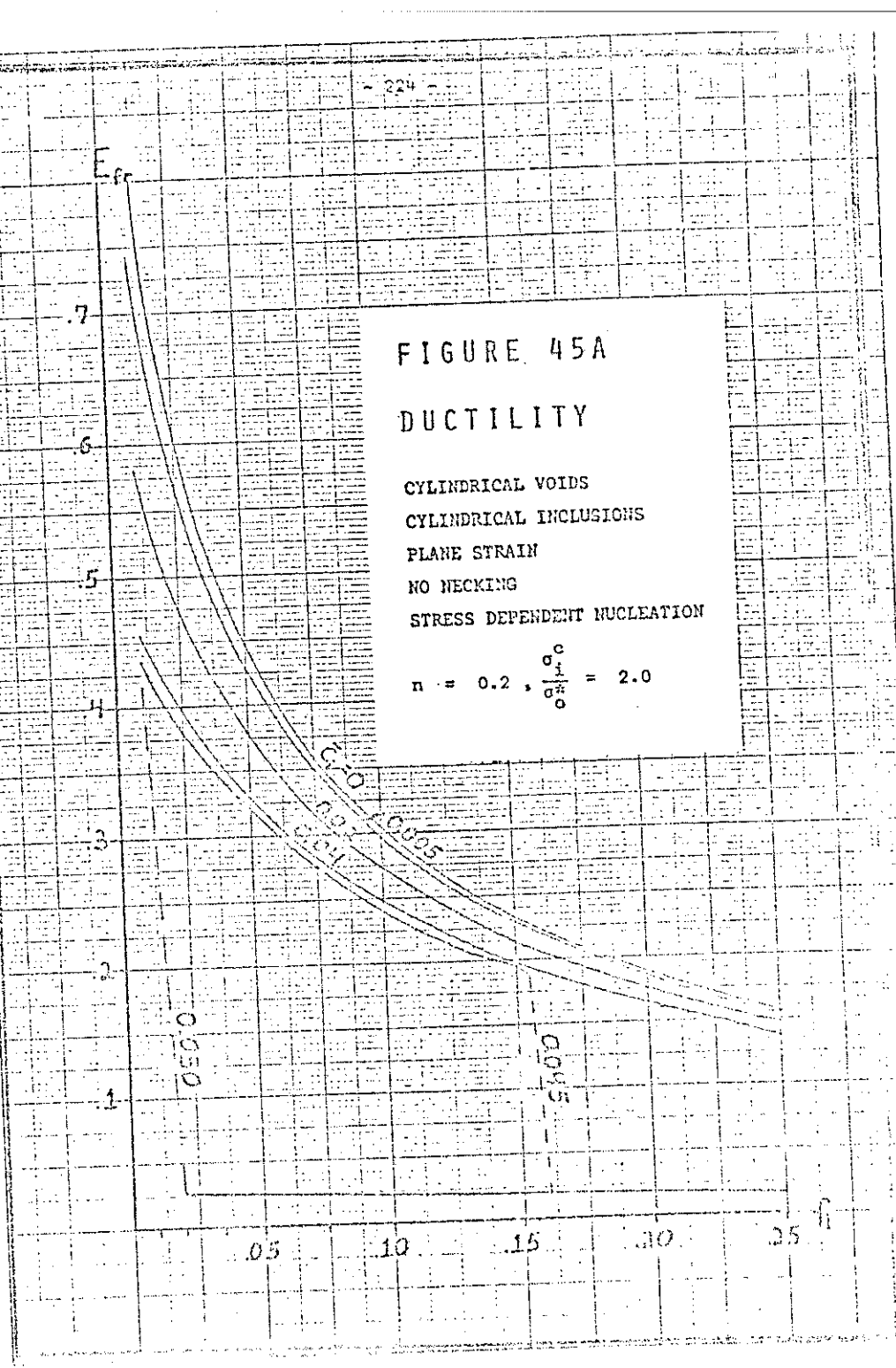

FIGURE 45A

DUCTILITY

CYLINDRICAL VOIDS

CYLINDRICAL INCLUSIONS

PLANE STRAIN

NO NECKING

STRESS DEPENDENT NUCLEATION

$n = 0.2$, $\frac{\sigma_i^c}{\sigma_o^*} = 2.0$

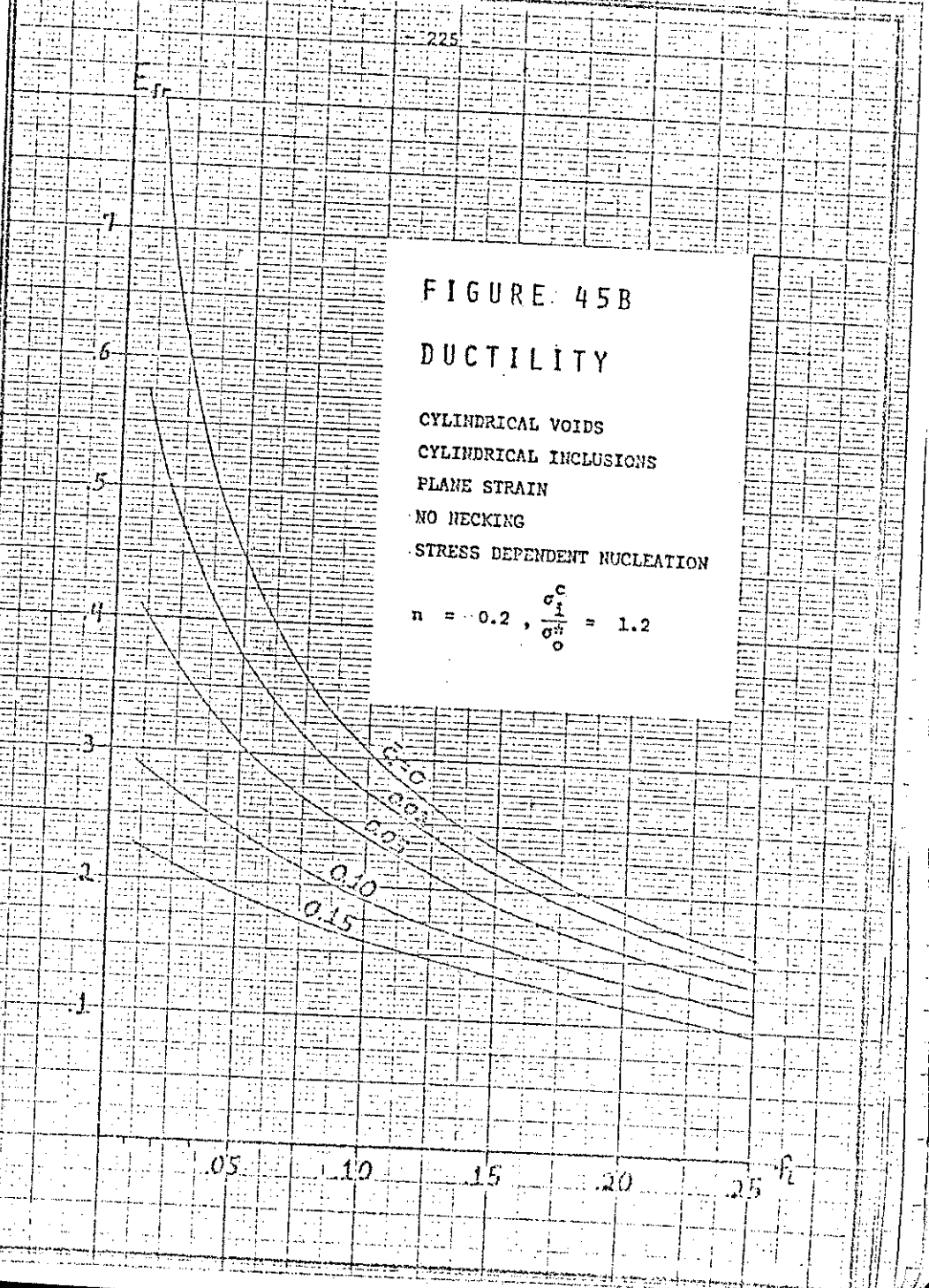

FIGURE 45B

DUCTILITY

CYLINDRICAL VOIDS

CYLINDRICAL INCLUSIONS

PLANE STRAIN

NO NECKING

STRESS DEPENDENT NUCLEATION

$n = 0.2$, $\frac{\sigma_i^c}{\sigma_o^*} = 1.2$

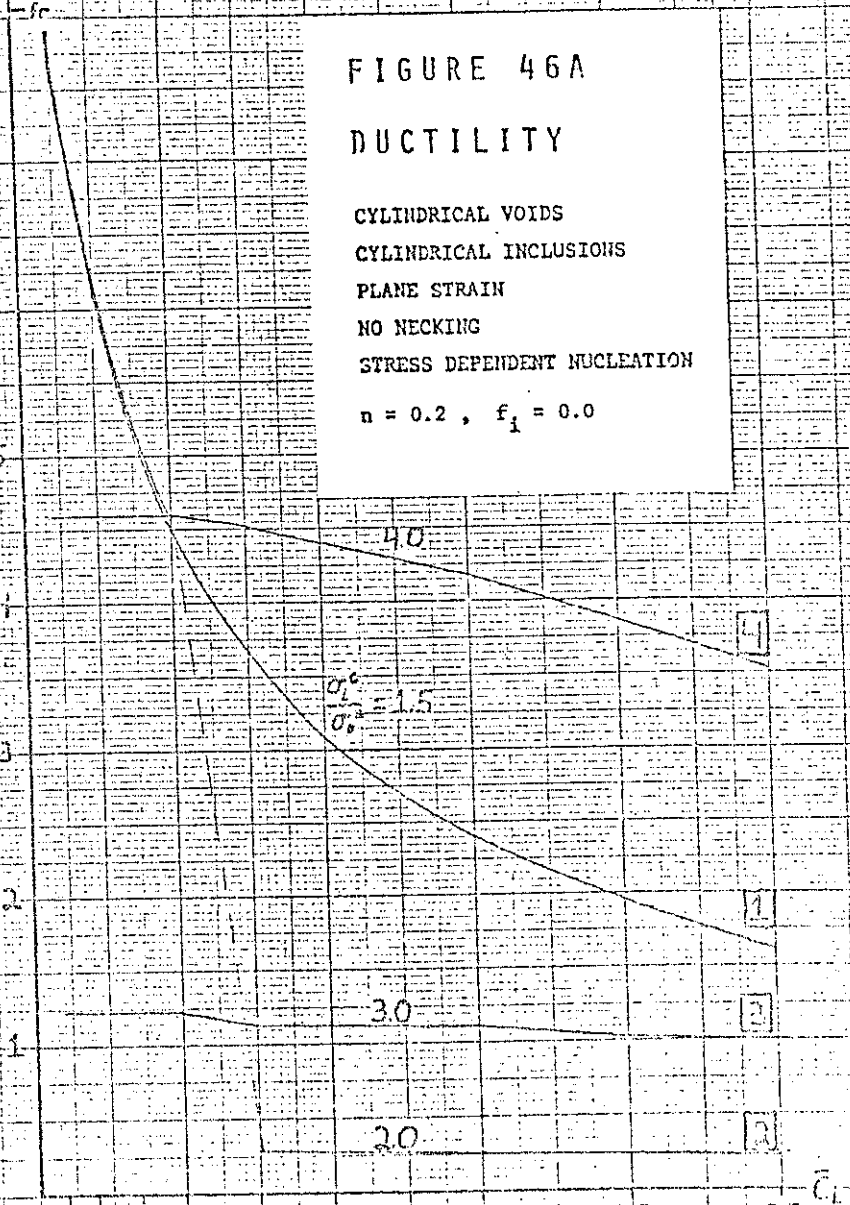

FIGURE 46A

DUCTILITY

CYLINDRICAL VOIDS
CYLINDRICAL INCLUSIONS
PLANE STRAIN
NO NECKING
STRESS DEPENDENT NUCLEATION

$n = 0.2$, $f_i = 0.0$

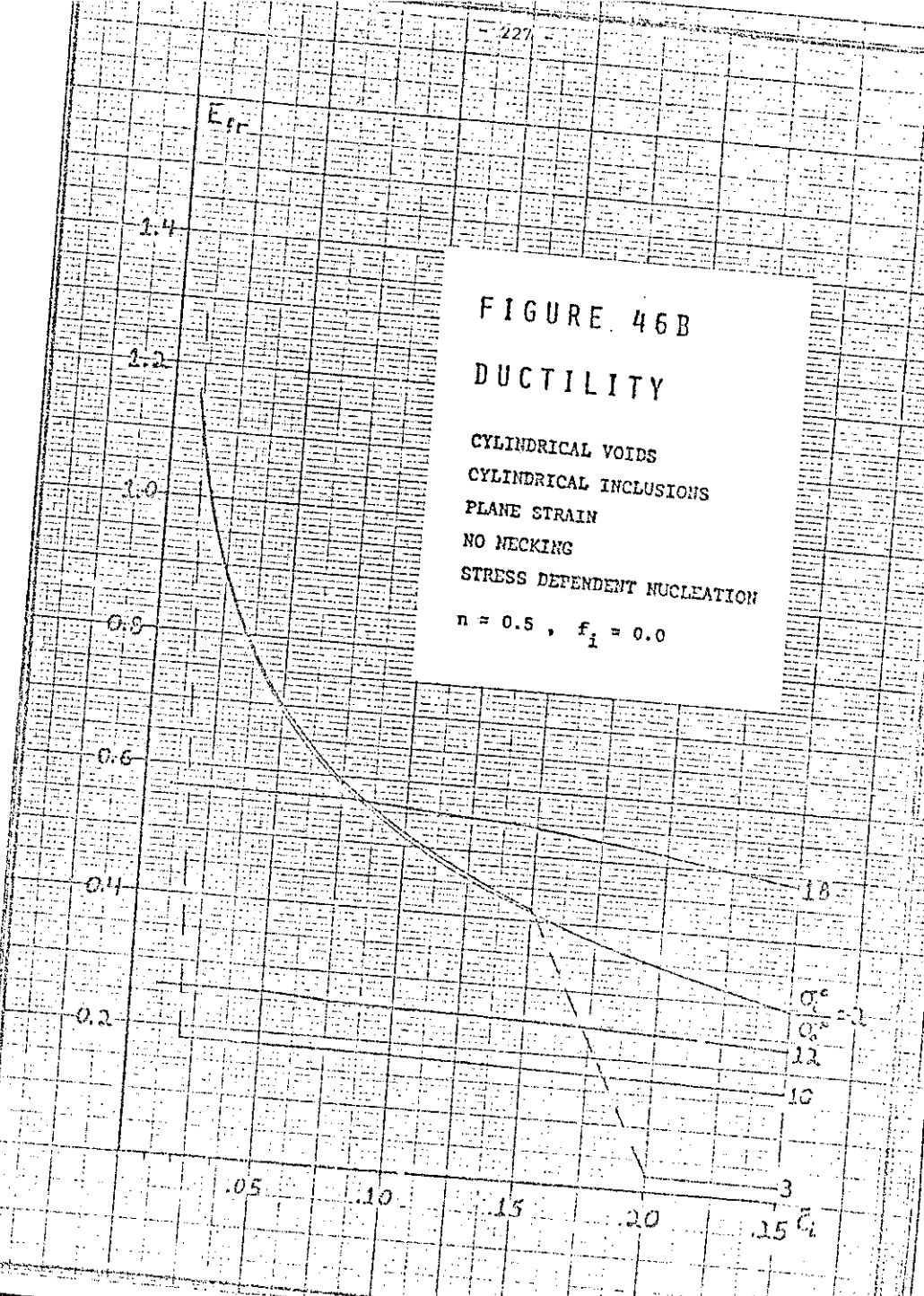

FIGURE 46B

DUCTILITY

CYLINDRICAL VOIDS

CYLINDRICAL INCLUSIONS

PLANE STRAIN

NO NECKING

STRESS DEPENDENT NUCLEATION

$n = 0.5$, $f_i = 0.0$

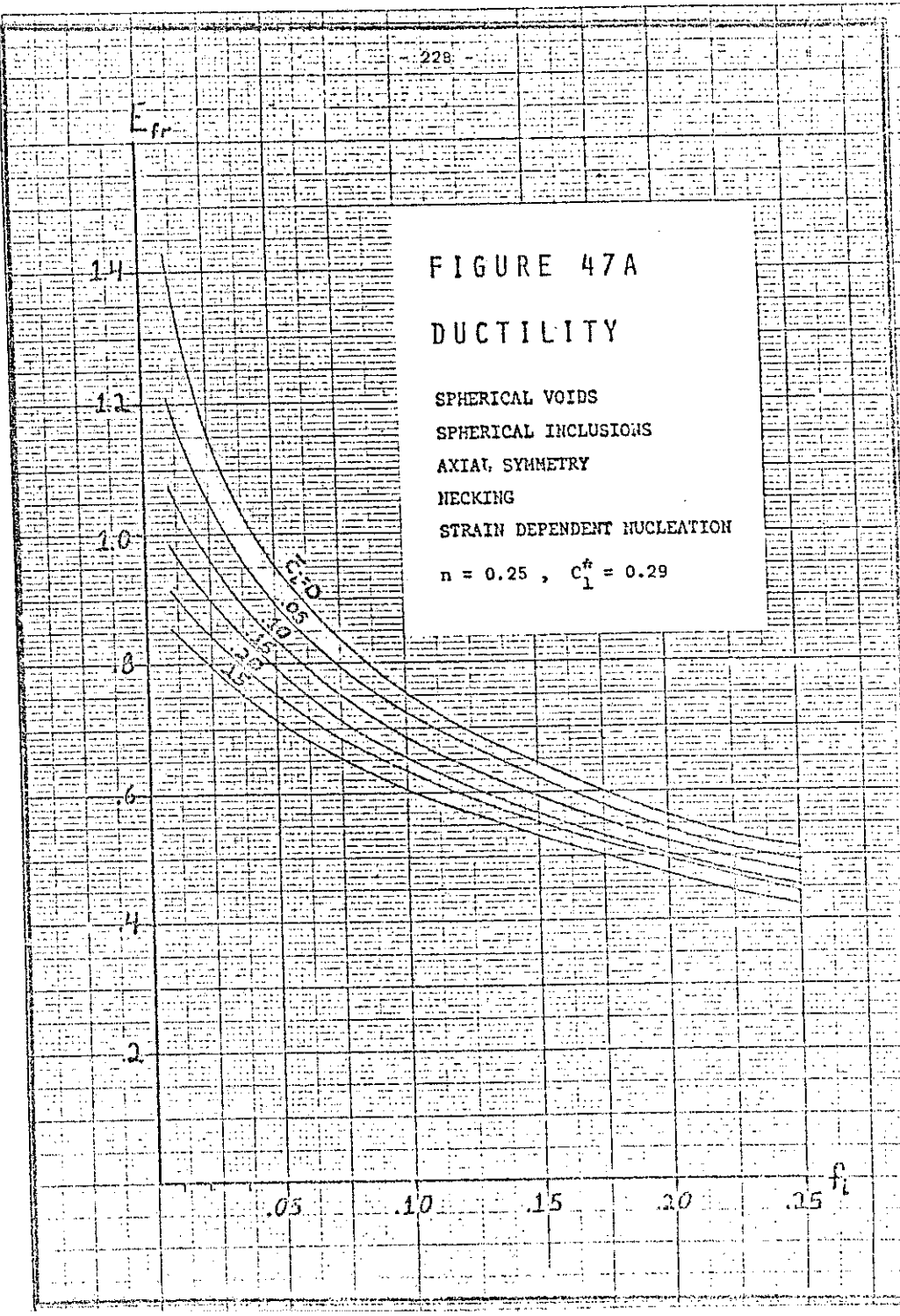

FIGURE 47A

DUCTILITY

SPHERICAL VOIDS

SPHERICAL INCLUSIONS

AXIAL SYMMETRY

NECKING

STRAIN DEPENDENT NUCLEATION

$n = 0.25$, $C_1^* = 0.29$

FIGURE 47B

DUCTILITY

SPHERICAL VOIDS
SPHERICAL INCLUSIONS
AXIAL SYMMETRY
NECKING
STRAIN DEPENDENT NUCLEATION

$n = 0.25$, $C_1^* = 0.29$, $f_i = 0$

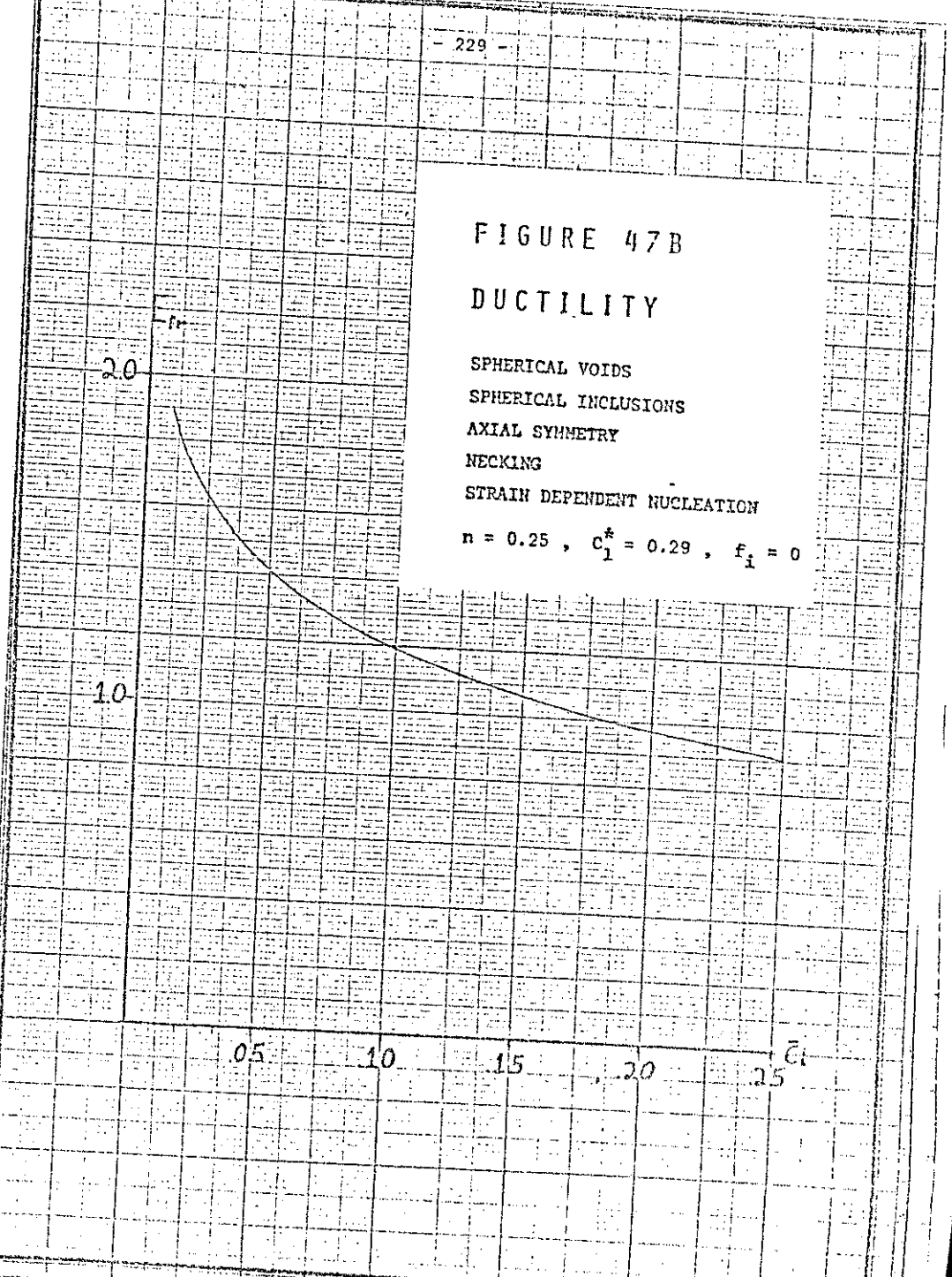

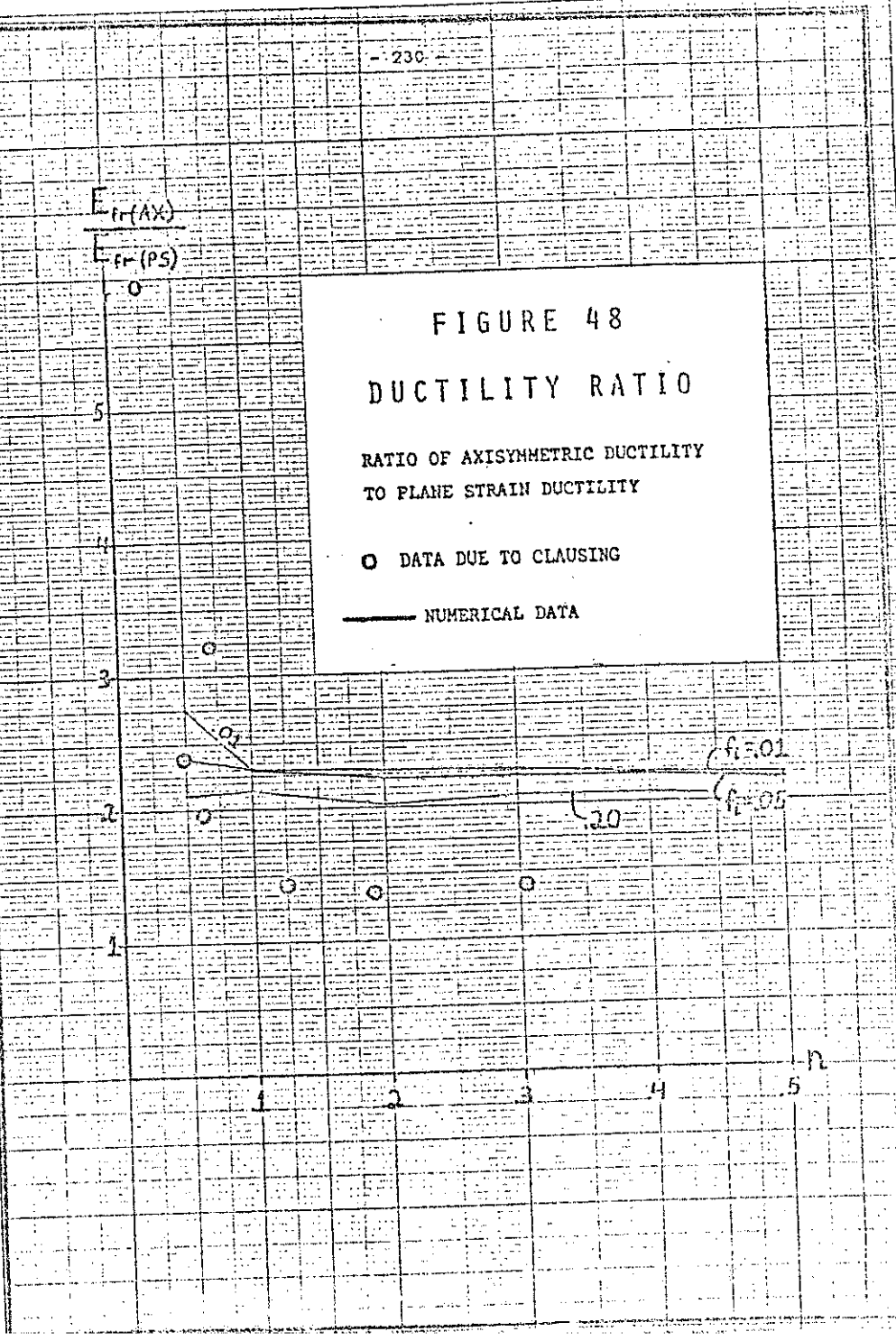

FIGURE 48

DUCTILITY RATIO

RATIO OF AXISYMMETRIC DUCTILITY TO PLANE STRAIN DUCTILITY

O DATA DUE TO CLAUSING

——— NUMERICAL DATA

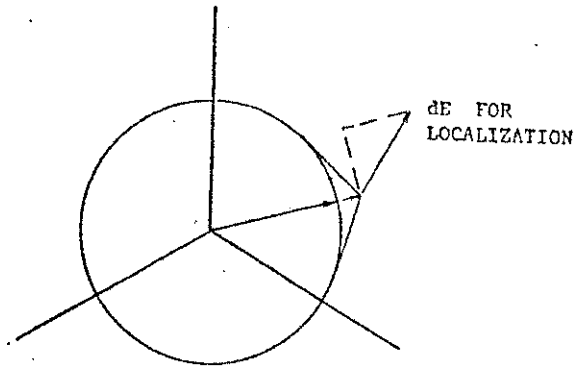

LOW n , HIGH TANGENTIAL STIFFNESS

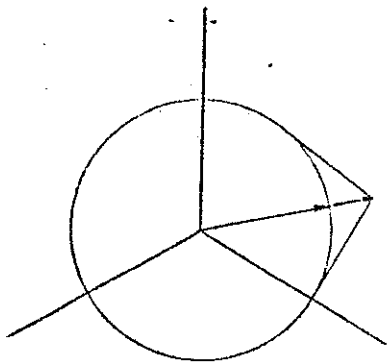

HIGH n , LOW TANGENTIAL STIFFNESS

VERTEX FORMATION
FIGURE 49

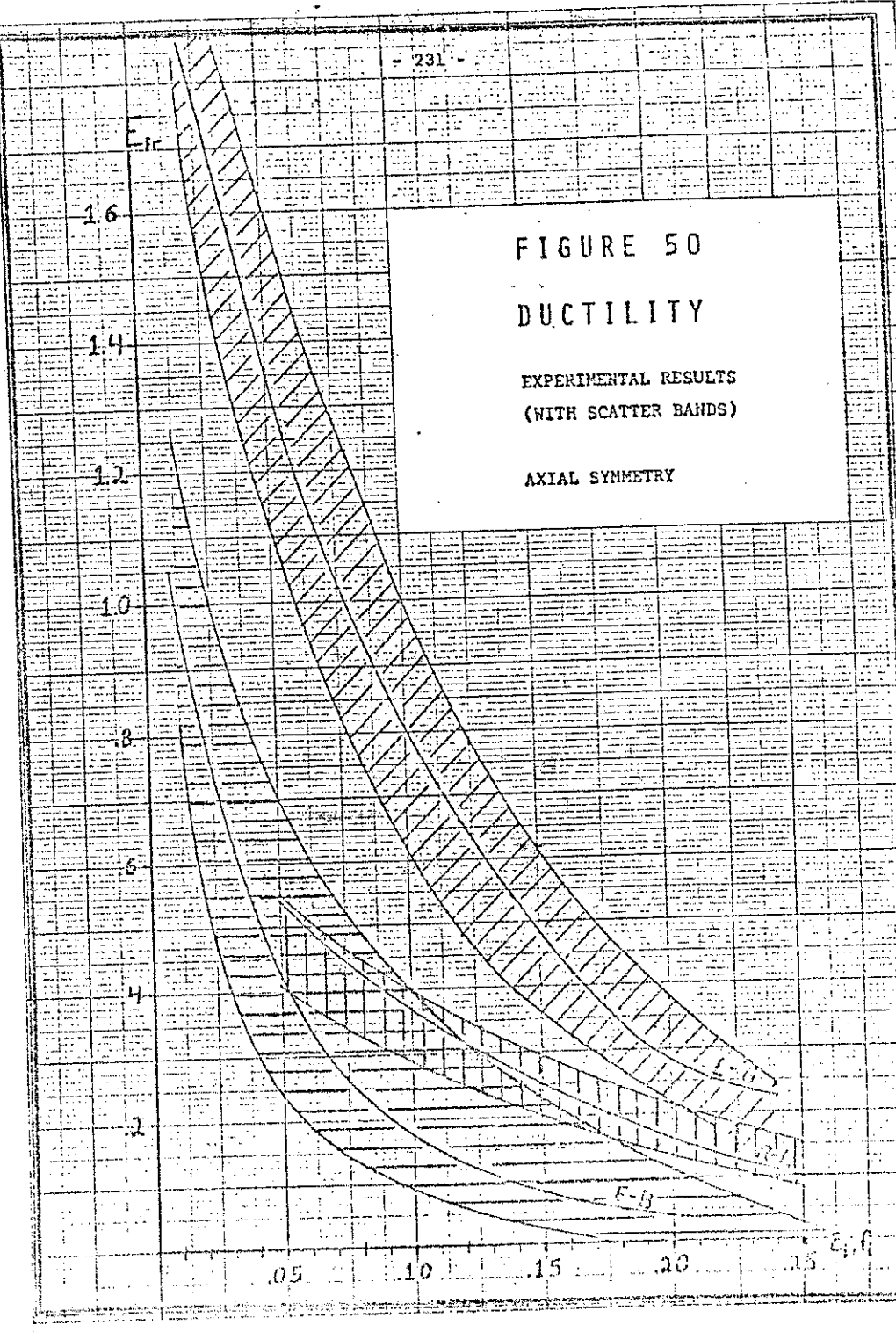

FIGURE 50

DUCTILITY

EXPERIMENTAL RESULTS
(WITH SCATTER BANDS)

AXIAL SYMMETRY